UNIVERSITÀ DEGLI STUDI DI NAPOLI
FEDERICO II
SCUOLA DI DOTTORATO IN INGEGNERIA INDUSTRIALE

DOTTORATO DI RICERCA IN
INGEGNERIA DEI SISTEMI MECCANICI
XXVIII CICLO

TESI DI DOTTORATO

BUILDING INDOOR AIR TEMPERATURE AND HUMIDITY CONTROL VIA INNOVATIVE TECHNIQUES

Supervisore:
Prof. ADOLFO PALOMBO

Dottorando:
UMBERTO MONTANARO

Coordinatore del dottorato
Prof. FABIO BOZZA

MARZO 2016

To my parents, sisters, nephews and niece.

To all wonderful human feelings that cannot be modeled by means of $\dot{x} = f\left(x,u\right)$.

CONTENTS

ACKNOWLEDGMENTS

The completion of the research that led to the results reported in this thesis would have not been possible without help, advice and support of people that I would like to thank in what follows.

First of all, I would like to thank my supervisor, Professor Adolfo Palombo for a variety of reasons. In particular, I want to thank him for having given me the possibility to perform my PhD under his supervision. His teachings, suggestions and comments have been fundamental for my work during these years. In addition, I really want to thank him for all the discussions we had, both scientific and non-scientific, they helped to improve me both scientifically and personally. I am sure they will be useful also in the future.

I want to thank Professor Stefania Santini for the scientific and personal support since I got my degree in engineering. She really deserves a special thank and our pleasant scientific collaboration has contributed a lot to this thesis. She is for me "my implicit supervisor" for this PhD and I am endlessly grateful to her.

I want to thank from the bottom of my heart Professor Annamaria Buonomano for having shared with me her code for the simulation of buildings (DETECt) which has been used to validate ideas and methods developed throughout the thesis. I want to thank her also for her constant support. But at the top of all, I want to thank her for her friendship, it counts a lot for me.

I would like to thank both Professor Buonomano and Professor Palombo for having welcomed me in their group, I will be always grateful to you for that.

I want to thank Professor Palombo and Professor Santini for trusting in me and for helping me with my career, but even more I want to thank them for understanding and supporting my decisions.

I would like to thank everyone in the group for creating a friendly and nice atmosphere. In particular Maria Vicidomini with whom I have shared the office. All these people made unique this Ph.D. experience.

Finally, I want to thank my Parents, my sisters Emilia and Maria Rosaria, my nephews Giampaolo, Michele and Francesco and my niece Sabrina for all their support and endless love. This thesis, as all my works, is dedicated to them and to all wonderful human feelings that cannot be modelled by means of $\dot{x} = f(x,u)$.

Umberto Montanaro,
Naples, March 2016.

Chapter 1
INTRODUCTION

Today a relevant amount of the total final primary energy is consumed in buildings, which are the largest energy consuming sector in the developed world [1]. Therefore, in the next years decision makers and planners are called to respond more effectively to a rising number of energy-related conflicting concerns dealing with energy saving, increasing of building energy and services demand, improved comfort life-time, satisfaction of indoor comfort indexes [2-5]. To this purpose, simulation-based methods have to be applied to solve sustainable building design problems and to dynamically predict the energy performance in a wide range of conditions.

Since the late '70s, building simulation is a well-recognized method for the building energy performance assessment [1]. Nowadays, due to mature and diffuse Information and Communication Technologies (ICT), its application is increasing wider and wider both to predict the indoor air temperature and humidity in time-dependent external weather conditions and to assess the influence of different buildings features (e.g. building use and envelope types, comfort parameters, building automation and control algorithms, occupants behaviour/preferences, etc.) on the building thermohygrometric behaviour and comfort [2]. Note that, building performance characterisation based on full scale testing of buildings is costly and difficult (e.g. due to changing structures, materials, ventilation strategy) and the real test of performance can be carried out only once the building is constructed and occupied. Therefore, the use of numerical models is a suitable tool for energy analysis during the very early stage of building design, e.g. for selecting innovative energy saving techniques or different construction materials like phase change materials (PCM) [3]. Finally, simulations help in control designing or control tuning, as well as in minimum disruption of the working system when deploying a new controller in a real environment.

Models used for simulation analysis can be classified as white-, black- and grey-box models [6]. White-box models (often referred as physics-based, analytical or forward models) fund on the understanding of the process physics and of its underlying engineering principles. Black-box models (or inverse and data-driven models) are based on measuring the system inputs and

outputs and then fitting them by a linear or nonlinear mathematical regressor to approximate the system behaviour during specific or standard operating conditions. Grey-box models are instead a combination of physics based and data-driven models and they are usually derived by using the equations within the white-box models and estimating parameters, or specific mathematical expressions, by using system measurements. Energy simulation programs usually exploit white-modelling approaches that ensure good prediction accuracy over a wide range of operating conditions without the need of providing additional measurement data [6]. They are embedded into commercial analysis tools (e.g. TRNSYS, Energy-Plus, ESP-r, etc. [6, 7]) or in generic programming environments [8] [9-11]. Commercial tools are regularly adopted among experts and professionals (architects, engineers, etc.) and they provide a variety of components in their libraries for a quick start of numerical analyses. Nevertheless, these programs are less flexible with respect to the controller development, the possible integration of new advanced controllers (alternative to standard strategies e.g. proportional-integral-derivative control (PID)) into the simulation code, and the implementation of specific mathematical models for describing the thermal dynamic of innovative materials like, for example, latent storage mediums [12].

As buildings continue to require increased energy performance and better comfort, control systems are becoming more and more complex and, hence, simulation codes based on generic programming environments offer a viable solution for testing new alternative control methodologies and for capturing the synergy between control algorithms and the forthcoming indoor thermohygrometric dynamics [9, 13-15]. With respect to the challenging multiple aim of fulfilling building cooling and heating requirements while guaranteeing indoor comfort, as well as of responding to variable weather conditions, thermal dynamics (due, for example, to the integration of energy storage elements with other building facilities), occupant behaviour and utility rate structures, existing control strategies currently implemented into buildings are still far away to reach their full potentials and, sometimes, are insufficient in accomplishing the ambitious expected benefits. Thus, there is still the need to examine existent strategies, to try to address the above issues by proposing alternative strategies and to test them via simulations tools [16]. Control techniques for energy buildings can be divided into different categories that essentially range from classical output control-loops (e.g. PID) to hard control (e.g. model predictive control (MPC), optimal control, adaptive control) and soft control (e.g. based on artificial intelligence tools, learning methods, agent based management algorithms). A scientific literature review and a detailed overview of the state-of-the-art in buildings control approaches can be found in [17]. Furthermore, although comfort level for building occupants also depends

on the indoor humidity levels, most of the control techniques presented in literature follows the classical approach of regulating only the building temperature to a certain set point [5].

Classical temperature control techniques basically consist of proportional-integral-derivative (PID) output feedback controls (and on their more recent implementation through fuzzy schemes [18]). The advantage of these schemes is their intuitiveness and simplicity and the absence of a precise mathematical models of the building system for the control design and implementation. Nevertheless, to achieve good performances a huge effort has to be spent for gains tuning (without providing the analytical proof of optimality, as well as closed-loop stability), while PID-controlled signals tends to result in overshoot (overheating) due to the weakness of the control scheme in processing disturbance inputs. As a further disadvantage, control parameters do not automatically adapt to changing in environmental conditions or building features and, hence, they have to be offline retuned every time that the working conditions evolve with time. In this regard, the lack of a very accurate and case specific gain tuning procedure effectively influences the reliability of parametric, multi-criteria and multi-objective analyses, which play a crucial role on the identification of optimal energy efficiency solutions and building features for the design of the next generation of buildings, such as net zero energy buildings (NZEBs)[19, 20]. In such analyses, multiple parameters, which may be related to the building features and to its boundary conditions (e.g. weather, usage, etc.), vary during the whole optimization procedure. Therefore, for efficient and reliable simulations, control parameters must be able to automatically adapt to such changes. Moreover, the tuning gains phase is very critical since an improper gains selection makes the entire system unstable and, for this reason, users are often not able to participate in the configurations scheme [5, 17]. As a result, tuning is always time-consuming and difficult. Different approaches, (based on artificial intelligence tools, such as, for example, learning methods [21] and agent-based energy management [15]), share with PID techniques the main advantage to be model-free, or better they do not need a detailed physics-based mathematical (ODEs) model of the building dynamics for the control design. The achievement of the thermal goal is reached, for example in the case of learning algorithms, by the choice of well-defined and huge training sets in different conditions or, for the case of agent-based solutions, by splitting the overall management problem into several well-posed sub-problems to be solved in order to find a balance among building energy requirement, thermal conditions and occupants comfort [17]. It is worth remarking that in the case of soft algorithms it is usually not possible to analytically guarantee the achievement of the control objective, or to analytically assess the stability and robustness of the overall system in perturbed situations. As a

result, as for PID schemes, great care has to be devoted to the selection of the training sets related to a wide range of different working conditions. As classical control schemes provide tuning-dependent results, hard techniques able to analytically guarantee the achievable performance have been proposed. Among them, Model Predictive Control (MPC) schemes are popular in the technical literature that deals with application to building-related systems [18].

MPC is a model-based controller which allows calculating an optimal command sequence. Particularly, MPC uses corresponding system dynamic models, such as building energy simulations models, to predict the system thermal behaviour. This prediction is then combined with optimization algorithms in order to determine the optimal control inputs. Note that, in order to elaborate the control sequence, not only a precise dynamic model of the system around the operating point, but also good estimations of all environmental conditions or disturbances acting on the system dynamics are needed, e.g. on-line whether forecast and time-history of the occupant behaviour. The need of an accurate system dynamic model for prediction purposes clamps down on the MPC application, since the effectiveness of the controller is significantly affected by the model accuracy. However, high accurate models are difficult to be developed due to the building systems complexity [22]. Further studies are hence still required to clearly disclose the robustness with respect to unmodelled nonlinear dynamics, such as the characteristics of innovative construction materials (especially in case of integrated thermal energy storage elements), and to reveal the effect of model prediction performance on control performance during practical system implementation. An optimal control sequence can be also determined by using optimal control techniques [23].

Although optimal control is an efficient mathematical tool for dealing with optimization problems through controlling engineering devices, it is not a viable solution in the case of building-related systems, since it is unable to deal with uncertain systems. Therefore, despite the effectiveness of the classical optimal approach (like linear quadratic algorithms, LQ) [23], changes in the operating condition and indoor disturbances affect the closed- loop behaviour; thus, the resulting trajectories can be strongly different from those optimal in real scenarios.

Since every building has its proper nonlinear thermohygrometric behaviour (due to the particular structure, construction materials, location, usage and climatic conditions), the problem to devise control schemes can be addressed by adaptive techniques that vary their parameters in order to accommodate changing dynamics in the system under control. This also provides a remarkable advantage with respect to the effectiveness of building simulation tools. In fact, this feature enables multiple building simulations (e.g. in case of sensitivity analyses and/or

optimization procedures) to run without the need of tuning the control system for each building model to be simulated. The different algorithms in the wide family of adaptive controllers can be classified into different categories according to the methods of adjusting controller parameters and to the approach with which they deal with the dependency on more or less accurate system models [24]. In spite of their adaptation features and, hence, their great robustness with respect to uncertainties, the application of innovative adaptive techniques to building-related systems is still rare [25, 26]. Possible reasons can be an excessive control effort or a high computational demand if choosing algorithms with complex adjusting lows for control or that exploits on-line parameter estimation techniques for their implementation. Moreover they may result to be less intuitive for engineers without knowledge of control.

1.1 **Aim of the thesis**

In this thesis, we design a novel Optimal-Adaptive scheme for controlling the air temperature and humidity for building indoor spaces in uncertain conditions, without requiring a priori knowledge of the building dynamics and/or its external disturbances. The algorithm, named LQ-EMRAC (Linear Quadratic - Enhanced Model Reference Adaptive Control) inherits the main advantages of Model Reference Adaptive Control (MRAC) and optimal control schemes (LQ) and it is able to appropriately and automatically vary its control gains, according to changes of the energy building behaviour, guaranteeing at the same time optimality with respect to a selected performance index that is function of the thermohygrometric requirements and the control effort.

Algorithms that belong to the MRAC family work on the principle of adjusting the controller parameters, so that the measured variables of the actual system under control track the dynamics of a Reference Model with the same reference input [24]. The Reference Model is used to give an ideal response of the controlled system to the reference input and it is selected just to specify the required performance. Therefore, it is different from complex system models, as those needed for the MPC implementation [18]. The controller is mathematically described by a set of adjustable parameters that are varied through an on-line adjustment mechanism, so that the actual system can track the reference model. To this aim, reference model dynamics are compared with real-time system operation variables and the difference between them defines the error signal, which is then used to adjust the control gains in order to reduce the tracking error to zero. Clearly, the main advantage of model-referenced adaptive control is that an accurate system model is not necessary for its deployment.

Differently from the classical MRAC approach, in the proposed LQ-EMRAC scheme the reference model is selected so as to provide optimal temperature and humidity profiles according to a cost function to be minimized. In so doing, the controller has the benefits of the adaptive strategy (such as robustness to perturbation and unmodelled dynamics and minimal knowledge of the plant dynamics for control design and implementation), while it also matches the performance dynamics of an optimal LQ-regulator, in order to impose an optimal thermohygrometric profile. Moreover, the LQ-EMRAC approach enhances the classical MRAC scheme by providing, in addition to the classical adaptive actions, novel control actions to improve the performance and the robustness of the scheme with respect to uncertainties and disturbances.

Summarizing, the main advantages of the proposed control are: i) robustness against a large class of perturbations, external disturbances, nonlinear unmodelled dynamics or parameters uncertainty that are suddenly counteracted by the control strategy; ii) ability to impose desired optimal dynamics; iii) reliance on a very reduced amount of information compared to other control techniques; iv) absence of on-line assessment of characteristic parameters of both building model or model reference; v) no need of a previous knowledge of the system initial conditions for the control implementation, vi) very accurate regulation and fast tracking of the optimal thermohygrometric profiles in case of stringent indoor air requirements (often mandatory in specific building spaces such as hospital units, museum display cases, laboratory chambers, etc.).

The above described control algorithm has been embedded in DETECt 2.3, a building energy performance simulation tool developed in MatLab® environment and based on a white-modelling approach [9, 26]. In particular, the LQ-EMRAC strategy has been implemented in this new release of DETECt, enhancing the previous ones [9, 26], in order to improve the robustness of the simulation results, especially in case of multiple simulations, such as parametric analyses. The code is able to dynamically predict: i) the building performance, in terms of both indoor air temperature and humidity; ii) the occupants' thermohygrometric comfort, through the assessment of several thermohygrometric comfort indexes (this is another novelty of DETECt 2.3 vs. the previous releases); iii) the sensible and latent heating and cooling energy demands and loads. In addition, the LQ-EMRAC strategy is also capable to deal with the nonlinear features of innovative construction materials (such as PCM), whose effects on the space heating and cooling demands can be suitably and consistently assessed through DETECt [26, 27]. Finally we remark that, thanks to the proposed control scheme, parametric analyses, performed through a single

simulation run, can be obtained with no need to tune the control system for each building simulation model.

In order to show the effectiveness of the adaptive solution, different case studies are developed throughout the thesis. In particular the numerical analysis can be divided as follows:

1. energy and comfort performance have been expounded by taking into account different buildings which are diverse with respect to the use, geometry and construction materials. In particular, geometry and usage of these sample buildings vary as a function of the square meters floor area, ranging from a basic small residential house to a large commercial mall. Furthermore, simulations are carried out by locating such buildings in different weather zones. For each case study, continuous and intermittent control system operating strategies are considered;
2. numerical analysis performed for different choices of the optimal reference profiles to impose to the thermohygrometric variables;
3. the analysis at point one has been done also when the building envelope integrates phase change materials (PCM), which are mainly used to improve energy reduction further especially during summer season by stabilizing indoor air temperature;
4. adaptive control of multi-zone systems when some zones are completely included in others and characterized by different thermohygrometric requirements. For this configuration two case studies have been developed. Specifically, we consider *i)* an expo indoor space of a museum building, including a display/case and *ii)* special indoor hospitals spaces including multiple infant-incubators.

Results confirm the ability of the proposed approach to reach the selected thermohygrometric requirements and comfort conditions for any investigated building. In particular the numerical analysis in point one is used to show the flexibility of the control solution to different buildings, climate weather conditions and use. The analysis in point two is exploited to study the effect of the choice of the reference model in terms of required sensible and latent heats and comfort indexes. Notice that the possible use of PCM layers make the parameters of the building model time-varying as the specific heat of these layers chance on the basis of their temperature. Consequently, control strategies with fixed control gains might fail in imposing the required thermohygrometric conditions. Instead the analysis carried out in point three have shown the ability of the controller to reconfigure its gains to regulate the required indoor air relative humidity and temperature also in this case. Finally the analysis in point four has been used to test the robustness of the adaptive systems for the control of buildings in presence of coupled

dynamics which have not been considered during the control design. Indeed, by neglecting the thermal coupling between zones the control design gets easier but during the simulation the mutual thermal effects play the role of additional disturbances that the control systems must be able to reject in closed loop.

Note that, even though the adaptive strategy is designed by considering an optimal reduced order reference model, the numerical analysis assesses the control performance on the detailed physical and nonlinear building models, included in DETECt [26, 27], which consist of several (more than 70) nonlinear differential equations. This further contributes to remove doubt on the robustness of the control approach with respect to unmodelled dynamics. We remark that the effectiveness of the adaptive approach to impose the required profiles to the indoor air temperature and humidity is proved in the thesis also analytically with a consistent proof of stability of the closed loop system in a more generic framework.

To compare the performance provided when the adaptive controller is exploited to tame the building dynamics with those given by state-of-art strategies available in the technical literature, both in terms of tracking of the required set points and energy demands, we have implemented a MPC strategy and additional numerical analysis are carried out in the thesis when these predictive controllers are inserted in the control loop.

We point out that, for the design of MPC algorithms it is crucial to have models of the building dynamics that are very predictive but yet simple so that it is possible to solve in an effective way the optimization problems required for the computation of the control action. Consequently, an additional aim of the thesis is that of proposing a systematic method for the generation of low order grey box building models. We remark that these models can be exploited also for aims different from the design of advanced model based controllers [17, 28]. Indeed by using reduced order models it is possible to *i)* reduce drastically the computation time to get an insight into building energy performance, especially when a large set of simulations are required to assess them [29] *ii)* derive mathematical models of building dynamics via reverse engineering methods when experimental data are available [30] and *iii)* simulate groups of buildings organized in districts with the aim to evaluate the overall energy performance [31]. Hence the design of methods for the building model reduction represent an additional result that is used in the thesis to devise predictive controllers but they have their own importance in the context of building performance analysis. We note that, in order to measure the effectiveness of the resulting low order building models to predict both indoor building temperature, heating and cooling energy demands, as well as comfort a set of performance indexes are defined to evaluate

the deviations of the outputs of the reduced order models with respect to the corresponding outputs of detailed models.

In addition to the work described in the thesis, additional results were obtained on modeling, simulation and analysis of buildings embedding novel technologies for reducing energy consumption [27, 32] (NZEBs in Mediterranean climates, see also List of Publications).

1.2 Outline of the thesis

The thesis is outlined as follows.

Chapter 2. This is a background chapter which provides to the reader some details about the in-house Building Energy Performance Simulation (BEPS) code DETECt and the building mathematical model which is implemented in it. This in-house code is indeed used throughout the thesis to confirm numerically the effectiveness of the adaptive control solution to impose to the indoor air temperature and humidity the required profiles. A more complete description of the code can be found in [9].

Chapter 3. In this chapter the control architecture used in the thesis is described in detail. In addition a first strategy is proposed for the control of the indoor air temperature with the aim of improving the pre-existing Proportional Integral (PI) control solution embedded in DETECt. Specifically the PI control gains are selected as the result of an optimization problem that takes into account indoor tracking error and the heating/cooling energy. Hence, it can be considered as an attempt to improve a classical control solution by imposing a sort of optimality to the control action.

Chapter 4. This chapter is completely dedicated to the design of the novel model reference adaptive control strategy for generic linear time invariant (LTI) dynamical systems subjected to parameter uncertainties and disturbances, as well as the steps required for its numerical implementation. Furthermore, the effectiveness of the control solution to impose the dynamics of the reference model is analytically proven by adopting both hyperstability theory and Lyapunov techniques.

Chapter 5. In this chapter the design of the adaptive solution proposed in Chapter 4 for the control of the termohygrometric variables in buildings is presented. The chapter opens with the design of a simplified building model to be used for the tuning of the reference model for the generation of the indoor air temperature and humidity profiles to be tracked in closed-loop. Then different case studies are presented to show numerically the effectiveness of the approach. Specifically, we consider

different buildings which are diverse with respect to the use, geometry and construction materials. Also a brief comparison with the PI solution presented in Chapter 3 is provided in order to point out the limitation of control strategies with fixed gains. Notice that the numerical analysis are carried out by using as building model that presented in Chapter 2.

Chapter 6. Here we further prove the ability of the adaptive control strategy to impose the required thermohygrometric dynamics in the case of multi-zone buildings where some thermal zones are completely included in others. As case studies we consider two possible scenario, i.e., *i)* an expo indoor space of a museum building, including a display/case and *ii)* special indoor hospitals spaces including multiple infant-incubators.

Chapter 7. This chapter is completely devoted to present the grey-box modelling approach to derive low order building models for the design of advanced model based control strategies, e.g., predictive controllers. To show the ability of the low order building models to predict indoor air temperature, heating and cooling as well as comfort indexes, e.g., PMV and PPD, the model reduction procedure is applied to the case studies in Chapter 5 and results are compared to those provided by the detailed model presented in Chapter 2. The comparison is carried out quantitatively by using a set of performance indexes which are also defined in the chapter.

Chapter 8. In the first part of the chapter, model predictive controllers are designed and numerically validated for the case studies in Chapter 5. For the design of these MPC controllers the low order models introduced in Chapter 7 have been exploited to predict buildings dynamics with a reduced computational effort and acceptable error. The second part of the chapter is instead dedicated to preliminary compare some features of the predictive approach to those of the adaptive solution proposed throughout the thesis both in the case of perfect knowledge of the weather data and internal loads as well as in the case of uncertain conditions.

Chapter 9. In the final chapter we summarize the main contributions of the thesis and some open problems are briefly given for the further research activities.

Appendix A. In this first appendix some details about adaptive control is given. The aim is to provide to the reader some basic concepts and definitions about this solution to the control of systems with uncertain parameters. In addition, a standard classification of

adaptive control schemes is also provided to better frame the adaptive technique proposed in the thesis.

Appendix B. This appendix reports additional details about the results of the model reduction procedure which have not been given in Chapter 7.

Chapter 2
BUILDING DYNAMIC MODEL

In this chapter, the dynamic model used to analysis building energy performance when advanced control algorithms for the optimal computation of the sensible and latent heats are exploited is presented together with some details about its implementation as numerical code. This in-house code, named DETECt, can be used for the testing of a variety of new building technologies to increase system energy efficiency before they are actually implemented. Therefore, it becomes a useful tool to carry out scientific research activities and it is used throughout the thesis as the numerical environment to prove the effectiveness of the novel control algorithms for the themohygrometric variable . As detailed described in the chapter, the outputs of this numerical code are not limited to the yearly heating and cooling load and energy demand, but they include the dynamic temperature profile of indoor air, indoor air humidity as well as the dynamic profile of the thermal fluxes through the building elements, just to name a few. The chapter summarizes briefly the basic features of the code, with particular care to those that are relevant for the following chapters where advanced methodologies for the computation of sensible/latent heats, which represent the aim of the thesis, are presented in depth. The material of this background chapter is taken from [9, 26, 27, 33] where the reader can find additional detail about DETECt. Here only some features are reported for the sake of completeness.

2.1 A brief introduction to DETECt in the framework of BEPS codes

Building Energy Performance Simulation (BEPS) codes have been used for decades for predicting the energy performance of buildings and energy savings associated with energy efficiency measures. In the last years, recent advances in analysis and computational methods as well as computer power have increased the opportunity for significant improvements in analysis tools developments. As a consequence, building energy performance simulations have become an irreplaceable tool for building design and energy diagnosis. Indeed, they are widely used for analyzing the energy consumption in buildings in order to assess buildings energy efficiency and

requirements, especially nowadays as a collaborative effort among researchers, building designers and government agencies have been built up with the aim to move towards the net zero energy building. Therefore, up-to-date building energy simulation codes are required for providing greater design flexibility in order to meet new targets in terms of buildings energy performance and occupants' thermal comfort. However, since building energy simulation is a complicated process involving modelling and analytical skills, the use of the building energy investigation tools and the analysis of the related results can be considered as a challenge for building designers and practitioners and often also advanced users doubt about the fidelity and accuracy of the related calculations results. From this point of view, in order to validate novel BEPS codes several general criteria and validation procedures (consisting of comprehensive and integrated suite of building energy analysis tool tests involving analytical, comparative, and empirical methods) have been developed and are available in literature [34]. Recently, the Energy Performance Building Directive (EPBD) issued by the European Union emphasizes the need of performance-based standards and requires the certification of new software developed for BEPS in compliance with the related standards. In this regard, the EN ISO 13790:2008 allows the assessment of the energy requirement for heating and cooling by means of several calculation methods [35]. For the dynamic one a specific validation procedure is described in the EN 15625:2008 [36]. Here, a set of assumptions and requirements that should be followed together with several tests for the validation of computer software are described. In particular, the dynamic calculation (with a time step of one hour or less) is referred to annual energy needs due to heating and cooling of a single space. No specific numerical technique is here imposed.

An alternative validation method for testing, diagnosing and validating the capabilities of BEPS codes is the BESTEST (Building Energy Simulation TEST) procedure [37]. This method consists of analytical techniques and tests that allow the results of a given BEPS program or design tool to be compared with those obtained by the current state-of-the-art codes. A number of the BESTEST cases have been incorporated into ANSI/ASHRAE Standard 140-2011 [38]. By the latter the original International Energy Agency (IEA) BESTEST is assumed as a standard method for BEPS codes validation. Note that the BESTEST procedure is adopted also by the European Committee for Standardization (CEN) as a test for checking the reference cooling load and energy calculation methods, based on the requirements of several standards addressing different aspects of the EPBD [39]. In accordance with these procedures, many BEPS codes have been validated [40-45]. Through these tools, the system behavior in terms of energy use for heating, cooling, lighting, etc., as well as indoor comfort and building operating temperatures,

can be usefully and accurately predicted. From this point of view, in order to carry out a BEPS analysis by suitable computer codes different approaches can be followed [46]. In general, the differences among them concern the fidelity and the accuracy by which the occurring physical phenomena are modelled. Usually, in order to realize straightforward tools, only few system phenomena can be modelled taking into account just the most significant physical aspects occurring in the building dynamics. This, for example, occurs in some models in which the conduction heat transfer is solved by lumping all the building thermal masses in a single node of a considered thermal network. Through this approach the integration of just one or two mathematical equations is necessary, avoiding the adoption and the resolution of many partial differential equations [47-49]. On the other hand, these simulation methods are mostly suitable for a basic building analysis only. In fact, they are not able to provide details about the building surfaces temperature or for simulating the frequent rapid variation of the thermal conditions occurring in buildings equipped by HVAC systems [50].

For all these reasons, more detailed simulation models are often used, as discussed above. Through these tools, in order to accurately predict the whole building dynamic behavior, the energy response of each thermal zone is analyzed taking into account almost all the physical phenomena by suitable mathematical models. In general, through these tools the simulations are carried out accounting time-variant parameters as: weather conditions, occupancy, lighting and machinery loads, building thermal inertia, etc.. Detailed output such as building energy heating and cooling demands, indoor and building surfaces temperature, humidity levels and even the operating system costs can be dynamically calculated for various design and operating conditions. A summary about assumptions, features and limitations of such standards are reported in [45, 51, 52]. Although all these standard tools are capable of a high level of flexibility, many new in-house BEPS codes have been developed mostly for research scopes. In addition, in the last years, the research in the building energy saving field led to investigate a lot of new building envelope technologies and innovative HVAC systems often supported by renewable energies or innovative control strategies [53]. In order to allow all these novel technologies to be implemented into commercial tools, a certain time-to-market is unavoidable. Thus, these fast growing research and development efforts often involve the development of suitable and flexible computer-based models for the energy performance calculation of innovative building-plant systems. Furthermore, in some of the above reported simulation codes, several household actions can be often simulated only in a rigid or basic way, without accurately emulating all the real interactions of occupants with the building [54-57]. As a result, depending

on the occurring physical phenomenon that has to be studied, specific in-house codes are more and more developed. In fact, recently, for research scopes, as alternative to commercial building simulators, several lumped parameter models have been developed and used for computer based optimization, analyzing the building envelope behavior, and to study distribution of internal solar radiation, etc. [40, 42, 58, 59].

In many of these models, the thermal resistance capacitance network approach is widely adopted [51]. In addition, although many reduced order models have been widely considered also for research scopes [47, 60], in order to analyze the effect of the spatial distribution of the heat capacity on the heat flux through the building envelope elements, a high number of thermal capacitances is taken into account through distributed parameters models [58, 61]. For all these reasons, several authors have developed building-plant simulation codes for the analysis of innovative and traditional systems, as reported in [62, 63].

In this framework, the code called DETECt has been proposed in [9, 62] as a simple but yet detailed code for assessing building envelope performance. Different from several of the above mentioned commercial codes, some simplifications are adopted but without renouncing to describe the main physical phenomena occurring in each building element. The main difference between DETECt and the most utilized commercial software lies in the adopted methods for the heat transfer in the building. In the following, the adopted methods for the one dimensional transient heat conduction through multi-layer envelope components, the solar and long wave radiation handling into and out of the building, ventilation and infiltration treatment, etc., are described. In the code developed in [9] all these models are grouped in a unique calculation tool. Notice that, a similar approach is adopted also in other works where in-house codes have been developed mostly for studying a single physical phenomenon [58, 59]. Obviously, at the code development status, in comparison with the presented code, commercial tools provide more complete user's interface and data libraries for building elements features, weather files, etc., as reported in [45, 52].

We point out that DETECt is implemented in MATLAB, which is well recognize as a standard tool for the scientific numerical computation [64]. Moreover, additional computer subroutines for the performance simulation of any kind of building plants (HVAC systems, renewable energy applications, etc) can be suitably linked to this tool obtaining a complete building-plant simulation code (e.g. [62, 63]). In addition, by using DETECt it is also possible to perform new and retrofit-oriented building sensitivity analyses, that can be used to assist the user in the retrofit selection process. These analyses can be easily performed though a specific code

interface by starting from a unique generated building model, without re-entering in the iterative simulation procedure the varied details of the different building features that have to be analyzed (e.g. thickness and stratification of building envelope elements, etc.).

It is important to point out that DETECt has been extensively validated in [9] by exploiting as validation method the BESTEST procedure. This choice fits fundamental criteria for the validation of BEPS codes such of completeness, accuracy, reproducibility and cost effectiveness of the test suite. Indeed, the BESTEST procedure presents widely available high quality empirical validation data sets. In particular, it includes detailed and unambiguous documentations of the input data for a selected number of representative design conditions. It is worth pointing out that DETECt results matched those of the BESTEST qualification cases in terms of heating and cooling annual energy demand and integrated peak-load, annual transmitted and incident solar radiation, annual hourly zone temperature, moreover, also hourly variables fit the reference trends. Briefly, DETECt exceeded the BESTEST reliability test as low or very low deviations of the results obtained by this code vs. those provided by BESTEST validation procedure has been observed. Note that DETEC underwent and additional code to code validation test for several commercial buildings located in different weather locations as reported in [9].

In the following sections, the main features of the model implemented in DETECt, which are essential for the rest of the thesis, are given in detail. Precisely, the heat transfer due to conduction and convection involving the building elements are shown in Section 2.2.1, while the nonlinear actions provided by radiation and solar radiation are presented in Sections 2.2.2 and 2.2.3, respectively. Indoor air temperature and humidity dynamics are instead presented in Sections 2.2.4 and 2.2.5. Finally, before summarizing the chapter content in Section 2.4, the input/output description, as well as an overview of the software modules composing the DETECt code are given in Section 2.3.

2.2 **Model Description**

The first steps to be carried out in a detailed building energy simulation analysis concern the calculation of building heating and cooling loads and demands. This calculation procedure starts from the heat flows analysis related to a building thermal zone. These flows, as is well known, depend on heat conduction through walls, internal and external convection and radiation, sun radiation transmission through fenestration, heat gains due to building equipment and occupants and ventilation [10, 50]. In general, the dynamic simulation methods mainly attempt to assess the

building energy balance by solving the heat transmission through the related envelope. From this point of view, suitable numerical and analytical algorithms are implemented in purposely designed performance simulation codes [50, 65-67].

In most of these tools the one-dimensional heat flow assumption is usually adopted. Even if through this hypothesis inaccurate results are achieved close to envelope corners, edges, etc., it can be generally accepted since transverse heat transfer often plays a minor role in the building conduction phenomena [68, 69]. The thermal network calculation techniques is usually used as an alternative to the simple energy balance assessment [42, 70, 71]. A very simple thermal network model consists of lumping all the system thermal mass in a single node [35, 48, 72-74]. In general, when low or null temperature gradient within the thermal mass are expected, the classical lumped parameters approach can be adopted. On the other hand, real building elements are often composed by different structural and energy saving insulation materials in mutual thermal contact. In these cases, being the allocation of heat capacity and thermal resistance a complex function of the space, a thermal model obtained by distributed parameters better describes the occurring transient physical phenomena [58]. Here, the distributed capacitances and resistances of a material layer are lumped together at nodes. In addition, by distributing these parameters on multiple nodes, the dynamic calculation of the indoor air and building surfaces temperatures can be also assessed. This method also allows the use of active climate controls for the detailed calculation of the building energy requirements. It must be said that in building dynamic analyses, a compromise between very simple models and those with a very high number of nodes should be also taken into account to keep the computation time at an acceptable level. Consequently, in order to consider both thicknesses and thermo-physical features of the different layers included in each considered building element, a minimum number of nodes have to be modelled.

2.2.1 *Heat flow calculation procedure*

In DETECt the thermal behaviour of each *m*-th multi-layer building element (wall, floor, roof, horizontal and vertical internal partition and window), is modelled through a thermal Resistance Capacitance (RC) network. Here, each building element construction material is considered as uniform and therefore its thermal mass and conductivity are uniformly discretized into a number of layers. Thus, each building element is discretized into a suitable number, *N*, of thin sub-layers of different thicknesses in function of the adopted discretization criterion [75, 76]. In each sub-layer a uniform temperature is supposed. The sub-layer temperature is represented with a single

node of the considered thermal network in order to account the related thermal mass. Each sub-layer includes two conductive resistances and a single capacitance, which is lumped in the middle of the layer. For each *m*-th building element two additional surface non-capacitive thermal nodes are accounted and considered as boundary nodes linked, in general, to the outdoor and indoor air temperatures. Figure 2.1 shows this thermal network composed by the *N+2* nodes for the generic *m*-th building element. Interface contact resistances are neglected, thus a perfect thermal contact of each adjacent inner homogeneous material layer to the connected ones is always supposed (i.e. identical interfacial temperatures are assumed). Furthermore, homogeneous, isotropic and time-invariant thermo-physical properties (i.e., density, specific heat and conductivity) are supposed. The heat transfer occurring out of each m-th building element is modeled via convective and radiative equivalent thermal resistances.

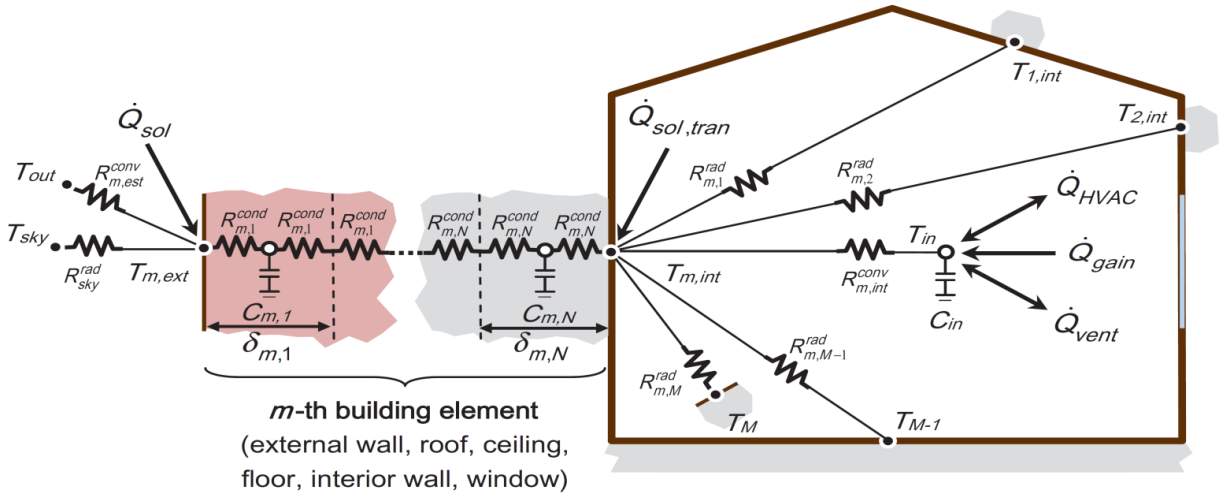

Figure 2.1. Schematics of the RC thermal network for the generic *m*-th element of the building envelope.

Therefore, in order to assess the system thermal response, the number of simultaneous equations to be solved is equal to *N+2* for each element. The higher the number of sub-layers, the lower the sub-layer thickness and capacity. Obviously, by using a high number of nodes the discretized model tends to become identical to the physical one and the accuracy of the simulation results improves (i.e., temperature gradients can be accurately accounted) [58]. On the other hand, beyond a certain *N*, the more accuracy of the numerical results becomes negligible despite the simulation time still increases.

For each capacitive *n*-th node ($1 \le n \le N$) of the *m*-th building element ($1 \le m \le M$) the differential equation describing the related heat transfer is (see also Figure 2.1):

$$C_{m,n}\frac{dT_{m,n}}{dt}=\sum_{j=n-1}^{n+1}\frac{T_{m,j}-T_{m,n}}{R_{m,j}^{cond}}, \tag{2.1}$$

where: *t* is the time, $C_{m,n}$ and $T_{m,n}$ represent the thermal capacitance and the temperature of the *n*-th node of the *m*-th building element, respectively. Moreover, $T_{m,j}$, with $j=n-1$ and $j=n+1$, are the temperatures of the neighbour nodes which are directly connected to the *n*-th layer; $R_{m,j}^{cond}$ is the sum of the halves sub-layers thermal resistances that couple the *n*-th node to their neighbour ones. Such total resistance is equal to the one of half sub-layer when $n=1$ and $n=N$ as the first and last capacitive nodes are connected to surfaces which are modelled as non-capacitive subsystems. For such outer ($n=0$) and inner ($n=N+1$) surface non-capacitive nodes, the algebraic equation describing the related heat transfer is:

$$\sum_{j=n-1}^{n+1}\frac{T_{m,j}-T_{m,n}}{R_{m,j}}+\dot{Q}_{m,n}=0,\ R_{m,-1}=R_{m,ext}^{conv},R_{m,N+2}=R_{m,int}^{conv},\ \text{otherwise } R_{m,n}=R_{m,n}^{cond}. \tag{2.2}$$

The extremal nodes of the *m*-th building element are linked to convective thermal resistances (external, $R_{m,ext}^{conv}$, and internal, $R_{m,int}^{conv}$, respectively, see Figure 2.1). Such resistances interconnect the above mentioned surface boundary nodes to the outdoor and indoor temperature nodes ($j=-1$ and $j=N+2$ for T_{out} and T_{in}, respectively). Although in Figure 2.1 some radiative thermal resistance are shown, in the model, all the radiation phenomena are lumped in $\dot{Q}_{m,n}$ (as it is described in the following). Hence, $\dot{Q}_{m,n}$ represents the generic thermal source term acting on the surface node. The thermal capacitance, $C_{m,n}$, of each sub-layer, the conductive resistance, $R_{m,n}^{cond}$, of each half sub-layer and the convective external, $R_{m,ext}^{conv}$, and internal, $R_{m,int}^{conv}$, ones, are computed as:

$$\begin{aligned}
C_{m,n}&=d\cdot c\cdot\gamma_{m,n}\cdot A,\\
R_{m,n}^{cond}&=\frac{\gamma_{m,n}/2}{k_{m,n}\cdot A}\quad \text{for } n=1 \text{ to } N,\\
R_{m,ext}^{conv}&=\frac{1}{a_{m,ext}\cdot A},\\
R_{m,int}^{conv}&=\frac{1}{a_{m,int}\cdot A},
\end{aligned} \tag{2.3}$$

where for each building element sub-layer: $\gamma_{m,n}$ is the thickness, $k_{m,n}$ is the thermal conductivity, *A* is the heat exchange surface area, $a_{m,ext}$ and $a_{m,int}$ are the outdoor and indoor

surface unitary convection heat transfer coefficients, respectively. In particular $a_{m,ext}$ is set as a constant on the basis of the surface type (rough, smooth, very smooth/glass, etc.) or can be optionally calculated, for rough surfaces, by empirical relationships as a function of the outdoor wind speed [77, 78]:

$$a_{m,ext} = \begin{cases} 3.8 \cdot v + 5.7 & \text{for } v \le 5 \text{ m/s}, \\ 7.0 \cdot v^{0.78} & \text{for } v > 5 \text{ m/s}, \end{cases} \tag{2.4}$$

where: v is the wind velocity, which can be set as a constant when its time-history is not given. Note that, constant properties of materials and no surface condensation or dust gathering are always assumed.

This *RC* model is applied to both opaque and transparent surfaces. It must be said that in most building energy simulation programs a negligible thermal inertia for thin glazing systems is assumed. This assumption may lead to remarkable errors when it is applied to thick or multi-layered glazing systems [79]. For this reason, the thermal inertia of glasses is always taken into account as an element of the system in Figure 2.1.

2.2.2 *Thermal network boundary conditions*

The forcing functions in (2.2) are basically composed by radiations and outdoor temperatures, which act only on the surfaces of each *m*-th building element. Precisely, the ambient temperature boundary condition is considered as convection load, while the radiation as a thermal source, $\dot{Q}_{m,n}$. The film resistances, see (2.3), interconnect the boundary outdoor, T_{out}, and indoor, T_{in}, temperature nodes with the related boundaries of the building element. Note that, in the presented model the occurring heat gains and/or ventilation and HVAC system effects are assumed to act only on the indoor air node, as reported in the following.

The radiation forcing functions is assumed acting on the outer ($n = 0$) and inner ($n = N+1$) surfaces of each *m*-th building element. Outer surfaces are here considered as in contact with indoor or outdoor space conditions. On an outer surface, the only considered boundary condition is the indoor air temperature of the related adjacent space. Such temperature can be kept as constant or follow a suitable time profile depending on whether it is switched-on or turned-off the building HVAC system, respectively. On the contrary, in case of an external outer surface the considered boundary conditions are the outdoor air and sky temperatures and the solar radiation.

The forcing function on external opaque and glazed surfaces describing both the solar and long wave radiations is denoted as Φ_m. On inner opaque and glazed surfaces (as well as on

internal facing surfaces of the gap of multi-layered glazing system), the accounted forcing function is the radiation incident on the *m*-th surface due to the solar radiation load entering through windows, Ψ_m, and to the net long wave radiation load, Γ_m, received by the other *i*-th ($1 \le i \le M$) internal surfaces of the considered thermal zone. In particular, for each *m*-th element with a heat exchange surface area *A*, those forcing functions are computed as:

$$\dot{Q}_{m,j} = \Phi_m \quad \text{for } j = 0,$$
$$\dot{Q}_{m,j} = \Psi_m + \Gamma_m \quad \text{for } j = N+1 \text{ or for a glazing gap,}$$

$$\Phi_m = \left[\varepsilon_{m,ext} \cdot \sigma \cdot f \cdot (T_{sky}^4 - T_{m,1}^4) + \alpha_{m,ext} \cdot I_m^{\text{ext}} \right] \cdot A_m, \tag{2.5}$$
$$\Psi_m = \alpha_{m,int} \cdot A_m \cdot I_m^{\text{int}},$$
$$\Gamma_m = \varepsilon_{m,int} \cdot \sigma \cdot A_m \cdot \sum_{i=1}^{M} G_{mi} \cdot (T_{i,N}^4 - T_{m,N}^4),$$

where *f* is the external surface view factor and T_{sky} is the sky temperature. If for the latter quantity a time history is not available, it can be computed as $T_{sky} = 0.0552 \cdot T_{out}^{1.5}$ in accordance with [80], where T_{out} is the outdoor air temperature. On the external and internal surfaces of each *m*-th element, $\varepsilon_{m,ext}$ and $\varepsilon_{m,int}$ are the selected emissivity, respectively; $\alpha_{m,ext}$ and $\alpha_{m,int\cdot}$, are the selected absorption factors, respectively; I_m^{ext} and I_m^{int} are the total solar radiation fluxes, respectively. In particular, the solar radiation entering through glasses is absorbed, reflected and distributed within the internal space by selected absorption, reflection and view factors, respectively, therefore, I_m^{int} is the total solar radiation flux received by an internal *m*-th surface including the solar irradiance reflected by other interior surfaces [81]. Such flux is the *m*-th entry of the total solar radiation flux vector, I^{int}, computed as:

$$I^{int} = \begin{pmatrix} I_1^{int} \\ I_2^{int} \\ \dots \\ I_M^{int} \end{pmatrix} = \begin{pmatrix} \left(1 - F_{11}\rho_1^S\right) & -F_{12}\rho_2^S & -\dots & -F_{1M}\rho_M^S \\ -F_{21}\rho_1^S & \left(1 - F_{22}\rho_2^S\right) & -\dots & -F_{2M}\rho_M^S \\ \dots & \dots & \dots & \dots \\ -F_{M1}\rho_1^S & -F_{M2}\rho_2^S & -\dots & \left(1 - F_{MM}\rho_M^S\right) \end{pmatrix}^{-1} \cdot \begin{pmatrix} I_1^0 \\ I_2^0 \\ \dots \\ I_M^0 \end{pmatrix}, \tag{2.6}$$

where the generic entries F_{ij} and ρ_j^S are the internal surfaces view factors and the solar reflectivity coefficients, respectively, while $I^0 = \left[I_1^0 \quad \dots \quad I_M^0 \right]^T$ is the vector of the solar radiation directly received by the interior surfaces; it depends on the solar radiation effectively

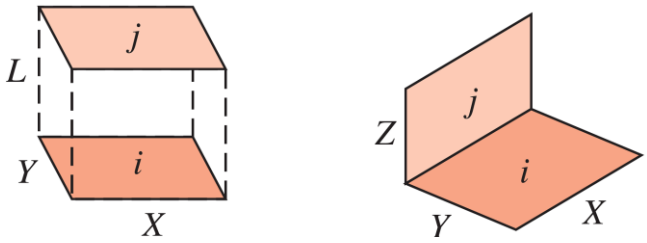

(a) **(b)**

Figure 2.2. Relevant three dimensional geometries: (a) Aligned Parallel Rectangles, and (b) Perpendicular Rectangles with common edge (Figure taken from [82]).

transmitted through windows. The latter is function of the equivalent solar transmission coefficient of the glazed surfaces. We point out that, the physical law (2.6) can be expressed synthetically as $I^{int} = (\bar{I} - FP_S)^{-1} I^0$, where $\bar{I}$ is the identity matrix of order *m*, and F and P_S are the internal surfaces view factors matrix and the solar reflectivity matrix, respectively. In addition, the coefficients F_{ij} are calculated for parallelepiped structure as in [78, 82]. Indeed, according with [82], the view factor between two generic surfaces A_i and A_j is given as

$$F_{ij} = \frac{1}{A_i} \iint_{A_i A_j} \frac{\cos(\theta_i)\cos(\theta_j)}{\pi R_{ij}^2} dA_i dA_j, \tag{2.7}$$

where R_{ij} is the distance between two generic infinitesimal elements dA_i and dA_j, while θ_i is angle between the normal vector to the surface dA_i and the vector connecting dA_i to dA_j. Analogously, θ_j is angle between the normal vector to the surface dA_j and the vector connecting dA_j to dA_i.

Even though the integral (2.7) can be discretized and computed numerically, for some relevant geometry, it can be solved analytically as a function of some relevant parameters of the surfaces. Of particular interest are the geometries reported in Figure 2.2. Precisely, in the case of aligned parallel rectangles with later lengths *X* and *Y* separated by a gap of length *L* (Figure 2.2a), we have

$$\begin{aligned} F_{ij} = \frac{2}{\pi \bar{X}\bar{Y}} \Bigg\{ & \ln\left[\frac{(1+\bar{X}^2)(1+\bar{Y}^2)}{1+\bar{X}^2+\bar{Y}^2} \right]^{\frac{1}{2}} + \bar{X}(1+\bar{Y}^2)^{1/2} \tan^{-1} \frac{\bar{X}}{(1+\bar{Y}^2)^{1/2}} + \\ & + \bar{X}(1+\bar{Y}^2)^{1/2} \tan^{-1} \frac{\bar{Y}}{(1+\bar{X}^2)^{1/2}} - \bar{X} \tan^{-1} \bar{X} - \bar{Y} \tan^{-1} \bar{Y} \Bigg\}, \end{aligned} \tag{2.8}$$

where $\bar{X} = X / L$ and $\bar{Y} = Y / L$.

In the case of perpendicular rectangles with common edge completely described by the lengths *X*, *Y* and *Z*, as shown in Figure 2.2b, the views factors can be evaluated as

$$F_{ij} = \frac{1}{\pi W}\left\{ W \tan^{-1}\frac{1}{W} + H \tan^{-1}\frac{1}{H} - (H^2+W^2)^{1/2} \tan^{-1}\frac{1}{(H^2+W^2)^{1/2}} + \right.$$
$$\left. + \frac{1}{4}\ln\left[\frac{(1+W^2)(1+H^2)}{1+H^2+W^2} \left(\frac{W^2(1+H^2+W^2)}{(1+W^2)(H^2+W^2)} \right)^{W^2} \left(\frac{H^2(1+H^2+W^2)}{(1+H^2)(H^2+W^2)} \right)^{H^2} \right] \right\}, \tag{2.9}$$

where $H=Z/H$ and $W=Y/H$.

When the view factors are known, the *m*-th entry of the total solar radiation flux vector can be calculated as in [81]

$$I_m^{int} = I_m^0 + \sum_{j=1}^{m} F_{mj}\rho_j^S, \tag{2.10}$$

From (2.10), expression (2.6) can obtained after some additional algebraic manipulations.

In Figure 2.1 the external and internal solar radiation fluxes are reported in terms of thermal load, $\dot{Q}_{sol}$ and $\dot{Q}_{sol,tran}$, respectively. In this regard, further details about the calculation of solar radiation incident on the building are reported in the following.

In order to calculate the long-wave radiation exchange on the internal surfaces within the zone, the Gebhart's absorption method is adopted [83]. Hence, Gebhart's factors must be computed and collected in the Gebhart's matrix *G*. We recall here that the Gebhart's factor, named G_{ij}, between a generic A_i and A_j is defined as the ratio between the energy absorbed at A_j originating as emission at A_i and the total radiation emitted from A_i. Alternatively, it represents the fraction of the emitted radiation from the *i*-th interior surface that is absorbed by the remaining *j*-th surface of the considered thermal zone.

In [83] it has been shown that such a coefficient is given by

$$G_{ij} = F_{ij}\varepsilon_j^{LW} + \sum_{k=1}^{M} \rho_k^{LW} F_{ik} G_{kj}, \tag{2.11}$$

with ρ_i^{LW} and ε_i^{LW} being the long wave reflectivity and emissivity coefficients of the *i*-th surface, respectively. From (2.11) the fraction of the emitted radiation from the *m*-th interior surface that is absorbed by the remaining surfaces of the considered thermal zone is computed by using the Gebhart's matrix, *G*, which consists of a number of *m* vectors of coefficients calculated as:

$$\begin{pmatrix} G_{1m} \\ G_{2m} \\ \dots \\ G_{Mm} \end{pmatrix} = \begin{pmatrix} \left(1 - F_{11}\rho_1^{LW}\right) & -F_{12}\rho_2^{LW} & -\dots & -F_{1M}\rho_M^{LW} \\ -F_{21}\rho_1^{LW} & \left(1 - F_{22}\rho_2^{LW}\right) & -\dots & -F_{2M}\rho_M^{LW} \\ \dots & \dots & \dots & \dots \\ -F_{M1}\rho_1^{LW} & -F_{M2}\rho_2^{LW} & -\dots & \left(1 - F_{MM}\rho_M^{LW}\right) \end{pmatrix}^{-1} \cdot \begin{pmatrix} F_{1m}\varepsilon_m^{LW} \\ F_{2m}\varepsilon_m^{LW} \\ \dots \\ F_{Mm}\varepsilon_m^{LW} \end{pmatrix}. \tag{2.12}$$

Notice that, the m^2 Gebhart's matrix coefficients only depend on surfaces geometry and materials thermal properties. Hence, it can be pre-computed on the basis of these proprieties. Notice that also (2.12) can be expressed systematically via linear algebra as $G = (\bar{I} - FP_{LW})^{-1} FE_{LW}$, where P_{LW} and E_{LW} are long wave reflectivity and emissivity matrices, respectively.

2.2.3 *Solar radiation calculation*

In order to calculate the solar radiation incidence angle on the building surfaces, as well as the global radiation striking of any arbitrarily tilted and orientated external or internal surface, different geometric relationships have to be taken into account [84]. Hence, to describe accurately their mathematical models in function of the hourly sun position, some preliminary fundamental relations are given below.

The solar azimuth given by the angle of the surface normal from the South, φ_s, and solar zenith representing the tilt angle from the horizontal, ϑ_s, are computed as:

$$\begin{aligned} \vartheta_s &= \arccos\left(\cos\lambda\cos\delta\cos\beta + \sin\lambda\sin\delta\right), \\ \varphi_s &= \arcsin\left(\frac{\cos\delta\sin\beta}{\sin\vartheta_s}\right), \end{aligned} \tag{2.13}$$

where λ is the latitude of the selected site, β is hourly solar angle, i.e., the angular displacement of the sun east or west of the local meridian due to rotation of the earth on its axis at 15° per hour (morning negative and afternoon positive), and δ is the declination angle, which is calculated in [84] as

$$\delta = 23.45\frac{\pi}{180}\sin\left[2\pi\left(\frac{284 + j_d}{36.25}\right)\right], \tag{2.14}$$

with j_d being the Julian day of the year.

Defining as φ_p, and ϑ_p the azimuth angle and the zenith angle of the generic building surface, the incident angle ϑ_i is computed as

$$\vartheta_i = \arccos\left(\sin\vartheta_s \sin\vartheta_p \cos(\varphi_s - \varphi_p) + \cos\vartheta_s \cos\vartheta_p\right). \tag{2.15}$$

(Notice that $\vartheta_p = 90°$ for vertical wall surfaces.) Consequently, The hourly incident beam, $I_m^{\text{ext,b}}$, and total, I_m^{ext}, solar radiation fluxes on a *m*-th building surface are calculated by:

$$\begin{aligned} I_m^{\text{ext,b}} &= I_{DN} \cdot \cos\vartheta_i, \\ I_m^{\text{ext}} &= I_m^{\text{ext,b}} + I_m^{\text{ext,d}}, \end{aligned} \tag{2.16}$$

where I_{DN} is the hourly direct normal irradiance, often available from database of weather data, and $I_m^{\text{ext,d}}$ is the diffuse irradiance. The latter can be computed by subtracting the beam irradiance on a horizontal surface from the global one or through properly relationships. In the first case, the beam irradiance on a horizontal surface can be calculated by the first relationship in (2.16) or directly obtained by database of weather data, similarly to the global one. It is noteworthy that nowadays the hourly direct normal irradiance as well as the global one on a horizontal surface are usually available, thanks to their large use in solar system performance investigations. However, in case of lack of such solar radiation data, the Hottel and Liu-Jordan methods for the direct and diffuse irradiances can be adopted and implemented [85, 86].

2.2.4 *Indoor air temperature model*

The energy rate of change connected to the indoor air mass is equal to the difference between the energy supplied to and removed from a thermal zone. The dynamical model of the thermal network node of the indoor air to be solved simultaneously with the system (2.1) and (2.2) is

$$C_{in}\frac{dT_{in}}{dt} = \sum_{m=1}^{M}\frac{T_{m,N} - T_{in}}{R_{m,\text{int}}^{conv}} + \dot{Q}_{gain} + \dot{m}_{vent}c_p\left(T_{out} - T_{in}\right) \pm \dot{Q}_{HVAC}, \tag{2.17}$$

where C_{in} is the thermal capacitance of the zone indoor air, whose temperature, T_{in}, is considered homogeneous in the space (perfect indoor air mixing). The first term on the right-hand side in (2.17) describes the heat exchange between the *M* internal surfaces nodes and the indoor air. Internal convective resistances, $R_{m,\text{int}}^{conv}$, are calculated as a function of the surfaces condition (vertical or horizontal wall; ascendant or descendant flow). We note that, in our modelling approach, with exception of the solar radiation thermal load transmitted through the windows and incident on the indoor surfaces, $\dot{Q}_{sol,tran}$ in Figure 2.1, all the sensible heat gains are considered networked to the indoor air node only, i.e., model (2.17). They include: *i)* the thermal zone internal load, $\dot{Q}_{gain}$, represented as a lumped heat source term and consisting of

convective sensible internal gains due to occupants (here due to the metabolic rate in function of the indoor air temperature), lights and equipment; *ii)* the ventilation thermal load, i.e., $\dot{Q}_{vent} = \dot{m}_{vent} c_p \left(T_{out} - T_{in}\right)$, where $\dot{m}_{vent}$ is the air ventilation mass flow rate (no distinction between infiltration and mechanical ventilation is assumed) and c_p is specific heat capacity of air, respectively ; *iii)* $\dot{Q}_{HVAC}$ is the sensible heat supplied to, or removed from, the building space by an ideal HVAC system in order to maintain the indoor air at the desired set point temperature. Note also that, $\dot{Q}_{HVAC}$ is here considered as acting on the node as purely convective. The design of algorithms in the form of feedback systems for the automatic computation of sensible heat is crucial [6, 7]. Indeed, features as energy consumptions and robustness to external disturbances are strongly connected to the performance of the resulting feedback control system. In this thesis, novel adaptive algorithms, belonging to the family of direct MRAC systems are designed and discussed in Chapter 4. (The reader is instead referred to Appendix A for the definition of this class of feedback controllers).

2.2.5 *Indoor humidity model*

To model indoor humidity dynamics, a temperature-humidity decoupled approach is adopted [9, 87]. Specifically, for each indoor space the moisture balance is calculated by neglecting the moisture exchange between the air node and the surrounding building surfaces. Consequently, the adopted moisture balance on the indoor space air is:

$$\Omega_{in} \frac{d\omega_{in}}{dt} = \dot{m}_{vent} \left(\omega_{out} - \omega_{in}\right) + \dot{m}_{wg} \pm \dot{m}_{vap}, \tag{2.18}$$

where Ω_{in} is the indoor dry air mass; $\dot{m}_{vent}$ is the air ventilation mass flow rate; ω_{out} and ω_{in} are the external and indoor air specific humidity, respectively; $\dot{m}_{wg}$ is the inlet water vapor mass flow rate to the thermal zone (e.g. due to occupants); $\dot{m}_{vap}$ is the water vapor mass flow rate delivered to (or removed from) the indoor space for maintaining a desired humidity set point. Notice that $\dot{m}_{vap}$ is equal to $\dot{Q}^{lat}_{HVAC} / \Delta h_{vs}$, where Δh_{vs} is the water latent evaporation heat at 0°C and $\dot{Q}^{lat}_{HVAC}$ is the latent heat supplied to, or removed from, the building space. As in the case of the computation of $\dot{Q}_{HVAC}$ in Section 2.2.4, also water vapor mass flow rate is computed in feedback according to the adaptive algorithm presented in Chapter 4.

2.2.6 *Modelling the effect of phase change materials*

In the conduction model presented in Section 2.2.1 it has been assumed that the specific heat of each capacitive node is constant. This hypothesis is not valid anymore when advanced Phase Change Material (PCM) are supposed to be integrated into the building envelope [26, 27]. Specifically, the thermal behaviour of PCM layers can be described by adopting an equivalent heat capacity whose value changes on the basis of the temperature layer including the PCM. More in detail, such a value rapidly increases in a specific temperature range reaching its maximum at the melting point temperature. This modeling approach allows to take into account the latent heat as an increased form of sensible heat in the transition phase, according to the effective heat capacity formulation approach [88, 89]. As shown in [88], this assumption has the main advantage of simplifying the mathematical representation of the phase-change heat transfer mechanism which can be studied as a single-phase non-linear conduction problem.

Hence, according to the technical literature, in the developed model, the behaviour of PCM undergoing phase change is taken into account in equation (2.1) by adopting a temperature dependent thermal capacitance for those nodes of building elements related to PCM layers ($C_{m,n} = C_{m,n}\left(T_{m,n}\right)$). In each modelled material layer, this parameter is considered as constant only in case of a single phase. In all the other cases, the specific heat of PCMs is assumed to be variable with the occurring temperature ($C_{m,n_{PCM}}\left(T_{m,n_{PCM}}\right)$), that influences the state of aggregation of the PCM layer (liquid state, solid state or undergoing the phase change). The above mentioned apparent PCM heat capacity fits a Gaussian shaped curve [88], where the maximum corresponds to the peak melting temperature as:

$$C_{m,n_{PCM}}\left(T_{m,n_{PCM}}\right) = M_{m,n_{PCM}}\, a \cdot e^{-\left(\frac{T-b}{c}\right)^2}, \tag{2.19}$$

where $M_{m,n_{PCM}}$ is the mass of the PCM layer, *a* is the maximum increment of the PCM specific heat due to the latent heat (height of the curve peak), *b* is the average temperature of the phase change for melting and solidification (which determines the curve peak position) and *c* is the range of the phase change (curve width). In the building simulation code, a database of materials properties is also included. Note that specific heat capacity, density and conductivity of such composite materials are dynamically assessed by manufacturers [90]. As a result, also PCM embedded in traditional building materials matrixes (gypsum, concrete, etc.) can be modelled and simulated. It is worth noting that in (2.19) the different parameters must be set in order to

take into account the different profiles of the equivalent heat capacity during the melting and solidification processes (a hysteresis phenomenon is typical for paraffin materials).

2.3 **Description of the numerical implementation of the building model**

The implementation in DETECt of the dynamical model of buildings described in Section 2.2 as well as the simulator logic are briefly described in this section for the sake of completeness. Figure 2.3 shows the software architecture and its kernel (light blue block) that summarizes the calculation procedure carried out through DETECt. The latter includes the heat conduction through building elements and the most important occurring phenomena, such as solar heat gains through windows, infrared heat exchanges, internal gains and ventilation. The input data taken into account in the simulation code are: hourly weather data (temperature, humidity, global and direct normal radiation), occupancy loads and schedules, ventilation flow rate, temperature set points, building size and orientation, thermal features of the building elements (conductivity, density, specific heat, absorption and emission coefficients, etc.). On the other hand, the DETECt output data can be selected according to the specific needs of the user. For instance, in addition to heating and cooling loads and yearly requirements, relevant time histories for building design can be obtained. These include the dynamic trends of temperatures (indoor air and building elements surfaces and layers), energy demands expressed as latent and sensible thermal loads, as well as spatial temperature gradients into walls. In addition, in the latest DETECt release, some comfort indexes widely adopted in the scientific literature has been included. Thus, in order to analyze the thermohygrometric comfort in each building thermal zone, the numerical code allows to calculate the following indexes:

- PMV (Predicted Mean Vote), i.e., the comfort perception of a large population of people exposed to a certain environment. It establishes a thermal strain based on steady-state heat transfer between the body and the environment assigning a comfort vote to that amount of strain;
- PPD (Predicted Percentage of Dissatisfied). It represents the predicted percentage of dissatisfied people at each PMV. As PMV changes away from zero in either the positive or negative direction, PPD increases.
- The mean radiant temperature of the indoor building space.

Additional details about the PMV and PPD are reported in [91, 92].

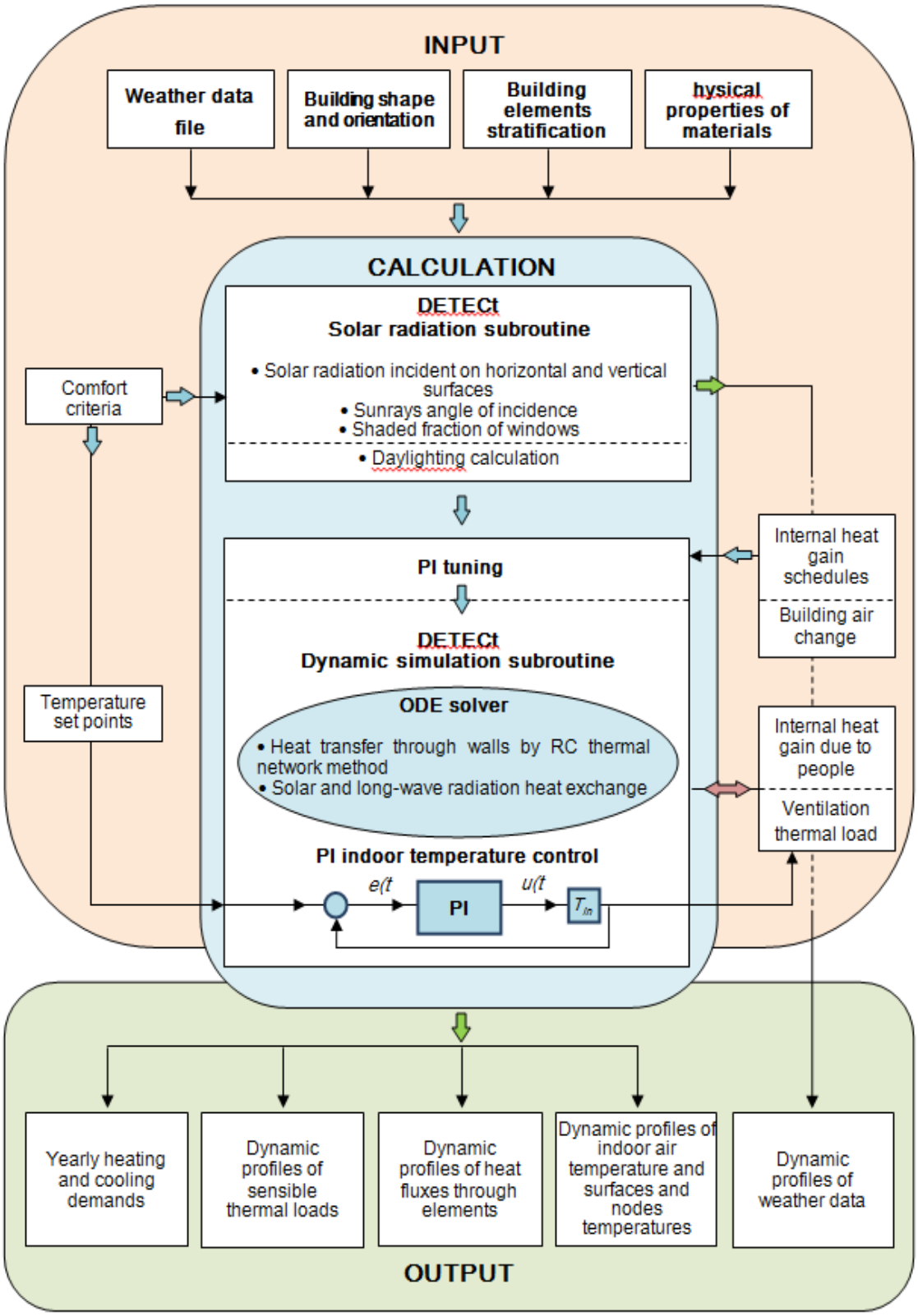

Figure 2.3. Input/Output schematization and fundamental modules of DETECt.

We explicitly point out that, through DETECt, in order to determine the effect of transparent elements on the space heating and cooling requirements, as well as to obtain the desired thermal transmittance, different and complex glasses can be simulated. In particular, by the presented model coated to tinted single or multi glazed windows filled by different gases can be selected, but in each wall only one window of rectangular shape can be modelled for sake of simplicity. For all the considered glazing systems, uniformly distributed absorption factors are considered. In addition, we note that, in the first versions of the presented code only constant normal incidence Solar Heat Gain Coefficients, SHGC, were implemented. Nevertheless, since the normal incident solar radiation is a very rare occurrence in dynamic buildings simulations, radiative properties of glazing systems must vary with the angle of solar incidence. For these reasons, optic features as well as solar radiation absorption, reflection and visible and solar transmission coefficients are calculated in the latest version of the code as a function of radiation incidence angle varying in function of the weather data file [84]. In particular, the equivalent solar transmission coefficient depends on the transmittance for direct radiation, which, for ordinary glasses, can be calculated by a fifth order polynomial expression, function of the solar incident angle [93]. Note that, the glass solar transmittance coefficient can be also calculated by interpolation of constant values imposed by the user. In the presented code the diffuse radiation entering through windows and the radiation transmittance coefficients are assumed as isotropic and hemispherical, respectively.

In order to modulate the solar heat gain, with the aim to increase and decrease the related effect during winter and summer, respectively, windows external solar shadings, overhangs and fins can be taken into account.

Before solving the model describing the buildings dynamics numerically (see Sections 2.2.1, 2.2.4 and 2.2.5), fundamental quantities are precomputed on the basis of the input data. For instance, at the beginning of the simulation the view factor matrix and the Gebhart's matrix in (2.6) and (2.12), respectively, are precomputed. When the Dynamic simulation subroutine starts, the simulation time domain is split in a large number of discretized time steps. The numerical integration of the set of differential equations presented in Sections 2.2.1, 2.2.4 and 2.2.5 is carried out simultaneously and iteratively as variable step size numerical schemes are adopted. Obviously, the maximum step size has to be selected with regard to the requested simulation fidelity and calculation efficiency. Indeed, the smaller the maximum step-size, the higher the accuracy of the resulting output data, but the higher the simulation time.

Analogously, the higher the number of thermal network nodes introduced in Section 2.2.1, the higher the accuracy of the resulting output data, but the higher the simulation time. Hence, for the routine for solving all the differential equations connected to the building model, thermal network nodes and maximum step-size (or maximum sample time) are set as trade-off between the desired calculation accuracy and simulation time [94]. Typically, in such kind of calculation procedures, a maximum sub-layer thickness of 1 cm and a maximum sample time of about 300 s are taken into account [58].

Note that, thanks to the efficiency of numerical integration methods as well as to the nowadays powerful computational systems and tools, long standing finite difference methods can be employed for the solution of such set of Ordinary Differential Equations (ODE). In the presented code, such equations are solved by a suitable tool, such as a built-in ODE solver included in MatLab, which employs variable step size Runge-Kutta and trapezoidal rule integration methods [95]. In each interval of integration the error of time discretization lies within a given range of tolerance, while the convergence criteria need to be satisfied within the maximum time step also defined.

It is important to point out that, during the simulation, not only the differential equations describing the plant dynamics are integrated, but also those of the control systems are solved at the same time. These dynamical systems must be introduced in the code to tame the dynamics of the indoor temperature and indoor relative humidity on the basis of some control objectives. In other words, they are used to impose either preassigned profiles or some given set points to the fundamental thermohygrometric variables, therefore allowing a precise calculation of the required sensible and latent heat to get some thermohygrometric working condition. Indeed, those dynamical systems decide online the amount of sensible and latent heat that must be either provided to or subtracted from the indoor node to achieve the required operating condition. To this aim, these systems compute their outputs, i.e., the control actions, not only as functions of the temperature and relative humidity references, but also by exploiting in feedback the current indoor air proprieties.

In the first releases of DETECt [9], only the indoor air temperature were controlled in feedback by means of a Proportional Integral (PI) strategy [96], schematized as the PI block in Figure 2.3, while a simple calculation of the latent heat were carried out for assessing the latent energy that has to be added to or subtracted from the examined thermal zone to keep the require specific humidity and a given value. This calculation procedure were based by solving in each simulation time step, τ, the space moisture balance. In particular, for each time step, the latent

energy calculation is based on the following logic. If the indoor air relative humidity is higher (lower) than the selected set point then the latent energy must be removed from (added to) the space. Consequently, the latent heat required in (2.18) is computed as $\dot{Q}_{HVAC}^{lat} = \Delta h_{vs}\Omega_{in}\left(\omega_{in}(t) - \omega_{sp}(t)\right)$ with being the required set point specific humidity. Additional details about this procedure can be found in [9].

As the thesis is devoted to improve the management of the sensible and latent heat, in the following subsection details about the pre-existing feedback control algorithm embedded in DETECt are given for the sake of completeness .

2.3.1 *Pre-existing controllers for the computation of sensible and latent heats*

In the first version of the DETECt code, the sensible heat supplied to, or removed from, the building space by an ideal HVAC system in order to maintain the indoor air at the desired set point temperature is computed according to a Proportional Integral (PI) control strategy [18]. This controllers are driven by the error signal *e(t)* (see also Figure 2.3) that in the case of temperature control represents the deviation between the indoor air temperature and the set point one, T_{sp}. Thus, in order to track the set point temperature, the sensible load to be supplied (heating mode) to or to be removed (cooling mode) from the thermal zone is function of the output control signal *u(t)*, which range from 0 to 100% [97]. Here, 0 corresponds to the HVAC system stand-by while 100% is proportional to the peak representing the design heating and cooling load of the space.

According with the PI strategy the sensible heat is computed in feedback as

$$u(t) = K_p \cdot e(t) + K_i \cdot \int_0^t e(t)dt, \qquad e(t) = (T_{sp} - T_{in}) \tag{2.20}$$

where K_p and K_i are the control gains, i.e., the proportional and integral gain, respectively. Such error is weighted on the basis of such proportional and integral gains, which vary in function of the heating or cooling HVAC mode. To simplify the tuning of the controller, the proportional gain is assumed as the ratio of the maximum controlled system output ($\dot{Q}_{HVAC}$ peak) to the throttling range ($\left|\min(T_{in}) - T_{sp}\right|$ and $\left|\max(T_{in}) - T_{sp}\right|$, for heating and cooling modes, respectively) [97]. The maximum and the minimum values of T_{in} can be considered equal to the relative outdoor air temperature or calculated by a free floating simulation (HVAC always turned off). The integral gain, added to the controller with the aim to eliminate the offset caused by the

proportional gain, is tuned by assuming a time scale (K_p / K_i) equal to the simulation time step. Notice that these gains are decided offline and kept constant during the simulations.

As any control strategy with fixed control gains, PI approach presents mainly two drawbacks: *i)* there is no guarantee that that selected control gains provide satisfactory performance, i.e., a satisfactory tracking of the reference temperature; and *ii)* the overall control system can be not robust with respect to external disturbances, parameter variation and unmodelled dynamics. It is interesting to note that all these uncertainties can affect building dynamics and consequently building performance in terms of energy consumption as well as thermohygrometric comfort of the occupants. For instance, and just to name a few, external temperature, ground temperature and solar radiation, i.e., whether conditions, act on the temperature dynamics as disturbances. Moreover, control strategies with fixed gains have to be retuned for the specific building on the basis of its parameters and actual weather conditions to get excellent taking performance of the reference thermohygrometric profiles. This can be a challenging task that can increase the design time of innovative buildings. To reduce this time it would be more convenient to assume during the design stage nominal building parameters and simplified models, but in this case the controller has to be robust to unavoidable parameter uncertainties and unmodelled dynamics. As additional drawback, in general PI control actions do not allow to include any optimality in terms of thermohygrometic comfort and energy consumption and phenomena like windup can jeopardize their performance. Those disadvantages will be tackled in the thesis systematically by proposing different feedback control strategies ranging from PI with optimal tuning of the control gains to model predictive algorithms and model reference adaptive control strategies.

2.4 **Discussion**

In this chapter, the mathematical model of building dynamics implemented in DETECt been briefly presented to give to the reader details about the BEPS code where both the optimal adaptive strategies for the computation of sensible and latent heat and algorithms for building model reduction (which are required, for example, by the application of model predictive controllers) have been implemented.

Hence, the aim of this chapter was also to present the features that will be used in the next chapters and the code architecture. Precisely, through DETECt the dynamic building behavior can be analyzed in case of different weather locations, envelope materials, building shape and orientation, as well as geometry. The outputs of this software include: sensible and latent heat demands for the whole year or for selected shorter periods, heating and cooling loads, operating

temperature and humidity of indoor air, building elements surfaces and nodes (modelled by a thermal network into each considered building element). In addition, dynamic profiles of building temperatures and heat fluxes are provided. The effectiveness of the model predictions have been shown in [9], where DETECt results have been proven to pass the BESTEST procedure and to be comparable to those provided by available commercial BEPS codes in large variety of working conditions. Obviously, as an in-house code, DETECt allows enhancements also depending on the research need. Hence, the control and model reduction approaches proposed in the rest of the thesis improve the available code as they have become additional routines of the latest DETECt release.

Chapter 3
PRELIMINARY ENHANCEMENTS TO BUILDINGS CONTROL

In this chapter we present the control architecture used to host the model reference adaptive control algorithm for the computation of the required sensible heat and water vapor mass flow rate. This architecture is basically composed by a couple of feedback controllers, a supervisor as well as air indoor temperature and relative humidity trajectory planner. In particular, the supervisory machine decides the activation/deactivation of the control algorithms on the basis of some feedback measurements and a given scheduled region on the psychometric chart where no sensible and latent heats have to be provided to the thermal zones, for example, because a satisfactory comfort level is there assured without any additional action.

As possible application of the control scheme, the chapter focus then on a methodology for selecting optimally, in accordance to a cost function which weighs both comfort and energy saving, the control gains of a PI control algorithm for the computation of the sensible heat to be provided by HVAC systems for the temperature control. Notice that, this represents also the first attempt in this work to seek for optimal control solutions for the control of thermohygrometric variables by means of control algorithms with fixed gains and it is presented in Section 3.3. To prove its effectiveness different case studies have been considered. Nevertheless, in the last section (Section 3.5) we stress the issues connected to this solution which motivates the need of adaptive strategies which are developed and implemented in the next chapters.

Material of this chapter has been published in [33, 98]. Precisely, the supervisory machine has been presented in [33] while the tuning method for temperature controllers with fixed gains has been published in [98].

3.1 **Architecture for the thermohygrometric control in buildings**

The control architecture used throughout the thesis for computing dynamically the amount of

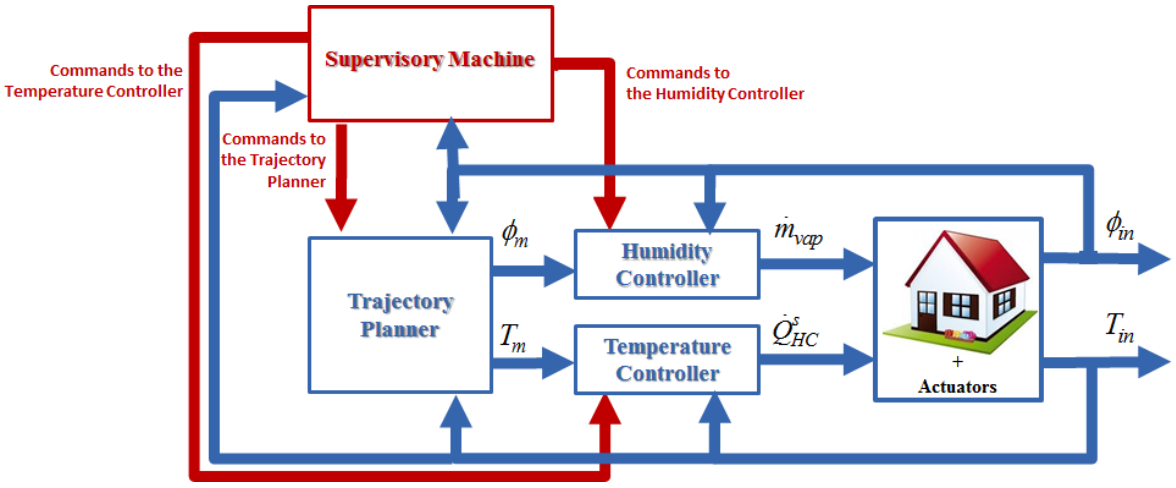

Figure 3.1. Schematics of the control architecture for the thermohygrometric variables.

sensible and latent heats to provide to or to remove form the thermal zone to get a suitable thermohygrometric condition is depicted in Figure 3.1. This architecture is based on three main blocks, i.e., *Feedback Controllers*, *Supervisor* and *Trajectory Planner*. Briefly, in the Trajectory Planner block are implemented strategies for the computation of paths on the psychometric chart from the point describing the initial state of the thermal zone at the beginning of the control horizon to a final point corresponding to the required set-point working condition. More in detail, defining t_0 as the initial time instant of the interest for the control of the thermal zone, and (T_{sp},ϕ_{sp}) the required set-points of temperature and relative humidity of the indoor air, respectively, the Trajectory Planner block computes its output, say $(T_m(t),\phi_m(t))$, so that $(T_m(t_0),\phi_m(t_0)) = (T_{in}(t_0),\phi_{in}(t_0))$ and $T_m(t) \rightarrow T_{sp}$, and $\phi_m(t) \rightarrow \phi_{sp}$, with $(T_{in}(t_0),\phi_{in}(t_0))$ being the current indoor air temperature and relative humidity at the time t_0 which are provided in feedback to this block. Notice that, different algorithms available in the literature can be implemented in the Trajectory Planner Block (see for example [99]). Nevertheless, in the thesis its outputs are chosen according to the procedure shown in Chapter 4, i.e., they are the outputs of an optimal reference model.

The required indoor temperature and relative humidity profiles are then imposed to the thermal zone by exploiting feedback control strategies implemented in the blocks *Temperature Controller* and *Humidity Controller* shown in Figure 3.1. These blocks compute dynamically, in accordance with the control algorithms which are actually implemented, the required sensible heat and the water vapor mass to add or subtract to the indoor zone in accordance with a decoupled approach.

We point out that the decupled approach to control temperature and humidity has used in the technical literature as a mean to improve energy saving in buildings [100] and it can be implemented via air conditioning systems which will be used for buildings of the next future [101].

Finally, the online activation/deactivation of both controllers and Trajectory Planner are orchestrated by the *Supervisory Machine* to reduce energy consumption when the thermohygrometric control is not required, allowing as a consequence the free-floating evolution of the indoor temperature and humidity. Basically there are two notable cases when the controllers have to be switched off. The first case is when buildings are operated according to the "intermittent running regime" [102, 103]. Here, for some hours, often nighttime, the control system is switched off because there are not occupants who demand thermal comfort, e.g., museums, malls, offices etc. The second reason for turning off the control algorithms is when the external/internal loads (outdoor temperature, radiation, etc…) can preserve the thermohygrometric comfort without any additional heating/cooling or humidification/dehumidification, i.e., when the external inputs are so that the indoor temperature and indoor relative humidity evolve within a preassigned comfort zone (as those presented in [104]). Notice that, the former case, activations/deactivations of controllers introduce time based switches in the overall scheme in Figure 3.1 [105], while the second case induces state based switches as activations and deactivations are functions of the thermohygrometic variables, i.e., indoor temperature and relative humidity, which define the working condition of the thermal zone. As for buildings operated according to intermittent running regime the time based commutations occur at a slow rate (several hours), it is reasonable to assume that they do not alter the performance of the underlying feedback temperature/humidity controllers [105]. On the other hand, the switching rate of state based commutations can become unbounded, i.e., the so called Zeno solutions [106]. As a consequence high frequency components will be induced in the control outputs, i.e., chattering phenomena on the control actions [107], which can be either not implementable by the underlying actuators or damage them [108]. For this reason, a particular care has been dedicated to the design of the Supervisor as an automaton [109] which will be illustrated in detail in the chapter.

3.2 **Supervising System and its modelling**

The supervisory system in Figure 3.1 is used to decide the activation/deactivation of the temperature and humidity controllers. To this aim each controller is switched on/off on the basis

of the evolution of an event driven automaton. As these systems have the same structure, in what follows we describe for the sake of brevity only that for the management of the temperature control. By denoting $t_{on}, t_{off} \in [0,24]$ as the time instants delimiting the time interval where occupants required thermohygrometric comfort, e.g., the working hours in the case of buildings for office use, and with T_l and T_u the lower and upper bounds for the indoor air temperature allowed for ensuring comfort, then the aim of the Supervisor is: *i)* to activate the temperature controller only when $T_{in} \notin (T_l, T_u)$ and $t_h \in [t_{in}, t_{off}]$ (with $t_h \in [0, 24]$ being the time *t* expressed as in the 24-hour clock system [110]), *ii)* to avoid numerical chattering (i.e., activation/deactivation of the underlying controller with infinite, or very high frequency [107]), and *iii)* to detect when the controller can be shut down without compromising comfort. To achieve these aims, an ad-doc finite state machine [111], which evolve on the basis of some events, has been designed and implemented.

The automaton describing the states and the transitions composing the Supervisor for the temperature controller is shown Figure 3.2a. For its description, we denote in what follows $e_T(t) = T_{sp} - T_{in}(t)$, with T_{sp} being either T_u (when $T_{in}(t_{on}) > T_u$) or T_l (when $T_{in}(t_{on}) < T_l$), and ε_T is a positive small threshold which is set to 0.05 in the code. The states of the system are *"Initialization"*, *"Tracking"*, *"Free Evolution" "Heating"* and "*Cooling"*. Specifically, *i)* the system is in the state *"Initialization"* when $t_h \notin (t_{on}, t_{off})$, i.e., for the time range which is not of interested for the control, e.g., nighttime; *ii)* in the state *"Tracking"* the underlying temperature contoller is active and the profile generated by the Trajectory Planner block (see Figure 3.1) is imposed to the indoor temperature; *iii)* the automaton is in *"Free Evolution"* , when the internal loads and disturbances, as external temperature, are so that the indoor air temperature dynamics are in the preassigned range of variation, i.e., $T_{in} \in (T_l, T_u)$, the controller is then switched off for reducing consumption*; iv)* in the state *"Heating"* the controller is active to keep the indoor temperature to T_l when the external disturbances tend to reduce it (for example in cold seasons), analogously *v)* in the state "*Cooling"* the controller is active to keep the indoor air temperature to T_u when the external disturbances tend to increase it (for example in summer seasons).

Briefly, independently on the actual state of the machine, if $t_h \in (t_{off}, 24) \cup (0, t_{on})$ then the next automaton state is "Initialization" till $t_h \geq t_{on}$ on the next day. When such event occurs, the next state can be either "Free Evolution" or "Tracking" on the basis of the actual indoor air temperature. In the case T_{in} is outside the required range, a reference trajectory is computed by

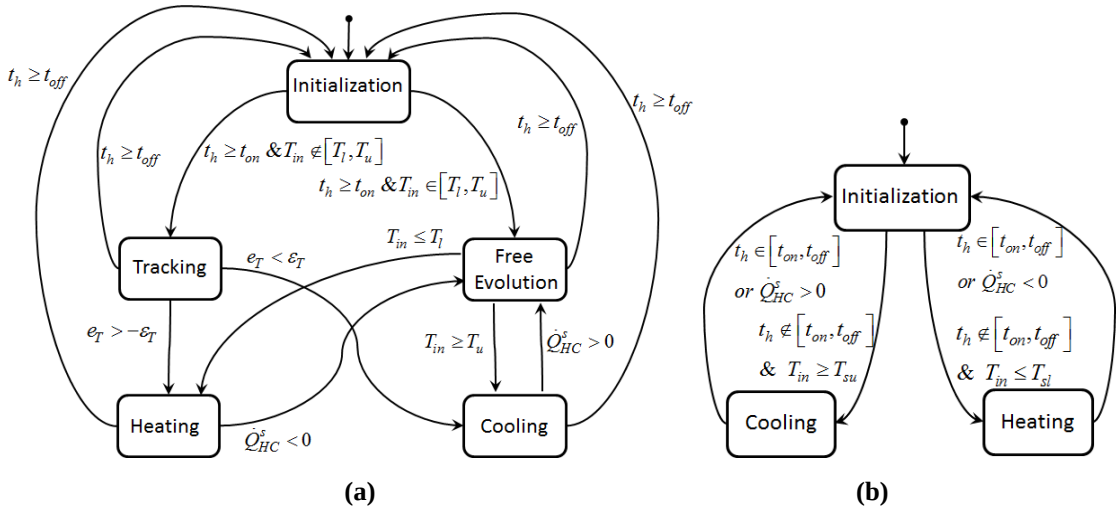

Figure 3.2. Automaton for the management of the activation/deactivation of the temperature controller for intermittent running building a) for $t_h \in [t_{on}, t_{off}]$, and b) $t_h \notin [t_{on}, t_{off}]$.

the Trajectory Planner and become the reference input to the underlying control temperature algorithm. Notice that, during the transition from "Initialization" to "Tracking", the reference trajectory is initialized with the actual indoor air temperature, and in the case $T_{in}(t_{on}) > T_u$, the resulting required temperature profile, T_m in Figure 3.1, is so that $T_m(t) \geq T_u$, $T_m(\infty) = T_u$, and T_{sp} is set equal to T_u. Analogously, if $T_{in}(t_{on}) < T_l$, then $T_m(t) \leq T_l$, $T_m(\infty) = T_l$, and T_{sp} .is set equal to T_l. Assuming, without loss of generality that, $T_{in}(t_{on}) > T_u$ and $T_{in}(t) \approx T_m(t)$ (as the underlying temperature controller is active), then $e_T(t)$ in the state "Tracking" is always positive and the switching to the next state occurs when this error becomes smaller than ε_T. As the initial indoor temperature was assumed to be above T_u, then a negative sensible load $\dot{Q}^s_{HC} < 0$ has been required during tracking, therefore to preserve continuity of the control variable the next scheduled state is "Cooling". In this state, the sign of the control action changes when the internal loads and external disturbances can drive the indoor air temperature in the acceptable range of variation, i.e., $T_{in} \in (T_l, T_u)$. Hence, if this case occurs, the next state of the automaton is "Free Evolution" where the temperature controller is switched off. The supervisory machine will remain in this state as far as the indoor temperature does not cross either T_u or T_l. Of course if $T_{in} \geq T_u$ a negative control action is required to keep $T_{in} = T_u$, therefore the state "Cooling" is restored. Instead, if $T_{in} \leq T_l$, a positive control action to regulate $T_{in} = T_l$ is provided after the automaton state is set to "Heating". We note that the automaton for the supervisory control of the relative humidity is similar to that in Figure 3.2a and it is not reported here for the sake of brevity. Indeed, it can be obtained substituting the indoor air relative humidity, say ϕ_{in}, to T_{in},

$\dot{m}_{vap}$ to $\dot{Q}^{s}_{HC}$, ϕ_u and ϕ_l to T_u and T_l, respective, with ϕ_u and ϕ_l being the lower and the upper bounds which delimit the acceptable range of variation of the relative indoor air humidity, while e_T is replaced with $e_\phi(t) = \phi_{sp} - \phi_{in}(t)$ where ϕ_{sp} is the relative humidity set point and ε_T is substituted with ε_ϕ. Finally the states Heating and Cooling are replace with "Humidification" and "Dehumidification", respectively.

We explicitly note that, by setting properly the parameters of the automaton in Figure 3.2a, different working conditions can be achieved. For example, to get a continuous running configuration, the user must set $t_{on} = 0$ and $t_{off} = 24$, while to keep the temperature to a given value, i.e., avoiding possible free-floating, it is enough to set $T_u = T_l = T_{sp}$, with T_{sp} being the required temperature.

In the case the building is designed to work in intermittent running regime, it is possible to use an additional automaton, which works in parallel to that depicted in Figure 3.2a, so that the temperature controller is restored in the loop also for $t_h \in (0, t_{on}) \cup (t_{off}, 24)$ providing that the indoor air temperature exceeds some boundaries. In so doing, it is possible to implement setback strategies to achieve additional energy saving [112]. Figure 3.2b shows such an automaton when this option is selected. In this case, when $t_h \notin [t_{on}, t_{off}]$, it is still possible that the temperature controller is switched on. Indeed, the finite state machine switches to the state "Heating", activating therefore the Temperature Controller block in Figure 3.1, in the case the indoor air temperature goes below the temperature T_{sl}. Analogously, the underlying temperature controller is activated also if the indoor temperature goes over the temperature T_{su} as the automaton switches to the state "Cooling". Notice that, T_{sl} and T_{su} are the parameters of the automaton in Figure 3.2b which need to be tuned in accordance with the specific use of the thermal zone.

We clearly point out that both the automatons in Figure 3.2 can be recast as flowcharts. For instance the finite state machine in Figure 3.2a can be described via the flowchart in Figure 3.3. When this formalism is adopted, the state of the supervisor is modelled as a flowchart variable named *State*, which can assume at any time instant $t \in \left[t_{init}, t_{end}\right]$, with t_{init} and t_{end} the time instate that delimit the beginning and the end of the control horizon, respectively, one of the values in the following finite set $\left\{\textit{Initialization}, \textit{Tracking}, \textit{Free Floating}, \textit{Heating}, \textit{Cooling}\right\}$. Notice that in Figure 3.3, Δt represents the simulation time step.

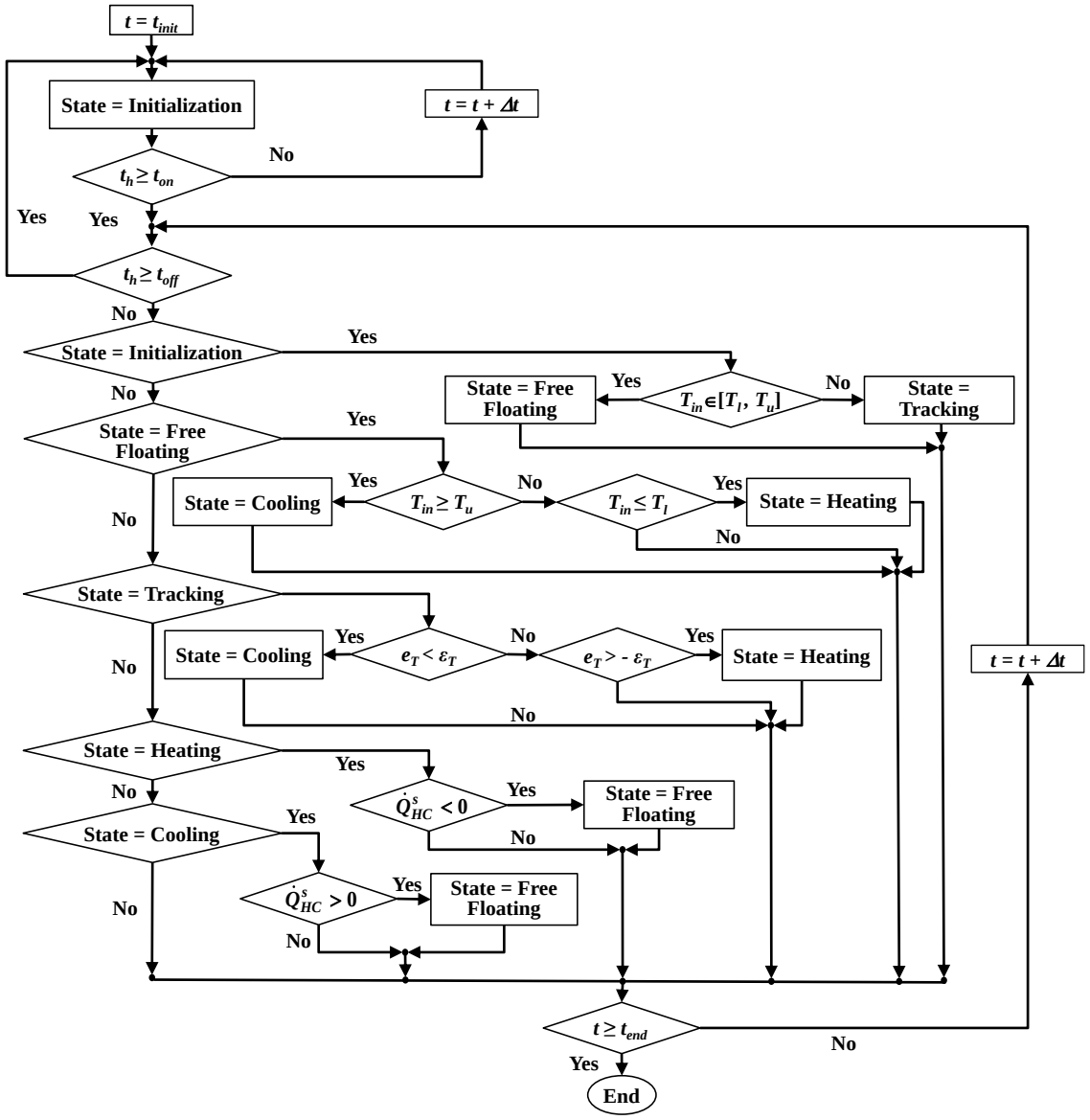

Figure 3.3. Flowchart describing the Supervisory machine in Figure 3.1a for activation/deactivation of the temperature controller.

Finally, we point out that the set of automatons described above have been implemented in SimuLink/Stateflow [95] and included in the latest version of DETECt.

3.3 **Optimal tuned PI strategy**

Nowadays, building automation and control systems play a remarkable role in order to achieve building energy efficiency and thermal comfort [6, 15]. In this regard, the feasibility of control schemes based on different techniques and their effectiveness for improving the accuracy of building energy performance simulation models have been recently analysed [15]. Nevertheless, such techniques can provide different results depending on the accuracy and

robustness of the adopted control solutions and building simulation approaches [15, 113]. With respect to control it is worth to be noted here that, although in the technical literature advanced control solutions have been recently proposed (see for example those based on model predictive control schemes [114] or artificial intelligence tools, such as, for example, learning methods [15]), fixed gains control algorithms, such as PI and PID controllers, are still widely used. These methods have the great advantage of being easy to be designed and to be implemented [115], but they require an appropriate tuning of control gains to be effective.

Automatic and well assessed methods for the tuning of PI/PID control parameters are today available in order to reduce the time required by the tuning phase [116]. Nevertheless, often these methods do not provide any optimality of the solution, which is essential, for example, in the context of indoor air temperature control. To overcome this limit, we propose a novel procedure for the optimal and automatic tuning of the PI gains. The approach is based on a purposely designed cost function to be minimized so to optimize the control gains over a finite control horizon. The adopted cost function weights both the temperature tracking error and the sensible thermal energy required to impose the demanded set-point. Due to the complexity of the building model, the resulting parameter optimization problem cannot be solved analytically. Hence, an iterative numerical procedure for its solution is also designed.

The optimized control algorithm has been embedded in the control architecture in Figure 3.1 for temperature control (Temperature Controller Block).

The control approach has been simulated in DETECt. As described in Chapter 2, this tool is able to analyse the building thermal behaviour and to assess the benefits of different and advanced building envelope techniques, solar gain controls and daylighting solutions in case of different weather locations, envelope materials, building shapes, orientations and geometries. In addition, temperatures dynamic profiles and time-variant spatial trends can be obtained. We note that, in the first release of DETECt, presented in [9] and in Section 2.3.1, the PI gains were selected by using an heuristic scheduling method [117]. Hence, the method here proposed can be seen as an alternative approach for a systematic tuning of the pre-existing controller.

3.3.1 *Procedure for the Optimal tuning of PI control parameters*

Given the tuple (A,B,C), with $A \in R^{n \times n}$, $B \in R^{n}$ and $C \in R^{1 \times n}$ we define the following system

$$\begin{cases} \dot{x} = Ax + Bu + F(x,t) \\ y = Cx \end{cases} \tag{3.1}$$

where $x \in R^n$ is the state vector, $u, y \in R$ are the system input and output, respectively, and $F(x,t) \in R^n$ is a vector function embedding all the time varying and nonlinear terms acting on the system dynamics. In what follows we assume system (3.1) to be controlled via a PI algorithm, hence

$$u(t) = K_p e(t) + K_I \int_{t_0}^{t} e(\tau) d\tau, \tag{3.2}$$

where $e(t) = r(t) - y(t)$ is the tracking error between the system output *y(t)* and a prefixed time-varying reference trajectory $r(t)$; K_P and K_I are control gains to be opportunely tuned; t_0 is the initial time instant.

As usual, closed-loop dynamics strongly depend on the specific choice of the control gains. Indeed a wrong selection of these parameters may jeopardize the system performance, leading to instability in some critical cases. Moreover, the tuning procedures, based on heuristic methods, may result to be time-consuming or not effective. To solve this problem, different experimental or model based methodologies have been proposed in the control literature for the appropriate gains tuning with the aim of guaranteeing stability and robustness (see for example [116], [118] and references therein for a complete overview of standard and innovative PI tuning procedures). Here we propose a different approach based on a purposely designed cost function to be minimized so to optimize the control gains. Specifically, consider a positive function, say $J(K_P, K_I)$, so that:

- $J(K_P, K_I)$ assumes finite values for stable solutions of system (3.1) under the control action (3.2);
- smaller values of $J(K_P, K_I)$ corresponds somehow to a better tracking of the reference trajectory;

the control gains are then set as $K_P = K_P^*$ and $K_I = K_I^*$ so that

$$J\left(K_P^*, K_I^*\right) = \min_{(K_p, K_I)} \left\{ J\left(K_p, K_I\right) \right\}. \tag{3.3}$$

According to this approach, different choices of $J(K_P, K_I)$ can be made in order to derive the PI gains according to (3.3). Here, we consider the following quadratic function measuring both mean squared tracking error and control effort over a finite control horizon as

$$J\left(K_p, K_I\right) = \int_{t_0}^{t_0+\Delta} \left[qe^2(\tau; K_p, K_I) + hu^2(\tau; K_p, K_I) \right] d\tau, \tag{3.4}$$

with q and h being positive constants that weigh the terms in the integral (3.4), and Δ the finite time interval that is of interest in the control problem (control horizon). Notice that the optimization problem discussed here is different from the one usually considered in optimal control theory where the controller structure is not a priori fixed [23]. Here instead the structure of the controller is fixed to the PI structure (3.2) and the aim is the parameters optimization.

Moreover, differently from the classical linear quadratic optimal control [23], here numerical methods are exploited to solve the parameter optimization problem in (3.4) that cannot be solved in closed form due to its complexity. The iterative procedure proposed to numerically solve the optimization problem is shown in Figure 3.4. This procedure is implemented by the following tools: *(i)* an optimization toolbox *(Optimizer)*, which decides the parameters $(K_P^{(i)}, K_I^{(i)})$ for the *i-th* interaction; *(ii)* a detailed simulator of the controlled system, i.e., system (3.1) under the control action (3.2). (Note that the *Simulation-Code* block in Figure 3.4 provides the data necessary to compute the function J); *(iii)* the *Compute-J* subsystem which allows the computation of the J-function at each interaction.

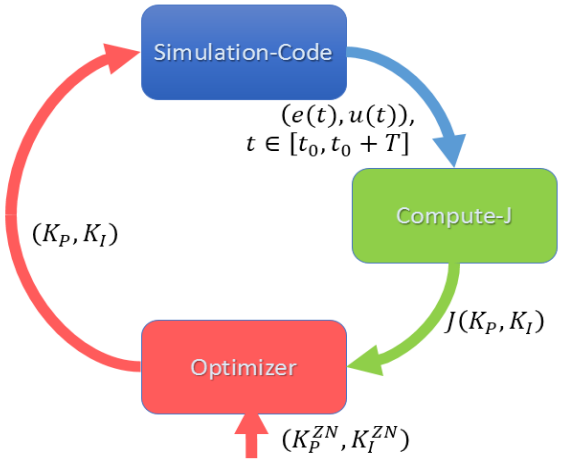

Figure 3.4. Iterative procedure adopted to numerically solve the optimization problem (3.4).

We remark that, as the optimization problem is numerically solved by an iterative procedure, the initial condition plays a fundamental role for the rate of convergence [119]. Moreover, initial conditions have to guarantee the stability of the controlled system at the very first interaction. Note that the stability at the generic *i*-th interaction (*i >1)*, is instead ensured by the Optimizer itself, since unstable solutions lead to high values of J in (3.4), and therefore they are automatically excluded. For these reasons, the optimization procedure is initialized by selecting the PI gains with the closed-loop Ziegler and Nichols method [116] (denoted as K_P^{ZN}, K_I^{ZN} in Figure 3.4). Furthermore, optimization toolboxes are available in most of the numerical software

packages (as, for example, MatLab, Maples, etc.), so the minimization problem of the equation (3.3) can be effectively solved. Note that, the proposed approach can be extended to the generic problem of tuning feedback control actions parameters described as:

$$\begin{cases} \dot{x}_c = f\left(x_c, e; \xi\right), \\ u = g\left(x_c, e; \xi\right), \end{cases} \tag{3.5}$$

where: x_c is the state of the controller; *f* and *g* are liner or nonlinear functions for mapping the tracking error and the state of the controller onto the state derivative and control action; while ξ is the set of the control parameters to be selected. In this case the cost function J must be a positive function of the parameter vector ξ.

In the next section, to show how to tune a PI strategy with gains optimally computed in accordance with the procedure discussed above, the effectiveness of this approach as well as its drawbacks, we illustrate in detail the design of the indoor air temperature controller block in Figure 3.1 for a set of thermal zones of different sizes and under different weather conditions. Humidity control is instead investigated in the next chapters when the model reference adaptive algorithm is introduced.

3.4 **Case Studies**

In order to show pros and cons of the proposed tuning method in Section 3.3.1 for an accurate tracking of a given indoor air temperature trajectory, which in turns allows a more accurate prediction of the heating and cooling demands in buildings, different case studies have been implemented and analysed by using DETECt [9]. More in detail, we have considered buildings of different geometry, construction materials and subjected to different weather conditions (external disturbances). In the following subsections we describe the typologies of buildings implemented in the simulation code in accordance with the model presented in Chapter 2 as well as the design of the optimized PI scheme in Section 3.3.1 for taming indoor air temperature dynamics.

3.4.1 *Description of buildings*

As case studies different buildig size, construction material as well as outdoor weather conditions are taken into account. In particular:

- we characterize the building geometry by its square meters floor area. Thus, a small size dwelling (48 m^2), a middle size office (200 m^2) and a large size mall (900 m^2) are

modelled. Some details about geometry and operating features are reported in Table 3.1;

	Building		
	Small	**Middle**	**Large**
Surface to Volume ratio (%)	1.3	0.53	0.30
Window to Wall ratio (%)	55	45	20
Air change (vol/h)	0.5	1.0	2.0
People vapour mass flow rate (g/h·p)	40	45	60

Table 3.1. Geometry features of the considered buildings.

- both light and heavy building envelopes have been considered. Table 3.2 shows the envelope stratification data for both the simulated buildings;

Building element	**Lightweight building**		**Heavyweight building**	
	Materials	**(mm)**	**Materials**	**(mm)**
wall	Plasterboard	12	Concrete block	100
	Fiberglass quilt	66	Foam insulation	61.5
	Wood siding	9.0	Wood siding	9.0
roof	Plasterboard	10	Identical to Lightweight case	
	Fiberglass quilt	111.8		
	Roof deck	19		
floor	Timber flooring	25	Concrete slab	80
	Insulation	1.003	Insulation	1.007
window	Glass	4.0	Identical to Lightweight case	
	Air	6.0		
	Glass	4.0		

Table 3.2. Envelope stratification (from inside to outside).

- input weather data (such as outdoor temperature, solar radiation, etc.) vary according to hourly profiles and are related to cold winter climates and temperate Mediterranean ones. Details on heating and cooling degree days, HDDs and CDDs respectively, of the investigated weather zones are reported in Table 3.3. Here, the annual Incident Solar Radiation (ISR) on the horizontal surface of each weather zones are also reported.

Location	**HDD (Kd)**	**CDD (Kd)**	**ISR (kWh/m^2y)**
Copenhagen	3757	77	988
Freiburg	2966	287	1470
Denver	2667	977	1662
Milan	2584	487	1114
Nice	1506	471	1562
Rome	1370	777	1430
Naples	1335	833	1825
Athens	1082	1284	1407

Table 3.3. Climatic zones, HDD and CDD indexes and ISR.

Hence, 48 case studies have been simulated and analysed, covering a wide range of operating conditions. Furthermore, we assume that the HVAC system of these buildings are intermittently operated [41], i.e. the temperature is not controlled all day long, but only in a given range of hours, defined as occupied hours.

Here we assume that the temperature must be constant to a given set-point from 08:00 to 18:00. In particular, the reference set-point is set at 20°C from the October 1st to April 30th and at 25°C from May 1st to September 30th. In addition, for each investigated case study the simulation horizon was set at one year to cover both winter and summer weather conditions (simulation starts on January 1st and ends on December 31st). Hence, the automaton in Figure 3.2a implemented in the supervisory machine in Figure 3.1 has been tuned so that $T_u = T_l = T_{sp}$, where the temperature set-point depends on the season.

3.4.2 *Design of the optimal PI algorithm for indoor air temperature*

In order to impose the required indoor air temperature set point over the daily interval of interest (from 08:00 to 18:00), a PI controller is adopted. The controller is tuned according to Section 3.3.1, by taking into account the following design options:

- for the optimization procedure presented in Section 3.3.1, we select as controlled variable, $y = T_{in}$, the indoor air temperature, and as control input, $u = \dot{Q}^s_{HC}$, the sensible load in (2.17);
- due to the rather slow dynamics of the building, the controller must be activated in advance with respect to the beginning of the occupied time slot [41]. In particular, the controller is activated at 07:00 each day;
- a smooth transition from the air temperature obtained at 07:00 to the demanded set-point required at 08:00 is imposed. This transition is guaranteed by Trajectory Planner block in Figure 3.1. Notice that in order to avoid discontinuities in the system dynamics, the output of this block is initialized to the indoor air temperature at 07:00;
- for the cost function in (3.4), we select $q = 100$ and $h = 0.1$. This imposes to the optimization procedure to search for the PI gains that allow the resulting indoor air temperature to closely match the reference trajectory;
- in order to reduce the computational time required for finding the optimal PI gains, few days have been considered in the optimization horizon, Δ in (3.4). Nevertheless, the procedure can also be applied to different days, random or not consecutive.

The numerical architecture depicted in Figure 3.4 adopted for solving the optimization problem of equation (3.3) was implemented in MatLab. In particular as *Simulation-Code*, the DETECt code [9], based on the thermal model of the building briefly described in Chapter 2, was adopted. The Optimizer block was implemented by using functions of the MatLab optimization toolbox and choosing as searching method the Interior Point algorithm [95]. The number of interactions required for solving the problem of equation (3.3) varied from 5, for the middle-size heavyweight building located in Denver, to 81, for the small-size lightweight building located in Naples.

3.4.3 *Numerical results*

We consider here the tracking performance achieved by the simulation code when the tuning strategy described in Section 3.3.1 is adopted for PI gains. In the following we analyse the time histories for the cases of heavyweight envelope buildings in a cold winter weather zone (Denver) and in a temperate climate one (Naples).

Even though the simulation time has set to one year (365 days, 8760 hours), we show in Figure 3.5a the performance of the closed-loop system only for a set of four sample days. Note that such time interval includes the change of the indoor set-point temperature (from 20 to 25°C). Here, it is clearly shown that adopting the control strategy presented in Section 3.3.1, the indoor air temperature is always controlled at the required temperature set-point (independently of the occurring: initial air temperature; building thermal inertia; weather conditions).

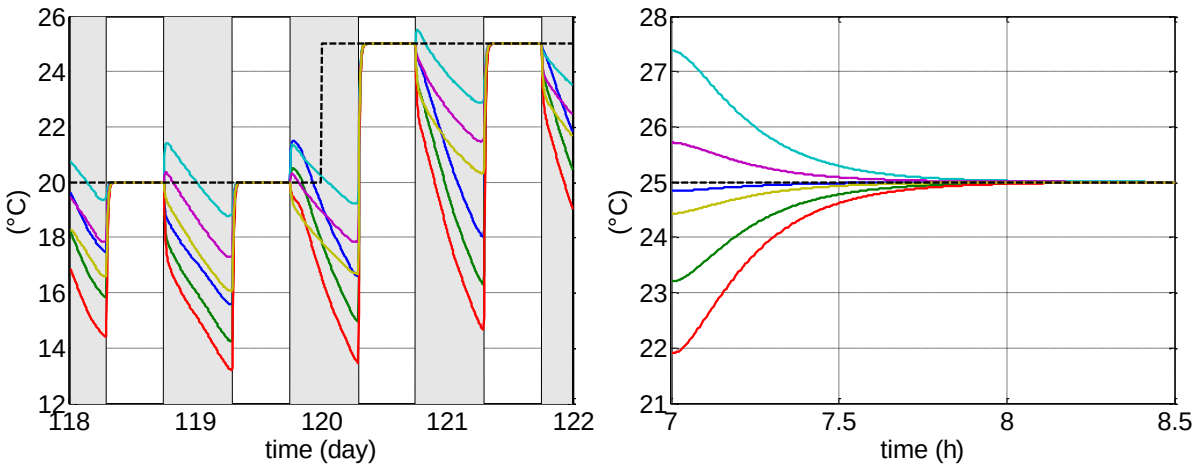

Figure 3.5. Indoor air temperature for heavyweight buildings (a) over a set of sample days (black line is referred to the temperature set-point) (b) for the 230-th day of the year. For both figures, solid lines denote for Denver: Small-size (blue), Middle-size (green), and Large-size (red), and Naples: Small-size (cyan), Middle-size (magenta), and Large-size (yellow).

Notice that, regions shaded in grey refer to hours in which the building is not occupied (switched off HVAC system, inactive control). Obviously, is such hours the indoor air temperature evolves in accordance with model (2.17) when $\dot{Q}_{HC}^{s} = 0$ (free floating indoor conditions).

We remark that, when the control system is activated the reference temperature is the output of a suitable designed second order LTI system with *(i)* an initial output equal to the indoor air temperature at 07:00; *(ii)* a settling time of one hour; *(iii)* absence of overshoots in the step response; and *(iv)* the demanded steady-state temperature for the occupied time as input. This feature is clearly shown in Figure 3.5b. Here, the time profile of the indoor air temperature subsequent to the controller activation is depicted for the 230-th day of the year.

We remark that similar tracking performance were achieved for all the investigated case studies (the remaining time histories are omitted for sake of brevity). The effectiveness of the control method to precisely impose temperature profiles can be detected also by Table 3.4.

Location	**Building**					
	Small-size		**Middle-size**		**Large-size**	
	Light	**Heavy**	**Light**	**Heavy**	**Light**	**Heavy**
Denver	0.02	0.017	0.028	0.023	0.0257	0.0254
Naples	0.018	0.018	0.027	0.022	0.035	0.0278
Rome	0.025	0.0159	0.0292	0.0243	0.037	0.031
Milan	0.019	0.016	0.0243	0.0251	0.0324	0.0294
Athens	0.02	0.0182	0.0267	0.024	0.0352	0.035
Freiburg	0.023	0.0176	0.0247	0.0271	0.038	0.032
Copenhagen	0.018	0.015	0.026	0.0293	0.041	0.029
Nice	0.019	0.018	0.0245	0.0232	0.0357	0.031

Table 3.4. Temperature mean squared error over the year (in °C).

Here, the temperature mean squared error for the entire year and for all the 48 developed case studies is reported.

Notice that for each indoor air set-point temperature imposed to the heating and cooling building simulation model, the resulted control action (i.e. the sensible load) can be exploited for obtaining the related yearly heating and cooling energy demands. Such information could be of a great interest for building designers and practitioners. In particular, Figure 3.6a and Figure 3.6b report the winter heating demand for the investigated lightweight and heavyweight buildings (dwelling, office and mall), respectively. As it is possible to observe, the amount of yearly heating demand strongly depends on the occurring Heating Degree Day (HDD): the higher the

HDD the higher the heating requirements. Furthermore, as expected, the heavier the envelope, the higher the heating demand.

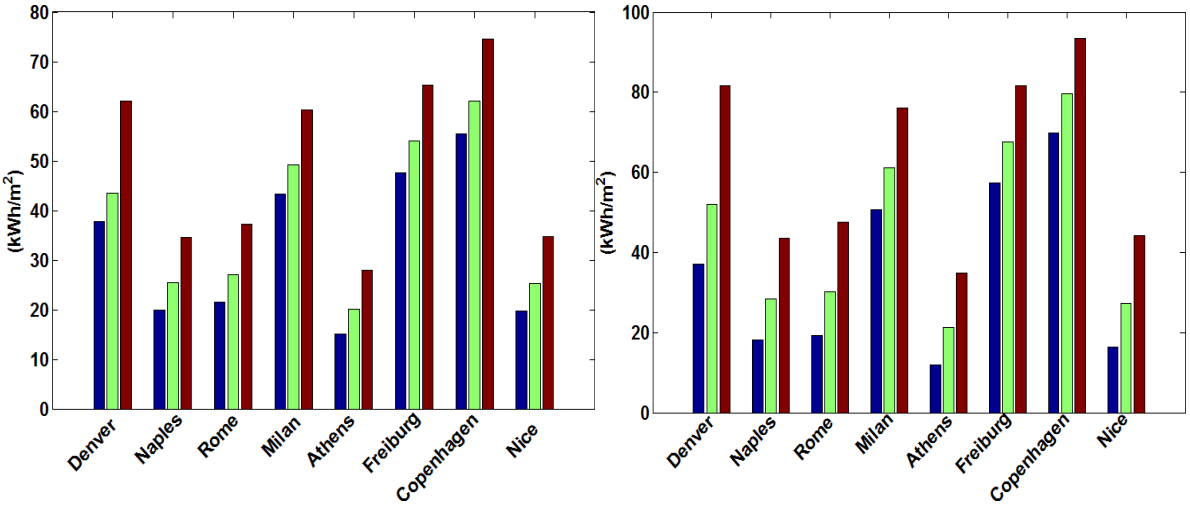

Figure 3.6. Yearly winter heating demand for (a) lightweight buildings and (b) heavyweight buildings, small-size (blue bar), middle-size (green bar) and large-size (red bar).

Analogously, Figure 3.7a and Figure 3.7b show the yearly summer cooling demands for the light and heavyweight buildings, respectively. In summer, as expected, the heavier the building envelope, the lower the cooling demand.

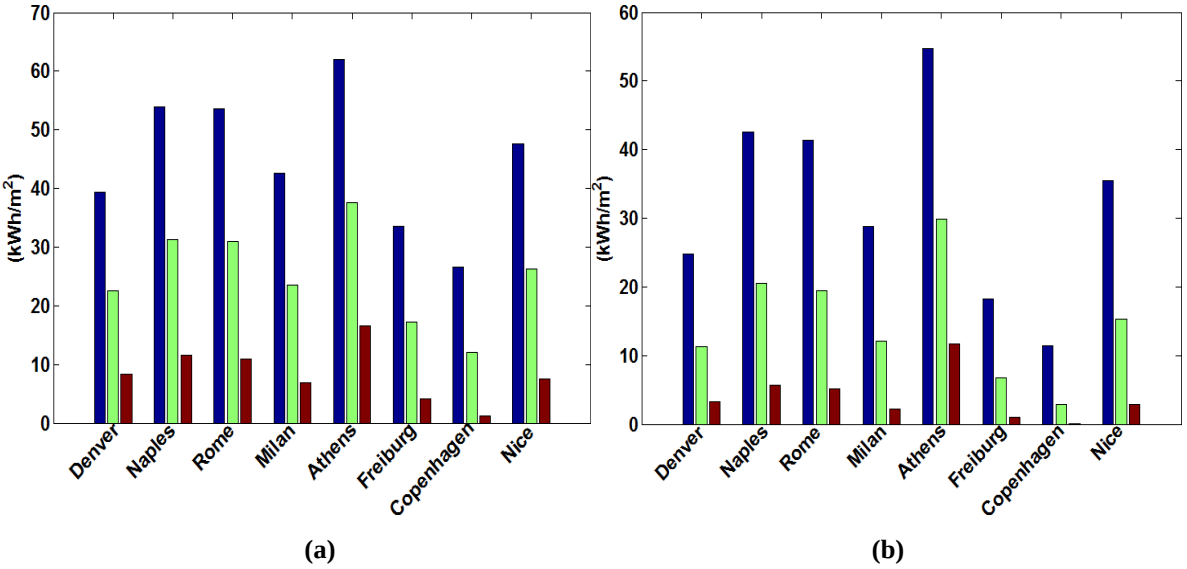

Figure 3.7. Yearly summer cooling demand for (a) lightweight buildings and (b) heavyweight buildings, small-size (blue bar), middle-size (green bar) and large-size (red bar).

.

Obviously, for all the investigated case studies, the highest heating demands are obtained for the large size (mall) building. The opposite occurs for the cooling demands. These results are due to the same internal gains per square meter of building floor assumed in all the cases. Such hypothesis was taken into account in order to analyse the only effects of the building geometry

and weather conditions on the heating and cooling buildings performance. Of course, the higher the heated (cooled) volume, the higher (the lower) the related demands.

As, expected, among all the analysed weather zones and for all the investigated buildings, the lowest heating and the highest cooling demands are always obtained in Athens (Mediterranean climate). The highest heating and the lowest cooling demands are always obtained in Copenhagen (highest HDD among the investigated weather zones).

Finally, in Figure 3.8a and Figure 3.8b, the calculated heating and cooling peak loads for all the investigated case studies are reported. Notice that for sake of brevity only the results related to the heavyweight building envelopes are shown. Here, it is possible to observe that the heating peak loads are much higher than the cooling ones. This is due to: i) the very low internal gains assumed for all the case studies; ii) the selected weather conditions (disturbances).

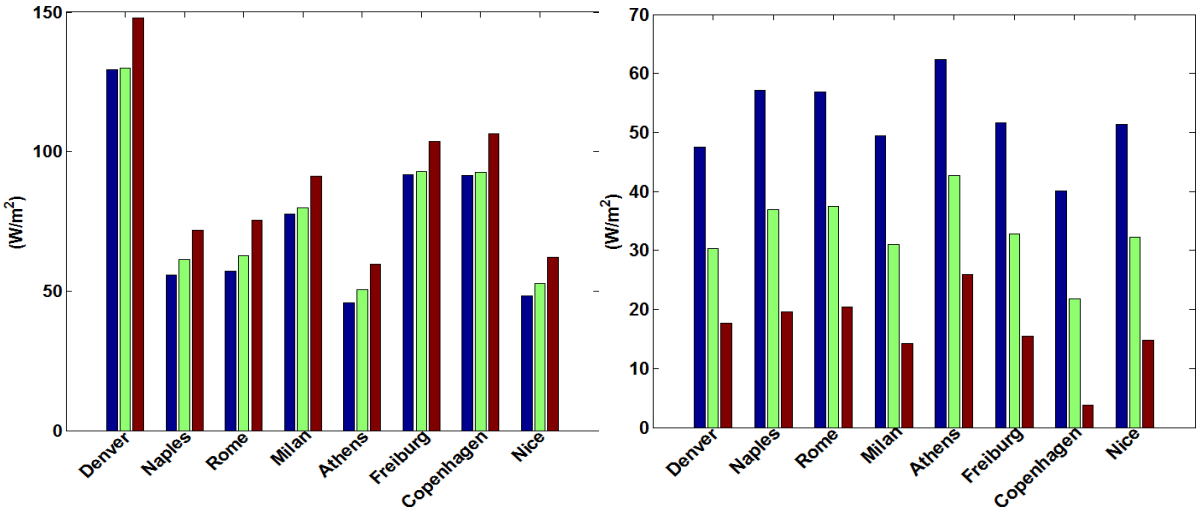

Figure 3.8. (a) Yearly Heating peak loads for heavy buildings and (b) Yearly Cooling peak loads for lightweight buildings, small-size (blue bar), middle-size (green bar) and large-size (red bar).

While the highest cooling load is obtained also in this case in Athens, the highest heating one is observed in Denver (and not in Copenhagen). Thus, the worst winter condition is obtained in Denver. Here, a cold clear winter and a hot dry summer is observed as well as large diurnal temperature variations throughout the year. Also such results can be useful for building designers.

Concerning plant disturbances, the winter outdoor air temperatures T_{out} resulted to be the most predominant among those taken into account. In fact T_{out} is almost always and everywhere lower than the selected indoor air set point of 20°C. It must be also noted that during summer T_{out} is averagely close to the indoor air temperature set-point, which in the investigated case studies was

fixed equal to 25°C. During such season and especially in Mediterranean weather zones, remarkable plant disturbances are caused also by sun radiation.

3.5 **Discussion**

In this chapter we have introduced the control architecture that will be used to host the model reference adaptive control algorithm. In addition to the feedback controllers for the online computation of the sensible heat and water vapor mass flow rate to impose a given thermohygrometric condition, this scheme includes two additional systems, i.e., the Supervisory Machine and Trajectory Planner. The former modelled via a set of event driven dynamical systems, i.e., automatons, is used to avoid the onset of unwanted chattering solutions for the sensible heat and water vapor mass flow rate, while the latter provides the references for the underlying controllers and will be used in the following chapters to generate humidity/temperature profiles in accordance with a quadratic cost function.

In the second part of the chapter an approach for the optimal tuning of parameters of a PI strategy (and more in general of a generic controller with fixed control gains) has been introduced for the building control. The main advantage of this tuning method is that the resulting controller minimizes the loss function in (3.4). In the case of the control of buildings, this cost function allows to measure in one single performance index both comfort (as the first term in (3.4) measures the distance to the required set-point) and energy saving (because the second term in (3.4) weights the energy demand). Consequently, the tuning of the coefficients of such a function provides solutions to the well-known tradeoff between cost reduction and improvement of the comfort that is one of the challenge in building management. Furthermore, the implementation of the proposed strategy in DETECt solves systematically the lack of optimality of the pre-existing control solution. Hence, both the novel control scheme and the tuning algorithm represent enhancements of such dynamic simulation code for the prediction of building heating and cooling requirements and loads. The effectiveness of the tuning procedure and the resulting control action to impose indoor air temperature profiles were also tested on a wide range of case studies related to several buildings of different geometry and construction materials, subjected to different weather conditions. In general, through the simulation results interesting guidelines, useful for building energy designers and practitioners, can be obtained. On the other hand three main issues remain open. Precisely:

- the solution of the optimization problem is done according to the numerical scheme in Figure 3.4 which requires the dynamics simulation of the building dynamics for an

unknown number of times. Hence, it can be time consuming in the case of slow convergence of the iterative algorithm to the optimal solution;

- the resulting control parameters strongly depend on the specific case (building physical parameters, weather conditions, scheduling of the occupants, etc), i.e., all the data required to run the simulator. Consequently, the optimization process must be redone for any case study. Indeed, the reuse of the control parameters tuned on a given building to another case not only can jeopardize comfort (as the resulting indoor air relative humidity and temperature can be quite different from those scheduled) but also closed loop instabilities can be induce [96];
- often classical control solutions with fixed gains, e.g., PI strategies, are not robust to parameters uncertainty, unmodeled nonlinear dynamics and disturbances. Nevertheless, in the case of the control of buildings robust control solution are desirable to provide a satisfactory comfort also in the case of uncertain conditions. Indeed building control algorithms have to tackle affectively not only whether uncertainties, e.g., external temperature and solar radiation etc., and unexpected thermal loads variations (external disturbances), but also parameter variations. The latter occurs because *i)* parameters of a dynamical building model are affected by uncertainties and *ii)* in the case of building envelopes that include advanced materials, e.g., phase change materials (see for instance Section 2.2.6 for its modelling) the system to be controlled is intrinsically a parameter varying system [120]. Consequently, control algorithms with fixed gains can be difficult to be tuned in real scenarios and fail to provide a satisfactory comfort level.

In the following chapters these issues will be tackled by introducing a novel model reference adaptive control algorithm with optimal choice of the reference dynamics. Precisely, the control gains of this strategy change on the basis of the actual system response with the aim of imposing to the system outputs a required behavior. Hence, robustness to parameters variations and disturbances are achieved without any preliminary setting of the control gains. In addition, as the control gains dynamically changed on the basis of the actual building conditions, the control design is simplified as no a priori numerical analysis, simulations, are required.

Chapter 4
OPTIMAL MODEL REFERENCE ADAPTIVE CONTROL

A crucial issue in building engineering is to accomplish the trade-off between reduction of energy consumption and high level thermal comfort for the occupants. To this aim, advanced control algorithms are fundamental to guarantee a certain optimality of the system performance also in working conditions that can be quite different from the nominal ones due to the presence, for example, of variable external wheatear conditions or parameter uncertainties. To impose an optimal profiles of the indoor air temperature and relative humidity while assuring robustness to plant parameter uncertainties and external disturbances, in this thesis we propose an extension of model reference adaptive scheme that embeds not only additional adaptive actions to improve tracking performance but also an optimal reference model tuned according to the LQ optimal procedure (see Appendix A for more details about adaptive control methods). Performance of the novel strategy to impose the desired thermohygrometric conditions are investigated both analytically and numerically. This chapter is completely devoted to present in detail this strategy, named LQ-EMRAC (Linear Quadratic - Enhanced Model Reference Adaptive Control), from an analytical prospective. The problem is formulated and solved by using a formalism so that the results presented here can be used not only for the control of buildings but easily extended to others mechanical systems described by a set of ODEs. Fundamental closed loop performance as stability and tracking ability of the closed loop system are investigated via hyperstability and Lyapunov theory. The effectiveness of the control to buildings is instead explored in the following chapters via a wide set of case studies. The application of the control algorithm presented in this chapter to the control of buildings has been published in [33, 121].

4.1 **Introduction to optimal MRAC**

In the control of buildings, as often happen also for other applications, it is required for the controller to minimize certain cost criteria while control is attained. It is common practice to address this requirement by using classical Optimal Control techniques such as the well-known Linear Quadratic Regulators (LQR) [23]. Their simplicity is indeed desirable to practitioners in

order to reduce costs and minimize the control design efforts. Briefly, the aim of optimal controllers is that of ensuring optimal performance through the minimization of specific cost functions. Classical optimal control schemes are usually characterized by fixed control gains. It has been shown that, typically, LQ schemes lack the flexibility and the structural stability of other more sophisticated control approaches as, for instance, exemplified by the two significative cases discussed in [122] and [123]. The lack of robustness to model uncertainties and nonlinear perturbation is, at times, a strong limitation for the use of LQ strategies. Many problems of relevance in applications contain uncertainties, model inaccuracies and other effects that can make unviable the use of classical optimal control schemes. One way of achieving greater control flexibility is to use adaptive control schemes where the control gains are appropriately varied (or adapted) according to the system behavior. The control algorithm proposed in this chapter extends the family of model reference adaptive controllers. The main idea behind the approach is to seek a simple and alternative route to implement the LQ regulator via self-organizing control algorithm which is effective also in those practical cases when the LQ action itself fails. In so doing, the derived controller has the benefits of an adaptive strategy (in terms of minimal knowledge of the plant, minimal design effort and robustness to uncertainties) while also matches the performance of an LQ regulator. (The reader is referred to Appendix A for some details about adaptive control methods and basic definition regarding this control strategy, more details about model reference adaptive control and linear quadratic regulator can be found in [24] and [23], respectively). The resulting control scheme, called LQ-EMRAC (Linear Quadratic - Enhanced Model Reference Adaptive Control) aims at achieving the desired performance by means of a model reference adaptive controller equipped with an optimally controlled reference model. Specifically, the reference model used to adaptively tune the MRAC gains is itself controlled via an LQR feedback strategy that requires the computation off line of the solution of the Riccati equation associated with the synthesis of the LQR control acting on the reference model. The underlying MRAC is also innovative and represent an enhancement of that proposed in [24]. Indeed, to improve tracking performance two additional control actions have been added to the original Landau's control scheme, i.e., an explicit integral adaptive action and an adaptive action based on the sign of the tracking error. The former is used for improving transient and the effect of a possible bias acting on the plant [124], while the latter enhances the robustness to unmodelled disturbances [125, 126].

A consistent proof of stability and closed-loop tracking performance the proposed control scheme are proved. Although it is not the scope of this Ph.D. thesis to derive a general class of

new optimal adaptive controllers, some remarks with respect to the wide literature on this research field are reported below for the sake of completeness. In particular the formal solution of the optimal adaptive control, starting from the pioneering work of Feldbaum (see for example [127] and references therein), usually implies stringent properties to be satisfied. In detail, in adaptive dual control systems the control signal has to be such as to guarantee the closest possible satisfaction of the control goal while sufficiently exciting the plant to allow the estimation. Within this context the problem can be solved through the use of dynamic programming, but the equations can neither be solved analytically nor numerically even for simple examples because of the growing dimension of the underlying state space (which has to be augmented by the parameter vector dynamics).

The difficulties in finding the optimal solution demand the use of some relaxation methods which lead to various approximations of the optimal adaptive problems (implicit methods) or reformulations of the problem itself by considering special cost functions (explicit methods).

Two surveys on optimal adaptive control methods can be found in [128]. For these reasons, most of the schemes attempting at merging on-line adaptation and optimality require intense computations, conservative hypotheses on the system nature, good knowledge of the plant and the absence of any nonlinear perturbation on the plant model. Some applicative examples can be found in [129-133] and in [134-136]. It is apparent that despite their potential benefits, such controllers are hardly used as general tools in generic applicative areas as they are too costly to design and implement.

In this framework, the LQ-EMRAC scheme, detailed in the following sections, is therefore an attempt to overcome the issues connected to the available approaches to the optimal control for uncertain system by achieving an optimal-like plant response by selecting, as a reference model, a nominal linear model of the plant controlled via a classical LQ strategy for the underlying model referenced adaptive controller. In so doing, any mismatch between the optimal model and the actual plant will be compensated by the adaptive action provided by the enhanced MRAC algorithm, which will also guarantee stability in those cases where the LQ strategy alone would fail [23, 122, 123].Thus, it is possible to consider the LQ-EMRAC as a simple and effective way to conjugate the simplicity and the optimality of the LQ action with the robustness of the MRAC control.

4.2 **The LQ-EMRAC strategy**

The idea behind the LQ-EMRAC approach is to recover robustness of the classical Linear-Quadratic (LQ) strategy with respect to unknown environmental conditions, disturbances, parameter uncertainties and unmodelled dynamics, that is typical in the optimal control theory [23], by implementing it via an Adaptive Model Reference Control (MRAC) scheme [24, 137], enhanced by two new additional control actions to improve tracking performance of the reference model dynamics.

As in the case of classical MRAC [24], also for the LQ-EMRAC strategy the Reference Model represents the desired dynamic performance to impose to a given uncertain system and the challenge is to find an Adaptive Mechanism so that the system state exactly tracks that of the reference model. The reference dynamics can be selected in terms of a requested behaviour in closed-loop and their design do not require a precise and detailed knowledge of the system under control. To accomplish optimality of the reference profiles, the Reference Model is chosen as a simplify Linear Time-Invariant (LTI) model of the system under control driven by an optimal LQ control action. In so doing, the reference model dynamics, say $x_m(t)$, are solutions of an optimization problem resulting from a minimization of a quadratic cost index J [23]. The mathematical formulation of the LQ-EMRAC strategy is given in what follows.

Consider the system dynamics described as

$$\dot{x} = A \cdot x + B \cdot u + f(x,t), \tag{4.1}$$

where $x(t) \in \mathbb{R}^n$ is the state of the system to be controlled; $u(t) \in \mathbb{R}$ is the control input; $f(x,t) \in \mathbb{R}^n$ is a bounded disturbance; $A \in \mathbb{R}^{n \times n}$ and $B \in \mathbb{R}^{n \times 1}$ are the dynamic and input matrixes, respectively.

The control objective is to find an adaptive strategy so that the system state tracks the trajectories of a simplified LTI model of the plant (4.1) controlled via an LQ strategy [23]. Although it is well known in the classical control theory [23], some details on the construction of the optimal reference model through the LQ approach are also here provided for the sake of completeness.

The first step is to describe the system dynamics (4.1) by selecting a very simple nominal LTI model of the form

$$\dot{x}_0(t) = A_0 \cdot x_0(t) + B_0 \cdot u_0(t), \qquad y_0(t) = C_0 \cdot x_0(t), \tag{4.2}$$

being $x_0 \in \mathbb{R}^n$ the state vector, $y_0 \in \mathbb{R}$ the output of the system, $A_0 \in \mathbb{R}^{n\times n}$ the dynamic matrix, $B_0 \in \mathbb{R}^n$ the input vector and $C_0 \in \mathbb{R}^{1\times n}$ the output vector. (Notice that, in the case of the control of building a possible choice can be based on some rough estimation of the plant matrices as illustrated in Section 5.1.) Then it is necessary to impose onto the system in (4.2) an optimal control signal $u_0(t) = u_{opt}(t)$ that minimizes the following quadratic functional cost:

$$J\left(x_0(t_0), u_0(\cdot)\right) = \int_{t_0}^{+\infty} \left[\bar{y}_0^T \cdot Q_1 \cdot \bar{y}_0 + \left(y_0 - r\right)^T \cdot Q_2 \cdot \left(y_o - r\right) + u_0^T \cdot R \cdot u_0 \right] \cdot d\tau, \tag{4.3}$$

where *r* is the given set point, t_0 is the initial time instant $Q_1 \in \mathbb{R}^n$ and Q_2, $R \in \mathbb{R}$ are positive matrices and the auxiliary variable $\bar{y}_0$ is defined as: $\bar{y}_0 = \bar{C}_0 \cdot x_0$, with $\bar{C}_0 = I_n - L \cdot C_0$ and $L = C_0^T \cdot \left(C_0 \cdot C_0^T\right)^{-1}$, being I_n the unit matrix in the vector space $\mathbb{R}^{n\times n}$.

According to optimal control theory [23, 138], the quadratic cost function in (4.3) is minimized by selecting:

$$u_{opt} = K^{opt} \cdot x_0 + K_R^{opt} \cdot r, \tag{4.4}$$

where the optimal constant gains are

$$K^{opt} = -R^{-1} \cdot B_0^T \cdot P \text{ and } K_R^{opt} = -R^{-1} \cdot B_0^T \cdot \left(A - B_0 \cdot K^{opt}\right) \cdot Q \cdot L, \tag{4.5}$$

with *P* being the solution of the following Riccati equation

$$\begin{aligned} &A_0^T \cdot P + P \cdot A_0 - P \cdot B_0 \cdot R^{-1} \cdot B_0^T \cdot P = -Q, \\ &Q = \bar{C}_0^T Q_1 \bar{C}_0 + C_0^T Q_2 C_0. \end{aligned} \tag{4.6}$$

Consequently the optimal reference model takes the following form:

$$\dot{x}_m(t) = A_m \cdot x_m(t) + B_m \cdot r(t), \tag{4.7}$$

where $x_m(t) \in \mathbb{R}^n$ is reference the state vector; $r(t) \in \mathbb{R}$ is the reference input signal; $A_m \in \mathbb{R}^{n\times n}$ and $B_m \in \mathbb{R}^n$ are the dynamic and input matrix, respectively, given by

$$\begin{aligned} &A_m = A_0 + B_0 K^{opt}, \\ &B_m = B_0 K_R^{opt}. \end{aligned} \tag{4.8}$$

To compensate adaptively any mismatch between the optimal reference dynamics $x_m(t)$ and the actual dynamics $x(t)$ the control input $u(t)$ in (4.1) is chosen as

4.2 The LQ-EMRAC strategy

$$u(t) = u_{MRAC}(t) + u_I(t) + u_E(t), \tag{4.9}$$

where

$$\begin{aligned} u_{MRAC}(t) &= K(t)\cdot x(t) + K_R(t)\cdot r(t), \\ u_E(t) &= K_E(t)\cdot \mathrm{sgn}\left(y_e(t)\right), \\ u_I(t) &= K_I(t)\cdot x_I(t), \\ x_I(t) &= \int_{t_0}^{t} x_e(\tau)\cdot d\tau, \end{aligned} \tag{4.10}$$

and the adaptive gains are on-line computed as

$$\begin{aligned} K(t) &= K^I(t) + y_e(t)x^T(t)\Gamma_\beta, \\ K_R(t) &= K_R^I(t) + y_e(t)r(t)\Psi_\beta, \\ K_I(t) &= K_I^I(t) + y_e(t)x_I^T(t)\Omega_\beta, \\ K_E(t) &= \gamma\int_{t_0}^{t} |y_e|\cdot d\tau, \end{aligned} \tag{4.11}$$

and

$$\begin{aligned} K^I(t) &= \int_{t_0}^{t} y_e\cdot x^T\cdot\Gamma_\alpha\cdot d\tau, \quad K^I(t_0) = K_0^I, \\ K_R^I(t) &= \int_{t_0}^{t} y_e\cdot r\cdot\Psi_\alpha\cdot d\tau, \quad K_R^I(t_0) = K_{R0}^I, \\ K_I^I(t) &= \int_{t_0}^{t} y_e\cdot x_I^T\cdot\Omega_\alpha\cdot d\tau, \quad K_I^I(t_0) = K_{I0}^I, \end{aligned} \tag{4.12}$$

where K_0^I, K_{R0}^I and K_{I0}^I are the initial values of the integral part of the adaptive gains at the initial time instant t_0; Γ_α, Γ_β, Ω_α, Ω_β $\in D_n$ (being D_n the subspace of diagonal matrices in $\mathbb{R}^{n\times n}$) and Ψ_α, Ψ_β, $\gamma\in\mathbb{R}$ are some adaptive weights with the same sign of K_R assumed as in [23] to be known.

Furthermore, the output error y_e necessary to online compute the gain dynamics is defined as:

$$y_e(t) = C_e\cdot x_e(t), \tag{4.13}$$

with $x_e(t)$ being the state tracking error, i.e., the distance between actual and optimal reference dynamics as:

$$x_e(t) = x_m(t) - x(t), \text{ and } C_e = B_m^T\cdot P_c, \tag{4.14}$$

and P_c is the solution of the following Lyapunov equation [139]

$$P_c \cdot A_m + A_m^T \cdot P_c = -M, \quad M > 0. \tag{4.15}$$

Figure 4.1 shows the LQ-EMRAC scheme. Notice that, the optimal choice of the reference model and the additional control actions (i.e., $u_I(t)$ and $u_E(t)$ in (4.10)) make the LQ-EMRAC different from the Landau's scheme depicted in Figure 4.2 for the sake of completeness.

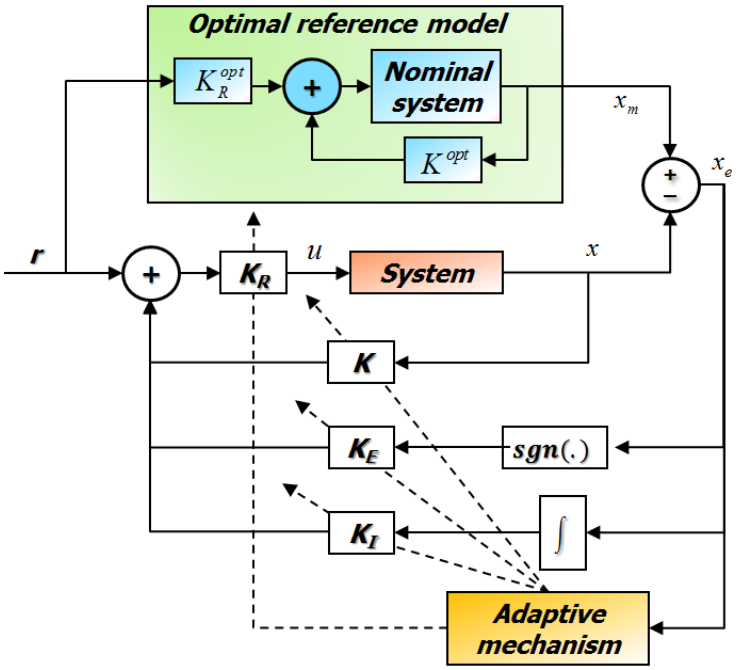

Figure 4.1. Model reference adaptive LQ-EMRAC scheme.

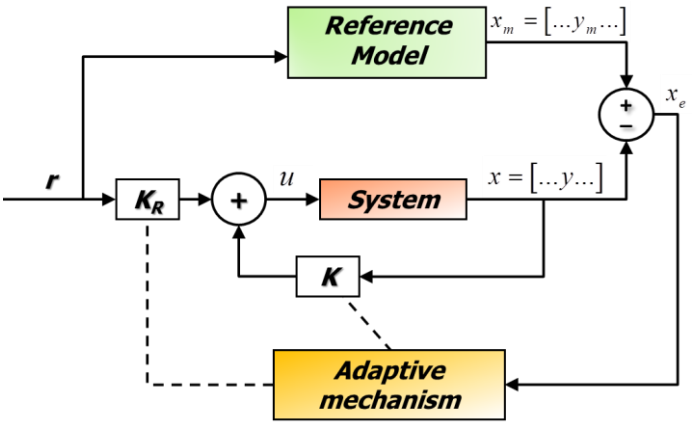

Figure 4.2. Landau's Model reference adaptive control scheme [24].

Remarks.

- The cost function in (4.3), which is exploited in the minimization process, is similar to the one used in (3.4) as it weighs both the distance between the actual plant trajectory and the reference one as well as the control effort via the quadratic form involving the control input $u(t)$. Hence, similar to the discussion in Section 3.3, in the case of the

control of buildings, this function provides a measurement for both comfort and energy saving. Consequently, the tuning of the matrices in (4.3) gives to practitioners a mean for solving the tradeoff between cost reduction and improvement of the comfort that is one of the challenge in building management. Nevertheless, different from the optimal PI tuning in Section 3.3, the optimization process is performed for the reference model and not for the control parameters whose, in the case of the LQ-EMRAC, changes online on the basis of the adaptive mechanisms in (4.11) to provide the required robustness to disturbances, parameter variations and unmodelled nonlinearities. This allows to prevent loss of tracking performance as we will show in the Section 5.4.4.

- As additional technical assumptions we supposed that the pair (A_0, B_0) in (4.2) is stabilizable and pair (A_0, Γ_0) is detectable, being $\Gamma_0 \in \mathbb{R}^{n \times n}$ so that $\Gamma_0 \Gamma_0^T = Q$ with Q defined in (4.6). Hence, the introduction of the auxiliary variable $\bar{y}$ in (4.3) allows to weight the complete state of the system (4.2) and therefore it is used for avoiding possible unstable solutions of non-observable parts of the closed loop system [23].
- We remark here that, when the optimal model in (4.7) (built according to the LQ approach) is chosen as reference model for the LQ-EMRAC scheme, the classical matching conditions, required to show the feasibility of the MRAC objective (see [140]) are automatically satisfied.
- According to [124], the main advantages, when the integral term $u_I(t)$ in (4.9) is used in the control-loop, are: i) the compensation of non-zero mean bias terms on the plant, not only in steady state conditions, but also during the transient phase when the plant has a low bandwidth bias; ii) in the case some locking strategies are used for the adaptive gains in (4.12), the control strategy has a structure comparable with a conventional PID controller, and this is a desirable property.
- Similar to the control scheme introduced in [125], the term $u_E(t)$ in (4.9) is a sliding action that ensures convergence to zero of the tracking error in the presence of bounded disturbances acting on the system to be controlled [141]. Notice that, the switching term in (4.10), which is based on the sign of y_e, is modulated via the adaptive gain K_E. Hence, different from [126] no apriority knowledge about the upper bound of the norm of the disturbance term in (4.1) is required.

- In the case u_E, u_I, Γ_α and Γ_β are set to zero the algorithm (4.9) reduces to the classical MRAC strategy given in [140]. Hence, both the novel adaptive control actions and the proportional terms of the adaptive gains enhance the pre-existing adaptive scheme.
- When u_E and u_I are set to zero and the matrices of system (4.1) and the reference model (4.7) are in control canonical form, the algorithm (4.9) reduces to the LQ-MCS strategy presented in [142].
- The solution of (4.15) exists as A_m is a Hurwitz matrix [23]. In addition choosing M in (4.15) as Q in (4.6), then $P_c = P$. Indeed, according to the LQ theory [23], $W(x_m) = x_m^T P x_m$, with P solution of (4.6), is a Lyapunov function of the LQ closed-loop system (4.7) with $r = 0$.
- Typically the adaptive gains are started from zero, i.e., $K_{E0} = 0$, $K_0^I = 0$, $K_{R0}^I = 0$, $K_{I0}^I = 0$ in (4.11) and (4.12).
- When implementing $u_E(t)$ in (4.9), the discontinuous control action can be replaced by a continuous one as

$$u_E(t) = K_E(t)\frac{y_e(t)}{|y_e(t)| + \varepsilon}, \tag{4.16}$$

  where K_E is that computed as in (4.11) and ε is a sufficiently small positive constant to be chosen appropriately. In so doing classical chattering phenomenon affecting the control variable can be avoided [109].

The steps required to design the LQ-EMRAC strategy are summarized in what follows.

1) Identify a nominal linear model of the plant of interest of the form (4.2). This model represents a rough estimate of the plant matrices that can be used to design a classical optimal control law.
2) Design a classical LQ optimal controller on the nominal plant model selected above in order to minimize the target cost function (4.3), with Q_1, Q_2 and R being appropriate weight matrices.
3) Implement the LQ-EMRAC scheme, see also Figure 4.1, by using the closed-loop LQ nominal plant in (4.7) as the reference model for the adaptive algorithm (4.9) acting on the real system dynamics (4.1).

The analytical proof of the asymptotic stability of the closed-loop dynamics, that is necessary to guarantee the effectiveness of the control action, is derived in Section 4.3 by using a Lyapunov approach [139] and, hence, by selecting a proper generalized energetic function depending on both tracking error and adaptive gains. Note that, differently from previous attempts [142], the convergence to zero of all the closed-loop dynamics is proven without assuming the plant structure to be in control canonical form and it is derived according to the Barbalat's Lemma [143]. An alternative proof of the closed loop stability and tracking performance based on the Hyperstability theory is provided instead in Section 4.4.

4.3 **Proof of closed loop stability via Lyapunov method**

The effectiveness of the control algorithm presented in Section 4.2 is analytically proven by showing the convergence to zero of the tracking error with a Lyapunov approach [139], i.e., by finding a generalized energetic function depending on both tracking error and adaptive gains.

Before showing in detail the proof, we disclose some technical aspects that are related to the mathematical derivation. In particular, in accordance again with the classical MRAC theory [24], we assume that the sign of the K_R^{opt} in (4.8) is known. As a further technical assumption, we assume that the nonlinear term acting on the plant dynamics (4.1) is bounded and it can be parameterized as $f(x,t) = B_m \cdot d(x,t)$ with $d(x,t)$ being a generic function of the plant state and the time. In addition, we assume that some saturation strategy and an anti-windup scheme are adopted when computing the integral x_I in (4.10) [96]. Moreover, we select the control weights Γ_α, Γ_β, Ψ_α, Ψ_β, Ω_α, Ω_β and γ in (4.11) and (4.12) with the same sign of K_R^{opt}. Note that, the boundedness of $f(x,t)$ implies the boundedness of $d(x,t)$, i.e. there exists a constant $D > 0$ so that $|d(x,t)| \le D$.

To derive the proof, we first recast the closed-loop state vector as $\left[x_e^T \quad \phi^T \quad K_E\right]^T$, being $\phi = \left[K^{opt} - K^I \;\vdots\; -K_I^I \;\vdots\; K_R^{opt} - K_R^I\right]$, so that the closed-loop dynamics under the LQ-EMRAC control action can be written as

$$\begin{aligned} \dot{x}_e &= A_m \cdot x_e + \frac{B_m}{K_R^{opt}} \cdot \phi^T \cdot \omega - \frac{B_m}{K_R^{opt}} \cdot y_e \cdot \omega^T \cdot \beta \cdot \omega - \frac{B_m}{K_R^{opt}} \cdot \left(d + K_E \cdot \mathrm{sgn}\left(y_e\right)\right), \\ \dot{\phi} &= -y_e \cdot \alpha \cdot \omega, \end{aligned} \tag{4.17}$$

where, $\omega^T = \left[x^T \;\vdots\; x_I^T \;\vdots\; r\right]$ and $\alpha = diag\left(\Gamma_\alpha, \Omega_\alpha, \Psi_\alpha\right)$ and $\beta = diag\left(\Gamma_\beta, \Omega_\beta, \Psi_\beta\right) \in D_{2n+1}$.

Notice that, since each entry of α and β have the same sign of K_R^{opt}, matrices α/K_R^{opt} and β/K_R^{opt} are positive definite.

Choosing now the following candidate Lyapunov function

$$V = x_e^T \cdot P_c \cdot x_e + \frac{1}{\left|K_R^{opt}\right|} \cdot \phi^T \cdot |\alpha|^{-1} \cdot \phi, \tag{4.18}$$

with $P_c > 0$ being the solution of (4.15) and $|\alpha| = diag\left(|\alpha_{11}|, |\alpha_{22}|, \ldots, |\alpha_{2n+1,2n+1}|\right)$, it is possible to prove that the derivative of (4.18) along the solutions of system (4.1) is

$$\dot{V} = -x_e^T \cdot M \cdot x_e - \frac{2}{\left|K_R^{opt}\right|} \cdot y_e^2 \cdot \omega^T \cdot |\beta| \cdot \omega - 2|y_e| \cdot \left[\frac{\mathrm{sgn}(y_e)}{\mathrm{sgn}\left(K_R^{opt}\right)} \cdot \frac{d}{\left|K_R^{opt}\right|} + \frac{K_E}{K_R^{opt}} \right], \tag{4.19}$$

where $|\beta| = diag\left(|\beta_{11}|, |\beta_{22}|, \ldots, |\beta_{2n+1,2n+1}|\right)$.

Now, since quantity K_E/K_R^{opt} is a positive increasing term, there exists a time instant, say t^*, so that $K_E(t)/K_R^{opt} > D/\left|K_R^{opt}\right|$ for all $t > t^*$. Hence, for $t > t^*$ also the last term in (4.19) is negative and, therefore, we can claim that

$$\dot{V} \le -x_e^T \cdot M \cdot x_e \le -\lambda_{\min} \cdot \|x_e\|^2, \tag{4.20}$$

where $\lambda_{\min}$ is the minimum eigenvalue of the *M*-matrix.

According to the Lyapunov theory [139], since $\dot{V}$ is definite negative than the origin of the closed-loop system is a globally stable equilibrium point, and all the closed-loop signals are bounded [143]. Moreover, from (4.20), after some algebraic manipulations, we have that for any $t > t^*$ it holds

$$\int_{t^*}^{t} \|x_e(\tau)\|^2 \, d\tau \le \frac{V\left(t^*\right)}{\lambda_{\min}}. \tag{4.21}$$

From inequality (4.21), we have that x_e is a square measurable function as time goes to infinity. Now, since all closed-loop dynamics are bounded and x_e is square measurable, it follows that x_e goes to zero as the time goes to infinity according to the Barbalat's Lemma [143].

4.4 **Proof of close loop stability via Hyperstability**

The convergence to zero of the tracking error can be also proven by showing that the error dynamics can be recast as an asymptotically hyperstable system [24, 144]. To this aim the proof

is composed by the following steps: *(i)* the closed-loop system is rewritten as an LTI feedforward system in feedback with an nonlinear system; *(ii)* the feedforward path is shown to be a Strictly Positive Real (SPR) block, and *(iii)* show that the feedback path satisfy Popov's integral inequality [144] (i.e., the feedback block is a passive nonlinear mapping). In accordance with Theorem in C-2, p. 385 in [24], the feedback system is then asymptotically hyperstable, and therefore closed-loop trajectories converge to zero for any initial state (i.e., $x_e \to 0$ as $t \to +\infty$).

Step (i): Recast the Error Dynamics as a Feedback System.

From (4.17), the error dynamics can be also easily represented as the feedback system shown in Figure 4.3. The feedforward block is described by the LTI model whose input-state-output representation is characterized by the triple (A_m, B_m, C_e), while the feedback block is a nonlinear mapping which depends on the output signal y_e and the adaptive gains.

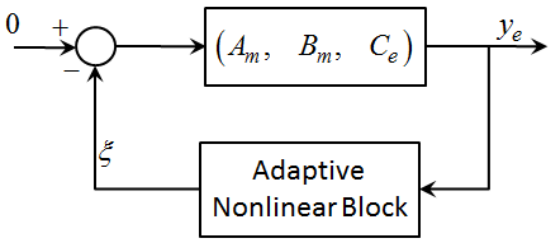

Figure 4.3. Closed-loop error dynamics (4.17) represented as an equivalent feedback system.

The feedback system in Figure 4.3 is mathematically described as

$$\dot{x}_e = A_m x_e + B_m \xi, \quad \text{and} \quad y_e = C_e x_e$$
$$\xi = \frac{\phi^T w}{K_R^{opt}} - \frac{y_e w^T \beta w}{K_R^{opt}} - \frac{K_E sign(y_e) + d}{K_R^{opt}}, \tag{4.22}$$

where the second equation represents the nonlinear mapping which transforms the y_e into the auxiliary variable ξ.

Step (ii): Strictly Positive Realness of the feedforward path.

Since A_m satisfies (4.15) and $C_e = B_m^T P_c$, then the Kalman-Yakubovich-Popov lemma holds, and therefore the feedforward path is an SPR system [24].

Step (iii): Passivity of the feedback path.

In order to prove that the feedback block in Figure 4.3 satisfies the Popov's integral inequality, it suffices to show that, for some finite constant c, it holds [24]:

$$I = \int_{t_0}^{t_1} -y_e \xi d\tau \geq -c^2, \tag{4.23}$$

for any generic time instant t_1.

Substituting (4.22) in (4.23) after some algebraic manipulations, we have

$$I = I_1 + I_2 + I_3, \tag{4.24}$$

with

$$\begin{aligned} I_1 &= \int_{t_0}^{t_1} \frac{y_e^2 w^T \beta w}{K_R^{opt}} d\tau, \\ I_2 &= \int_{t_0}^{t_1} -y_e \frac{\phi^T w}{K_R^{opt}} d\tau, \\ I_3 &= \int_{t_0}^{t_1} y_e \frac{K_E \operatorname{sgn}(y_e) + d(\tau)}{K_R^{opt}} d\tau. \end{aligned} \tag{4.25}$$

Since each element of the β-matrix has the same sign of K_R^{opt}, we have that $w^T \beta w / K_R^{opt} = w^T |\beta| w / \left|K_R^{opt}\right| \geq 0$, for all $w \in \mathbb{R}^{2n+1}$, with $|\beta| = diag\left(|\beta_{11}|, |\beta_{22}|, \ldots, |\beta_{2n+1,2n+1}|\right)$. Consequently,

$$I_1 \geq 0 \tag{4.26}$$

for all time instants.

Consider now I_2 in (4.25). By exploiting the second equation in (4.17) we can solve the integral that defines I_2 as follows

$$I_2 = \int_{t_0}^{t_1} -y_e \frac{\phi^T w}{K_R^{opt}} d\tau = \int_{t_0}^{t_1} \frac{\phi^T \alpha^{-1} \dot{\phi}}{K_R^{opt}} d\tau = \frac{1}{2} \frac{\phi^T(t_1) \alpha^{-1} \phi(t_1)}{K_R^{opt}} - \frac{1}{2} \frac{\phi^T(t_0) \alpha^{-1} \phi(t_0)}{K_R^{opt}} \tag{4.27}$$

Since each element of the α-matrix has the same sign of K_R^{opt}, we have that $\phi^T(t_1) \alpha^{-1} \phi(t_1) / K_R^{opt} = \phi^T(t_1) |\alpha|^{-1} \phi(t_1) / \left|K_R^{opt}\right| \geq 0$, for any generic time instant t_1, where the matrix $|\alpha|$ is defined as $|\alpha| = diag\left(|\alpha_{11}|, |\alpha_{22}|, \ldots, |\alpha_{2n+1,2n+1}|\right)$, therefore

$$I_2 = \int_{t_1}^{t_1} -y_e \frac{\phi^T w}{K_R^{opt}} d\tau \geq -\frac{1}{2} \frac{\phi^T(t_0) \alpha^{-1} \phi(t_0)}{K_R^{opt}} \triangleq -c_1^2. \tag{4.28}$$

Final, consider the term I_3, after simple algebraic manipulations we have

$$y_e \frac{K_E \operatorname{sgn}(y_e) + d}{K_R^{opt}} = |y_e| \cdot \left[\frac{\operatorname{sgn}(y_e)}{\operatorname{sgn}\left(K_R^{opt}\right)} \cdot \frac{d}{\left|K_R^{opt}\right|} + \frac{K_E}{K_R^{opt}} \right]. \tag{4.29}$$

Taking into account (4.29) and that the quantity K_E/K_R^{opt} is a positive increasing term as K_E has always the same sign of K_R^{opt}, there exists a time instant, say t^*, so that $K_E(t)/K_R^{opt} > D/\left|K_R^{opt}\right|$ for all $t > t^*$, with D the positive constant so that $|d(t)| \le D,\ \forall t \ge t_0$ (which exists as the disturbance was assumed to be bounded). Consequently also the term (4.29) is positive for $t > t^*$. Hence,

$$\begin{aligned} I_3 &= \int_{t_0}^{t_1} y_e \frac{K_E \operatorname{sgn}(y_e) + d(\tau)}{K_R^{opt}} d\tau \\ &= \int_{t_0}^{t^*} y_e \frac{K_E \operatorname{sgn}(y_e) + d(\tau)}{K_R^{opt}} d\tau + \int_{t^*}^{t_1} y_e \frac{K_E \operatorname{sgn}(y_e) + d(\tau)}{K_R^{opt}} d\tau. \\ &\ge -\left| \int_{t_0}^{t^*} y_e \frac{K_E \operatorname{sgn}(y_e) + d(\tau)}{K_R^{opt}} d\tau \right| \ge -c_3^2. \end{aligned} \tag{4.30}$$

From (4.26), (4.28) and (4.30) follows immediately that $I \ge -(c_2^2 + c_3^2) \triangleq -c^2$, therefore the Popov's integral inequality (4.23) is fulfilled. In so doing the feedback system Figure 4.2 is hyperstable and their dynamics converge to zero according to [24].

Notice that, for any time instant $t < t^*$ the bounded input-output property of the feedback passive systems guarantees boundedness of the error dynamics [126]. Furthermore, the convergence of the adaptive gain K_E to a finite value in the absence of persistent perturbations can be easily shown by following the approach in [125]. In practice, it might keep growing if persistent disturbances are present. In this case, a simple implementation solution is to lock the evolution of over a certain threshold.

4.5 **Discussion**

In this chapter, we have presented a novel model reference adaptive control algorithm. The aim of the controller is for the adaptive strategy to match the dynamic behavior of an LQ-regulator which would be unsuitable because of the uncertain, time-varying nature of the plant. The idea is to use an optimally controlled reference model and implement the control action onto the plant by means of an adaptive controller consisting of state feedback and feedforward actions enhanced by means of a switching action and an integral action. In so doing the adaptive gains of the algorithm change to compensate online any mismatch between the dynamics of the system to be controlled and the optimal reference trajectories. The additional control terms are added to further improve tracking. In particular the adaptive action based on the integral of the tracking

error is used to improve steady-state regime, while the action depending of the sign of the tracking error is used to tackle disturbance during transients.

In this chapter we have also shown the analytical proof of the closed-loop asymptotic stability when the novel control action, named LQ-EMRAC, is inserted in the control loop by using both Lypunov techniques and hyperstability theory.

We wish to emphasize that the control scheme presented in this work could be a practical alternative to other more sophisticated adaptive-optimal controllers which is easy to implement and do not require a large amount of off-line analytical work to design the control parameters or select initial conditions on the adaptive gains.

For its feature, the LQ-EMRAC is proposed in this thesis as a novel approach to control the dynamics of buildings. In particular, the underlying adaptive mechanism allows to impose the required LQ optimal model dynamics to the building termohygrometric variables also in presence of unmodeled conditions, e.g., uncertain or time-varying building parameters (for instance in the case of PCM materials), change of the weather conditions and occupants. In the next chapters the effectiveness of the proposed algorithm will be shown on a variety of case studies together its design.

Chapter 5
DESIGN AND NUMERICAL ANALYSIS OF THE EMRAC TO BUILDINGS

In this chapter, in order to investigate the effectiveness of the method presented in Chapter 4 for imposing some profiles to the thermohygrometric variables in buildings, the model reference adaptive control strategy has been implemented in DETECt. This tool enables multi-zone building simulation analyses and is capable to dynamically predict: i) spaces sensible and latent heating and cooling demands and loads; ii) indoor air temperatures and humidity, as well as building envelope internal and external temperatures; iii) the performance of phase change materials (PCM) embedded in building enclosures and; iv) the thermohygrometric comfort of occupants (see Chapter 2 and [9] for further details).

In order to analyze the effectiveness and robustness of the proposed control strategy, in this chapter several case studies are proposed. They refer to some reference buildings with different geometry, use and construction materials (also including PCM integrated into the building envelope) simulated in different weather conditions. For each case study, both continuous and intermittent control system regimes are considered. Results confirm the ability of the developed approach to achieve the selected indoor air temperature and humidity conditions in order to guarantee indoor comfort in uncertain conditions. In addition, before showing in detail the numerical results, a simplified physical based dynamical model of building dynamics given in Chapter 2 is here derived and used for the design of the reference dynamics as required by the design procedure of the optimal model reference adaptive control in Chapter 4. Such a procedure is also reformulated in this chapter for its specific use to the control of thermohygrometric variables in buildings. The material of this chapter has been published in [33, 121].

5.1 **Reduced heat flow calculation procedure**

In order to apply the adaptive control in Chapter 4, a linear and low-order nominal building model must be developed and used in the optimal LQ procedure. In what follows such a simplified model is obtained by the high order physical based building model in Chapter 2 for

the sensible load calculation. Specifically, the building model reduction is carried out by lumping all the thermal capacitances of the building envelope in a single node. As a result, an equivalent thermal resistance of the whole building envelope is adopted and weighted average thermal properties are taken into account. Through such approach, the reduced low-order thermal network system includes two temperature nodes, one for the lumped building envelope and one for the indoor air. Due to such a simplification, the set of algebraic and differential equations given in Chapter 2 becomes

$$\begin{cases} C_w \dfrac{dT_w}{dt} = \dfrac{T_{out} - T_w}{R_{ext}^{eq}} + \dfrac{\bar{I}_{ext} \cdot h_o^{-1}}{R_{ext}^{eq}} + \dfrac{T_{in} - T_w}{R_{int}^{eq}} + \dfrac{T_{gr} - T_w}{R_{gr}^{eq}}, \\ C_{in} \dfrac{dT_{in}}{dt} = \dfrac{T_w - T_{in}}{R_{int}^{eq}} + \dfrac{T_{out} - T_{in}}{R_v} + \dot{Q}_g + \dot{Q}_{HC}^s, \end{cases} \tag{5.1}$$

where R_{gr}^{eq} is the equivalent thermal resistance between the node related to the lumped envelope temperature and the ground, R_v is the resistance equivalent to air ventilation and infiltration, $C_w = \sum_{n=1}^{N} C_{m,n}$ is the lumped thermal capacitance of the whole building envelope, with $C_{m,n}$ being the capacitances of the layers of the *m*-th building element (see Section 2.2.1), whose temperature is T_w, while the indoor air temperature is denoted as T_{in}. The equivalent internal and external thermal resistances of the building envelope, i.e., R_{int}^{eq} and R_{ext}^{eq}, are calculated as the sum of: *i)* a half conductive resistance $\left(\bar{R}^{cond}/2\right)$, with $\bar{R}^{cond} = (\sum_{m=1}^{M}(\sum_{n=1}^{N} R_{m,n}^{cond})^{-1})^{-1}$ calculated from series ($1 < i < N$) and parallel resistances ($1 < j < M$), for both opaque and transparent elements (see Section 2.2.1); *ii)* combined radiation and convection heat transfer resistances, for internal $R_{m,0}^{cr}$ and external $R_{m,N+1}^{cr}$ surfaces. Additional average thermal properties, weighted on the building surface areas, are taken into account, such as combined radiation and convection average external (h_o) and internal (h_i) heat transfer coefficients and the average incident solar radiation flux, $\bar{I}_{ext}$. Note that the model related to the latent load calculation is already suitable for control application in its form in (2.18). In model (5.1), the input signals acting on the nodes are: the outdoor temperature, T_{out}, the average incident solar radiation flux, $\bar{I}_{ext}$, the ground temperature T_{gr}, while $\dot{Q}_g$ is a lumped heat source term which consists of convective sensible internal gains due to occupants, lights and equipment, and $\dot{Q}_{HC}^s$ is the additional sensible heat to add or subtract to control the indoor air temperature.

We remark that this simplified model is only used for the computation of the reference dynamics, while the actual control gains adapt in accordance to the adaptive mechanisms in (4.11)-(4.12).

5.2 **LQ-EMRAC Design for Thermohygrometric control**

As recently proposed for NZEBs, energy saving and indoor comfort can be achieved simultaneously by independently controlling sensible loads and the water vapour mass flow rate [101]. Following this approach (also adopted in [9]), here an independent temperature and humidity control, where two separate LQ-EMRAC actions drive each of the variables of interest, is proposed.

The general steps required to design the LQ-EMRAC strategy in Chapter 4 can be summarized as follows:

Step 1. Select a nominal linear model of the plant of interest, i.e., the matrices A_0 and B_0 in (4.2).

Step 2. Optimize the nominal model selected above by designing a classical LQ optimal action able to minimize the target cost function J in (4.3).

Step 3 Implement the LQ-EMRAC scheme in Figure 4.1 by using the model designed in *Step 2* as the reference model for the adaptive algorithm in (4.9)-(4.12).

According to this procedure, the first step for the design of the LQ-EMRAC in the specific thermohygrometric case is the choice of nominal linear models for both the indoor air temperature and humidity (*Step 1*). To this aim, for the temperature dynamics, we reduce the nonlinear physical building model in Chapter 2 in accordance with the approach discusses in Section 5.1. In so doing, the state vector in (4.2) is $x_0(t)=\left[T_w(t) \quad T_{in}(t)\right]^T$ (being T_w and T_{in} the temperatures of lumped thermal capacities of the whole envelope and indoor air temperature, respectively); $u_0=\dot{Q}_{HC}^s$ is the sensible heat to be supplied to or removed from the building space and the system matrices are

$$A_0=\begin{bmatrix} -\dfrac{\left(R_{int}^{eq}+R_{ext}^{eq}\right)\cdot R_{gr}^{eq}+\left(R_{int}^{eq}\cdot R_{ext}^{eq}\right)}{R_{int}^{eq}\cdot R_{ext}^{eq}\cdot R_{gr}^{eq}\cdot C_w} & \left(R_{int}^{eq}\cdot C_w\right)^{-1} \\ \left(R_{int}^{eq}\cdot C_{in}\right)^{-1} & -\dfrac{R_v+R_{int}^{eq}}{R_{int}^{eq}\cdot R_v\cdot C_{in}} \end{bmatrix}, \tag{5.2}$$

$$B_0=\begin{bmatrix} 0 & C_{in}^{-1} \end{bmatrix}^T,$$

$$C_0=\begin{bmatrix} 0 & 1 \end{bmatrix},$$

being R_{int}^{eq}, R_{ext}^{eq} and R_{gr}^{eq} the equivalent thermal resistances between the nodes related to the lumped envelope temperature, T_w, and the indoor air temperature, T_{in}, the outdoor air temperature, T_{out}, and the ground temperature, T_{gr}, respectively; R_v is the resistance equivalent to air ventilation and infiltration; C_{in} and C_w are the lumped thermal capacities of the indoor air and the building envelope, respectively. (The reader is referred Section 5.1 and Chapter 2 for further details on building modelling.)

For the humidity dynamics the nominal model is obtained from (2.18). The nominal model in this second case is a first order linear system of the form in (4.2) where $x_0(t) = \omega_{in}(t)$ and the system input is the water vapour mass flow rate to be supplied to or removed from the indoor space (which is proportional to the space latent load, $\dot{Q}_{AC}^{lat}$, i.e. $u_0 = \dot{m}_{vap}$), while

$$A_0 = -\dot{m}_v \cdot \omega_{in}, \quad B_0 = \Omega_{in}^{-1}, \quad C_0 = 1 \tag{5.3}$$

It is worth remaking that the choice of these very simplified reference models, one for the temperature dynamics and one for the humidity behaviour, reduces the complexity of the control design without jeopardizing the close-loop performance, whose robustness is guaranteed by the evolution of the adaptive actions aimed to compensate any unmodelled dynamic and parameters mismatch.

Once the nominal models for the temperature and humidity have been selected, it is necessary to impose an appropriate LQ action (see (4.4)) on each of the nominal models whose matrices are given in (5.2) and (5.3), respectively, in order to achieve the optimality of the reference profiles (Step 2). The weight matrices have been selected to impose a settling time of 1 hour avoiding overshoots for a step variation of the reference signal for both temperature and humidity dynamics [102]. Different choices can be obviously made according to different thermohygrometric behaviours to be imposed during transients. Notice that when the optimal reference model is designed it is implemented in the Trajectory Planner block in Figure 3.1.

As it usually occurs when implementing adaptive strategies [24], the scalar quantities modulating the adaptive gains can be heuristically obtained as a tradeoff between convergence time and reactivity of the control action. Here, we select for the temperature control: $\Gamma_\alpha = 50 I_2$, $\Psi_\alpha = 50 I_2$, $\Omega_\alpha = 5 I_2$ and $\gamma = 2$ with I_2 being the identity matrix in $\mathbb{R}^2$; while for the humidity control: $\Gamma_\alpha = 1$, $\Psi_\alpha = 0.1$, $\Omega_\alpha = 0.5$ and $\gamma = 0.01$. For both temperature and humidity controls, $\Gamma_\beta = 10^{-1}\Gamma_\alpha$, $\Psi_\beta = 10^{-1}\Psi_\alpha$ and $\Omega_\beta = 10^{-1}\Omega_\alpha$ are also chosen.

Once the Reference Model is built, the closed-loop dynamics are driven by the adaptive actions according to the block scheme reported in Figure 5.1 (*Step 3*). Here, two separate control loops are designed for the indoor air temperature and humidity, each one with its proper reference model.

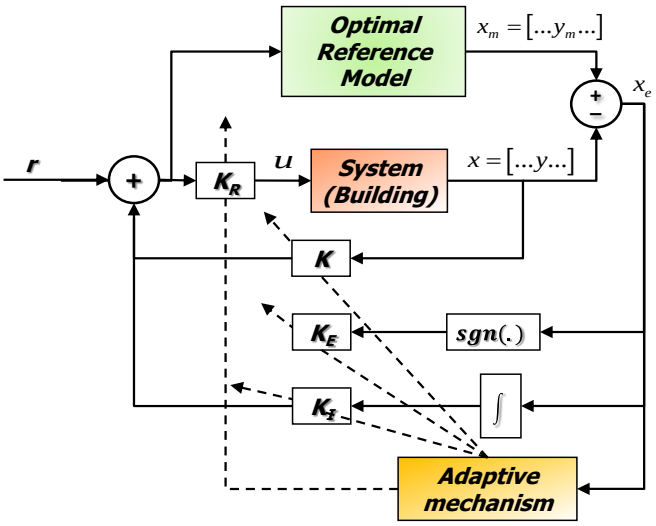

Figure 5.1. Enhanced Model Reference Adaptive Control algorithm with optimal reference dynamics applied to buildings.

With respect to the temperature control, it must be noted that, if wall temperature measurements are not available, the control strategy can be applied by setting to zero the adaptive gains $K_1^I(t)$ and $K_{I1}^I(t)$ in (4.11) for the temperature control-loop. This implementation choice has been already used in the adaptive control literature [145] and the results reported in Section 5.4 show that it does not affect the overall performance of the temperature controller. Furthermore, although humidity and temperature variables are controlled independently by adopting a decoupled approach for the sensible and latent heat, the indoor air specific humidity set point is calculated as a function of the selected indoor air temperature and relative humidity set points, as reported in [146].

5.3 **Case Studies**

In order to show the effectiveness of the proposed approach, the energy analysis is carried out by taking into account several buildings, with different geometry and construction materials, located in diverse weather zones (therefore, they are subjected to different external disturbances due to the variable weather conditions).

The geometry and use of the sample buildings vary as a function of the square meters floor area. In particular, a small size House (48 m^2), a middle size Office (200 m^2) and a large size

Mall (900 m^2) are taken into account. The different building shapes are selected by also considering: *i)* different heat transfer Surface to heated/cooled Volume ratios (S/V); *ii)* different construction materials for taking into account light and heavyweight building envelopes. Details regarding building features and envelope layers are summarized in Figure 5.2, Table 5.1 and Table 5.2. Note that: *i)* the assumptions related to all the building envelope features (e.g. materials thickness in Table 5.1, thermodynamic properties, etc.) are made in agreement to the BESTEST procedure [147], while *ii)* the assumptions made for the House building (S/V ratio, internal sensible heat gains and windows to wall ratio, WWR, calculated only for the South facing walls) are reported in Table 5.2 and refer to BESTEST reference building [147].

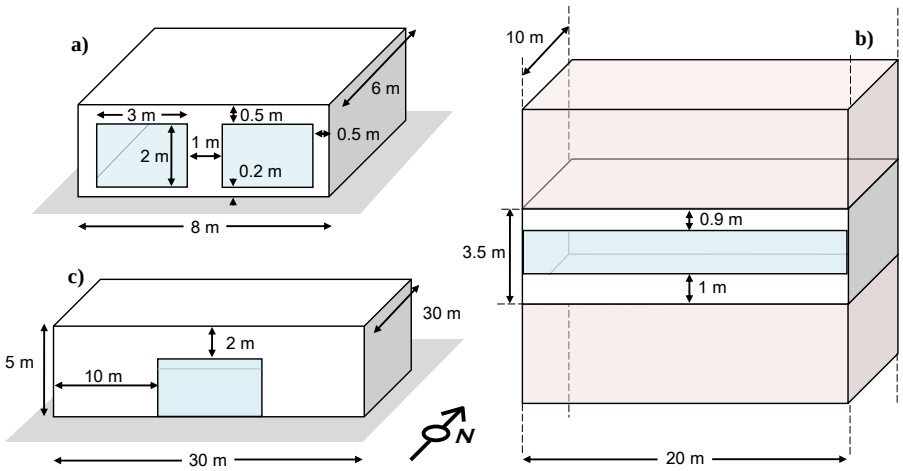

Figure 5.2. Case studies buildings: a) House; b) Office; c) Mall.

Building element	Lightweight envelope		Heavyweight envelope	
	Materials	**Thickness (mm)**	**Materials**	**Thickness (mm)**
wall	Plasterboard	12.0	Concrete block	100
	Fiberglass quilt	66.0	Foam insulation	61.5
	Wood siding	9.0	Wood siding	9.0
roof	Plasterboard	10.0	Identical to the lightweight case	
	Fiberglass quilt	111.8		
	Roof deck	19.0		
floor	Timber flooring	25.0	Concrete slab	80.0
	Insulation	1003	Insulation	1007
window	Glass	4.0	Identical to the lightweight case	
	Air	6.0		
	Glass	4.0		

Table 5.1. Buildings envelope layers (from the inside to the outside).

	Building		
	House	**Office**	**Mall**
Surface to Volume ratio (%)	1.3	0.53	0.30
Window to Wall ratio (%)	55	45	20
Air change (vol/h)	0.5	1	2
Internal sensible heat gains (W/m^2)	4.2	9.4	22.5
Vapour mass flow rate due to people (g/h·p)	40	45	60
WWRs only refer to the South façades. During night time the air change is decreased to 0.5 vol/h and occupancy and internal gains are assumed equal to zero.			

Table 5.2. Simulation assumptions for the investigated buildings.

In this analysis, input climate data (such as outdoor temperature, solar radiation, etc.) vary according to hourly Meteonorm weather data files. In particular, such data refer to 9 weather zones which range from cold winter areas to temperate Mediterranean ones. The Heating and Cooling Degree Days (calculated by assuming a base temperature of 20 °C) as well as the annual Incident Solar Radiation on the horizontal surface (HDD, CDD and ISR, respectively) of each weather zones (sorted for decreasing HDDs) are reported in Table 5.3.

Weather zone	**HDD (Kd)**	**CDD (Kd)**	**ISR (kWh/m^2y)**
Copenhagen	3700	79	988
Denver	2924	740	1832
Freiburg	2894	295	1114
Milan	2519	501	1253
Rome	1507	784	1563
Nice	1454	485	1470
Naples	1279	860	1529
Jerusalem	1214	1031	2093
Athens	1044	1313	1562

Table 5.3. Climatic zones, HDD and CDD indexes and ISR.

The simulation horizon is set at one year in order to cover both the heating and cooling dominated seasons (simulation starts on January 1st and ends on December 31st). Additional building design and operating parameters can be found in [9]. With respect to the comfort analysis, the metabolism of all occupants is set equal to 1.2 Met (light work) during the simulations, while the dressing thermal resistances are set at 1.0 and 0.5 Clo for winter and summer, respectively. Finally, the indoor air velocity varies between 0 and 1.0 m/s according to the building use [34]. As a consequence of combination of buildings and weather zones, the results of this analysis are related to 54 different case studies. For each of them, two different heating and cooling regimes are investigated:

i) *Continuous running* (24/24h all over the year). The indoor air temperature and specific humidity set points are set, as an example, at 20°C and 50% (i.e. specific humidity is set to 7.5 g/kg), respectively. In general, this condition has to be tackled for special kind of

environments where strict thermohygrometric conditions must be always ensured (e.g. medical wards, laboratories, industrial chambers, etc.). This is a strict regulation problem were the set-point has to be guaranteed although the system is subjected to unknown time-varying disturbances, which have to be counteracted;

ii) Intermittent running. The ideal heating and cooling system is intermittently operated in order to combine energy saving with an indoor thermohygrometric quality acceptable for the occupants. Note that the analysis of the impact of operational zoning and operation strategies on both energy consumption and acceptable comfort is behind the scope of the thesis. Therefore, here, only the ability of the proposed approach in Chapter 4 in tracking the desired temperature and humidity profiles (in case of predefined scheduled intermittent operation of the heating and cooling system) is analyzed. Hence, according to a given management policy, the adaptive controllers are active in some temperature/humidity regions depending on the season and the buildings features. Table 5.4 summarizes the exemplar intermittent operation strategy selected in the carried out analysis. The supervisor, modelled as a finite-state dynamical system in Section 3.2, easily implements the activation/deactivation of both the temperature and relative humidity controllers according to the required strategy.

Building	**Winter**				**Summer**			
	Scheduling		**Control deactivation**		**Scheduling**		**Control deactivation**	
			$\boldsymbol{T}$ [°C]	$\boldsymbol{\phi}$ [%]			$\boldsymbol{T}$ [°C]	$\boldsymbol{\phi}$ [%]
House	October 1st to April 30th (24/7)	7:00–18:00	20–33	45–55	May 1st to September 30th (24/7)	14:00–18:00	10–25	45–55
Office		7:00–18:00	20–28	45–55		12:00–18:00	10–25	45–55
Mall		9:00–18:00	20–28	45–55		11:00–18:00	10–25	45–55

Table 5.4. Intermittent operation policy.

An additional investigation is carried out in case of the integration of PCM into the building envelope that has been modelled as in Section 2.2.6. In particular, for the examined buildings, the following layers layouts were investigated:

- House and Mall buildings: a 3 cm PCM layer is integrated in the building roof externally to the thermal insulation layer (between the fiberglass quilt and roof deck, see Table 5.1);
- Office buildings: a 3 cm PCM layer is positioned into the East and West perimeter walls internally to the insulation layer (between the plasterboard and the fiberglass quilt for the lightweight building and between the concrete block and the foam insulation for the heavyweight one, see Table 5.1).

Note that, in the developed case studies each simulated PCM layer refers to a composite material panel, obtained by mixing gypsum with suitable PCM paraffin microcapsules (BASF - Micronal®), whose content is about 42% of the whole mass fraction of the panel. Thermal properties, specific heat, density and conductivity, are accounted by the correlations reported in [90]. In particular, the PCM microcapsules density and conductivity are set equal to 980 kg/m^3 and 0.18 W/mK, respectively. The specific heat of solid and liquid phase is set equal to 2.5 and 2.0 kJ/kgK, respectively, reaching about 28.9 kJ/kgK at the nominal peak melting temperature of 26 °C (note that the transition between solid and liquid phase goes from about 19 to 28 °C). Note that the cooling/solidification curve is shifted of 1 °C towards lower temperatures vs. the melting one [148].

Details about the remaining simulation assumptions are reported in Table 5.2.

5.4 **Numerical Results**

In this section, for the sake of brevity, only results obtained in some exemplar cases, selected among those included in the carried out numerical investigation, are reported. Nevertheless, for the case of the intermittent regime, a more comprehensive numerical analysis is presented, with the purpose to delve deeper into the robustness of the control system with respect to different possible choices of the Reference Model (in terms different modulations of the transient reference trajectories).

As already mentioned, the adaptive algorithm, designed by considering simplified second and first order systems for the temperature and humidity building dynamics, is implemented to tame the dynamics of a detailed physics-based nonlinear model of the building consisting of more than 70 differential equations (as described in Chapter 2). This further confirms the robustness of the control approach against unmodelled dynamics.

At last, the proposed strategy is also compared to a classical PI control algorithm, which is frequently adopted as the common practice for energy building control. The PI gains have been selected as shown in Chapter 3 (see also Section 3.4.2).

5.4.1 *Analysis in continuous running*

The effectiveness of the adaptive control strategy in satisfying strict thermohygrometric requirements, despite of the presence of time-varying disturbances, is confirmed by all the indoor air temperature and humidity mean square root errors calculated with respect to the required set-points over a time horizon of one year. They resulted to be always less than 10^{-3} for every

building use, in every weather zone and for both the light and heavyweight building envelopes. The very good performance for the indoor air temperature and humidity regulations is mainly due to the ability of the control strategy to automatically adapt its gains, in order to tailor its action according to the different scenarios, without any participation of designers/occupants and precise knowledge of environment/building features.

The energy demands required to achieve this fine regulation are reported in Table 5.5 and Table 5.6.

Weather zone	**Mode**	**House**		**Office**		**Mall**	
		Light (kWh/m^{2}y)	**Heavy** (kWh/m^{2}y)	**Light** (kWh/m^{2}y)	**Heavy** (kWh/m^{2}y)	**Light** (kWh/m^{2}y)	**Heavy** (kWh/m^{2}y)
Copenhagen	*H*	156.46	139.38	169.05	160.00	194.49	193.12
	C	-43.13	-26.46	-19.75	-10.45	-3.24	-1.34
Denver	*H*	130.42	96.46	140.70	121.10	170.97	166.90
	C	-96.25	-62.08	-50.00	-30.00	-15.66	-10.90
Freiburg	*H*	135.63	117.50	148.30	137.40	170.41	167.62
	C	-57.08	-38.75	-29.30	-18.00	-8.27	-4.81
Milan	*H*	120.42	102.08	132.25	120.50	152.73	149.27
	C	-72.50	-53.75	-38.70	-26.40	-12.70	-8.46
Rome	*H*	76.88	54.38	89.45	73.85	108.58	104.17
	C	-104.79	-81.25	-57.80	-41.25	-19.98	-14.51
Nice	*H*	71.46	49.79	84.85	69.85	104.29	100.61
	C	-94.79	-72.29	-50.35	-34.40	-14.62	-9.88
Naples	*H*	71.88	51.67	84.75	70.35	101.99	97.63
	C	-103.33	-82.29	-57.85	-42.35	-20.94	-15.47
Jerusalem	*H*	65.8	38.96	77.80	57.85	95.64	89.13
	C	-132.08	-104.17	-75.20	-54.20	-27.52	-19.83
Athens	*H*	54.79	38.54	66.40	55.00	81.66	78.02
	C	-119.38	-101.67	-69.40	-56.75	-30.98	-26.09

Table 5.5. Continuous running: sensible (heating (*H*) and cooling (*C*)) energy demands.

Here, results about sensible and latent heating and cooling demands for all the investigated buildings (House, Office and Mall) and envelope thermal inertia (light and heavy) are summarized. Note that the weather locations are sorted in descending order of HDDs. By analyzing such data, related to the continuous running regime, several conclusions can be pointed out: *i)* the lower the HDDs, the lower the building heating demands (a decreasing trend is not strictly detected because of the effect of heat gain due to the solar radiation); *ii)* the envelope thermal inertia has a significant effect on the calculated building sensible heating and cooling requirements (the higher the mass of the envelope, the lower the heating and the cooling demands); *iii)* in general, the higher the HDDs, the lower the difference between light and heavy envelope requirements. Obviously, as expected latent requirements are not influenced by the building thermal inertia.

Weather zone	Mode	House		Office		Mall	
		Light (kWh/m^{2}y)	**Heavy** (kWh/m^{2}y)	**Light** (kWh/m^{2}y)	**Heavy** (kWh/m^{2}y)	**Light** (kWh/m^{2}y)	**Heavy** (kWh/m^{2}y)
Copenhagen	*H*	3.79	3.79	3.83	3.82	2.64	2.64
	C	-25.98	-25.97	-25.65	-25.65	-28.87	-28.87
Denver	*H*	3.42	3.41	3.51	3.51	2.58	2.58
	C	-33.54	-33.54	-33.21	-33.21	-37.59	-37.60
Freiburg	*H*	5.48	5.47	5.59	5.58	3.97	3.96
	C	-22.99	-22.99	-22.66	-22.66	-25.58	-25.59
Milan	*H*	14.60	14.60	14.79	14.78	12.40	12.39
	C	-18.99	-18.99	-18.73	-18.73	-21.13	-21.13
Rome	*H*	19.39	19.38	19.71	19.70	16.73	16.72
	C	-10.86	-10.86	-10.70	-10.70	-13.08	-13.08
Nice	*H*	17.37	17.36	17.60	17.59	14.67	14.66
	C	-11.84	-11.84	-11.68	-11.68	-14.15	-14.15
Naples	*H*	22.28	22.26	22.58	22.56	19.49	19.48
	C	-9.87	-9.87	-9.69	-9.70	-11.90	-11.90
Jerusalem	*H*	22.60	22.59	23.06	23.05	19.75	19.74
	C	-8.08	-8.08	-7.94	-7.94	-10.20	-10.20
Athens	*H*	15.21	15.19	15.56	15.54	12.31	12.29
	C	-8.68	-8.68	-8.55	-8.55	-10.77	-10.77

Table 5.6. Continuous running: latent (heating (H) and cooling (C)) energy demands.

5.4.2 *Analysis in intermittent running*

In this section some results, exemplar with respect to the energy building dynamic behaviour, are presented. The first aspect to be discussed concerns the transient dynamic at the switching on of the heating and cooling system, as it is scheduled in Table 5.4. Note that such table also reports the control deactivation ranges, comprised by the indoor air temperature and humidity set points, which change, according to the selected schedules, from the winter (heating dominated) to the summer (cooling dominated) season and vice versa.

In order to analyze the dynamics of indoor air temperature and humidity, several figures are presented. In particular, Figure 5.3 shows the time history of the indoor air temperature and relative humidity during the winter season (360th day of the year) for a Mall building located in the weather zone of Rome. The switching on policy of the heating and cooling system depends on the transient time allowed to reach the thermohygrometric comfort conditions. In this analysis, we assumed that such conditions must be reached one hour after the activation of the heating and cooling plant. As shown in Figure 5.3, both the thermohygrometric variables exactly track their reference behaviour, designed (through the Reference Model) to ensure a smooth transition during transient operations, which goes from the occurring initial air temperature and humidity levels towards the admissible thermohygrometric conditions (corresponding to the deactivation of the temperature and humidity control, as reported in Table 5.4).

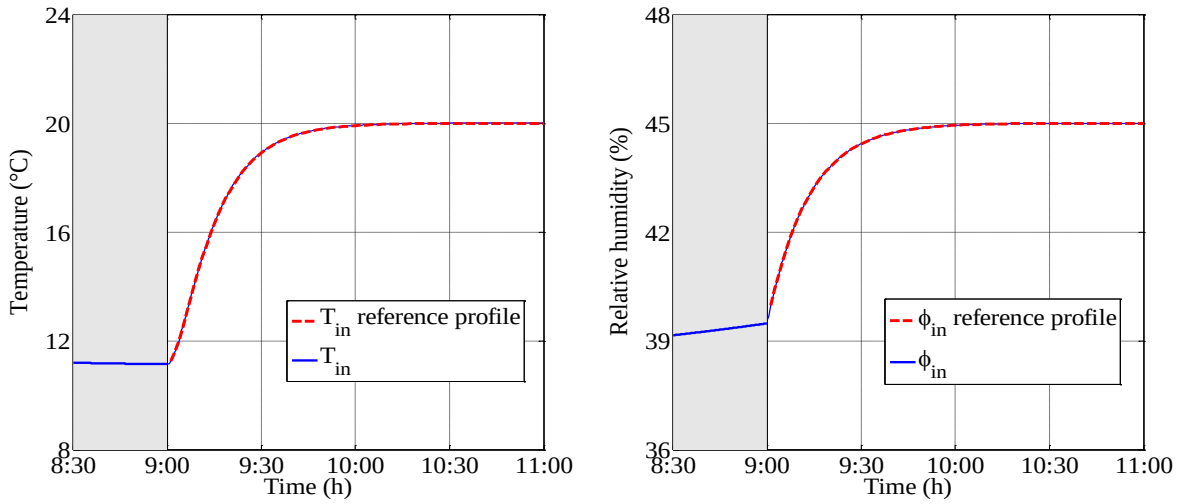

(a) **(b)**

Figure 5.3. Winter season, 360th day of the year. Transient dynamics of (a) indoor air temperature and (b) indoor air relative humidity. Mall building - Rome.

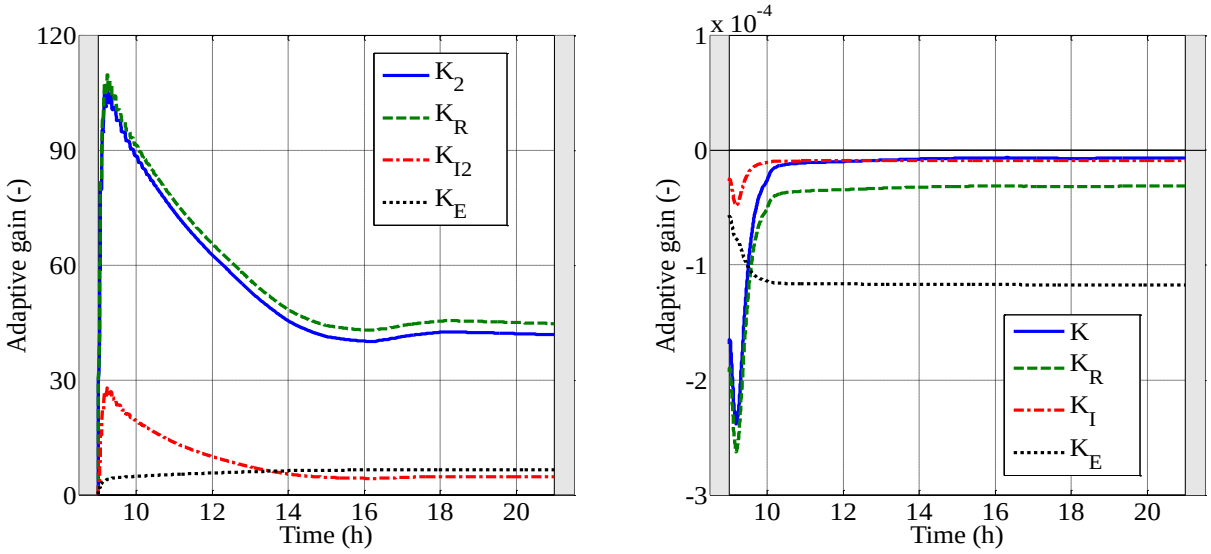

(a) **(b)**

Figure 5.4. Winter season, 360th day of the year. Time history of the evolution of the adaptive gains within the: (a) temperature control loop and (b) humidity control loop. Mall building – Rome.

The resultant bounded dynamic behaviour of the adaptive gains is reported in Figure 5.4 for both the indoor temperature and humidity loops. Similar results are achieved also in the remaining investigated weather zones, where the thermohygrometric conditions reach the different boundaries of the operational zone depending on the different initial conditions. An example is depicted in Figure 5.5 for light and heavyweight Mall buildings located in four different weather zones. For such zones, the indoor air dynamic routes (from point 1 to point 2)

on the psychrometric chart are shown in Figure 5.6. Note that, through the temperature and humidity profiles assigned by the control Reference Model, the selected thermohygrometric comfort domain (area delimited by the magenta dashed line in Figure 5.6) is always reached for any initial indoor air condition (points 1).

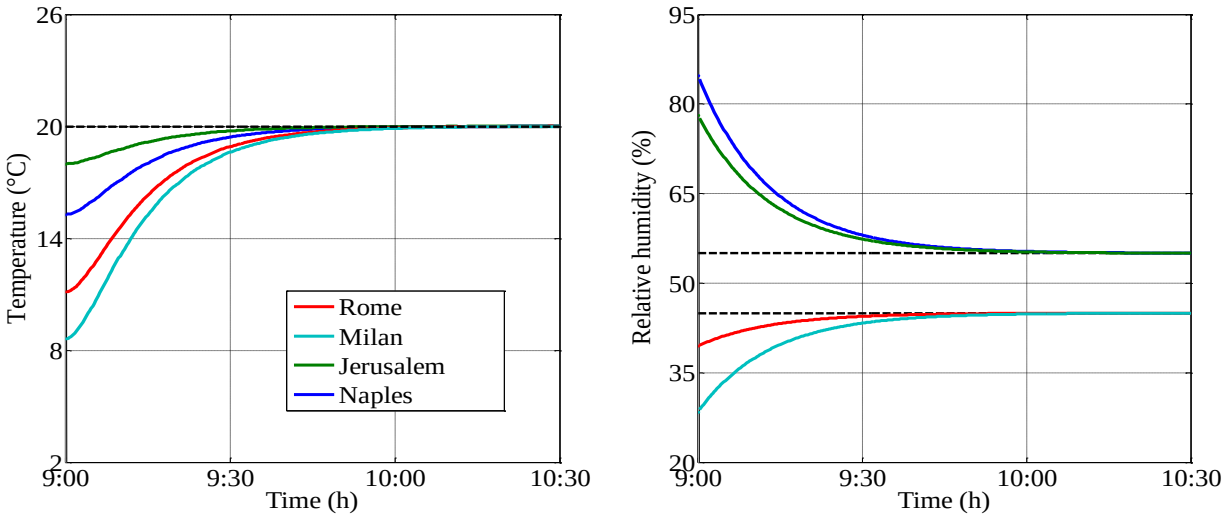

Figure 5.5. Winter season. Transient dynamics of (a) the indoor air temperature and (b) indoor air humidity. Lightweight Mall building - Naples and Jerusalem (290th day of the year), heavyweight Mall building - Rome and Milan (360th day of the year).

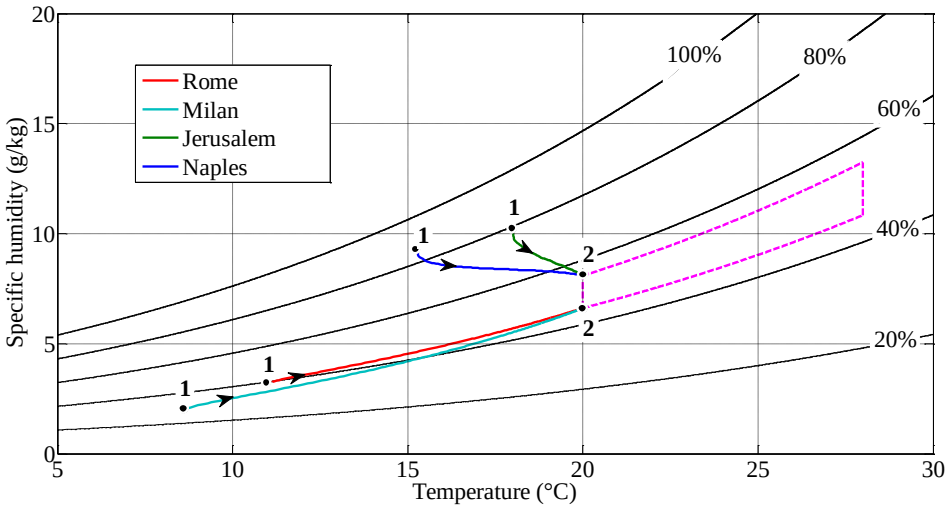

Figure 5.6. Winter season. Indoor air routes on the psychrometric chart for Mall buildings. Lightweight building - Naples and Jerusalem (290th day of the year), heavyweight building - Rome and Milan (360th day of the year).

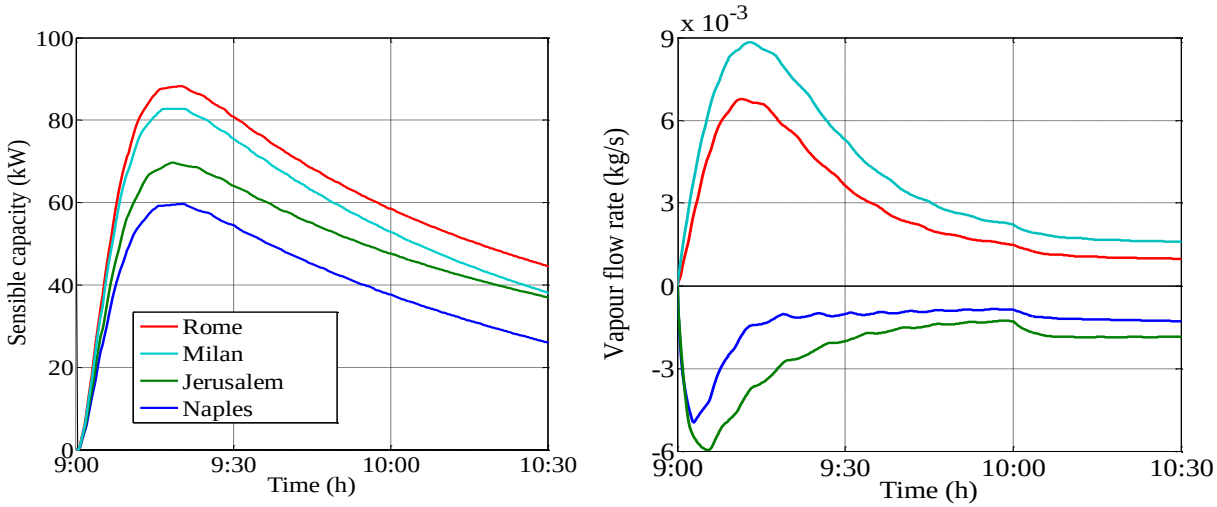

Figure 5.7. Winter season. Time history of the control actions at the control activation (a) sensible load and (b) water vapour mass flow rate. Lightweight Mall building - Naples and Jerusalem (290th day of the year), heavyweight Mall building - Rome and Milan (360th day of the year).

Furthermore, for all the case studies, the boundedness of the adaptive gains implies the boundedness of the control actions, obtained by modulating the sensible heating (or cooling) system capacity and the water vapour mass flow rate (to be added to or subtracted from the indoor space), indoor space), as shown, for example, in Figure 5.7 for the Mall building in the same weather conditions of Figure 5.5 and Figure 5.6. Note that the control signals, tailored by the adaptive actions, satisfy the physical constraints and always result within the selected region of admissible thermohygrometric variables.

In Figure 5.8, for heavyweight House buildings located in several cold winter zones, the performance of the closed-loop system is shown over a set of sample days, related to scheduled changes of the selected indoor air temperature set points (winter to the summer season, occurring at the 120th day of the year) according to the management policy in Table 5.4.

Results refer to the exemplar case of heavyweight House buildings located in several cold winter regions. The white areas reported in Figure 5.8 are related to hours during which the heating and cooling system is switched on, if necessary. Results clearly show the decoupling of the indoor air temperature and relative humidity control loops. For example, at the 120th day of the year and for the case study related to the house located in Freiburg, in order to guarantee the desired comfort level it is sufficient to regulate only the relative humidity, while the indoor air temperature is free to float (no control is required). The remaining grey shaded regions in Figure 5.8 refer to hours during which the control system is scheduled as inactive and in which free floating indoor air temperature and humidity are obtained.

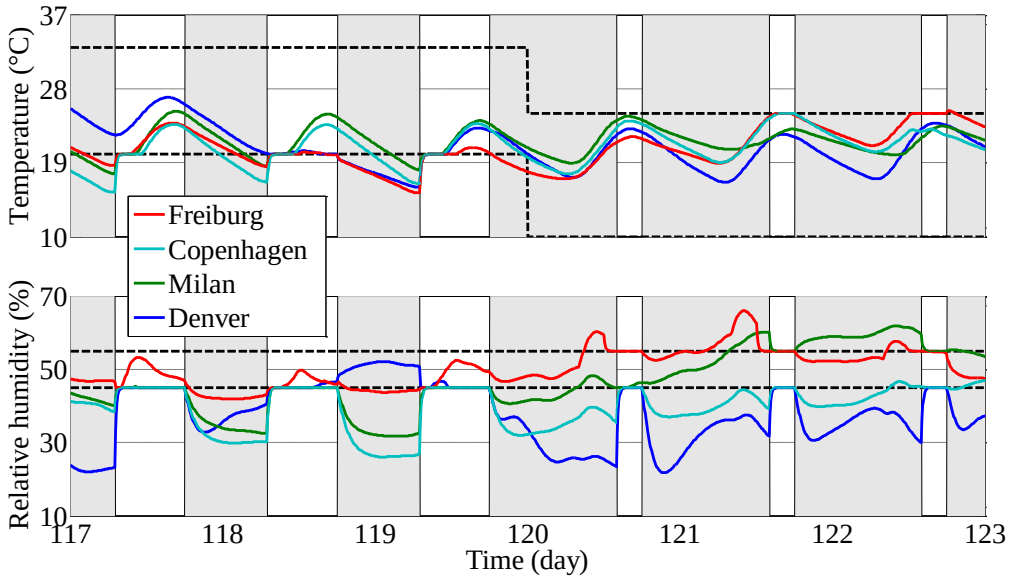

Figure 5.8. Heavyweight House buildings in cold winter regions. Time history of indoor air temperature and relative humidity (scheduled controls depend on the winter and the cooling seasons, Table 5.4). The dashed lines delimit the free floating region.

Closed-loop performance are also provided for lightweight Office buildings located in several hot summer zones. Results, reported in Figure 5.9, refer to a set of sample days related to scheduled changes of the selected indoor air temperature set points (summer to winter the season, occurring at the 273th day of the year) according to the management policy in Table 5.4. Again, results show how the control strategy suddenly reacts, once it is activated, recovering the required indoor conditions after the night stop. Moreover, it is evident that the control action is able to automatically adapt to the very different conditions and to tame the thermohygrometric dynamics only when it is necessary (as a function of the weather zone and the indoor conditions). Note that also in this case, the very low mean squared errors (always lower than 10^{-3} for all the analyzed cases) highlight the control effectiveness.

The calculated energy demands are reported in Table 5.7 and Table 5.8. Here, the building sensible and latent, heating and cooling, demands for all the investigated buildings and envelopes in case of the intermittent regime are reported. Similarly to Table 5.5 and Table 5.6 for the continuous regime, in Table 5.7 and Table 5.8 the obtained results are sorted in descending order of the investigated weather locations HDDs. From the analysis of these tables, several considerations can be underlined. For example, as for the continuous running, the lower the HDD, the lower the building heating demand (although a strictly decreasing trend cannot be detected because of the solar radiation effects). For severe cold climates (very high HDDs and low ISR), the higher the thermal inertia, the higher the heating demands.

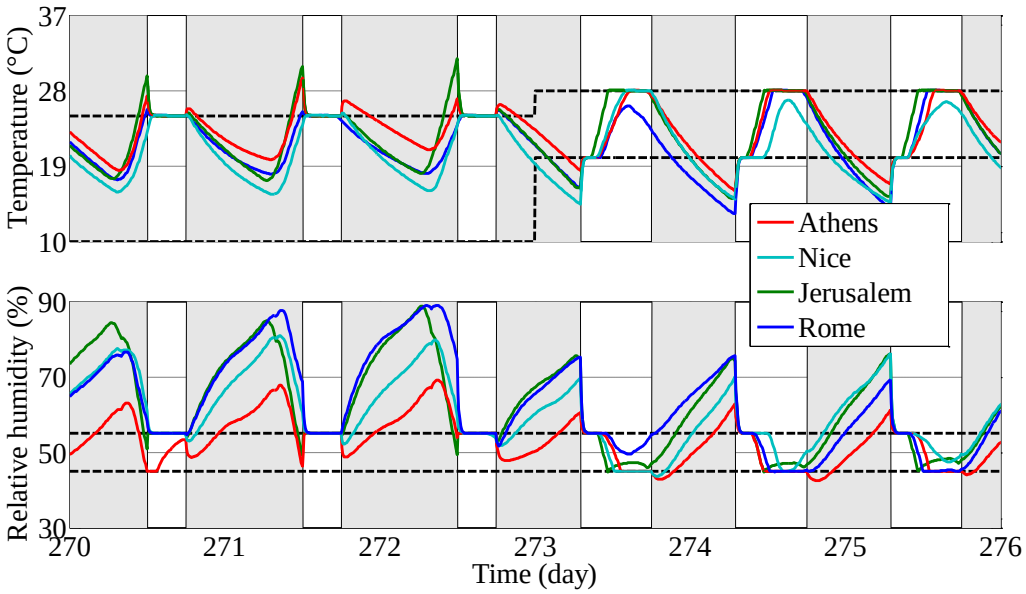

Figure 5.9. Lightweight Office buildings in hot summer regions. Time history of indoor air temperature and relative humidity (scheduled controls depend on the winter and the cooling seasons, Table 5.4). The dashed lines delimit the free floating region.

Weather zone	Mode	House		Office		Mall	
		Light (kWh/m²y)	**Heavy** (kWh/m²y)	**Light** (kWh/m²y)	**Heavy** (kWh/m²y)	**Light** (kWh/m²y)	**Heavy** (kWh/m²y)
Copenhagen	*H*	57.75	73.71	64.31	83.30	77.66	96.60
	C	-16.71	-5.46	-6.58	-0.57	-0.32	0.00
Denver	*H*	37.94	35.88	43.96	53.62	62.10	82.81
	C	-32.71	-14.54	-19.25	-6.50	-5.81	-1.65
Freiburg	*H*	49.46	60.13	56.04	70.72	66.45	83.65
	C	-23.19	-10.50	-11.64	-3.42	-2.24	-0.22
Milan	*H*	44.88	52.90	51.01	63.99	60.94	77.78
	C	-30.40	-18.04	-17.61	-7.74	-4.49	-0.99
Rome	*H*	21.94	19.10	27.94	31.44	36.07	47.86
	C	-41.83	-26.54	-27.30	-14.36	-8.72	-4.06
Nice	*H*	20.44	16.21	26.30	28.72	33.40	44.45
	C	-36.83	-22.73	-22.34	-10.90	-5.44	-1.63
Naples	*H*	20.44	18.10	26.52	29.45	32.85	43.61
	C	-41.83	-27.02	-27.93	-15.49	-9.53	-4.46
Jerusalem	*H*	14.04	9.40	19.31	19.46	26.63	36.58
	C	-53.85	-30.60	-37.09	-18.60	-11.82	-4.50
Athens	*H*	15.73	11.83	21.07	22.42	26.44	34.51
	C	-48.54	-35.10	-34.92	-23.66	-16.54	-11.52

Table 5.7. Intermittent running: sensible (heating (H) and cooling (C)) energy demands.

Conversely, for low HDDs, the lighter the building envelope, the higher the heating demands in case of House buildings, and the lower the heating demands in case of Office and Mall buildings. This dissimilar behaviour is justified by the higher outdoor air infiltration rate adopted in Office and Mall buildings (selected according to their non-residential usage). In other words,

higher air infiltration rates cause an increase of the external solicitation effect (due to the outdoor ambient temperature) on the indoor air condition, resulting in a trend (i.e. thermal inertia vs. heating demand) similar to that one observed in higher HDDs weather zones. On the other hand, a decrease of the calculated cooling demands is always observed by shifting from the light to the heavyweight envelope, for all the investigated buildings and weather zones. Finally, differently from the continuous running regime, a remarkable effect of the building thermal inertia is observed also for the latent energy requirements. Note that in the developed model the air humidity is dependent on the air temperature and independent of the building envelope mass.

Weather zone	**Mode**	**House**		**Office**		**Mall**	
		Light (kWh/m^2y)	**Heavy** (kWh/m^2y)	**Light** (kWh/m^2y)	**Heavy** (kWh/m^2y)	**Light** (kWh/m^2y)	**Heavy** (kWh/m^2y)
Copenhagen	*H*	9.90	5.66	8.53	5.85	8.86	6.94
	C	-0.96	-0.68	-1.12	-1.62	-2.62	-3.69
Denver	*H*	22.27	10.88	15.30	9.93	14.28	12.32
	C	-0.71	-0.43	-0.68	-0.78	-1.40	-1.49
Freiburg	*H*	10.40	5.07	8.57	5.12	8.23	6.07
	C	-1.36	-1.07	-1.29	-1.73	-2.42	-3.30
Milan	*H*	10.40	3.92	7.88	4.12	7.32	4.93
	C	-3.37	-2.91	-3.75	-4.25	-5.58	-6.50
Rome	*H*	9.85	1.80	5.73	1.59	3.80	2.25
	C	-4.52	-3.61	-4.65	-5.03	-6.32	-7.35
Nice	*H*	10.22	2.04	5.41	1.71	4.22	2.47
	C	-3.75	-2.88	-3.82	-4.26	-5.48	-6.47
Naples	*H*	8.39	1.74	5.10	1.38	3.52	1.86
	C	-5.06	-4.17	-5.62	-6.19	-7.68	-8.60
Jerusalem	*H*	9.68	2.38	4.80	0.92	2.43	1.43
	C	-5.02	-3.66	-5.30	-5.36	-6.94	-7.87
Athens	*H*	8.55	1.90	3.86	1.16	2.93	1.65
	C	-3.25	-2.61	-3.28	-2.74	-2.72	-3.04

Table 5.8. Intermittent running: latent (heating (H) and cooling (C)) energy demands.

In modern smart buildings the thermohygrometric comfort requirements must be accurately fulfilled. Therefore, in order to analyze the system performance with respect to this target, the time histories of PMV, PPD and mean thermal radiant temperature, T_{mr}, (see Section 2.3), are assessed all over the year. For the investigated case studies, such analysis showed that good PMVs and PPDs are always and everywhere achieved. While this result is obvious for the case of continuous running conditions, simulation results confirm the capability of the proposed approach to restore high comfort levels (lost during control deactivation intervals because of the change of the external conditions and the variable internal thermal loads) also for the intermittent regime. In this paragraph, the thermal comfort performance is discussed by means of several

figures related to different sample days, simulated buildings and weather locations. In particular, Figure 5.10 and Figure 5.11 show the thermal comfort (described by means of PMV, PPD and T_{mr}) related to the simulated Mall buildings located in some weather zones with cold winters and hot summers.

Specifically, Figure 5.10 refers to several winter days, ranging from January 16th to 22nd, related to heavyweight buildings located in Freiburg, Copenhagen, Milan and Denver. Here, it is clearly shown that during the steady state regime (subsequent to the switching on transient time), very good PMVs (always included between -0.5 and 0) and PPDs (always less than the 10%) are achieved, despite of rather low T_{mr}. Such low temperatures basically depend on the occurring building envelope features (the adopted high U-values and low masses are selected according to the BESTEST assumptions [147]). As a result, during the night, the lower the outdoor ambient temperature (e.g. Denver), the lower the mean radiant one and, consequently, the lower the thermal comfort level (e.g. on January 20th low PMVs and very high PPDs occur).

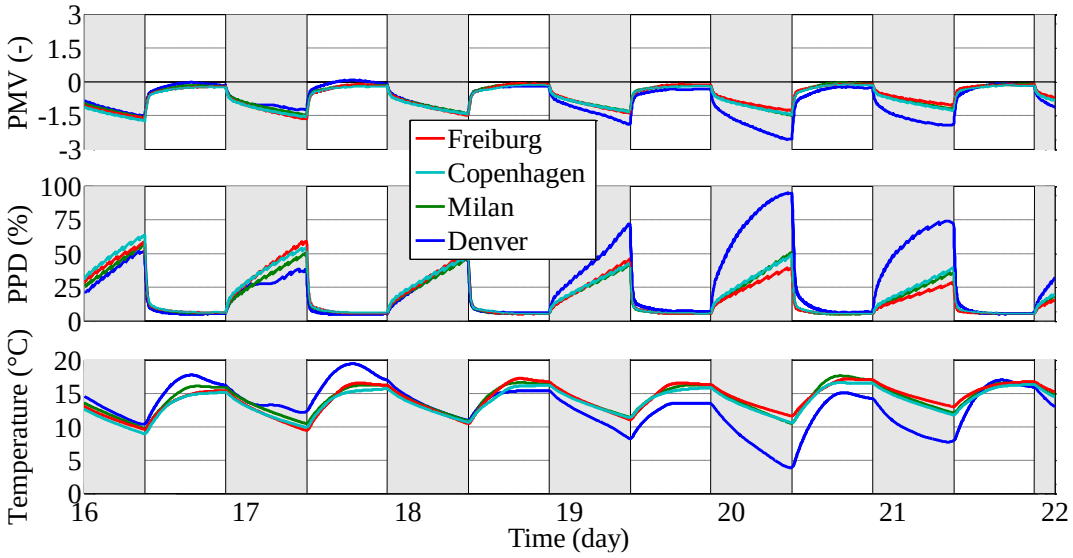

Figure 5.10. Heavyweight Mall buildings in cold winter zones. Time history of PMV, PPD and T_{mr}.

Similar results are obtained during the summer season, as shown in Figure 5.11. Such figure refers to the days ranging from July 21nd to 26th (i.e. 202nd - 207th days of the year) and to the lightweight Mall buildings located in Athens, Nice, Jerusalem and Rome. Here, as a result of the optimal performance of the control actions, good PMVs (always included between 0 and 0.75) and PPDs (always less than the 20%) are obtained during the steady state regime. The mean radiant temperatures, T_{mr}, of the buildings envelopes are highly fluctuating during control deactivation intervals, due to the low thermal inertia of the simulated lightweight buildings. The comfort analysis is completed through Figure 5.12 and Figure 5.13.

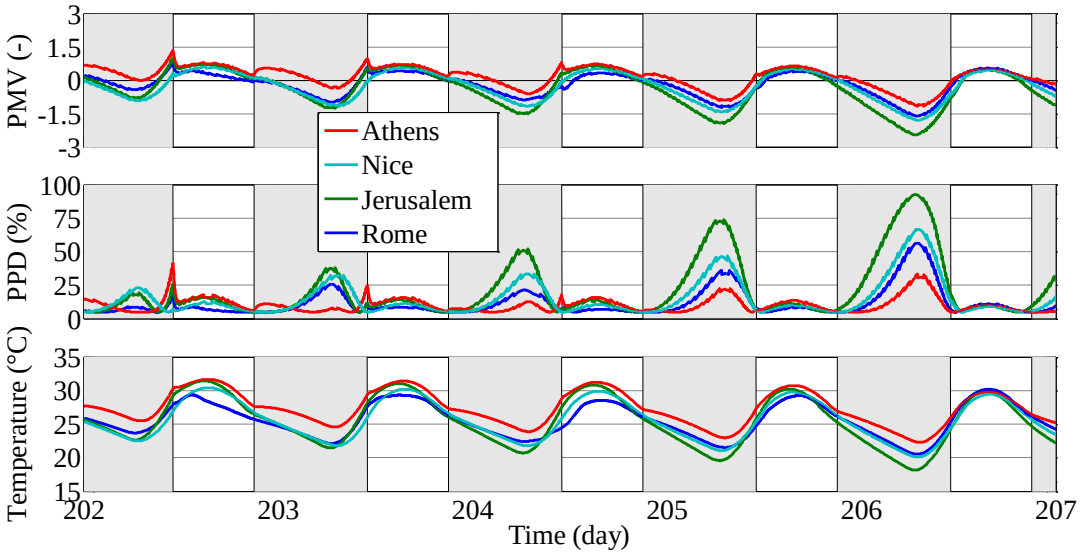

Figure 5.11. Lightweight Mall buildings in hot summer zones. Time history of PMV, PPD and T_{mr}.

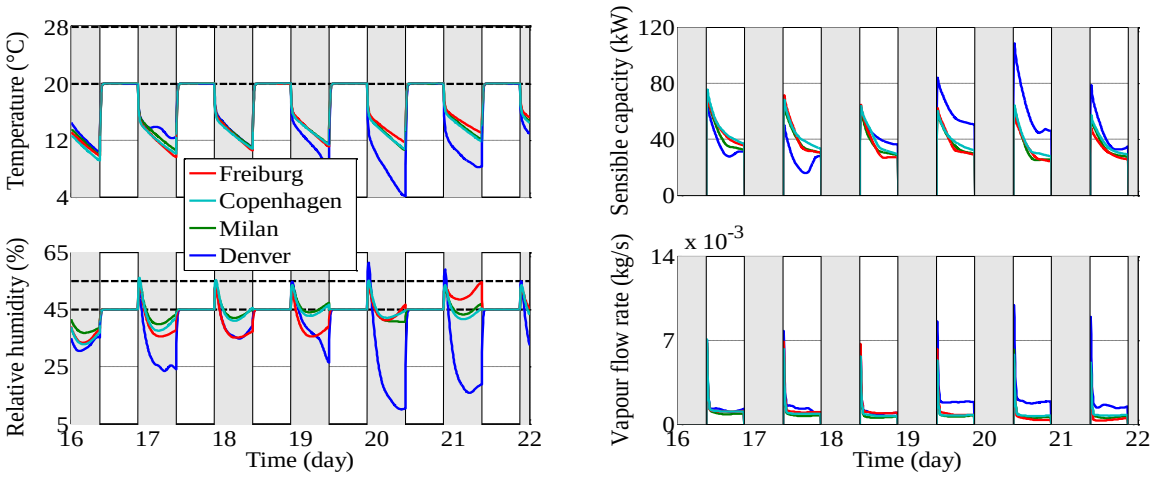

(a) **(b)**

Figure 5.12. Heavyweight Mall buildings in cold winter zones. Time history of (a) indoor air temperature, relative humidity and (b) sensible load and water vapour mass flow rate.

Here, we show the dynamic trends of the indoor air temperature and relative humidity, as well as of the related control actions (sensible heating/cooling and water vapour mass flow rate added to/subtracted from the space). Such analysis takes into account the same weather zones, buildings, and weather conditions investigated in Figure 5.10 and Figure 5.11. Specifically, Figure 5.12 refers to several cold winter days in Freiburg, Copenhagen, Milan and Denver and to heavyweight Mall buildings, while Figure 5.13 is referred to some hot summer days in Athens, Nice, Jerusalem and Rome and to lightweight Mall buildings. In these figures it is possible to

observe a proportional dependence of the control actions occurring in the investigated weather conditions.

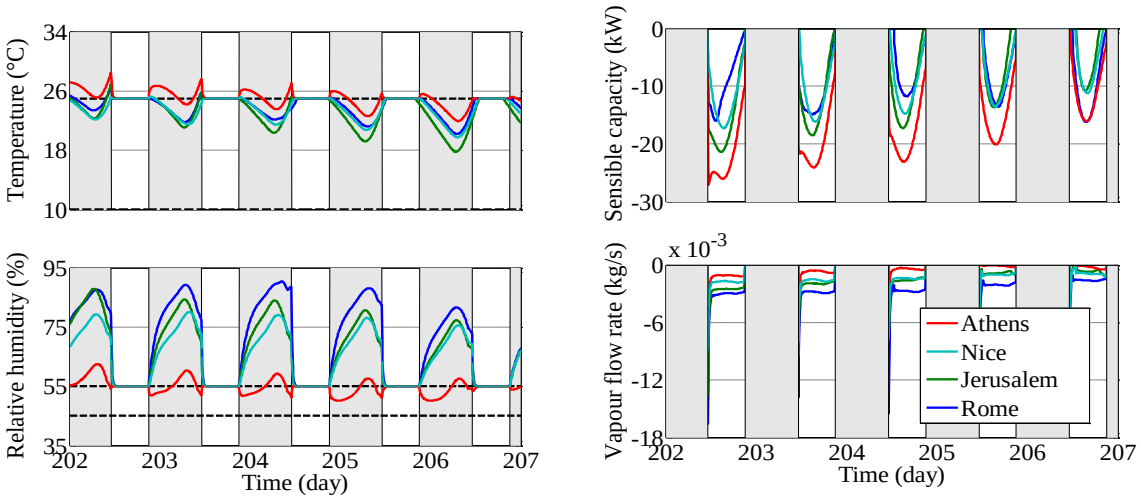

(a) **(b)**

Figure 5.13. Lightweight Mall buildings in hot summer zones. Time history of (a) indoor air temperature, relative humidity and (b) sensible load and water vapour mass flow rate.

As an example, in Figure 5.12 is clearly shown that the lower the indoor air temperature (during the heating system switching off) the higher the sensible heating necessary at the control activation (e.g. Denver day 20th). A similar result can be observed in case of hot summer days, as shown in Figure 5.13. Note that, according to the simulated weather conditions, the magnitudes of the control actions, necessary to reach the desired transient dynamics and to achieve the imposed set points and comfort levels, are fairly different and depend on the specific case study. For example, the sensible cooling demand in Rome is about half of the Athens one. According to the adopted thermohygrometric model, such conclusions can be also observed for the control actions related to the indoor air humidity control (i.e. water vapour mass flow rate). In fact, the farther the indoor air humidity from the set points, the higher the humidification/dehumidification requirements. In Rome, the water vapour mass flow rate to be subtracted from the indoor space doubles those calculated for Nice and Jerusalem, Figure 5.13.

Finally, note that, due to low thermal inertia of the investigated buildings and the adopted design and operating assumptions, in day hours during which the system control is switched off (grey regions of the above discussed figures), both the indoor air temperature and the relative humidity are averagely far from the related selected set points.

5.4.3 *Energy and comfort analysis for different choices of the reference models*

As above discussed, the reference trajectories can be modulated by opportunely choosing the weight parameters of the cost function (4.3). These parameters balance the tradeoff between control reactivity and control effort. According to the LQ control theory [23], different optimal transient behaviours can be indeed associated to different choice of the values assumed by the parameter *R* in (4.3) that weighs the control effort, i.e., the sensible and latent loads in the case of the control of indoor air temperature and humidity, in the computation of the cost function. Roughly speaking, by reducing the *R*-parameter, the LQ optimization provides a greater control effort without altering the value of the final cost (4.3). As a consequence, the reference set point can be reached with a smaller relaxation time. On the contrary, by increasing *R*, high control efforts have a severe impact on the final cost (4.3). Hence, the LQ procedure yields a more moderate control effort at the expense of a larger settling time. In so doing, the *R*-parameter can be exploited to calibrate the dynamic performance of the close-loop system. To better illustrate this feature, results for different choices of the *R*-parameter in the temperature and relative humidity control loops are shown for two heavyweight House buildings located in Denver and Rome. For Denver the transient evolution of indoor air temperature and relative humidity as well as of the related control actions (when control is activated according to the intermittent strategy, see Table 5.4) is reported for a sample winter day (January 2nd) in Figure 5.14.

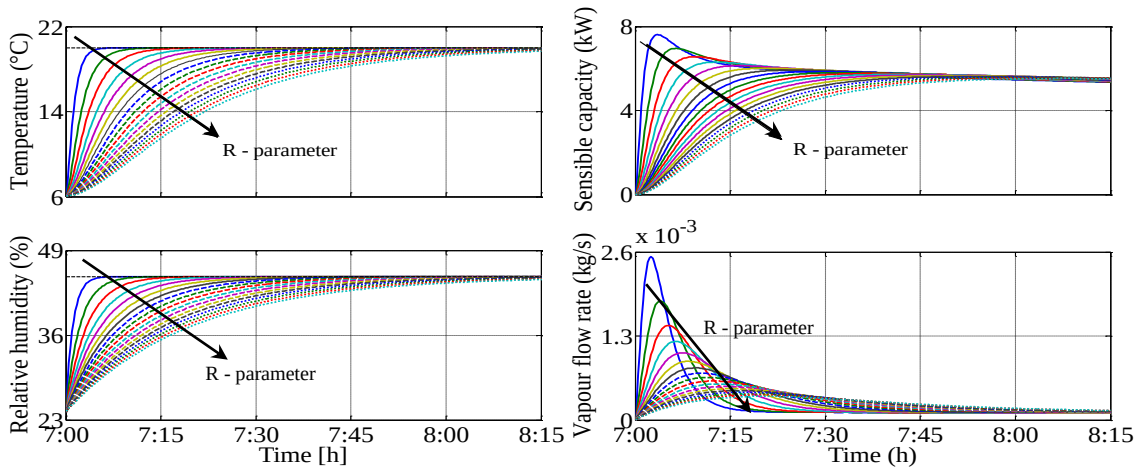

Figure 5.14. Heavyweight House building in Denver. Transient dynamics of (a) indoor air temperature, relative humidity and (b) sensible load and water vapour mass flow rate at the control switching on for different choices of the Reference Model.

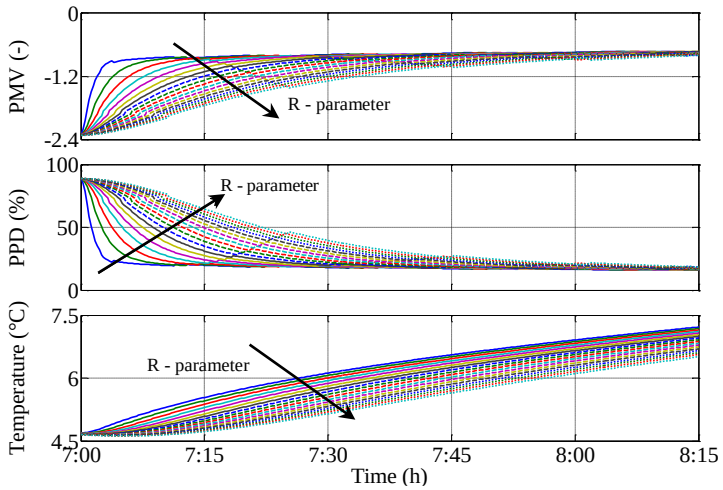

Figure 5.15. Heavyweight House building in Denver. Time history of PMV, PPD and T_{mr} at the control switching on for different choices of the Reference Model.

As expected, to lower values of the *R*-parameter corresponds a faster behaviour (in terms of both settling and rise time), but the price to be paid for an increase of control reactivity is the necessity of a higher control effort to be supplied (i.e. a higher energy consumption), as shown by the depicted sensible heating and water vapour mass flow rate added to the indoor space (as a function of *R*). For the same sample day, the results of the comfort analysis are shown in Figure 5.15. Here, it is possible to observe that the choice of the *R*-parameters clearly affects the comfort level of occupants. Note that, for each value of *R* the achievement of a satisfactory comfort level (detected by suitable PMVs and PPDs) is obtained in different time intervals from the instant of heating and cooling system switching on (for the selected time range T_{mr} is always very low).

In Figure 5.16 and Figure 5.17 the results of a similar investigation for a sample summer day in Rome (July 18th) are shown.

The tuning of the *R*-parameter provides to designers a degree of freedom for selecting the dynamic behaviour and the comfort level to be imposed to the system with respect to the energy demands. In other words, as a function of the building usage, suitable *R*-parameters (which influence the dynamics of the indoor air temperature and humidity) must be selected. In general, the selection of a suitable combination of values of the *R*-parameter in the temperature and humidity control loops has to be done for each building use by taking into account the minimum time in which a certain comfort condition must be reached. Obviously, such choice has a remarkable effect on the building dynamics as well as on the indoor comfort, as shown in Figure 5.14, Figure 5.15, Figure 5.16, and Figure 5.17. In this regard, through the simulation code, it is possible to provide and/or create suitable maps containing many combinations of the values to be

assumed by the *R*-parameter, which allow achieving different comfort levels starting by various temperature and humidity initial conditions. As a result, by means of such maps, the minimization of the sensible and latent energy requirements, given the desired comfort level, can be carried out by selecting the appropriate combination of the values assumed by the *R*-parameter for the temperature and humidity control loops.

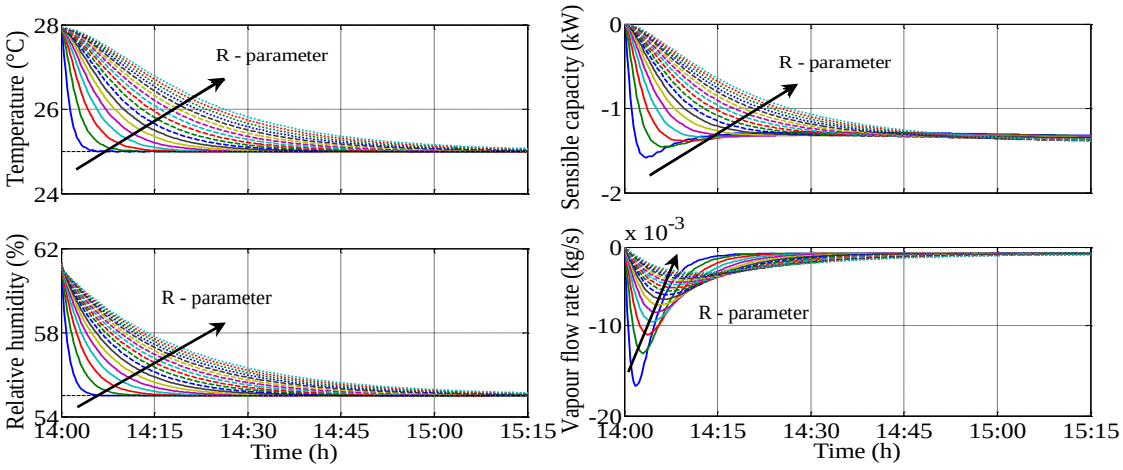

(a) **(b)**

Figure 5.16. Heavyweight House building in Rome. Transient dynamics of (a) indoor air temperature, relative humidity and (b) sensible load and water vapour mass flow rate at the control switching on for different choices of the Reference Model.

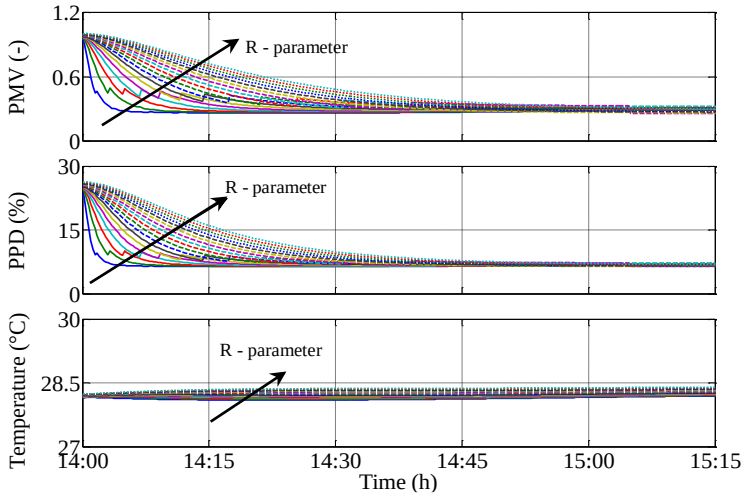

Figure 5.17. Heavyweight House building in Rome. Time history of PMV, PPD and Tmr at the control switching on for different choices of the Reference Model.

5.4.4 *A brief comparison with the PI algorithm*

In the control literature [149], the adaptive controllers are well known to be very effective to handle situations in which the parameter variations and environmental changes are frequent. Although this is especially true when adaptive controllers are compared to conventional fixed

gain controllers, as PID, in this section we briefly compare the LQ-EMRAC scheme with the optimal PI controller proposed in Chapter 3 (see also [98]). It is worth nothing that here an accurate tuning of PI action can improve steady state performances by reducing the steady state errors, whereas PD controller may improve transient period by reducing the maximum overshoot. Nevertheless, the adaptive controllers have the major advantage, with respect to PID ones, of maintaining constant dynamic performance in presence of unpredictable and immeasurable variations, as well as to improve and to shape opportunely the entire dynamic characteristic of the system under control, making the plant dynamics as close as possible to the reference model. To show this feature in the case of the thermohygrometric control, we applied both strategies to the case of the lightweight Office building located in Denver during a sample winter day. Note that the PI control was previously optimally tuned with respect the heavyweight Office building model (while the LQ-EMRAC controller does not have precise knowledge of the building features, such as building shape, envelope materials, etc.).

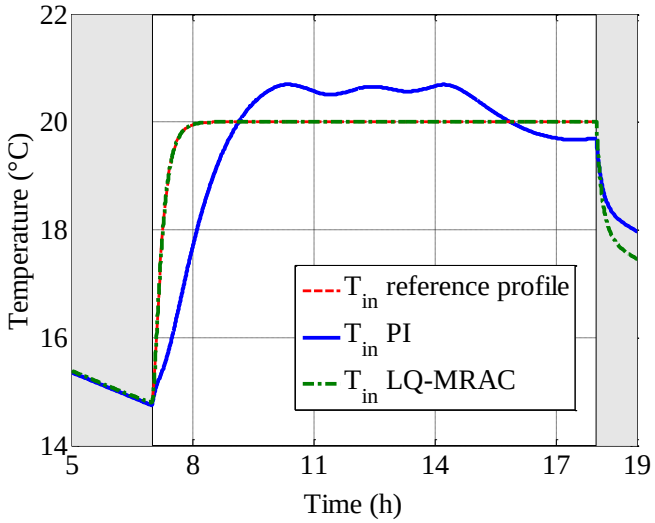

Figure 5.18. Lightweight Office building in Denver (at December 1st). Comparison among the time histories of the indoor air temperatures obtained by PI and LQ-EMRAC control schemes.

Despite of this, the worsening PI control performance, compared to the adaptive scheme, is clearly visible in Figure 5.18, where the time-histories of the indoor air temperatures are reported for both the controllers. In such figure, it is possible to observe that the PI control is not able to accurately overlap the temperature set-point of 20 °C.

To better understand this loss of performance we have computed for the heavyweight Office building model located in Denver the phase margin and the crossover frequency of the closed loop system when the PI strategy is used to impose the required temperature dynamics (see [96] for the definition of such quantities). These performance indexes have been computed both when the PI gains are tuned according to the optimization procedure proposed in Section 3.3 and in the

case these gains are selected by using the Ziegler–Nichols rule [116]. As the Ziegler–Nichols PI gains have been chosen as initial guess for the optimization procedure in Section 3.3, the aim is to evaluate the effect of the optimization method on the phase margin and the crossover frequency. We recall here, for the sake of completeness, that some relevant features, like robustness and settling time (i.e., the time required for the output to track the desired reference input) of classical closed loop control systems embedding linear controllers with fixed gains can be assessed by computing such performance indexes [96]. In particular the phase margin, say ψ_m (deg), can be used to evaluate both closed loop stability and the magnitude of the oscillatory response to step variations of the input to the control system [96]. Specifically, a negative value of this parameter indicates that the closed loop system is unstable; low values (up to 35°) imply the presence of oscillations in the step response which cannot be neglected and small robustness to plant parameter variations and unmodelled dynamics, e.g., delays; while high values of ψ_m provide step responses of the closed loop system without overshoots and more robustness to uncertainty. Instead the crossover frequency, say ω_c, can be used to get some information about the closed loop "readiness" as $\tau_s \propto 4.6/\omega_c$, with τ_s being the closed loop settling time. Hence, higher values of the crossover frequency corresponds to smaller settling times and vice versa.

In the case of heavyweight Office building model located in Denver the phase margin changed from about 65° (Ziegler–Nichols tuning) to 12° for the optimal tuning, while the crossover frequency shifted from 0.00142 rad/s to 0.00223 rad/s for the optimal PI. Hence the optimization procedure improved the settling time of about three times at the expense of closed loop robustness, making the resulting controller not suitable to impose the temperature reference for different building parameters (see Figure 5.18). We point out that, for the adaptive strategy is not possible to define the phase margin and crossover frequency as the control gains are not constant but they change according to nonlinear adaptive mechanism (4.11)-(4.12), therefore a similar analysis cannot be carried out for the adaptive scheme. Nevertheless, the adaptive controller is intrinsically robust to parameter variations as the control gains change online on the basis of the actual building response.

At last, we underline that numerical results are obtained by using the same work-station (Intel i7, 3.60 GHz, 32 Gb Ram) and the time saving through the LQ-EMRAC controller vs. the PI one was of about 180 minutes (-20%) to perform the entire set of simulations.

5.4.5 *Analysis in case of PCM materials*

From a control prospective, dealing with PCM layers implies that the building envelope is a time-varying system, i.e. a linear system where the entries of the systems dynamic matrices are not fixed, but vary as a function of the plant state (e.g. temperatures) and time [120]. In this case, the design of fixed gain strategies (such as PID) can be ineffective, since this would require a different gain tuning for each value assumed by the matrices entries, i.e. for each of the different admissible system configurations. Conversely, adaptive strategies automatically adapt control gains to compensate dynamic changes occurring in the thermal capacitances of PCM layers. In order to provide evidence of this last aspect, several simulations are carried out for all the above examined buildings operating in intermittent regime. It is worth noticing that the adaptive controllers was not re-tuned with respect to the case when the PCM is not taken into account.

Exemplar results reported in this section refer to a heavyweight House located in Freiburg (cold winter zone) and a lightweight Office in Nice (hot summer zone). This analysis aims to compare building energy and comfort performance obtained with and without PCM integrated into the building envelope. In particular, results highlight how the adoption of PCM allows reducing the energy consumption providing at the same time a better thermohygrometric comfort. Specifically, results reported in Figure 5.19 confirm the effectiveness of the controller in ensuring the required indoor air temperatures (according to the intermittent control system regime) with and without PCM. The figure refers to the heavyweight House building located in Freiburg and to five sample days, i.e. March 26th - March 31st (corresponding to the 85th - 90th days of the year).

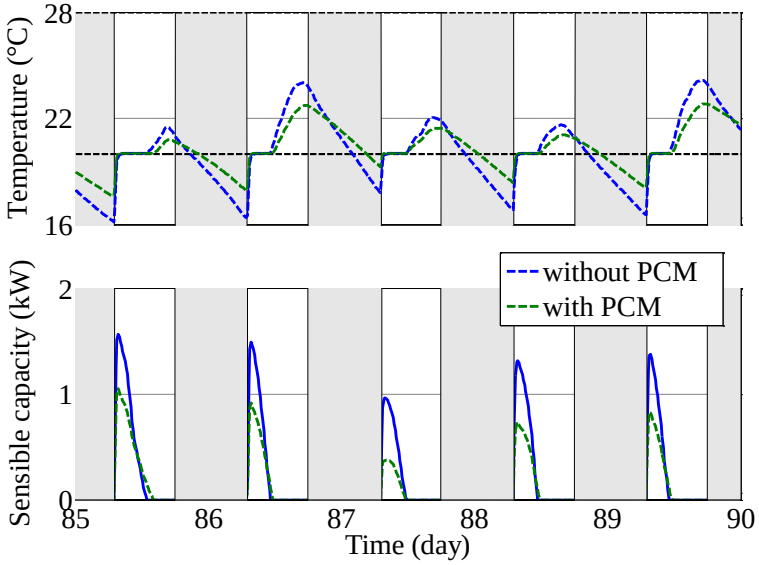

Figure 5.19. Heavyweight House building in Freiburg. Time history of indoor air temperature and sensible heating capacity.

In such figure, in case of PCM adoption, the decrease of the indoor air temperature minimum and maximum peaks (lower fluctuation) is clearly visible. In addition, a reduction of time delay, calculated between the temperature peaks (in free floating regime) occurring without and with PCM, is also obtained, as shown in Figure 5.19. As a consequence, due to the lower indoor air temperature fluctuation, milder control actions (i.e. lower heating energy demand) are required when PCM is adopted.

Note that, dealing with PCM is more challenging, since the control action has to neutralize the effect of uncertainties due to the high variability of the temperature-dependent thermal capacitances. Nevertheless, the adaptive terms can effectively tackle this additional on-line variation of the plant parameters and provide at the same time temperature tracking errors that are comparable to those obtained without PCM. As a result, it is possible to reliably compute energy savings with respect to commonly used building materials. Also for this analysis, the heating and cooling energy calculation is carried out for all the investigated case studies. As an example, for the heavyweight House building located in Freiburg, the application of PCM materials reduces the winter heating demand of about 10.8%, while a summer cooling demand decrease of about 25.1% is obtained in the case of the lightweight Office located in Nice.

In Figure 5.20 the simulated thermal behaviour of the outer, the middle and the inner PCM layers is reported for the same sample days of the end of March. Here, it is clearly visible how the thermal capacitance of such layers is time-variant according to the variable external disturbances.

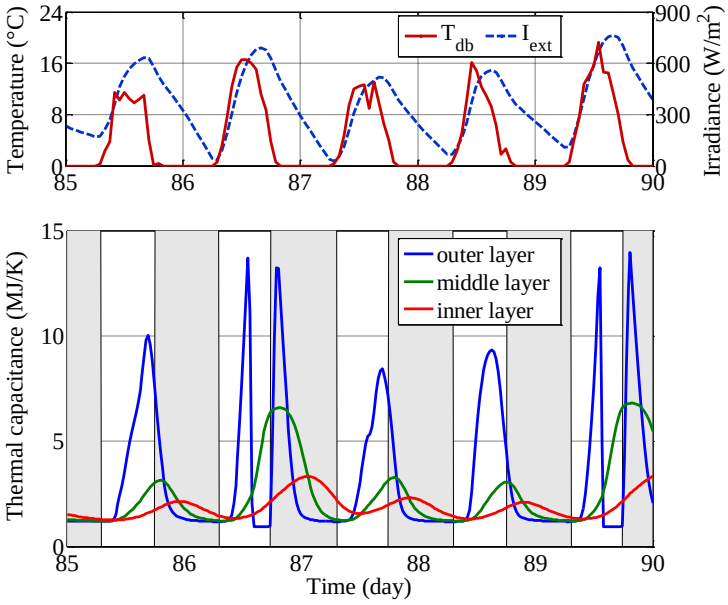

Figure 5.20. Heavyweight House building in Freiburg. Time history of outdoor air temperature, solar radiation and thermal capacitance of three PCM roof layers.

In all the cases, the thermal capacitance fluctuation is higher in the outer PCM layer than in the middle and inner ones. Note that on March 27th and 30th, for the outer PCM layer a complete melting and a subsequent solidification processes occur, due to the combined effects of outdoor air temperature and solar radiation (a temperature of the layer higher than 26 °C can be observed). Therefore, the thermal capacitance of the outer PCM layer reaches two consecutive peaks, while its minimum, occurring between such peaks, is related to the liquid phase.

By integrating PCM layers into the envelope, higher levels of comfort are detected even during night hours during which temperature and humidity controls are deactivated, as shown in Figure 5.21. Here, it is clearly evident that in case of PCM adoption, the obtained PMVs are always closer to zero (minimum PPDs) and, as expected, the mean radiant temperature oscillation is always lower. Similar results regarding the control scheme reliability and interesting energy and comfort benefits are also detected for the summer season. For the sake of brevity, such results are reported only for the lightweight Office building located in the weather zone of Nice for several sample, i.e. July 14th – July 19th (corresponding to the 195th - 200th days of the year).

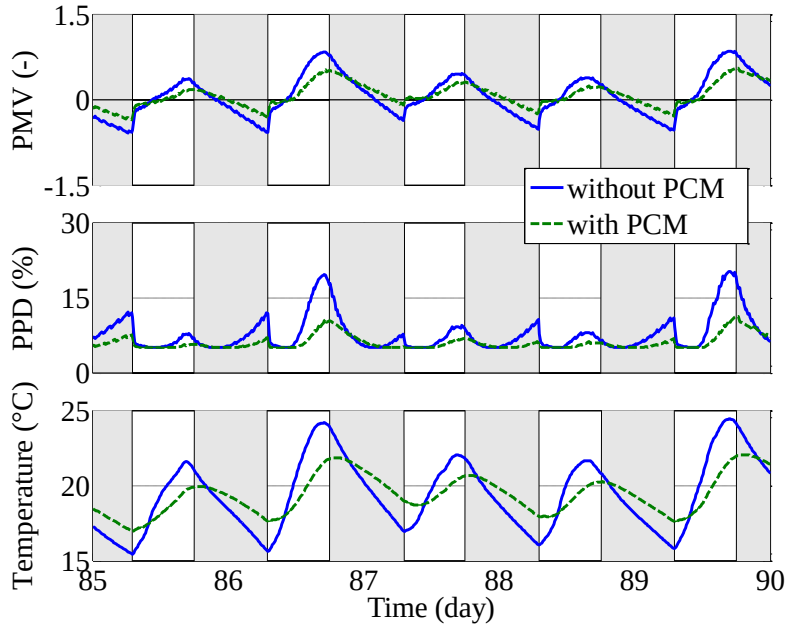

Figure 5.21. Heavyweight House building in Freiburg. Time history of: PMV, PPD and mean radiant temperature.

In particular, Figure 5.22 shows that the adoption of PCM implies a lower cooling demand (thus a milder control action), which is always detected when compared to the case without PCM. On July 14th, no cooling energy is even required (no control action) in case of PCM adoption, due to the quite low hourly outdoor air temperatures and solar radiations.

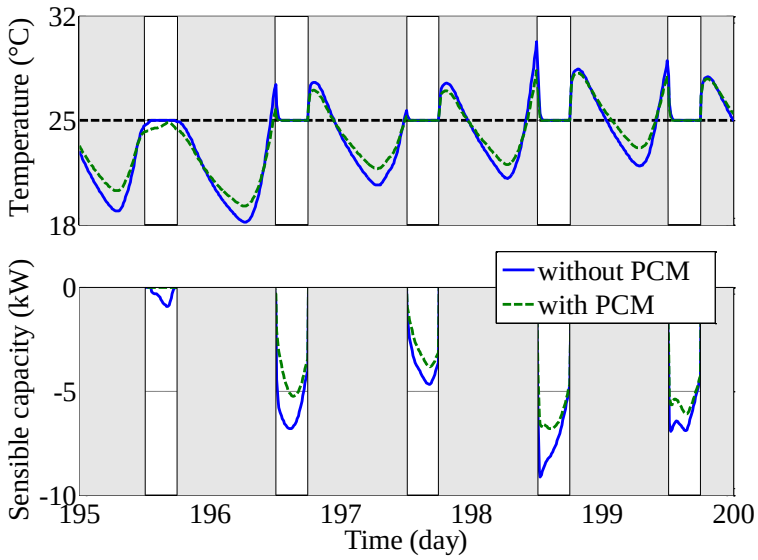

Figure 5.22. Lightweight Office building in Nice. Time history of: indoor air temperature and sensible cooling capacity.

5.5 **Discussion**

In this chapter the novel Enhanced Model Reference Adaptive Control (EMRAC) scheme proposed in Chapter 4 have been applied to the control of the thermohygrometric variables in buildings. The reference model is obtained by a Linear-Quadratic (LQ) optimization and it is developed for controlling nonlinear building dynamics. The goal of this control scheme is to strictly control the thermohygrometric behaviour of buildings in uncertain conditions (also for guaranteeing indoor comfort). This is obtained through the control ability to appropriately and automatically vary its control gains, without requiring a priori knowledge of the building dynamics. The LQ-EMRAC performance (in terms of control robustness against disturbances) was extensively analysed through the development of 54 different case studies. In particular, they refer to: i) three different building uses (small house, office building and large commercial mall); ii) two diverse building envelopes (lightweight and heavyweight); iii) nine different European weather zones (ranging from cold winter climates to temperate Mediterranean ones). Energy and comfort analyses were also carried out for continuous and intermittent control system operating strategies, as well as for different choices of the reference profiles. Additional tests have been performed by taking into account the nonlinear thermal behaviour of roof and walls integrated with Phase Change Materials (PCM).

Simulation results show that the proposed control strategy is able to impose the reference behaviours to both indoor air temperature and humidity, in any simulated conditions and for both

the continuous and intermittent regimes. As a result, indoor air temperature and humidity tracking mean squared errors, for each investigated case study, resulted to be always negligible. Due to such accurate thermohygrometric control, high occupants' comfort levels are also achieved, obtaining good PMVs (ranging from -0.5 to 0.75) and PPDs (less than 10% in winter and 20% in summer) for all the investigated case studies.

In addition, due to the LQ-EMRAC ability, simulation results also show: i) smooth transitions of both the indoor air temperature and humidity during transient operations; ii) bounded dynamic behaviours of the adaptive gains; iii) bounded sensible and latent heating and cooling control actions. Additional feature will be analyzed in the next chapters. In particular the control of thermohygrometric variables for multi-zone systems, where some zones are totally included in others, will be considered in the next chaper.

Chapter 6
ADAPTIVE CONTROL OF MULTI-ZONE THERMAL SYSTEMS

The aim of this chapter is twofold. The first is to extend the model implemented in DETECt (see Chapter 2) so that it is possible to simulate also multiple thermal zones totally enclosed into others. The second aim is to control the resulting multi-zone system when different thermohygrometric conditions are required for each zone. The regulation of indoor air temperature and humidity, according to the different specific requirements of each zone, is guaranteed by the adaptive model reference scheme embedded into the code, namely LQ-EMRAC, Linear Quadratic Extended Model Reference Adaptive Control, presented in Chapter 4. Such algorithm allows the control of the different indoor spaces thermo-hygrometric variables in uncertain conditions through the on-line variation of its control gains. As a result, a great control flexibility and robustness is achieved and the control action is able to automatically counteract unexpected and unknown thermo-hygrometric behaviour deviations (e.g. due to external disturbances acting on the different zones), without requiring, for its design or on-line implementation, an a priori knowledge or a detailed mathematical description of the overall dynamics.

In order to show the effectiveness and robustness of the control approach to multizone systems when some of them are totally included in others, two case studies are developed throughout the chapter. In particular, the first refers to an indoor hall of a museum building with an included glass display case. Here, an accurate climate control (rigid constraints of temperature and humidity of the case indoor air) is required. As it is well known, such occurrence is mandatory in case of particular exhibited items contained in museums glass cases (e.g. archival artifacts, paper-based objects, etc.). Here, preservation techniques must be emphasized in order to avoid eventual irreversible damages. In this specific case there are two thermal zones to be modeled and controlled. The first one, i.e., the hall of a museum, is operated according to an intermit running regime, while for the included zone a continuous running mode is adopted. Hence, we test the robustness of the adaptive approach for the included zone to sudden variation

of the thermohygrometric conditions of the surrounding environment caused by the activation/deactivation of the controllers for the hall of a museum.

The second case study is referred to a Neonatal Intensive Care Ward (NICW) where several Neonatal Intensive Care Units (NICUs) for premature and full-term newborn babies are located. In each NICU, an accurate climate control of air temperature and humidity is required for producing healthful micro-environment for the hosted babies. Although many works in literature highlighted the need of a neutral thermal environment for increasing the survival rate of preterm infants [150, 151], the adoption of accurate and advanced regulation of both the temperature and the relative humidity within the NICUs have been only recently emphasized [152]. For this second case study, the main idea is to analyze the effect of sudden disturbances, e.g., windows and NICUs openings, and how the adaptive control tackle such unexpected events.

At the best of the authors' knowledge, the presented dynamic BEPS code is the first one in literature in which: i) an innovative and optimal adaptive scheme for controlling indoor air temperature and humidity is implemented; ii) the thermo-hygrometric behaviour of multiple thermal zones totally included into larger ones can be assessed. The chapter opens by considering the modelling of multi thermal zones where some of them are totally included in other as this modelling is common to both case studies shown after. The material of this chapter has been partially published in [153-155].

6.1 **Modelling thermal multi-zones systems**

In order to analyse the effectiveness and robustness of the LQ-EMRAC control algorithm for assessing the thermo-hygrometric behaviour of different building thermal zones enclosed into others, a suitable simulation model was developed. The model is based on the resistive-capacitive (RC) thermal network approach and extend that presented in Chapter 2 based on [9] to the case that there are Z zones and Z-1 of them are completely enclosed into a main one. Through such model, the dynamics of temperatures and humidity, as well as of heating and cooling loads and demands, occurring within each modelled zone, can be assessed. A sketch of the modelled RC thermal network, related to Z thermal zones (one main zone including the remaining Z-1 zones) is showed in Figure 6.1.

The calculation procedure takes into account the heat flows between: *i)* the outdoor environment and the main thermal zone (Zone 1 in Figure 6.1); *ii)* the main thermal zone and the enclosed ones (zones 2 to Z in Figure 6.1). Several simplifications are taken into account, such as:

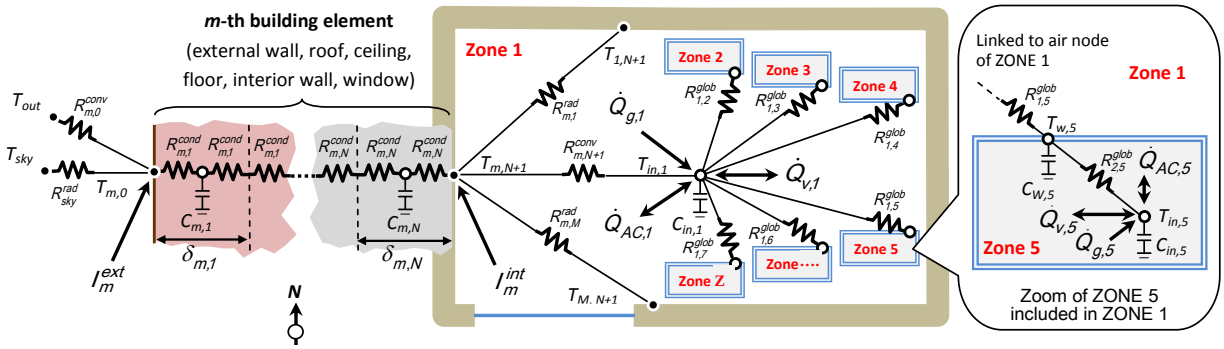

Figure 6.1. Sketch of the modelled *RC* thermal network.

- the indoor air of each thermal zone is considered as uniform and, thus, modelled as a single indoor air temperature node;
- the building envelope of the main Zone 1 is subdivided into *M* multi-layer elements, subdivided in *N* sub-layers (of different thicknesses), where thermal masses and conductivities are uniformly discretised (see also Chapter 2). For each m-th envelope component of Zone 1 (main zone), *N* capacitive and *2* surface nodes are taken into account; the construction envelope of the enclosed zones (from 2 to Z) is lumped in a single node.

As a result, the whole system is modelled through a high order *RC* thermal network of: *i)* $M \times (N+2)$ nodes in which the building envelope of the main zone is subdivided (consisting of *M* envelope elements ($m = 1, \ldots, M$) and *N* sub-layers $(n = 1, \ldots, N)$, see also Chapter 2 for further details on the modelling of Zone 1); *ii) Z-1* nodes of the lumped envelopes of each enclosed zone; *iii) Z* nodes related to the indoor air of each enclosed zone and the main one.

The set of differential equations describing the energy rate of change of the envelope of Zone 1 are those described in detail in Chapter 2 (see Section 2.2 and [9]). Instead a simplified approach is adopted for the enclosed zones (z = 2,…,Z). Here, the differential equation describing the energy rate of change of the temperature node of each enclosed zone envelope ($T_{w,z}$) is calculated as:

$$C_{w,z}\frac{dT_{w,z}}{dt} = \frac{T_{in,1} - T_{w,z}}{R_{1,z}^{glob}} + \frac{T_{in,z} - T_{w,z}}{R_{2,z}^{glob}}, \qquad z = 2\ldots Z, \tag{6.1}$$

where $C_{w,z}$ is the envelope lumped thermal capacitance, whose indoor air temperature is $T_{in,z}$; $R_{j,z}^{glob}$ is a global thermal resistance that takes into account all the heat transfer effects. At the exterior of the enclosed zones, $R_{1,z}^{glob}$ is calculated by adding the half sub-layer conductive thermal resistance of each enclosed zone envelope node to the equivalent convective and radiative thermal resistance (modelled by a combined linearized convective-radiative thermal

resistance). In addition, the radiative exchange includes the heat transfer between the enclosed zones envelopes and the main zone, disregarding the long-wave fraction of each enclosed zone vs. the remaining ones. Within the enclosed zones, the equivalent global thermal resistance ($R_{2,z}^{glob}$) includes combined conduction and convection phenomena only.

The dynamics of the indoor air of the main zone $T_{in,1}$ and of each enclosed zone $T_{in,z}$ are described as

$$C_{in,1}\frac{dT_{in,1}}{dt}=\sum_{m=1}^{M}\frac{T_{m,N}-T_{in,1}}{R_{m,int}^{conv}}+\frac{T_{out}-T_{in,1}}{R_{v,1}}+\sum_{z=2}^{Z}\frac{T_{w,z}-T_{in,1}}{R_{1,z}^{glob}}+\sum_{z=2}^{Z}\frac{T_{in,z}-T_{in,1}}{R_{v,z}}+\dot{Q}_{g,1}\pm\dot{Q}_{AC,1}, \tag{6.2}$$

and

$$C_{in,z}\frac{dT_{in,z}}{dt}=\frac{T_{w,z}-T_{in,z}}{R_{2,z}^{glob}}+\frac{T_{in,1}-T_{in,z}}{R_{v,z}}+\dot{Q}_{g,z}\pm\dot{Q}_{AC,z},\qquad z=2\ldots Z, \tag{6.3}$$

where $R_{m,int}^{conv}$ are the thermal resistances defined in Section 2.2 and $R_{v,1}$ and $R_{v,z}$ are the thermal resistances that describe the air ventilation and infiltration thermal loads. Specifically, $R_{v,1}$ links the indoor air node of Zone 1 to the external one (outdoor air at T_{out}), whereas $R_{v,z}$ links the indoor air node of the Z-th zone to the one of Zone 1. The sensible heat gains include: *i)* the thermal zone internal gains due to occupants, lights and equipment, $\dot{Q}_{g,1}$ and $\dot{Q}_{g,z}$; *ii)* the sensible heat to be supplied to (or removed from) the building space by an ideal HVAC system, aiming at maintaining the indoor air at the desired set point temperature, $\dot{Q}_{AC,1}$ and $\dot{Q}_{AC,z}$, respectively. (We remark that (6.2) replaces (2.17) for modelling the dynamics of indoor air temperature of Zone 1 in the case it contains additional thermal zones that are completely included. Hence, the reader is referred to Section 2.2.4 for further details and comments for this dynamical system.)

For each indoor space, the moisture balance is calculated by neglecting the moisture exchange between the air node and the surrounding building surfaces. As a result, the adopted moisture balances for the main zone and the enclosed ones are described

$$\Omega_{in,1}\frac{d\omega_{in,1}}{dt}=\dot{m}_{v,1}\left(\omega_{out}-\omega_{in,1}\right)+\sum_{z=2}^{Z}\dot{m}_{v,z}\left(\omega_{in,z}-\omega_{in,1}\right)+\dot{m}_{wg,1}\pm\dot{m}_{vap,1}, \tag{6.4}$$

and

$$\Omega_{in,z}\frac{d\omega_{in,z}}{dt}=\dot{m}_{v,1}\left(\omega_{in,1}-\omega_{in,z}\right)+\dot{m}_{wg,z}\pm\dot{m}_{vap,z},\qquad z=2\ldots Z, \tag{6.5}$$

where $\Omega_{in,z}$ in is the indoor dry air mass; $\dot{m}_{v,z}$ is the air ventilation mass flow rate; $\dot{m}_{wg,z}$ is the inlet water vapour mass flow rate to the thermal zone (due to occupants), $\omega_{in,z}$ is the indoor air

specific humidity, $\dot{m}_{vap,z}$ is the water vapor mass flow rate delivered to (or removed from) the indoor space for maintaining a desired humidity set point in accordance with the decoupling approach in [87], with $z = 1 \ldots Z$ (i.e., for each zone), where ω_{out} is the outdoor air specific humidity.

Notice that $\dot{m}_{vap,z}$ is equal to $\dot{Q}^{lat}_{HVAC,z} / \Delta h_{vs}$, where Δh_{vs} is the water latent evaporation heat at 0°C and $\dot{Q}^{lat}_{HVAC,z}$ is the latent heat to supply to, or to remove from the z-th zone to keep its humidity to a given set point. Again we remark that (6.4) replaces (2.18) for modelling the dynamics of indoor air specific humidity of Zone 1 in the case it contains additional thermal zones that are completely included. Hence, the reader is referred to Section 2.2.5 for further details and comments for this dynamical system.

6.2 **Case Study 1: two zones**

As first case study to show the effectiveness of the design approach presented in Chapter 4 also for the precise control of multi-zone systems with different thermohygrometric needs, we start to consider the simple case of two zones as depicted in Figure 6.2.

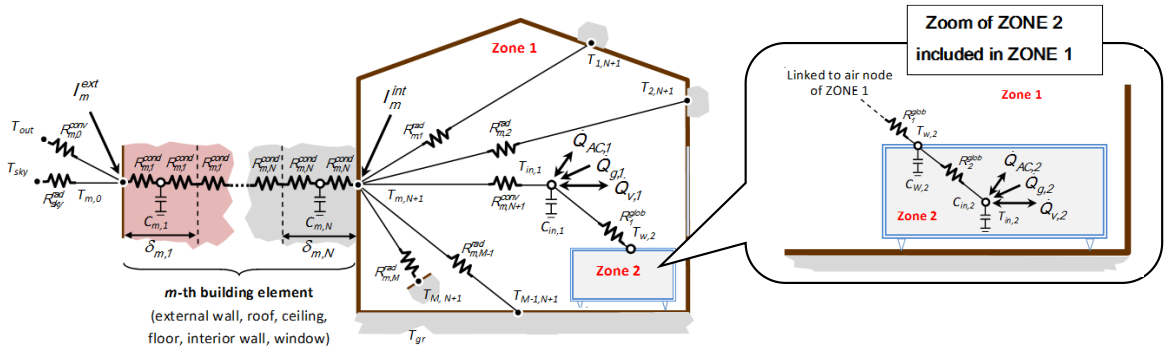

Figure 6.2. Sketch of the modelled RC thermal network in the case when a zone is totally included in another.

The presented case study refers to a possible museum indoor space in which two thermal zones are modelled. In particular, the first zone is referred to a museum hall while the second one (totally included in first zone) to a glass display case with an accurate climate control (rigid constraints of temperature and humidity of the case indoor air) necessary to preserve collected exhibits such as: paints, woods, papers and leathers (which require suitable conditions of indoor air temperature and relative humidity, simultaneously). The numerical analysis, carried out in the next section, is referred to the weather zones listed Table 5.3.

For Zone 1, it is considered a length, width and height equal to 20, 10 and 3.5 m, respectively. The building longitudinal axis is East–West oriented and a South facing windows (4-6-4 air filled double-glazed system) of 32 m^2 is taken into account. The thickness of the building walls and floor/ceiling are 25 and 30 cm, respectively. Their stratigraphy is designed by concrete bricks (λ = 0.51 W/mK, ρ = 1400 kg/m^3, c = 1000 J/kgK) and thermal insulation (λ = 0.04 W/mK, ρ = 15.0 kg/m^3, c = 1400 J/kgK). Note that each building element is subdivided in 10 sub layers of equal thickness. The direct solar radiation transferred through the windows to the inside zone is assumed to be absorbed by the floor with an absorption factor of 0.3. The absorption and emission factors of interior surfaces are assumed to be equal to 0.15 and 0.9, respectively. For such zone, a ventilation rate equal to 1 Vol/h and a crowding index of 0.12 person/m^2 are taken into account. A cubic shaped zone 2 with 1 m length side is considered. In particular, a glass envelope of 3 cm thickness, with an occurring air infiltration of 2 l/h is modelled.

The simulation starts on 0:00 of January 1st and ends at 24:00 of December 31st. For zone one it is assumed an intermittent running regime similar that considered in Section 5.3. In particular, the heating/cooling system of the thermal Zone 1 is switched on from 08:00 to 18:00, from November 1st to March 31st (heating mode) and from 14:00 to 20:00, from June 1st to September 30th (cooling mode). The heating/cooling system is activated for indoor air temperatures lower than 20°C and higher than 28°C, during heating mode, and for indoor air temperatures lower than 10°C and higher than 25°C, during cooling mode. Simultaneously, humidification and dehumidification are required for indoor relative humidity lower than 45% and higher than 55%. Notice that, for this case study also setback strategies have been considered. In particular, during the heating mode the temperature controller is activated also for simulation time t $\notin$ [08:00, 18:00] providing that the indoor air temperature goes below 10 °C, while in the case of the cooling mode the temperature controller is re-activated when the indoor air temperature becomes higher that 28 °C and the simulation time t $\notin$ [14:00, 20:00]. Consequently also the automaton in Figure 3.2b has been used for the simulation of Zone 1. Notice that additional thermal loads due to people effect the indoor temperature/relative humidity evolution from 09:00 to 18:00 and from 15:00 to 20:00 during winter and summer season, respectively.

The heating/cooling system for the thermal Zone 2 is switched on 24/7 for accurately conserving the case exhibited items. Here, the indoor air temperature and relative humidity are controlled all over the year at 20°C and 65%, respectively.

The LQ-EMRAC presented in Chapter 4 has been implemented to control the air temperature and humidity, simultaneously, of both the modelled thermal zones. In particular, following a decentralized control approach (where each control variable is used to impose the dynamic behaviour of only one variable to be controlled according to decentralized control scheme [156], while coupling between zones are assumed to be as additional unmodelled dynamics to tackle in closed-loop), four different and independent adaptive controllers have been designed. In order to design the LQ-EMRAC control, the simplified models (see Section 5.1) was adopted as nominal models to be optimized via the LQ approach. Note that, the choice of these simplified models reduces the complexity of the control design, without jeopardizing the closed-loop performance. On the other hand, the robustness of the closed-loop control is guaranteed by the adaptive actions, whose gains evolve to compensate any parameters mismatch and/or presence of unmodelled dynamics (see Chapter 4). The weight matrices, which define the cost function (4.3), were set in order to impose: *i)* a settling time of 50 minutes for Zone 1 and 10 minutes for Zone 2; *ii)* absence of overshoots for any step variation of the reference signal. The choice of the relaxation time for Zone 1 is done according to [103] with the aim to ensure a smooth daily transition during the transient operation toward the regime set-point. Finally, the reference input signals (i.e., *r* in Figure 4.1) depends on the selected temperature and humidity set points. Note that, the humidity control is obtained through the input reference set point of indoor air specific humidity, in order to achieve the selected relative humidity set-point.

6.3 **Numerical results**

In the following subsection we discuss the results of the numerical analysis first for the Zone 1, i.e., the museum hall, and then those of Zone 2, i.e., the glass display. We note that during the design of the adaptive control schemes the mutual thermal effects between the zones have not been taken into account. Hence, the coupled dynamics in Section 6.1 are considered as additional uncertainties to tackle in closed loop to impose the required indoor air temperature and humidity set points.

6.3.1 *Analysis for Zone 1 (Outer zone)*

As mentioned above, for Zone 1 indoor air temperature and humidity are daily controlled only for some hours. Hence, at control activation both these thermohygrometric variables have to be regulated to the desired set points if they are not inside the admissible range of variation. In this case, as discussed in Chapter 4, for each variable, the gains of the corresponding controller adapt

so that it is possible to track in closed loop the output of the reference model which converges to the required set point. The tracking of the reference model dynamics are imposed despite external disturbances, e.g., solar radiation, external temperature and internal loads, and the thermal coupling with Zone 2. To better illustrate this feature, Figure 6.3 shows the evolution of indoor air temperature and humidity and the corresponding reference models at the control activation occurring at the 319th day of the year in Denver. (Notice that, in this figure, as in those in the rest of the section, grey shaded area denote the time range where the controllers are not activated according to the scheduling discussed in Section 6.2.) Here it is clear that adaptive strategies can impose the demanded thermohygrometric regime also in this challenging case as a satisfactory performance of the developed closed-loop control scheme can be observed (coincident references and obtained temperature/humidity profiles).

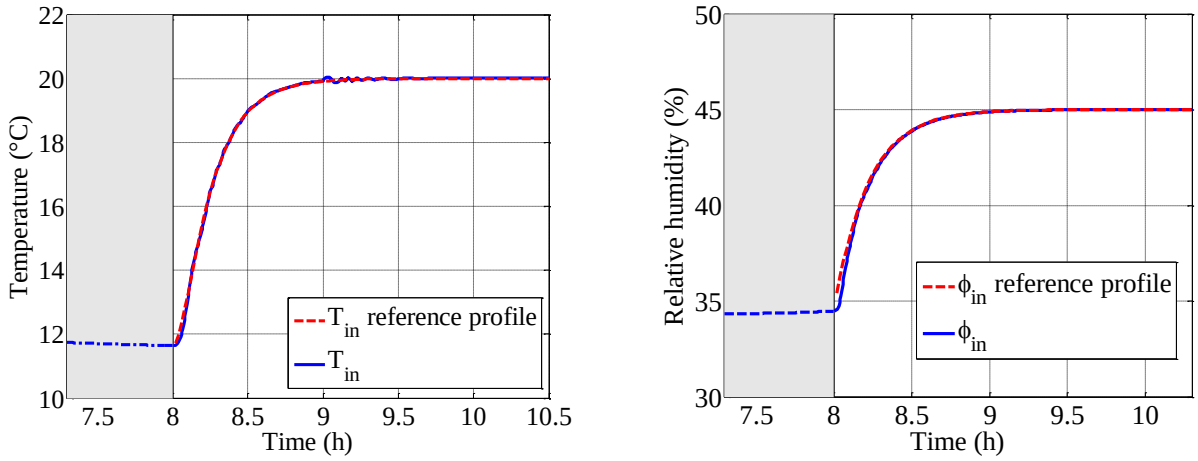

(a) **(b)**

Figure 6.3. Time history of (a) indoor air temperature and (b) together with the corresponding reference profiles in the case of Denver (319th day of the year).

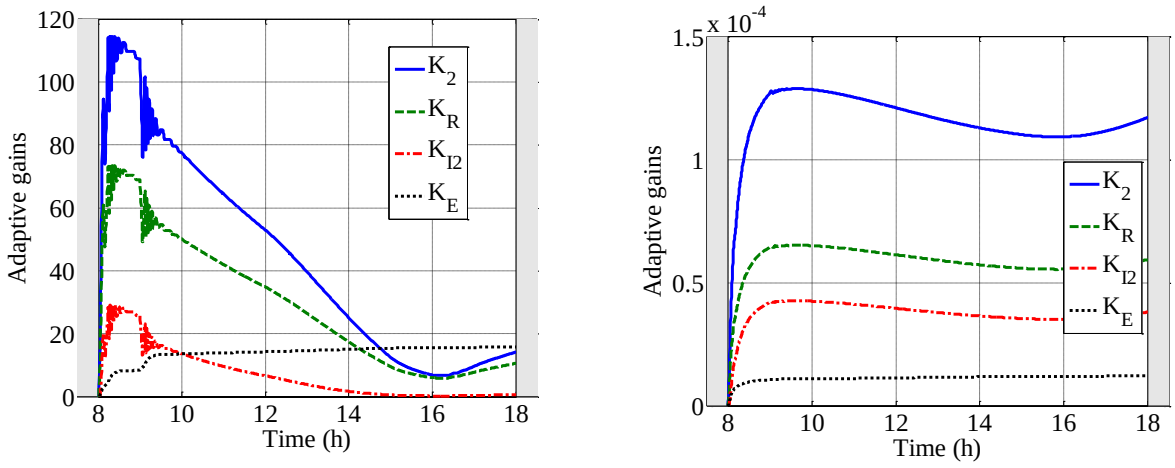

(a) **(b)**

Figure 6.4. Time history of the adaptive gains for the case of Denver (319th day of the year.) for (a) indoor air temperature control and (b) indoor air relative humidity.

The evolution of the adaptive gains (4.11)-(4.12) to obtain the tracking performance in Figure 6.3 are shown in Figure 6.4 for the sake of completeness. In particular, in Figure 6.4a, we note a change of the rate of variation of the adaptive gains around 9:00. This is mainly due to the effect of additional internal loads caused by the arrival of people in the room. Despite this effect, tracking of the reference profiles is not jeopardized as the adaptive system fast adjusts its gains to face the new working condition.

Similar tracking performance have been obtained for other weather zones and different days of the year, some of them have been depicted in Figure 6.5.

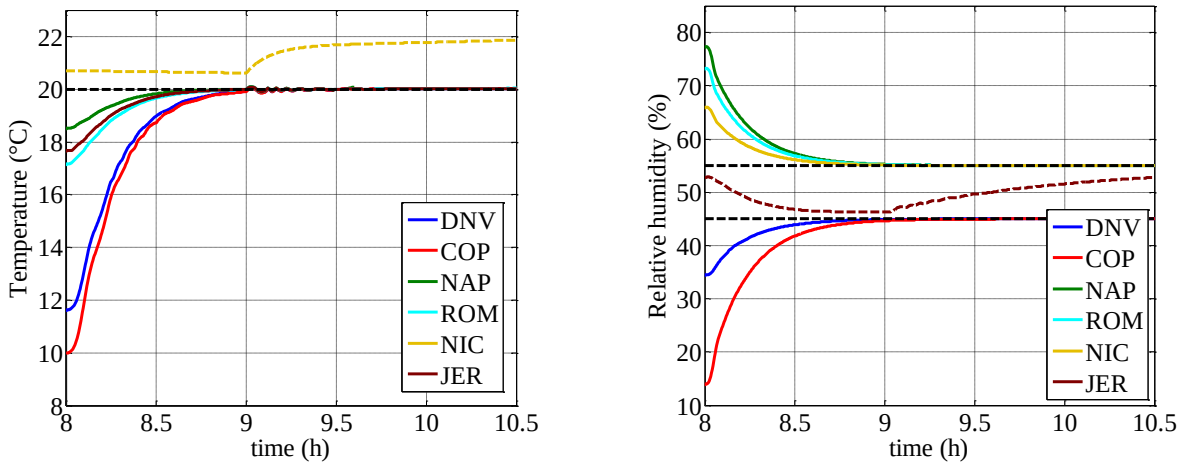

(a) **(b)**

Figure 6.5. Transient dynamics of (a) the indoor air temperature and (b) humidity for some selected days. Denver (319th day of the year), Copenhagen (11th day of the year), Naples (99th day of the year), Rome (114h day of the year), Nice (278h day of the year), Jerusalem (280th day of the year).

In particular from Figure 6.5a we note that in the case of the 99th day of the year in Nice (dashed dark yellow line), when the control system is switched on, the indoor air temperature is already within the acceptable range of variation given in Section 6.2. Consequently, additional heating/cooling is not provided and the sensible heating is set to zero (see also Figure 6.6a). In this case the change of the derivative of the indoor air temperature at 9:00 and its increase towards 22 °C is caused by the arrival of people in the room.

Similarly, in the case of relative humidity control the adaptive strategy is not switched on when the room is located in Jerusalem on the 280th day of the year, as shown in Figure 6.5b, because the indoor air relative humidity already belongs to [45, 55] % at 8:00. In this specific case, when people arrive at 9:00, the indoor air temperature has been already driven to 20 °C (see dashed dark red line in Figure 6.5a) by the temperature controller with the control action (sensible heating) in Figure 6.6a. Hence, additional latent loads due to people increase the indoor

air relative humidity which continues to free float in the preassigned range of variation while the vapour flow rate is constantly set to zero (see dark red line in Figure 6.6b).

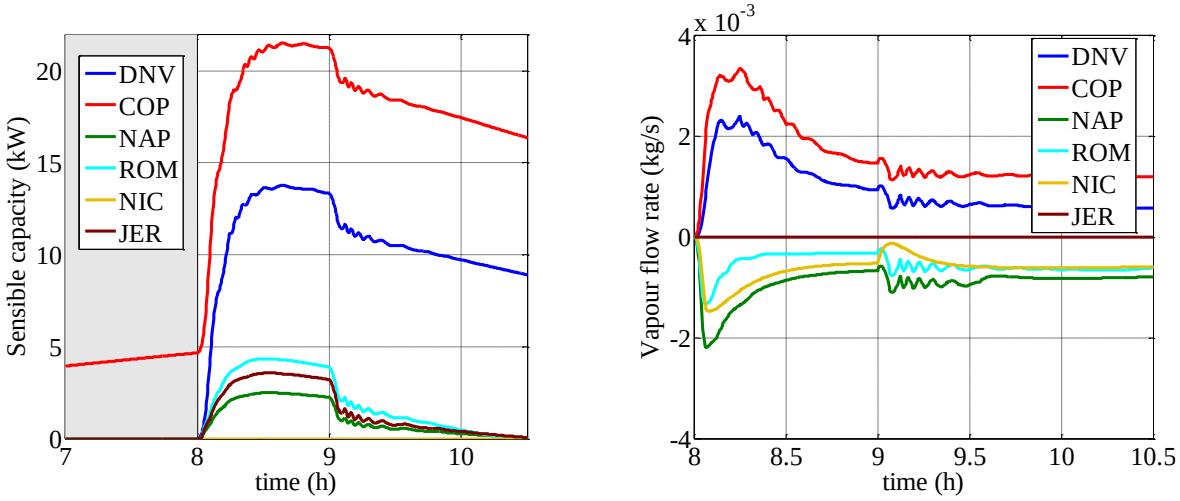

(a) **(b)**

Figure 6.6. Time history of the control actions at the control activation for some selected days. Denver (319th day of the year), Copenhagen (11th day of the year), Naples (99th day of the year), Rome (114h day of the year), Nice (278h day of the year), Jerusalem (280th day of the year) (a) sensible heat and (b) water vapour mass flow rate.

From Figure 6.6 we can also remark that for the temperature control of the room located in Copenhagen on the 11th day of the year, the setback strategy was activated to keep indoor air temperature at 10 °C during nighttime, while for the other weather zones, the indoor air temperatures were above 10 °C and therefore none additional heating was required according to the scheduling given in Section 6.2. Also the effect of the arrival of people at 9:00 is clear in Figure 6.6. Indeed, additional internal loads imply that lower sensible heats can be supplied to keep the indoor air temperatures at the required set-point. Consequently, the adaptive temperature controllers adapt their gains automatically so that required thermohygrometric conditions are preserved also for the new operative working regime. We clearly not that, the additional internal loads due to people were not able to increase indoor air temperature so that free floating ware allowed. Free evolution of the indoor air temperature has been detected for some cases in Figure 6.5a only after 10:30, e.g., for Naples (99th day of the year), Rome (114h day of the year), Nice (278h day of the year), Jerusalem (280th day of the year) where the required sensible heat in Figure 6.6a converged to zero.

The phase portrait of the thermohygometric variables over the time interval 8:00÷9:00 for the weather zones in Figure 6.5 is shown on the psychrometric chart in Figure 6.7. Here, in accordance with Figure 6.6, it is clear that for rooms in the weather zone of Naples and Rome, at the beginning of the 99th and 114th day of the year, respectively, heating and dehumidification

are required to enter in the admissible region defined by the constraints introduced in Section 6.2 (see trajectories D4 and E4 in Figure 6.7). On the other hand heating and humidification have to be provided in the case of Denver (319th day of the year) and Copenhagen (11th day of the year), i.e., trajectories A1 and B1. Finally a pure heating is required for Jerusalem (280th day of the year) and only dehumidification is needed for Nice (278th day of the year). Notice that, the resulting trajectories, i.e., C2 and F3 are almost a horizontal and vertical segment, respectively, as the indoor specific humidity, in the case of Jerusalem, and the indoor air temperature, in the case of Nice, vary in a small range during the first hour after the control activation.

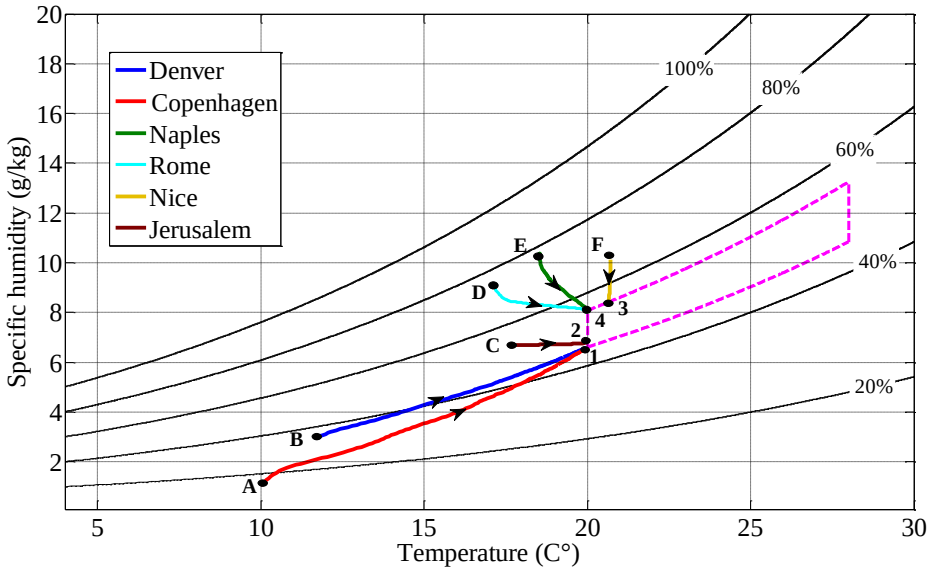

Figure 6.7. Winter season. Indoor air routes on the psychrometric chart for mall buildings. Denver (319th day of the year), Copenhagen (11th day of the year), Naples (99th day of the year), Rome (114th day of the year), Nice (278th day of the year), Jerusalem (280th day of the year).

We remark that for the control of the room the maximum root mean squared tracking error for the weather zones in Table 5.3 where about 0.0373 °C for the indoor air temperature control and 0.28 % for the indoor humidity control. These are small residual errors considering also the thermal effect of Zone 2 on Zone 1 which was not considered during the design of the control strategy.

The energy demands required to achieve this fine regulation is reported in Table 6.1. Similar considerations as those given in Section 5.4.2 for Table 5.7 and Table 5.8 can be redone also for data in the first two columns in Table 6.1. In particular, it is possible to note that the lower the HDD, the lower the building heating demand (although a strictly decreasing trend cannot be detected because of the solar radiation effects). Conversely, lower the HDD, the higher is the building cooling demand.

Weather zone	Mode	Energy Demand		Peak Load		Comfort	
		Sensible (kWh/m^2y)	**Latent** (kWh/m^2y)	**Sensible** (kW)	**Latent** (g/s)	**PMV** (-)	**PPD** (%)
Copenhagen	*H*	80.35	13.18	21.34	3.23	-0.589	12.2
	C	-1.24	-1.67	-4.29	-2.64	-0.132	5.35
Denver	*H*	54.31	21.64	26.09	3.57	-0.378	7.97
	C	-10.59	-1.01	-9.45	-2.16	0.116	5.27
Freiburg	*H*	66.32	11.37	20.93	3.09	-0.513	10.5
	C	-5.69	-1.52	-8.81	-2.22	-0.056	5.06
Milan	*H*	59.17	9.23	19.24	2.88	-0.137	5.38
	C	-11.43	-5.57	-8.36	-4.6	-0.013	5.01
Rome	*H*	25.7	3.84	15.17	2.38	0.143	5.42
	C	-19.29	-6.42	-11.28	-5.21	0.27	6.51
Nice	*H*	22.08	4.35	12.22	2.17	0.043	5.03
	C	-14.79	-4.84	-9.27	-3.62	0.245	6.25
Naples	*H*	23	3.23	14.12	2.17	0.131	5.35
	C	-20.53	-8.23	-10.97	-5.54	0.297	6.82
Jerusalem	*H*	15.78	3.26	11.71	1.99	0.201	5.84
	C	-21.92	-7.43	-11.52	-7	0.572	11.9
Athens	*H*	16.03	3.39	11.94	2.09	0.318	7.11
	C	-31.81	-3.05	-12.93	-2.6	0.406	8.43

Table 6.1. Man value data for Zone 1: average PMV and PPD during winter (H) and summer (C) seasons, heating (H) and cooling (C) energy demand and peak load.

As the size and the scheduling policy for the winter season of the building considered in this section are similar to office buildings in Chapter 5 under intermit regime, some additional consideration can be done. Precisely, even though the building described in Section 6.2 is heavier than the heavy office building in Chapter 5 and possible setback can be activated during the nighttime, the heating demand are smaller. This is mainly because of the presence of Zone 2 whose air temperature is constantly controlled at 20 °C. This is also the low-bound set-point indoor air temperature for the room. Consequently, Zone 2 heats the surrounding environment to the required set point and then less sensible heat is required to control the indoor air temperature.

Table 6.1 also reports the peak load demands both for heating/cooling and humidification/dehumidification. These values can be used for the design of conditioning systems that must provide the required sensible and latent heats for the control of Zone 1.

To give some concise overview about comfort in Zone 1, Table 6.1 reports also the mean value of the PMV and PPD computed in steady state (i.e., after transient due to control system activation). We note that the mean PMV value never exceeds 0.6 and consequently PPD is limited 12.2%. In addition, for many weather zones smaller PMV mean values are achieved. For those cases the mean PPD is around 5% which corresponds to the minimum value for this comfort index.

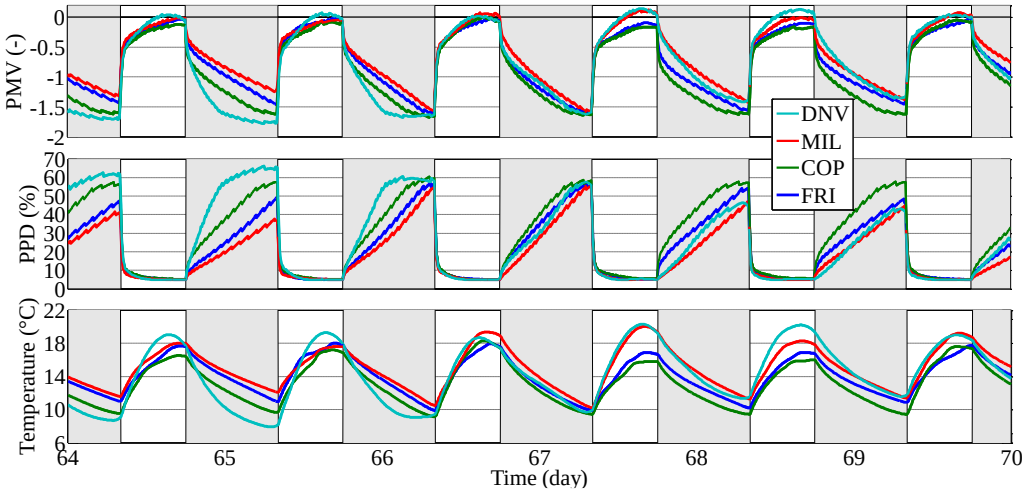

Figure 6.8. Time history of PMV, PPD and mean radiant temperature for cold winter zones.

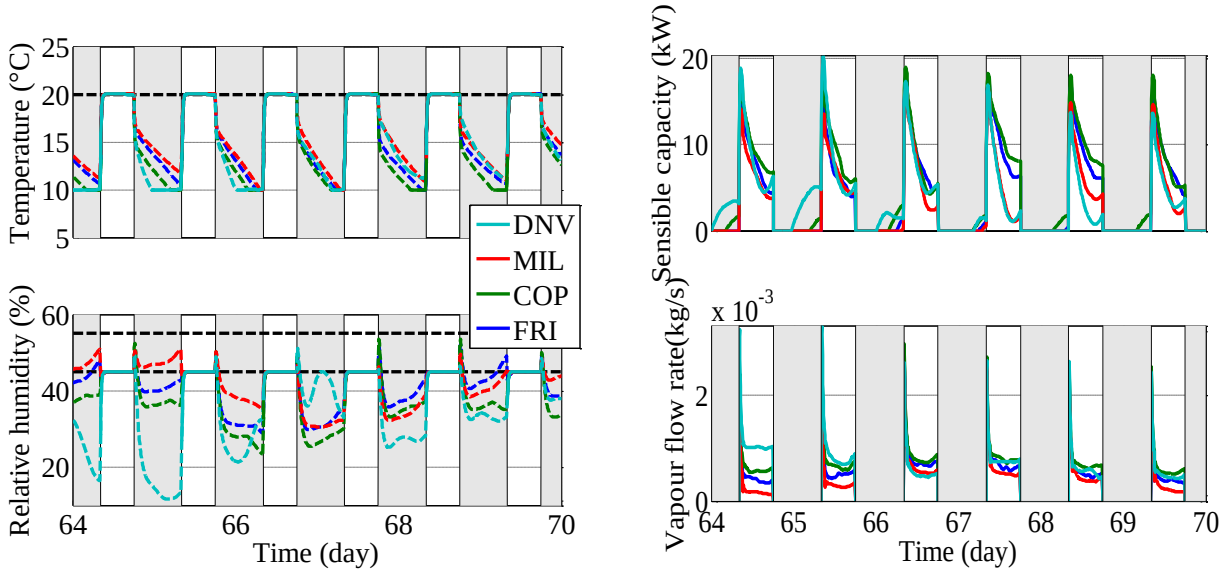

(a) **(b)**

Figure 6.9. Time history of (a) indoor air temperature, relative humidity and (b) sensible load and water vapour mass flow rate for cold winter zones.

To better illustrate the dynamics of the comfort indexes, Figure 6.8 shows the time history of PMV, PPD and mean radiant temperature for cold weather zones for a set of days during the winter season. Here, it is clear that comfort is fast imposed when the control systems are activated (white regions in Figure 6.8). For example, a PPD below 10% is always achieved also when its initial value is about 70%. The indoor air temperature and relative humidity dynamics for the same days in Figure 6.8 and the corresponding control actions required for their control are given in Figure 6.9a and Figure 6.9b, respectively. These figures also show that over the selected days the setback strategy was activated several times, avoiding therefore the indoor air temperature to go below 10 °C. In particular, the temperature controller is switched on also

during the nighttime (grey shaded area in Figure 6.9) for Denver and Copenhagen over the first four days, but for former weather zone an increase of the outdoor temperature was noted on the 68th day of the year, which prevented the reactivation of the setback strategy.

For the sake of completeness, Figure 6.10 and Figure 6.11 show a similar comfort analysis but for warm summer zones.

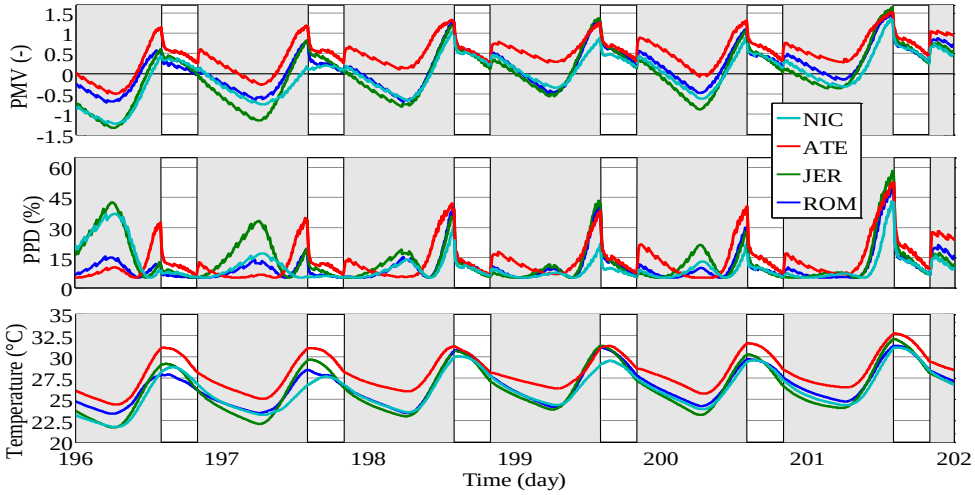

Figure 6.10. Time history of PMV, PPD and mean radiant temperature for warm summer zones.

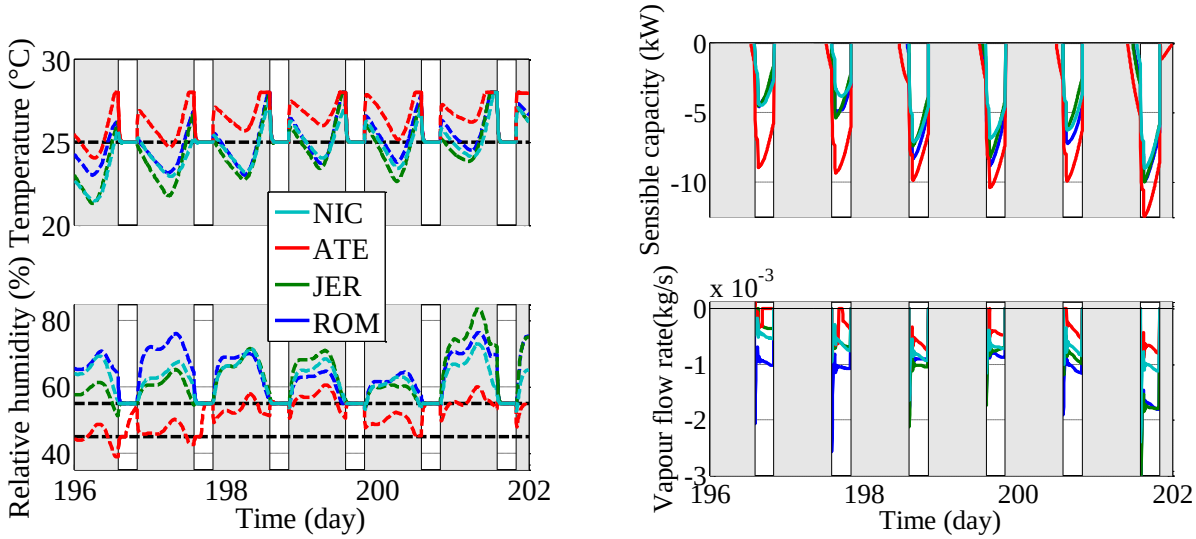

(a) **(b)**

Figure 6.11. Time history of (a) indoor air temperature and relative humidity, and (b) sensible load and water vapour mass flow rate for warm summer zones.

6.3.2 *Analysis for Zone 2 (Included zone)*

For the included thermal zone, i.e., Zone 2 or equivalently the museum display case, we start noticing that the air temperature and humidity mean square root errors calculated with respect to

the required set-points over a time horizon of one year were small, confirming therefore the effectiveness of the adaptive control strategy in satisfying strict thermohygrometric requirements, despite the coupling with Zone 1 which was not taken into account during the control design. Precisely, they resulted to be always less than 10^{-3} for every weather zone.

Figure 6.12 shows the sensible heat and the vapour flow rate (control actions) required to achieve this precise regulation in the case of a set of winter days for cold zones. In particular, we remark that, as for the winter season the indoor air temperature of Zone 1 is controlled at 20 °C from 8:00 to 18:00 (see Figure 6.9a), which is also the air temperature set point for Zone 2, in steady state there is not a gradient temperature between the two zones.

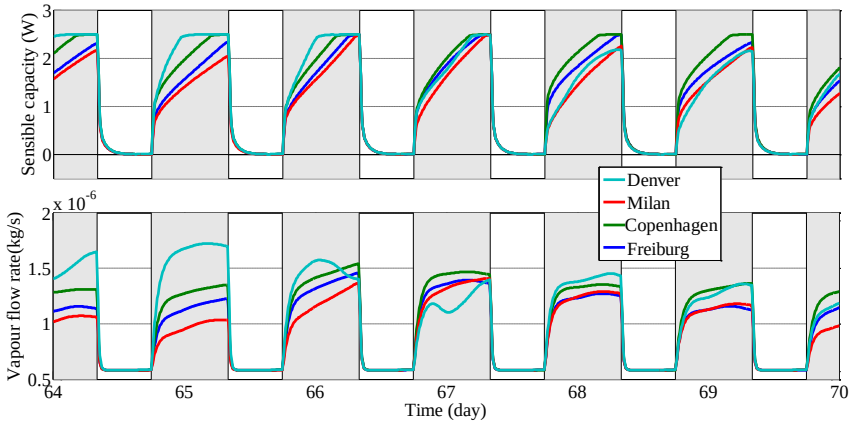

Figure 6.12. Winter season. Time history of the control actions of the sensible load and the water vapour mass flow rate for Zone 2.

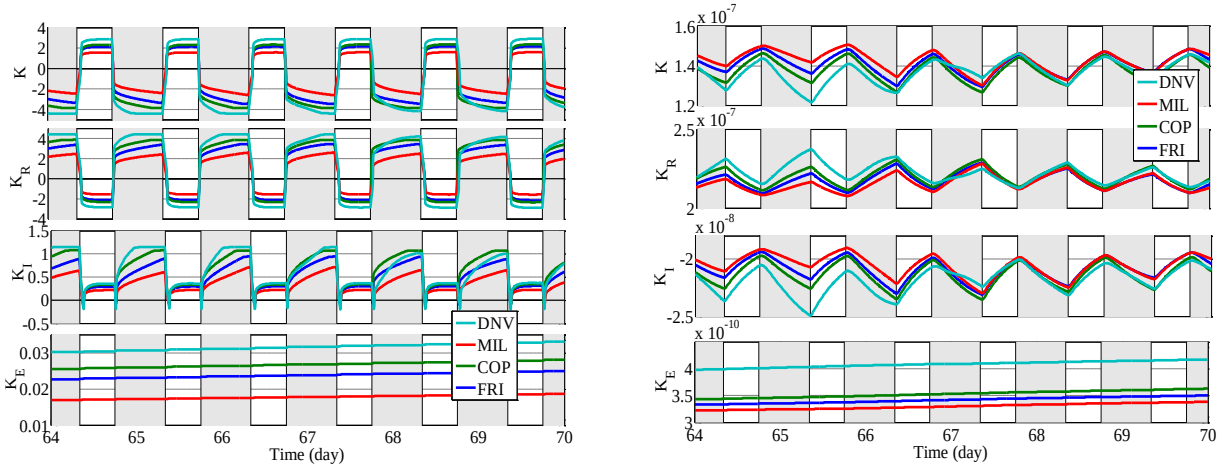

(a) **(b)**

Figure 6.13. Winter season. Time history of the adaptive gains for Zone 2 (a) for the air temperature control and (b) for the air relative humidity control.

Consequently, the sensible heat to add to Zone 2 converges to zero when the temperature controller for Zone 1 is active (white area in Figure 6.12). A different steady state regime is

achieved also during the nighttime for those weather zones where the setback strategy is activated, e.g., Copenhagen. In this case the sensible heat to provide to Zone 2 to regulate its air temperature to 20°C when the indoor air temperature of Zone 1 is 10 °C is about 2.5 W (see grey shaded area in Figure 6.12 and Figure 6.9a). A similar analysis can be carried out also for the humidity control in Zone 2 for cold winter zones. Specifically, from 8:00 to 18:00 and from the 64th to the 70th day of the year, the indoor air relative humidity is controlled at 45%. On the other hand the required set point for Zone 2 is 65%. Hence, to balance the difference between the indoor air humidity in Zone 1 and the demanded one a vapour flow rate of about 0.25 mg/s has to be provided to Zone 2 (see white area in Figure 6.12). Instead, when the humidity control of the room is deactivated (shaded grey area in Figure 6.9a) the vapour flow rate to provide to Zone 2 varies on the basis of the free floating evolution of the indoor air relative humidity in the surrounding zone (Zone 1).The adaptive gains to obtain the regulation of the thermohygrometric variables for cold winter zones are given in Figure 6.13 for the sake of completeness.

A similar analysis can be done also for hot summer zones. In this case, an example of the required control actions are given in Figure 6.14 while the related adaptive gains are depicted in Figure 6.15.

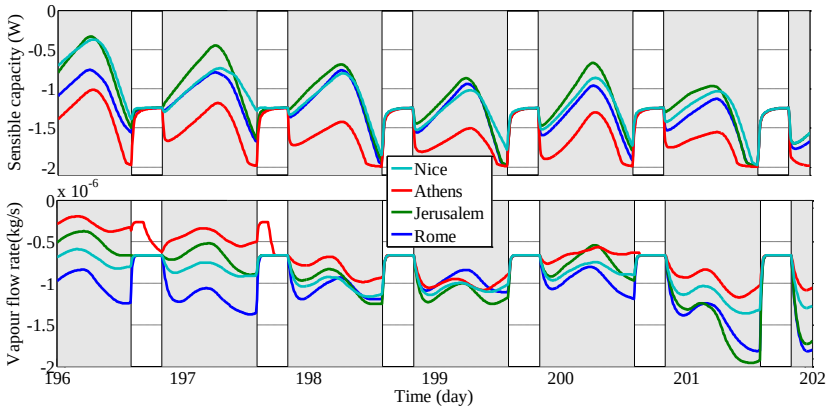

Figure 6.14. Summer season. Time history of the control actions (sensible load and the water vapour mass flow rate) for Zone 2.

For the temperature control we only remark that, as the air temperature of Zone 1 is controlled at 25 °C from 15:00 to 20:00 (see white area in Figure 6.11a), for these hours a constant cooling of about -1.25 W is required to keep temperature of Zone 2 at 20 °C. Instead a steady state of the cooing demand is not achieved when the temperature controller for Zone 1 is deactivated (see grey shaded area in Figure 6.11a).

For the included Zone 2 (glass display case), the calculated energy demands, both for sensible and latent heats, are reported in Table 6.2.

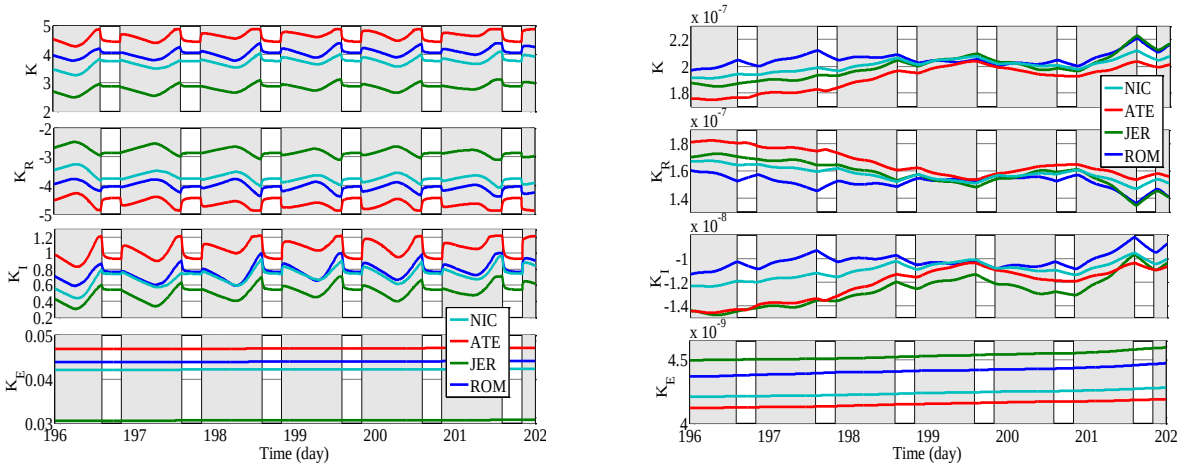

(a) **(b)**

Figure 6.15. Summer season. Time history of the adaptive gains for Zone 2 (a) for the air temperature control and (b) for the air relative humidity control.

As in the case of the room, also these data can be used by practitioners to estimate both consumptions and tune proper air conditioning systems. In particular it is possible note that for many weather zones the sensible demand has the same order of magnitude of the latent energy demand. Furthermore, for high HDD (first four weather zones in Table 5.3) the heating demand differs from the humidification demand at most of 37.14% (Milan).

Weather zone	**Mode**	**Energy Demand**		**Peck Load**	
		Sensible (kWh/m^2y)	**Latent** (kWh/m^2y)	**Sensible** (W)	**Latent** (mg/s)
Copenhagen	*H*	5.15	3.76	2.99	1.68
	C	-0.92	-0.48	-1.35	-0.93
Denver	*H*	4.61	6.18	3	1.85
	C	-2.3	-0.29	-1.99	-1.01
Freiburg	*H*	4.47	3.25	2.99	1.62
	C	-1.66	-0.43	-1.97	-0.79
Milan	*H*	4.2	2.64	2.99	1.53
	C	-2.73	-1.59	-1.98	-1.34
Rome	*H*	2.47	1.1	2.55	1.35
	C	-3.66	-1.83	-2.00	-1.49
Nice	*H*	2.16	1.24	2.10	1.28
	C	-3.34	-1.38	-1.99	-1.23
Naples	*H*	2.27	0.92	2.46	1.28
	C	-3.78	-2.35	-2.00	-1.62
Jerusalem	*H*	1.92	0.93	2.13	1.21
	C	-3.8	-2.12	-2.00	-1.88
Athens	*H*	1.66	0.97	2.03	1.25
	C	-4.78	-0.87	-2.01	-0.9

Table 6.2. Man value data for Zone 2: heating (H) and cooling (C) energy demand and peak load.

6.4 **Case Study 2: multi-zones**

To further prove the effectiveness of the adaptive strategy to suppress the coupled dynamics of thermal systems in Figure 6.1 also when more than one inner zone dynamics have to be tackled, we consider here an additional case study that refers to a Neonatal Intensive Care Ward (NICW) in which six Neonatal Intensive Care Units (NICUs), for premature and full-term newborn babies, are placed. In each NICU, an accurate climate control provides exact suitable conditions of air temperature and relative humidity, simultaneously. The sketch of the modelled seven-zones building is shown in Figure 6.1 with Z=7.

For the NICW, Zone 1, a heavy building envelope, with length, width and height equal to 8, 7 and 3.5 m, respectively, is considered. The building longitudinal axis is East-West oriented and a South facing window (4-6-4 air filled double-glazed system) of 12 m^2 is taken into account. The thickness of the building walls and floor/ceiling are 35 and 25 cm, respectively. Their stratigraphy is designed by concrete (λ = 0.51 W/mK, ρ = 1400 kg/m^3, c = 1000 J/kgK), semi-aerated bricks (λ = 0.6 W/mK, ρ = 1000 kg/m^3, c = 840 J/kgK) and thermal insulation (λ = 0.04 W/mK, ρ = 15.0 kg/m^3, c = 1400 J/kgK). The direct solar radiation transferred through the window to the inside zone is assumed to be absorbed by the floor with an absorption factor of 0.3. The absorption and emission factors of interior surfaces are assumed to be equal to 0.15 and 0.9, respectively. For such zone, a ventilation rate equal to 0.8 Vol/h and a crowding index of 0.054 person/m^2 (3 pers.) are adopted. Each NICU (zones 2 to 7 in Figure 6.1) has length, width and height equal to 1.3, 0.77 and 0.60 m, respectively. In such zones, a polycarbonate envelope of 2.0 cm thickness is assumed and an occurring air infiltration of 0.5 Vol/h is modelled. In order to assess the effectiveness and robustness of the control algorithm, several accidental, heavy and intensive thermo-hygrometric disturbances are simulated. They regard*: i)* the opening of Zone 1 windows, simulated by an additional outdoor air flow rate of 1.4 kg/s, occurring at 9:00 and 16:00 (for 1 hour); *ii)* the opening of the 6 NICUs, modelled as additional outdoor air flow rates of 3.5 g/s for each NICU, occurring for 10 minutes every 6 hours; *iii)* a steep increase of internal gains, simulated from 14:00 to 16:00 by increasing the crowding index to 0.142 person/m^2 (9 pers.).

The computer simulation model of the neonatal ward, including the incubators systems, was implemented in a MatLab/Simulink environment. The simulation starts at 0:00 on January 1st and ends at 24:00 on December 31st. In zone 1, heating and cooling are activated for indoor air temperature lower than 20°C and higher than 26°C, respectively. Simultaneously, humidification and dehumidification are required for relative humidity lower than 45% and higher than 55%,

respectively. Inside the NICUs, different indoor air temperature and humidity set points are taken into account as a function of the mass of infants, gestational age and days of life Table 6.3 [152].

Characteristics	*NICU1*	*NICU 2*	*NICU 3*	*NICU 4*	*NICU 5*	*NICU 6*
Birthweight [kg]	0.90	1.35	1.75	2.85	2.05	2.35
Gestational age in weeks [w]	25	32	27	24	28	30
Days [d] or weeks [w] of life	3 d	10 d	8 d	13 d	4 w	6 w
Temperature set point [°C]	34	33	32	32	30	29
Humidity set point [%]	85	40	60	85	60	40

Table 6.3. NICUs temperature and humidity set points as a function of the mass of infants, gestational age and days of life

In the NICW and NICUs zones, air temperature and humidity are controlled 24/7. Sensible and latent losses of each premature infant are calculated by adopting a decoupled approach [87]. Such physical and biological model includes conduction, convection, radiation, evaporation, breathing and heat generation from the infant, as described in [152]. Finally, in the following numerical analysis we consider as weather zones those in Table 5.3.

6.5 **Numerical results**

In the following subsection we discuss the results of the numerical analysis first for the Zone 1, i.e., Neonatal Intensive Care Ward (NICW), and then those of Zone 2-7, i.e., the six Neonatal Intensive Care Units (NICUs). As in Section 6.3, during the design of the adaptive control schemes the mutual thermal effects between the zones have not been taken into account. Hence, the coupled dynamics in Section 6.1 are considered as additional uncertainties to tackle in closed loop to impose the required indoor air temperature and humidity set points.

6.5.1 *Analysis for Zone 1 (Outer zone)*

In this section we stat considering the closed-loop dynamics of the Neonatal Intensive Care Ward (NICW). For the evolution of the thermohygrometric variable, when the adaptive controller is used to tackle external disturbances, many observations can be done. The classification of the resulting system dynamics can be done mainly on the basis of the weather zones in Table 5.3 as well as the time range of interest. For example, for cold zone there is never free floating of the indoor air temperature and humidity and the required set points are constantly 20 °C and 45%, respectively. On the other hand, for weather zones with smaller HDD in Table 5.3 free floating was not detected for hot summer days. Consequently, for these cases the adaptive controllers impose an indoor air temperature of 26 °C with a relative humidity of 55% despite the activation and deactivation of the sudden disturbances described in Section 6.4 As

detected for the case study illustrated in Section 6.2 and Section 6.3, also in this case the regulation error is always below 10^{-3} for every weather zone. The sensible heat and the vapour flow rate (control actions) for a set of weather zones and some sample days are reported in Figure 6.16. In these figures different colors for the shaded areas are used to denote the activation and deactivation of different disturbances acting on Zone 1. The meaning of each color is reported in Table 6.4. From Figure 6.16, it is clear that the dominant disturbance to be rejected to preserve the required thermohygrometric conditions is the window opening.

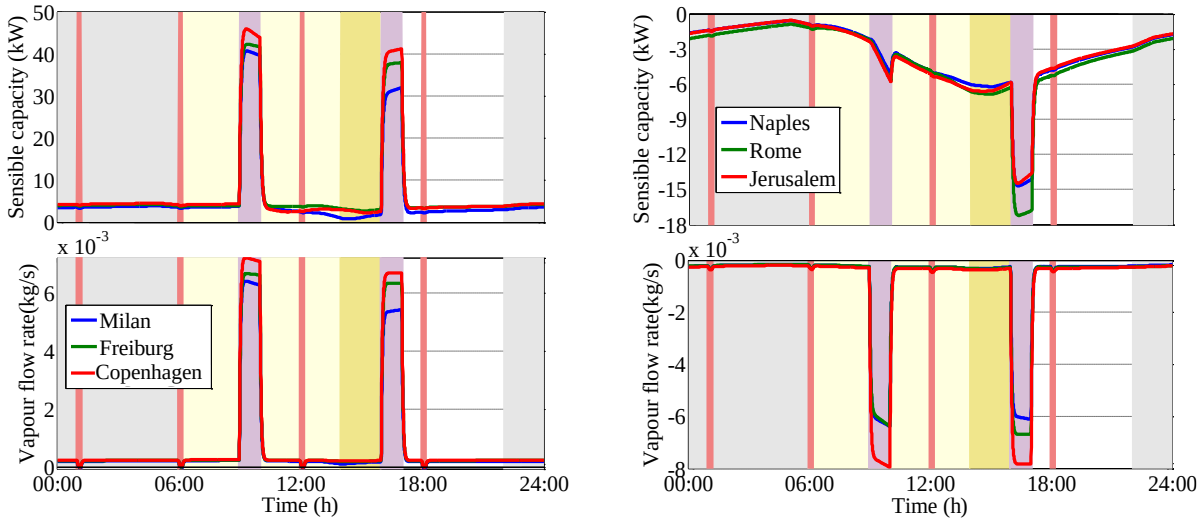

Figure 6.16. Sensible heat and vapour flow rate (a) cold winter zones during the 14th day of the year and (b) hot summer regions during the 230th day of the year. See Table 6.4 for details on colour shaded areas.

Time range	Description of the disturbance	Color of the shaded area
1	No lightning, and a crowding index equal to 0.036 person/m^2	Grey
2	Opening of Zone 1 windows, simulated by an additional outdoor air flow rate of 1.4 kg/s, occurring at 9:00 and 16:00 (for 1 hour)	Light Purple
3	Opening of the 6 NICUs, modelled as additional outdoor air flow rates of 3.5 g/s for each NICU, occurring for 10 minutes every 6 hours	Dark Pink
4	A first steep of internal gains, simulated from 06:00 to 12:00 by increasing the crowding index to 0.054 person/m^2	Light Yellow
5	A second steep of internal gains, simulated from 14:00 to 16:00 by increasing the crowding index to 0.142 person/m2 (9 pers.).	Dark Yellow
6	Lighting on and a crowding index equal to 0.036 person/m^2	White (no color)

Table 6.4. Activation/deactivation of disturbances.

Indeed, from 9:00 to 10:00 and from 16:00 to 17:00 the control actions increase, reaching higher values with respect to the other hours of the day. Precisely, in the case of cold winter zones during the 14th day of the year (Figure 6.16a) both additional sensible and latent heats are required to control the indoor air temperature to 20°C and the indoor relative humidity to 45%. While in the case of hot summer regions during the 230th day of the year (Figure 6.16b)

additional cooling and dehumidification are needed to keep the indoor air temperature and humidity to 26°C and 55%, respectively. For the sake of completeness, Figure 6.17 shows the adaptive gains corresponding to the days in Figure 6.16.

Free floating evolution of the thermohygrometric variables have been obtained in the case of cold weather zones during warm days. The the joint effect of the presence of the NICUs and higher external temperature allow both the indoor air temperature and the humidity to evolve within the possible admissible ranges.

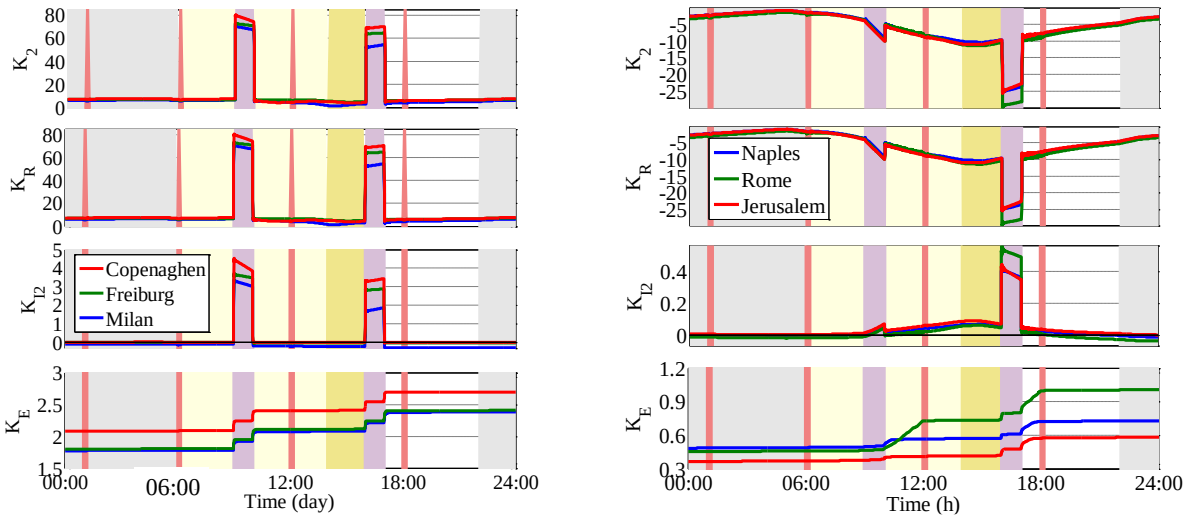

Figure 6.17. Adaptive gains: (a) cold winter zones during the 14th day of the year and (b) hot summer regions during the 230th day of the year. See Table 6.4 for details on colour shaded areas.

For istance, Figure 6.18 shows the indoor air temperature and relative humidity evolution during May 28th-29th. It is interesting to remark that for these days the indoor air temperature evolve in free evolution as far as windows are kept closed. Nevertheless the adaptive controller has to be reactivated to avoid that such temperature goes below the admissible low value during window openings. On the other hand openings of NICUs have a small effect of this temperature and only a small increase has been detected. This is possibly due to the small time range (10 min) that this systems are open.

The effect of NICUs openings is more severe in the case of indoor air relative humidity as clearly shown in Figure 6.18 where sudden and not negligible increase of this quantity, as response to this impulse disturbance, has been observed.

Similar considerations can be done for warm weather zones during winter season (see for example Figure 6.19). In this case it is interesting to point out that without the presence of the NICUs, free floating would not been possible. Precisely, in this case the NICUs provide to Zone

1 a sufficient extra heating which allows, taking into account also outdoor air conditions, to switch off the heating system.

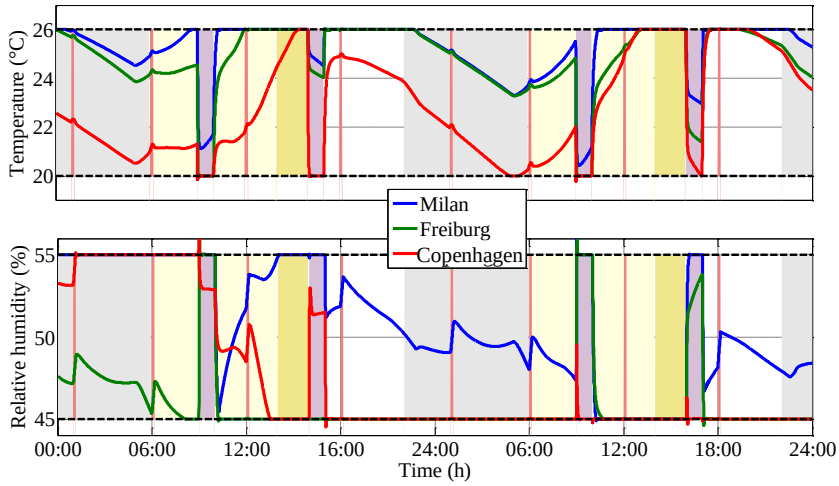

Figure 6.18. Evolution of the indoor air temperature and relative humidity for cold weather zones during a set of warm days (148th -149th day of the year). See Table 6.4 for details on colour shaded areas.

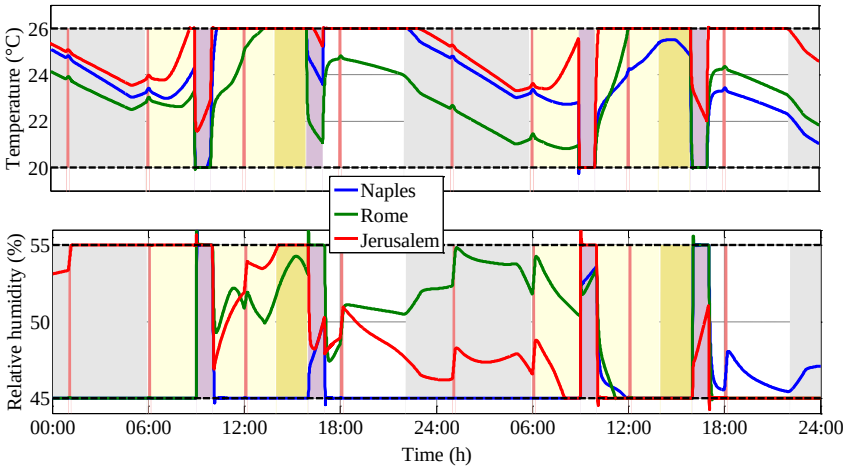

Figure 6.19. Evolution of the indoor air temperature and relative humidity for hot weather zones during a set of winter days (314th -315th day of the year). See Table 6.4 for details on colour shaded areas.

For the sake of completeness Figure 6.20 reports the control action for some days for the cases in Figure 6.18 and Figure 6.19. Here it is evident, that conditioning systems must be reactivated to tackle the effect of window openings.

We finally conclude by considering the energy demands, peak loads and comfort for all weather zones in Table 5.3 which results are concisely reported in Table 6.5. It is possible to note that for any generic day, a suitable mean value comfort, expressed in terms of mean PMV and PPD, is always achieved despite the HDD value. In particular PMV varies from -0.574 to 0.513, consequently the mean PPD is always below 12%.

Energy demand strongly depends on the HDD. Precisely, for high HDD, heating demand is dominant. On the other hand, when HDD decreases the need for cooling cannot be neglected. In addition, window openings for two hours per day strongly effect heating/cooling demand and higher values have been obtained with respect to those in Section 5.4.1. Such energy demands were expected as during window openings the required sensible heat increase also up to ten times with respect to the hours when this disturbance is deactivated (see Figure 6.16). Similar considerations can be done also for latent energy demands and the required peak load.

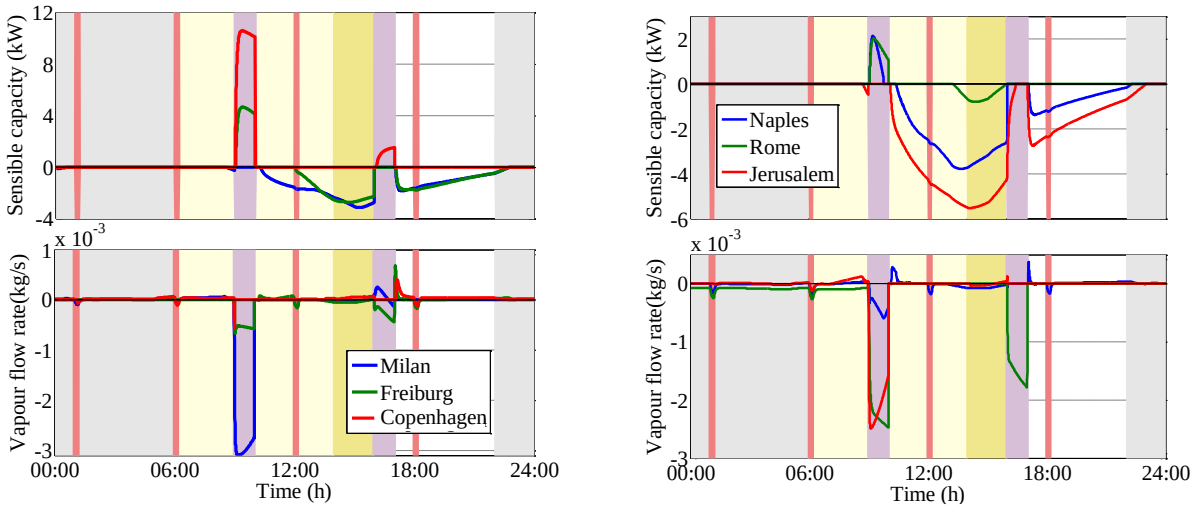

Figure 6.20. Control actions for the case of (a) cold weather zones during the 148th day of the year and (b) hot weather zones during the 315th day of the year. See Table 6.4 for details on colour shaded areas.

Weather zone	Mode	Energy Demand		Peck Load		Comfort	
		Sensible (kWh/m^2y)	Latent (kWh/m^2y)	Sensible (kW)	Latent (g/s)	PMV (-)	PPD (%)
Copenhagen	*H*	317.48	60.05	49.74	7.41	-0.574	11.90
	C	-32.22	-4.24	-5.54	-0.76	-0.045	5.04
Denver	*H*	237.48	98.97	74.3	10.97	-0.165	5.56
	C	-79.77	-3.37	-16.74	-2.58	0.124	5.39
Freiburg	*H*	261.47	54.67	46.09	7.72	-0.202	5.85
	C	-55.9	-3.41	-15.93	-0.74	0.045	5.04
Milan	*H*	229.53	43	42.19	7.61	0.132	5.36
	C	-88.03	-16.92	-13.42	-2.1	0.102	5.21
Rome	*H*	104.98	28.64	30.8	2.55	0.295	6.81
	C	-125.8	-23.29	-17.49	-5.01	0.364	7.75
Nice	*H*	89.38	33.08	26.58	2.15	0.235	6.15
	C	-103.99	-18.81	-11.72	-3.89	0.391	8.18
Naples	*H*	92	26.93	29.92	2.14	0.295	6.80
	C	-129.96	-27.14	-17.18	-5.62	0.399	8.31
Jerusalem	*H*	71.62	24.58	26.61	1.62	0.324	7.18
	C	-137.63	-24.84	-17.23	-7.97	0.554	11.43
Athens	*H*	64.4	27.28	27.18	2.56	0.383	8.05
	C	-179.08	-6.81	-22.33	-0.74	0.513	10.49

Table 6.5. Man value data for Zone 1: heating (H) and cooling (C) energy demand and peak load, average PMV and PPD during winter (H) and summer (C) seasons.

6.5.2 *Analysis for the included zones*

Different from a Neonatal Intensive Care Ward (NICW), the Neonatal Intensive Care Units (NICUs) require the exact regulation of both indoor air temperature and relative humidity (see Table 6.3) for 24/7. As detected for the case study illustrated in Section 6.2 and Section 6.3, also in this case the regulation error is always below 10^{-3} for every weather zone. Figure 6.21a shows, as an illustrative example, results achieved during several hours of the same winter day (January 25th) in the case of the weather zone of Naples. Specifically, the profile of the heating control actions necessary to keep the NICUs 1-6 (or equivalently Zones 2-7) air temperatures perfectly constant and equal to their required set-points during the 24 h are depicted together with the dynamic profiles of the previously described sensible load disturbances. Obviously, the thermal loads of the Zones 2-7 are much smaller than those related to Zone 1.

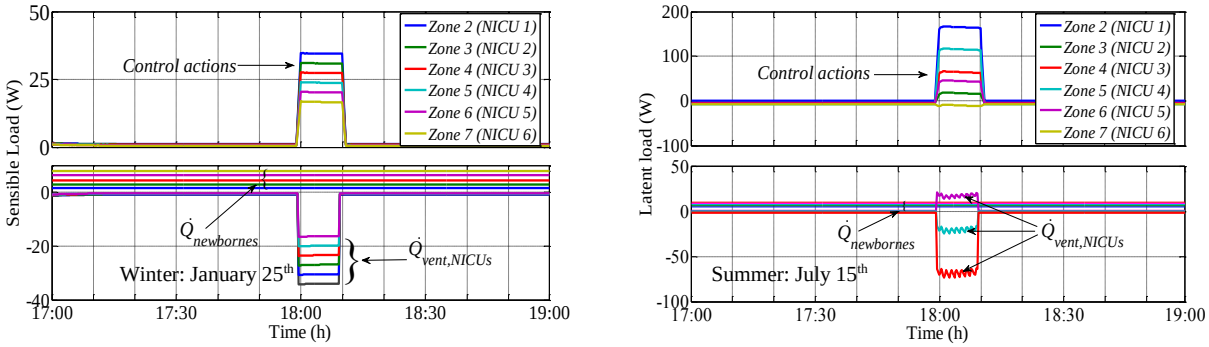

(a) **(b)**

Figure 6.21. NICUs – Indoor air temperature and humidity control actions and simulated disturbances in the case of the weather zone of Naples.

In Figure 6.21b the profile of the humidification/dehumidification control actions necessary to keep the NICUs at their required relative humidity set-points for the selected summer day (July 15th) are reported together with the occurring latent load disturbances. Note that, in several cases the NICUs disturbances overlap each other.

With the help of the obtained numerical results, some conclusions can be highlighted, such as: *i)* temperature and humidity set points (control targets) for the enclosed Zones 2-7 are always achieved for all the investigated sensible and latent load disturbances; *ii)* in all the zones (where a continuous control of both the temperature and humidity is required) very low regulation errors for the indoor air temperature and relative humidity are obtained despite of the oscillation of outdoor and Zone 1 climate conditions.

Since Zone 1 is controlled, for Zones 2-7 (NICUs 1-6) the external temperature always oscillates between 20 – 26 °C with a relative humidity between 45% and 55%. Consequently,

different from Zone 1, the maximum control actions (sensible heat and vapour flow rate) are required during the openings of the NICUs, i.e., window openings do not effect NICUs thermohygrometric dynamics. In addition, in the case the indoor temperature of the surrounding zone (Zone 1) is controlled at either 20 °C or 26 °C (analogously, the indoor relative humidity is controlled at either 45% or 55%) the maximum sensible heats (analogously, vapour flow rate) for the included zones do not depend on the day and take a constant value, while when there is free floating in Zone 1, the maximum value of the control actions in Zones 2-7 cannot be predicted easily. For example, Figure 6.22 shows the case of Copenhagen. Here, it is clear that for this weather zone and for almost all winter days, the indoor air temperature and relative humidity for Zone 1 are controlled at 20 °C and 45%, respectively. Furthermore, the maximum sensible and vapour flow rate peak loads scale on the basis of the NICU as a function of the reference temperature set point and the relative humidity set point, respectively (see Table 6.3). In addition, free floating of the thermohygrometric variables of Zone 1 occur during the summer season.

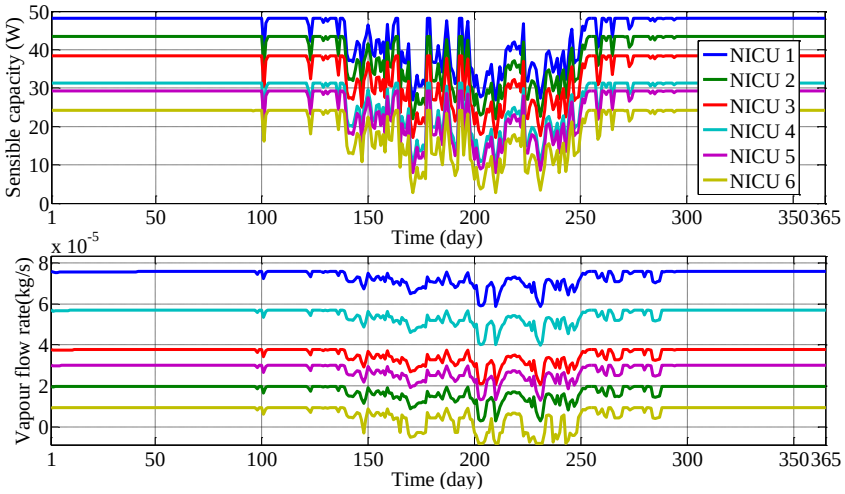

Figure 6.22. Maximum value of the control actions (sensible heat and vapour flow rate) for each day of the year in the case of Copenhagen.

Similar considerations can be done also for the Jerusalem weather zone in Figure 6.23. Nevertheless, different from Figure 6.22, in this case there is not free floating for the thermohygrometric variables of Zone 1 also for hot summer days. Hence, for those days, a constant maximum sensible and vapour flow rate peak loads are required for the included zones.

Table 6.6 and Table 6.7 report the sensible heating and latent heating/cooling demands, respectively, computed on the yearly basis for all the investigated thermal zones and weather conditions. For NICUs (zones 2-7), the obtained sensible and latent energy demands basically depends on the required indoor conditions (see Table 6.3).

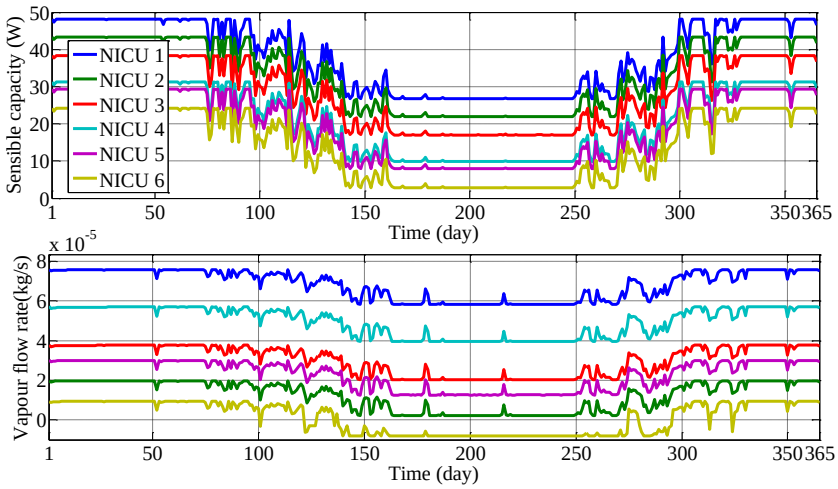

Figure 6.23. Maximum value of the control actions (sensible heat and vapour flow rate) for each day of the year in the case of Jerusalem.

It is interesting to note that such energy demands do not change too much on the basis of the weather zone. Again, this is mainly due to the precise control of the indoor air within Zone 1 whose thermohygrometric state variables are bounded in the design set by means of the adaptive control despite the selected weather zone.

	NICU 1 (kWh/m^{2}y)	**NICU 2** (kWh/m^{2}y)	**NICU 3** (kWh/m^{2}y)	**NICU 4** (kWh/m^{2}y)	**NICU 5** (kWh/m^{2}y)	**NICU 6** (kWh/m^{2}y)
Copenhagen	10.8	9.38	7.96	5.91	5.46	4.07
Denver	9.49	8.07	6.66	4.64	4.19	2.83
Freiburg	10.37	8.95	7.53	5.49	5.04	3.66
Milan	10.05	8.63	7.22	5.18	4.74	3.36
Rome	9.19	7.78	6.37	4.36	3.91	2.55
Nice	9.18	7.78	6.37	4.35	3.9	2.55
Naples	9.17	7.76	6.36	4.34	3.89	2.54
Jerusalem	8.66	7.25	5.85	3.85	3.4	2.05
Athens	8.82	7.42	6.01	4.01	3.55	2.21

Table 6.6. Sensible heating demands for the NICUs for the weather zones in Table 5.3.

6.6 **Discussion**

In this chapter we have investigated the capability of the LQ-EMRAC strategy proposed in Chapter 4 to control a novel configuration of multi-zone thermal systems, where some zones are totally included in others. To this aim the building model embedded in DETECt (see Chapter 2) has been extended to take into account this novel scenario. To test the effectiveness of the adaptive strategy two case study have been proposed. The first one considers two thermal zones of a museum building. Here, a glass display case with a rigid temperature humidity micro-climate control is enclosed in a large indoor space. In particular the museum hall has been

operated via an intermittent regime, while for the glass display case a continuous running mode has been adopted.

Weather zone	**Mode**	**NICU 1** (kWh/m^{2}y)	**NICU 2** (kWh/m^{2}y)	**NICU 3** (kWh/m^{2}y)	**NICU 4** (kWh/m^{2}y)	**NICU 5** (kWh/m^{2}y)	**NICU 6** (kWh/m^{2}y)
Copenhagen	*H*	57.58	7.88	20.13	32.87	14.47	1.71
	C	-0.04	-31.54	-30.49	-55.01	-47.82	-60.79
Denver	*H*	53.65	5.92	17.5	30.23	11.99	1.15
	C	-0.24	-33.7	-31.99	-56.49	-49.46	-64.33
Freiburg	*H*	56.48	7.33	19.47	32.2	13.83	1.52
	C	-0.05	-32.1	-30.93	-55.45	-48.28	-61.7
Milan	*H*	56.14	7.23	19.4	32.13	13.76	1.43
	C	-0.03	-32.32	-31.19	-55.7	-48.53	-61.94
Rome	*H*	54.97	6.7	18.92	31.66	13.29	1.15
	C	-0.02	-32.95	-31.87	-56.39	-49.22	-62.82
Nice	*H*	54.66	6.49	18.66	31.4	13.03	1.1
	C	-0.01	-33.04	-31.91	-56.43	-49.27	-63.07
Naples	*H*	54.11	6.29	18.47	31.21	12.84	1.09
	C	-0.03	-33.41	-32.29	-56.81	-49.65	-63.63
Jerusalem	*H*	53.41	5.89	18.06	30.8	12.44	0.83
	C	-0.03	-33.7	-32.57	-57.09	-49.94	-64.07
Athens	*H*	53.42	5.79	17.93	30.67	12.32	0.84
	C	-0.01	-33.58	-32.42	-56.94	-49.79	-64.05

Table 6.7. Latent heating (H) and cooling (C) demands for the NICUs for the weather zones in Table 5.3.

Hence, we have tested the control capability to provide to the inner zone the required temperature/humidity micro-climate conditions (for preserving aims) also for not negligible change of the thermohygrometric conditions of the surrounding zone.

The second case study is instead connected to a neonatal intensive care ward. Here, a rigid temperature/humidity the micro-climate control is simulated for six enclosed neonatal intensive care units for newborn babies. The analysis of the effect of different accidental, heavy and intensive thermohygrometric disturbances on the resulting control actions have been then considered for both the included zones and the surrounding one, including window openings. In this case, the adaptive solution has shown to cope very well with these unexpected change of the operative conditions.

It is interesting to note that for both cases the adaptive controllers had to tackle coupled thermal dynamics that were not considered during the design of the control strategy. In so doing we have proven also the effectiveness of the adaptive approach to impose the required thermohygrometric conditions in the presence of unmodelled dynamics.

Chapter 7
DESIGN OF REDUCED ORDER MODEL FOR BUILDING DYNAMICS

In this chapter we propose and grey box approach to design high predictive mathematical models of the thermohygrometric variables in buildings but with a reduced number of differential equations. We point out that reduced models are of a great importance for research in the building sector. Indeed by using low order models it is possible to *i)* reduce drastically the computation time to get an insight into building energy performance when BEPS are used, especially when a large set of simulations are required to assess them [29] *ii)* derive mathematical models of building dynamics via reverse engineering methods when experimental data are available [30] and *iii)* design advanced model based controllers for ensuring energy saving and comfort [17, 28]. In particular, to optimize energy consumption, advanced control algorithms, as those belonging to the class of model predictive controllers (which will be designed in Chapter 8), need building models for the estimations of the dynamic evolutions of the thermohygrometric variables for future time instants. Models used to obtain these predictions must be accurate but simple as much as possible in order to keep the complexity of the computation of the control strategy acceptable especially for its implementation via cost effective microprocessors. An additional reason for developing simple building models is provided by the increasing interest to evaluate energy performance at the district scale [31]. In this case detailed models cannot be used because the large number of buildings to consider rapidly increase the complexity of the entire model making it useless. Hence, the current attention is limited to a rough estimation of the total energy consumptions.

In this thesis, reduced models are developed to devise up-to-date control strategies for buildings with the aim to compare their energy performance with those obtained via the adaptive strategy proposed in Chapter 4 and used in Chapter 5 and Chapter 6.

This chapter is divided into two parts. In the first we show in detail the grey box approach used to approximate the temperature dynamics of each building element with low order thermal networks. The second part is instead completely dedicated to prove the effectiveness of the modelling procedure on a set of case study of the interest. The analysis of the numerical results is

carried out quantitatively via a set of performance indexes that measures the deviation of the reduced model outputs with respect to those provided by a detailed building model both in terms of predicated *i)* indoor air temperature; *ii)* heating and cooling demands; *iii)* maximum peak load and iv) comfort (mean radiant temperature, PMV and PPD). An additional investigation is carried out also to evaluate the simulation time reduction when these simplified models are exploited. A statistical analysis is used to represent the trend of these indices in an effective and compact way.

From an implementation viewpoint the proposed framework is composed by a set of routines which have been integrated into the DETECt code. Hence, it represents a novel tool of this BEPS code that allows to users the automatic generation of low order models which can be exploited, for instance, for the cases described above where simple but reliable models are fundamentals.

7.1 **Description of the gray box model reduction approach**

According to [157] a grey-box model is one that has a known structure but has unknown parameters. The structure of these models derive from the physical or mechanistic knowledge of the underlying phenomenon that they have to reproduce including the delineation of subsystems and their interconnections. The challenge when deriving grey–box model is twofold *i)* develop meaningful reduced-order models that reflect the system behavior, while being better suited to identification, simulation and control design than a more complicated detailed but cumbersome model; *ii)* identify the unknown parameters.

In the case of buildings, it is required that reduced order models predict with a small deviation not only energy demand but also comfort of the occupants so that they can effectively substitute more complex models for some applications, e.g., design of control algorithms [17, 28] where the precise knowledge of the spatial gradients through the building elements are not required. As the comfort indexes PMV and PPD depend not only on indoor air temperature but also on the temperature of the elements of the building that face to the indoor zone of interest (through the mean radiant temperature), these temperatures become the key thermodynamical variables to match in order to obtain reliable low order systems. Consequently, the idea is to substitute each building element in Figure 2.1 with a simplified one so that $T_{i,N}$, i.e., the temperature of the layer of the i-th element connected to the indoor air temperature node, is well reproduced. The complete reduced building model is then obtained by connecting the simplified element models in accordance with their original interconnection.

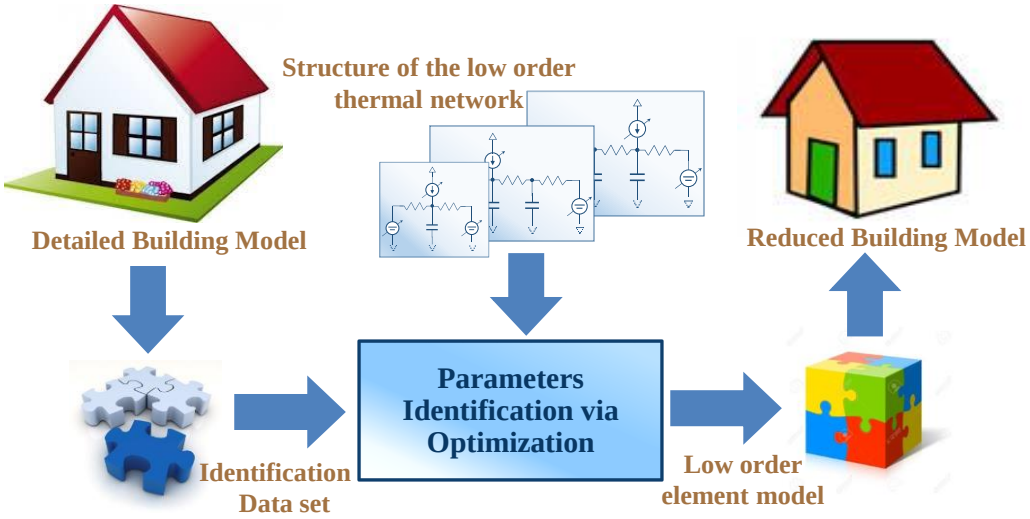

Figure 7.1. Schematization of the working principle of the building model reduction procedure.

In so doing the problem of model reduction of the entire thermal zone is recast as the model reduction of its *M* elements. Each of this *M* problem is expected to be easier to solve. We point out that, each building element is assumed to be described by a low order thermal network whose parameters are tuned by minimizing a cost function that measures the mismatch of the network output with respect to the behavior of the corresponding building element.

Figure 7.1 shows a schematization of the required steps to generate a reduced model of a thermal zone of interest from its detailed description. Those steps are outlined as follows.

1) Identify the number of elements of the thermal zone which effect the indoor air temperature and comfort indexes and how they are interconnected.
2) For each of them choose a low order thermal network and select as output variable the temperature of the node that faces to the indoor zone of interest.
3) Select a cost function that measures, for each set of the network parameters, the deviation of the output of the reduced element model with respect to the detailed one and use the complete model to generate data required for the computation of this cost function (i.e., Identification Data set in Figure 7.1).
4) Choose for the network parameters those that minimize the cost function defined at Step 3.
5) Connect the simplified models in accordance with the interconnection scheme in Step 1.

To implement the above procedure there is the need to specify the topology of the thermal network in Step 2 and the cost faction in Step 3. Indeed different choices in these steps lead to

different reduced models which can perform differently for example in terms of simulation time, energy demand, and comfort predictions, just to name a few. In the following subsections we describe in detailed all the design choices that have been considered in this thesis for constructing reduced models in accordance to the scheme in Figure 7.1 and the procedure sketched above.

7.1.1 *Low order thermal networks*

In what follows we consider two low order thermal network topologies to be used in Step 2. Precisely, we model each building element either as a first order or a second order network which are shown in Figure 7.2a and Figure 7.2b, respectively.

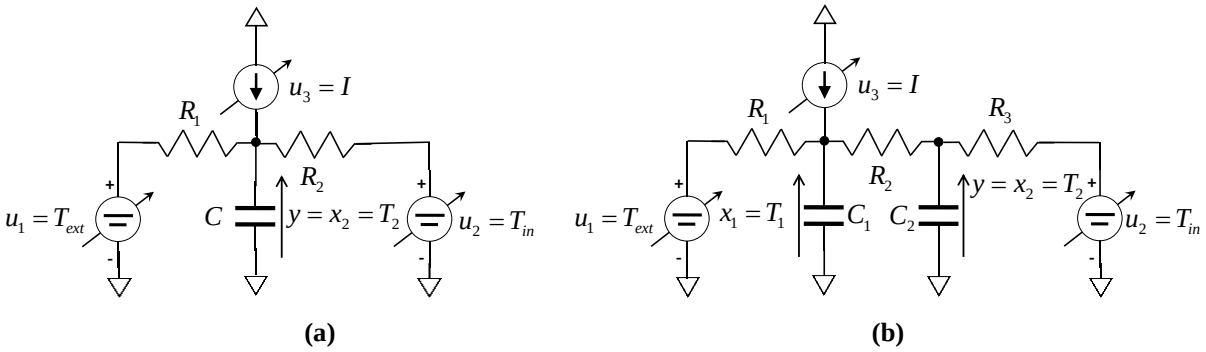

Figure 7.2. Low order thermal network used for the building model reduction: (a) first order model and (b) second order model.

According to Figure 7.2, each network has three inputs, i.e., an external temperature u_1, the indoor air temperature u_2 and a possible solar radiation u_3. Notice that, on the basis of the building element, the first input can represent either the outdoor temperature, in the case of walls, roof and windows, or the ground temperature when considering the floor element. In the latter case, in accordance with the hypothesis done in Chapter 2, I, i.e., u_3, models the solar radiation effectively transmitted through windows to the floor, therefore the source current generator for the second order network (see also Figure 7.2b) is connected to the second node, between R_2 and R_3.

By applying the Kirchhoff's laws to the networks in Figure 7.2 and defining $u = \begin{bmatrix} u_1 & u_2 & u_3 \end{bmatrix}^T$ the stack of the inputs, the first order system in Figure 7.2a is described by the following Linear Time Invariant (LTI) system

$$\begin{aligned} \dot{x} &= -\frac{1}{C}\left(\frac{1}{R_1}+\frac{1}{R_2}\right)x + \begin{bmatrix} \frac{1}{CR_1} & \frac{1}{CR_2} & \frac{1}{C} \end{bmatrix} u, \\ y &= x, \end{aligned} \tag{7.1}$$

with x being the temperature of the only node.

On the other hand, in the case of second order model in Figure 7.2b, by defining $x=\begin{bmatrix}x_1 & x_2\end{bmatrix}^T$ the stack of the temperature of the capacitive nodes, the second order network dynamics are

$$\dot{x}=\begin{bmatrix}-\frac{1}{C_1}\left(\frac{1}{R_1}+\frac{1}{R_2}\right) & \frac{1}{C_1R_2}\\ \frac{1}{C_2R_2} & -\frac{1}{C_2}\left(\frac{1}{R_2}+\frac{1}{R_3}\right)\end{bmatrix}x+\begin{bmatrix}\frac{1}{C_1R_1} & 0 & \frac{1}{C_1}\\ 0 & \frac{1}{C_2R_3} & 0\end{bmatrix}u, \qquad (7.2)$$

$$y=\begin{bmatrix}0 & 1\end{bmatrix}x.$$

From Figure 7.2 it is clear that in the case of a first order thermal network the vector parameter of model (7.1) is $p=\begin{bmatrix}R_1 & R_2 & C\end{bmatrix}$, while for the second order network in (7.2) this vector parameter is $p=\begin{bmatrix}R_1 & R_2 & R_3 & C_1 & C_2\end{bmatrix}$.

Notice that different from the approach presented in [158, 159] we use as output of the simplified networks the temperature of the node that face to the indoor zone of interest instead of the heat flows at both sides of each the building element. In so doing, if these output variables predict well the corresponding temperatures of the detailed model in Chapter 2, also the mean radiant temperature, and as consequence PMV and PPD, are well predicted.

7.1.2 *Cost Functions*

As in [160], also in this work we use two different cost functions to measure the distance between the output of the reduced models of the building elements and the corresponding outputs of the detailed model in Chapter 2. Precisely, the first cost index is set in the frequency domain. Hence, the idea is to tune the model parameters so that the frequency response of the low order thermal networks in Figure 7.2 match those of the detailed model. Consequently, the identification data set, required for Step 3 in the procedure above, is composed by the frequency response of the building element of the interest for each input of the network. These functions can be computed via the detailed model in Chapter 2 in a preassigned range of frequencies.

The frequency response of models in (7.1) and (7.2) can be instead computed analytically starting from the system response in the Laplace domain [161, 162]. Precisely, for models in (7.1) and (7.2) the output in the Laplace domain $Y(s)$ is computed as $Y(s)=G_1(s)U_1(s)+G_2(s)U_2(s)+G_3(s)U_3(s)$, where $U_i(s)$, for *i = 1,2,3,* is the Laplace transform, at the complex frequency $s\in\mathbb{C}$, of the i-th input, while $G_i(s)$, is the transfer function between the i-th input and the output. Then, the frequency response to the i-th input at the frequency ω is

$G_i(j\omega) = |G_i(j\omega)| e^{j\arg(G_i(j\omega))}$, for $i = 1,2,3$, where j is the imaginary unit, and $|G_i(j\omega)|$ and $\arg(G_i(j\omega))$ are the modulus and argument of the complex number $G_i(j\omega)$, respectively.

In the case of the first order model in (7.1) the transfer functions, $G_i(s)$, for $i = 1,2,3$, are

$$
\begin{aligned}
G_1(s) &= \frac{R_2}{R_1+R_2}\frac{1}{1+\frac{CR_1R_2}{R_1+R_2}s}, \\
G_2(s) &= \frac{R_1}{R_1+R_2}\frac{1}{1+\frac{CR_1R_2}{R_1+R_2}s}, \\
G_3(s) &= \frac{R_1R_2}{R_1+R_2}\frac{1}{1+\frac{CR_1R_2}{R_1+R_2}s},
\end{aligned}
\tag{7.3}
$$

while for the second order network in Figure 7.2b we have

$$
\begin{aligned}
G_1(s) &= \frac{R_3}{s^2+\left(R_3C_2(R_1+R_2)+R_1C_1(R_2+R_3)\right)s+(R_1+R_2+R_3)}, \\
G_2(s) &= \frac{s+R_1+R_2}{s^2+\left(R_3C_2(R_1+R_2)+R_1C_1(R_2+R_3)\right)s+(R_1+R_2+R_3)}, \\
G_3(s) &= \frac{R_1R_3}{s^2+\left(R_3C_2(R_1+R_2)+R_1C_1(R_2+R_3)\right)s+(R_1+R_2+R_3)}.
\end{aligned}
\tag{7.4}
$$

The mismatch between the frequency response of the reduced model (7.3) or (7.4) with the complete model is computed by the following cost index, which is a function only of the network parameters

$$
J_f(p) = \sum_{i=1}^{3}\sum_{k=1}^{z}\left(m_i \frac{\left|\left|\overline{G}_i(j\omega_k)\right| - \left|G_i(j\omega_k;p)\right|\right|}{\left|\overline{G}_i(j\omega_k)\right|} + \theta_i \frac{\left|\arg(\overline{G}_i(j\omega_k)) - \arg(G_i(j\omega_k;p))\right|}{\left|\arg(\overline{G}_i(j\omega_k))\right|} \right)
\tag{7.5}
$$

where $\overline{G}_i(j\omega_k) = \left|\overline{G}_i(j\omega_k)\right| e^{j\arg(\overline{G}_i(j\omega_k))}$ is the actual frequency response of the building element of interest with respect to the i-th input, $i = 1,2,3$, computed at the frequency ω_k, $k = 1,2,\ldots z$, while m_i and θ_i are positive constants that weight the relative difference between the building frequency response to i-th input with respect to that of its reduced model when the vector network parameters is p.

Notice that the set of frequencies $\omega_1 < \omega_2 < \omega_3 < \ldots < \omega_z$ to evaluate (7.5) must be chosen so that they cover the frequency spectrum of the input signals (e.g., solar radiation, outdoor temperature, ground temperature etc.) which are relevant for the building element. As rule-of-thumb we can choose $\omega_z \geq \max\{5\omega_T, 2\omega_N\}$, where ω_N is the Nyquist frequency of the input

signal and ω_T is the cutoff frequency of the building element of interest. In addition we point out that this approach does not depend from the actual time history of the input signals (or equivalently, on the weather zone where the building is located), but only from the frequency response of the thermal zone to be modelled.

An alternative approach to measure the output deviation of models (7.1) and (7.2) from the actual dynamics of the corresponding building element is that of using the following cost index defined in the time domain

$$J_t(p) = \sqrt{\frac{1}{m(\Omega)}\int_{\Omega}\left(\bar{y}(t) - y(t;p)\right)^2 dt} \tag{7.6}$$

where $y(t;p)$ is either the output of the model (7.1) or (7.2) with parameter p at the time $t \in \Omega$, where Ω is the time range of interest for the identification procedure with $m(\Omega)$ being its length, while $\bar{y}(t)$ is the output of the building element to be reduced, i.e., the temperature of the node which faces to the indoor zone of the building element, computed by means of detailed building model in Chapter 2.

Notice that the identification data set for computing the index (7.6) is $\bar{y}(t)$ with $t \in \Omega$. This function can be calculated from the time history of the inputs, e.g., solar radiation, outdoor temperature etc by integrating numerically either (7.1) or (7.2). Consequently, the J_t-index depends on the weather zone where the building is located. In addition these time histories must be also used to compute the output $y(t;p)$ of the thermal networks in Figure 7.2.

When the cost index is selected, the parameter vector of the low order model is set as follows:

$$p_{opt} = \arg\min_{p \in \mathrm{P}} J(p) \tag{7.7}$$

with J being either J_f in (7.5) or J_t in (7.6) and P is the admissible parameter set.

It is interesting to note that parameters of systems with structure (7.3) or (7.4) can be identified, after some additional manipulation, by using a black box time domain approach, e.g., least square methods [163]. Nevertheless when these approaches are used it is not easy to impose physical constraints on the admissible parameter set (i.e., P in (7.7)), and only combinations of physical parameters can be identified, i.e., the coefficients of polynomials in (7.3) and (7.4). Consequently, it is not possible in general to tune models with structures (7.1) and (7.2), whose state variables have a physical meaning, but only input-output models whose depend on the output variable y and its derivatives.

Finally, we remark that neither the minimization of the cost in (7.5) nor that in (7.6) can be solved analytical. Hence, numerical methods must be used. In this thesis the seeking of the

minima for both (7.5) and (7.6) is done by exploiting interior point algorithms which are available in the MatLab Optimization Toolbox [95] (the reader is referred to [164] for additional details on iterative and interior point optimization algorithms). In addition, as iterative optimization algorithms can stuck in local minima, also advanced genetic optimization methods have been used for the minimization of the cost index (7.5). Precisely the genetic algorithm used is that presented in [165] (the reader is referred to [166] for an introduction to the genetic algorithm and their application in engineering). We point out that genetic algorithms have not been used for the minimization of the cost function (7.6). The main reason for not seeking for global minima via genetic algorithms in the case of the optimization in the time domain is that the evaluation of J_t in (7.6) is more complex and time-consuming than the computation of J_f in (7.5). Indeed, for computing (7.6) it is required to solve a set of ODEs (7.1) or (7.2) which is more complex, from a numerical viewpoint, than the evaluation of the static function (7.5). As genetic optimization procedures often require a large number of evaluations of the cost function to find the global minima, we have decided to apply them only for the easy-to-compute cost indexes as those required for the model reduction in the frequency domain.

7.2 Add-on for the automatic building model reduction and simulation

The method for generating low order models of buildings described in Section 7.1 has been implemented in MatLab/Simulink language as a novel Add-on integrated in DETECt. The tool not only allows to generate reduced order DETECt models of buildings but also to simulate them and, if required, compare the simulation results with those provided by the detailed model described in Chapter 2

The main modules composing the software are shown in Figure 7.3. Briefly, for each building element composing the detail model, the user can select how to approximate its dynamics in accordance to the decision tree in Figure 7.4, i.e., the complexity of the element model η (fist or second order thermal network), the cost index between (7.5) and (7.6) to be minimized and the numerical method to find its minimum.

The software module “Model Splitting” decomposes the building model provided by DETECt in M sub-models, one for each building element, with M being the number of constructive elements delimiting the thermal zone of interest. Now, in the case the user selects the time domain cost function (7.6), these dynamical sub-models are integrated over the time range Ω (required as input) to compute the M functions $\overline{y}(t)$ in (7.6). Instead, when the frequency domain identification method is selected, the “Model Splitting” routine computes for each constructive

element the frequency response with respect to each input and over the frequencies required by the user, .i.e., $\bar{G}_i(j\omega_k)$, $i = 1,2,3$, and $k = 1,2,\ldots z$.

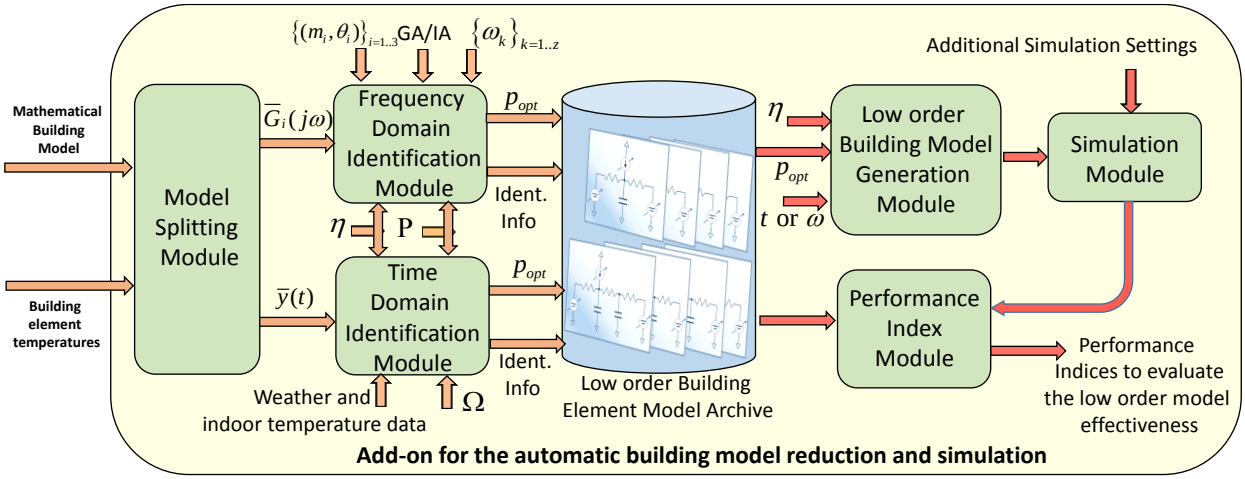

Figure 7.3. Module decomposition of the automatic building model reduction.

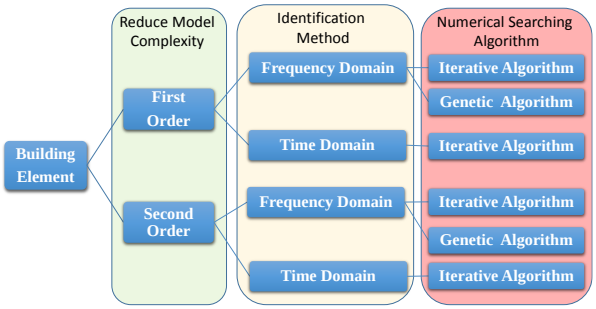

Figure 7.4. Decision tree of all the possible choices for the model reduction of each building element.

The modules "Frequency Domain Identification" and "Time Domain Identification" include the code and call to other MatLab functions and Simulink schemes to set and solve the optimization problem in (7.7) when the frequency domain or the time domain approach is used, respectively, and the parameter vector is constrained in the set P. In particular in the case of the Frequency Domain Identification" module the transfer functions in (7.3) or (7.4) are computed for the evaluation of (7.5) as required by the underlying numerical optimization procedures (iterative algorithms of the MatLab Optimization Toolbox [95], indicated as IA in Figure 7.3, or the Genetic Algorithm presented in [165], indicated as GA in Figure 7.3) taking also into account the value of the input parameters η, and the weights (m_i,θ_i), $i = 1,2,3$. Similarly, for the "Time Domain Identification" module, a Simulink scheme is used to integrate either (7.1) or (7.2) over

the time range Ω, on the basis of the input parameter η, to generate $y(t; p)$ for the evaluation of (7.6) as required by the underlying numerical optimization procedures.

The optimal parameters of the reduced model of each building element are then stored into an archive for future use together additional information ("Ident. Info" in Figure 7.3) that include:

- the number of interaction required by the optimization procedure to converge (in the case of iterative optimization numerical algorithm);
- the time required by the optimization procedure to converge (in the case of iterative optimization numerical algorithm);
- the position of the eigenvalues of the reduced and detailed building element;
- The cost value for the first and last interaction, i.e., the initial cost and the optimal cost, respectively.

There are basically two software modules that can access to the archive in Figure 7.3. The fundamental one is the module "Low Order Building Model Generation" which accesses to the archive to collect, for each building element, the optimal parameters of a pre-simplified constructive element. When the parameters of all elements have been collected, the module constructs for each of them either the mathematical model (7.1) or (7.2) and assembles the resulting systems by connecting them as in the detailed DETECt model, generating in turns the low-order complete model of the entire building. We point out that, the user can select for the reconstruction process the model order (η-parameter in Figure 7.3) for each building element as well as if the parameters to be used must be those derived by the time domain optimization or the frequency domain optimization ("*t-or-ω"*-parameter in Figure 7.3). In so doing model of mixed order can be generated.

Often reduced order building models are used to design advanced controllers to tame optimally the building dynamics. Nevertheless, on the user demands, the low-order building model can be exploited by the "Simulation" module. This module is mainly developed in Simulink and it used to solve the set of differential equations composing the complete low order building model to perform, for instance, energy and comfort analysis. To this aim the user must specify also the time range where the set of ODEs must be solved, the time histories of all building inputs (e.g., outdoor temperature, solar radiation, etc) as well as control specifications (indoor temperatures set points, time of control activation and deactivation, possible setback temperatures etc.). It is important to point out that, for temperature control, the "Simulation" module uses the control architecture presented in Chapter 3 embedding the optimal model reference adaptive controller presented in Chapter 4. In so doing a precise control of the

temperature profile can be achieved without a preliminary study of the dynamics of the reduced building system.

The additional module that can use the data in the archive in Figure 7.3 is the "Performance Index". This module uses the stored data to perform analysis, via a set of performance indexes both on the identification and simulation results. These indexes will be introduced in the following subsections.

Finally, we point out that users can combine easily the identification modules on the basis of their needs and required precision. For example, frequency domain and time domain identification methods can be merged as shown by the algorithm in Figure 7.5.

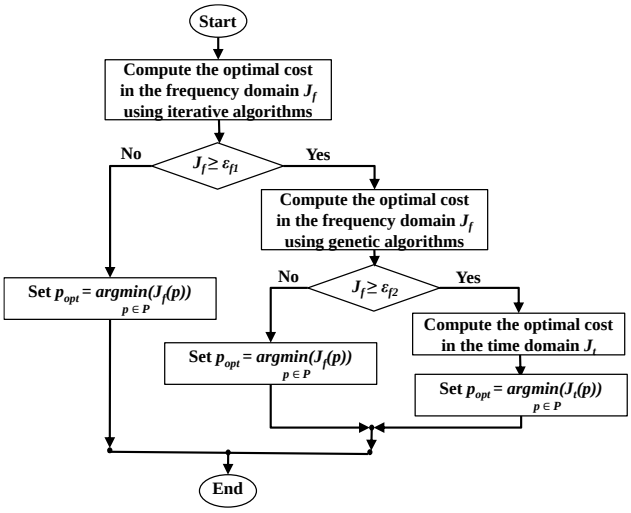

Figure 7.5. Possible combination of the proposed identification methods for each building element.

In this case, the user decides to use at first the identification in the frequency domain and solve the minimization of the cost function (7.5) initially by means of iterative optimization algorithms. In the case the resulting optimal cost is not satisfactory (this is if $J_f \geq \varepsilon_{f1}$ with ε_{f1} some positive constant), e.g., the iterative algorithm was stuck in a local minima, the same optimization can be performed via genetic algorithms. If also this result is not acceptable, e.g., $J_f \geq \varepsilon_{f2}$ with ε_{f2} some positive constant, then the user can choose to use also weather data to improve the matching between the reduced model and the detailed one by optimizing the cost function in the time domain (7.6). Of course in the later case the identification result will strongly depend on the weather zone, i.e., building location.

7.2.1 *Performance indices for evaluating low order building models*

When the low order building model has been found the tool allows to compare its dynamics and performance with those of the detailed model, A set of indexes have been implemented to

evaluate quantitatively the results of the add-on in Figure 7.3. These indexes can be dived in two sets. By defining Θ the time interval of interest, e.g., day, week, year. The first set of performance indexes measure the mismatch between the low order model and the detailed one in term of energy prediction and indoor air temperature. In particular we measure the indoor air temperature prediction capability as

$$Max\Delta T = \max_{t\in\Theta}\left|T_{in}^{d}(t) - T_{in}^{l}(t)\right|, \tag{7.8}$$

with T_{in}^{d} and T_{in}^{l} being the indoor air temperature of the detailed model and that of the low order model, respectively.

In addition we evaluate the mismatch in predicting energy demands as

$$\begin{aligned}\Delta E &= 100\frac{\left|E^{d} - E^{l}\right|}{\left|E^{d}\right|},\\ \Delta P &= 100\frac{\left|\max_{t\in\Theta}\left|Q_{HC}^{sd}(t)\right| - \max_{t\in\Theta}\left|Q_{HC}^{sl}(t)\right|\right|}{\max_{t\in\Theta}\left|Q_{HC}^{sd}(t)\right|}.\end{aligned} \tag{7.9}$$

where E^{d} and E^{l} are the heating/cooling demands computed on the time range Θ by using the detailed and reduced model, respectively, while Q_{HC}^{sd} and Q_{HC}^{sl} are the sensible heats computed by feedback controllers, designed as in Chapter 4, for the detailed and reduced model, respectively. Consequently, ΔP gives a measure of the deviation between the low order building model and the detailed one in terms of the peak sensible loads.

The second set of performance indexes is used instead to evaluate the accuracy of comfort predictions. Hence, by denoting as T_r^d, PMV^d and PPD^d the mean radiant temperature, the predicted mean vote and the predicted percentage dissatisfied, respectively, for the detailed model, and T_r^l, PMV^l and PPD^l, the same quantities but computed for the low order building system, we define

$$\begin{aligned}\Delta Tr &= \max_{t\in\Theta}\left|T_r^{d}(t) - T_r^{l}(t)\right|,\\ \Delta PMV &= \max_{t\in\Theta}\left|PMV^{d}(t) - PMV^{l}(t)\right|,\\ \Delta PPD &= \max_{t\in\Theta}\left|PPD^{d}(t) - PPD^{l}(t)\right|.\end{aligned} \tag{7.10}$$

Finally, the benefit of the use of low order model in terms of simulation time reduction is measured as

$$\Pi = 100\frac{\kappa^d - \kappa^l}{\kappa^d}, \tag{7.11}$$

Where κ^d (κ^l) is the time required to perform a simulation of one year in the case the detailed (reduced order) model is exploited.

7.3 **Numerical validation of the building model reduction procedure**

To test the effectiveness of the reduced modelling approach in Section 7.1, we consider the 54 case studies presented in Chapter 5. For each of them we have designed the grey box models in Table 7.1. Notice that, for the model Gm we have chosen to use a first order system for modelling window, roof and north wall as for these building elements acceptable frequency responses can be obtained also with the simplest thermal network (see Figure 7.2a).

Model Name	Description	Color
G8	Grey model where all the building elements are described as first order networks (see Figure 7.2a) tuned in the frequency domain, i.e., minimizing (7.5). The complete model is composed by a set of 8 ODEs.	Dark Blue
G15	Grey model where all the building elements are described as second order networks (see Figure 7.2b) tuned in the frequency domain, i.e., minimizing (7.5). The complete model is composed by a set of 15 ODEs.	Red
Gm	Grey model where some building elements, i.e., window, roof and north wall, are described as fist order networks (see Figure 7.2a) while the remaining elements are second order networks (see Figure 7.2b). For all elements, the tuning is carried out in the frequency domain, i.e., minimizing (7.5). This mixed order model is composed by a set of 12 ODEs.	Orange
Gt	Grey model where all the building elements are described as second order networks (see Figure 7.2b) tuned in the time domain, i.e., minimizing (7.6). The complete model is composed by a set of 15 ODEs.	Black

Table 7.1. Grey box models and colors associated to each of them for the figures in the following sections.

To better point out the effectiveness of low order grey box models, in what follows we compare the performance of these reduced systems in terms of temperatures, energy and comfort predictions with those provided by reduced order white box models. These white box systems have been derived from the detailed one in Chapter 2 by using two or three capacitive nodes for each building element. A summary of these additional building dynamical systems is given in Table 7.2. Notice that W2 is a white box model composed by two equations, one for the envelope and one for the indoor air temperature, similar to that used in [103]. Furthermore the detailed model is composed by and ODE of 71 equations.

Model Name	Description	Color
W22	Building model tuned by means of physical parameters and composed by a set of 22 ODEs.	Green
W15	Building model tuned by means of physical parameters and composed by a set of 15 ODEs.	Light Blue
W2	Building model tuned by means of physical parameters and composed by a set of 2 ODEs see also [103].	Magenta

Table 7.2. White box models and colors associated to each of them for the figures in the following sections.

We remark that also for each white model in Table 7.2 we have considered the 54 case studies in Chapter 5. Hence, in the following subsections we consider 432 numerical simulations on a yearly basis. Consequently, to compare this large set of data concisely and effectively, statistical analysis are performed. The mathematical expression of the resulting Probability Density Functions (PDF) of interest have been collected in Appendix B, where for each of them we point out its parameter vector. The values of these parameter vectors are reported in tables in the following sections. Concerning all the figures shown in the next subsections, the meaning of the different color lines is that summarized in Table 7.1 and Table 7.2 when not indicated explicitly in the figure caption.

7.3.1 *Grey box identification results*

The parameters of models G8, G15 and Gm in Table 7.1 have been identified in the frequency domain. For constructing the cost function in (7.5), we have chosen frequencies belonging to the range $\omega \in [0, 10^{-3}]$ rad/s which contains the relevant part of the frequency spectrum of the external inputs, i.e., outdoor temperature and solar radiations, of the weather zones taken into account in Chapter 5. This is also confirmed by Figure 7.6 which shows the Fast Fourier Transform of the solar radiations. A similar range of frequencies have been found suitable also for the spectrums of external temperatures, but they are not reported here for the sake of brevity.

Some statistical results about the frequency domain identification are reported in Table 7.3.

Index	Mean	Variance	Maximum	PDF	PDF Parameters		
J_{opt} - 1° order model	281.86	$1.68 \cdot 10^5$	1500	Rayleigh	349.04		
J_{opt} - 2° order model	2.85	16.67	15.1	Rayleigh	3.5		
$\Delta\lambda_1$-1° order model	-13.77	346.32	65	Normal	-13.77	18.56	
$\Delta\lambda_1$-2° order model	-1.04	16.38	11.1	t-location Scale	-0.46	1.16	2.19
$\Delta\lambda_2$-2° order model	24.14	560.35	95.15	Gen.Extreme Value	1.07	8.74	6.12

Table 7.3. Statistical analysis of the identification result in the frequency domain.

We remark that the random variables that model the numerical data for any generic index in Table 7.3, as well as their parameters, are the result of another optimization problem based on the outcome of the identification and it is solved in Matlab via the routines in [167].

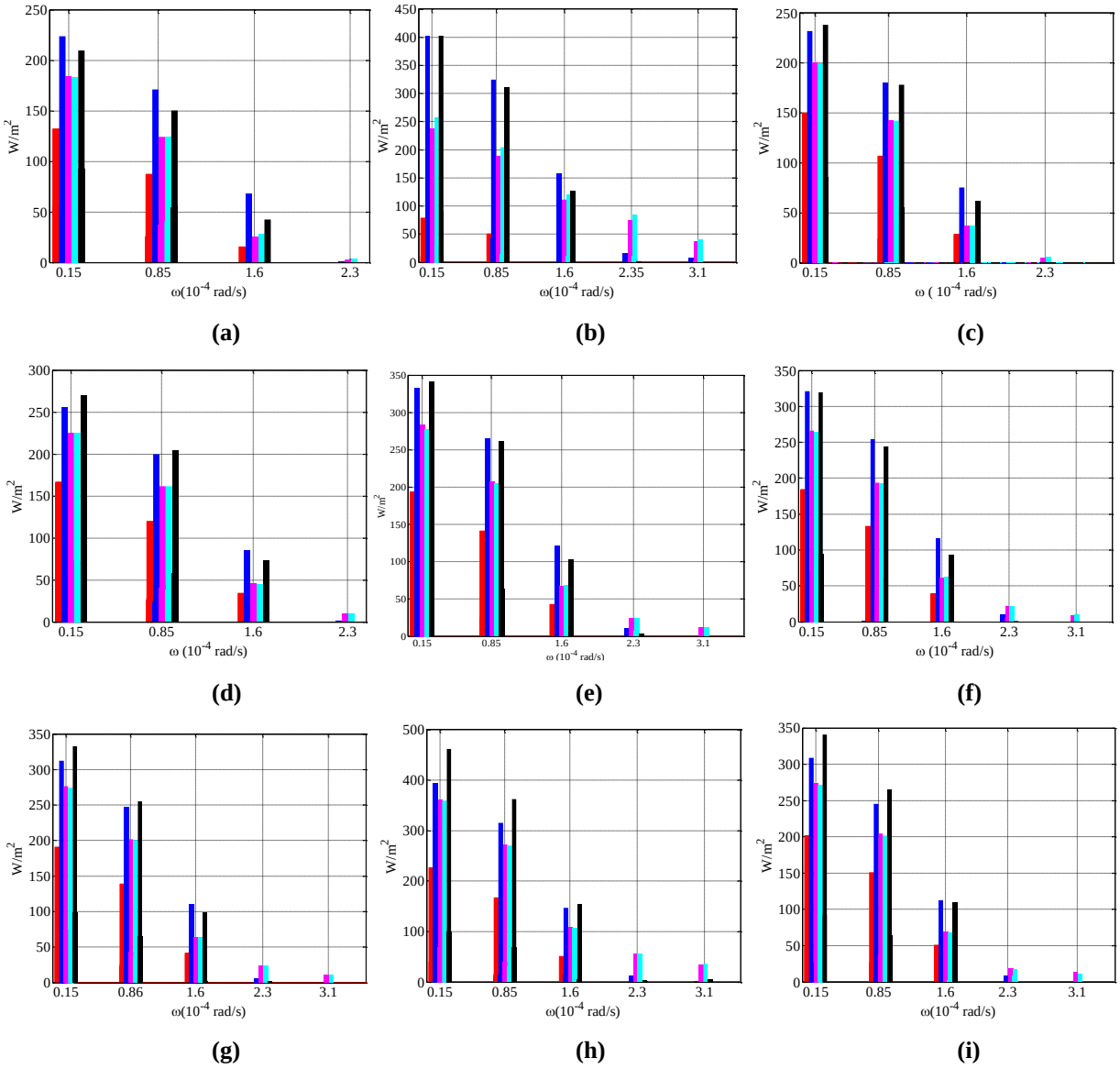

Figure 7.6. Fast Fourier Transform of the solar radiations for the weather zone of interest, North wall (red), South wall (blue), West wall (magenta), Est wall (cyan), roof (black): (a) Copenhagen; (b) Denver, (c) Freiburg; (d) Milan; (e) Rome; (f) Nice; (g) Naples; (h) Jerusalem (i) Athens.

In addition to the Probability Density Function (PDF) for the optimal cost $J_{opt,}$ (i.e., the results of the minimization of (7.5) for each element of each model G8, Gm and G15) we have also computed the PDF of the percentage variation of the eigenvalues of the reduced thermal networks with respect those of the corresponding detailed building elements. To define formally this measure, assume to sort the eigenvalues of a given LTI system in a descending order. Hence, for each low-order model we compute

$$\Delta\lambda_i = 100\frac{\lambda_i^d - \lambda_i^l}{\lambda_i^d}, \tag{7.12}$$

with $i = 1$, for first order networks, or $i=1,2$ for second order networks, while λ_i^d and λ_i^l are the i-th eigenvalues of the detailed and low order model, respectively.

As clearly shown in Table 7.3 and Figure 7.7, the optimal costs of first order thermal models are much larger than those of second low order systems. This is mainly due to the impossibility of first order models to match the frequency response of detailed building elements at high frequencies.

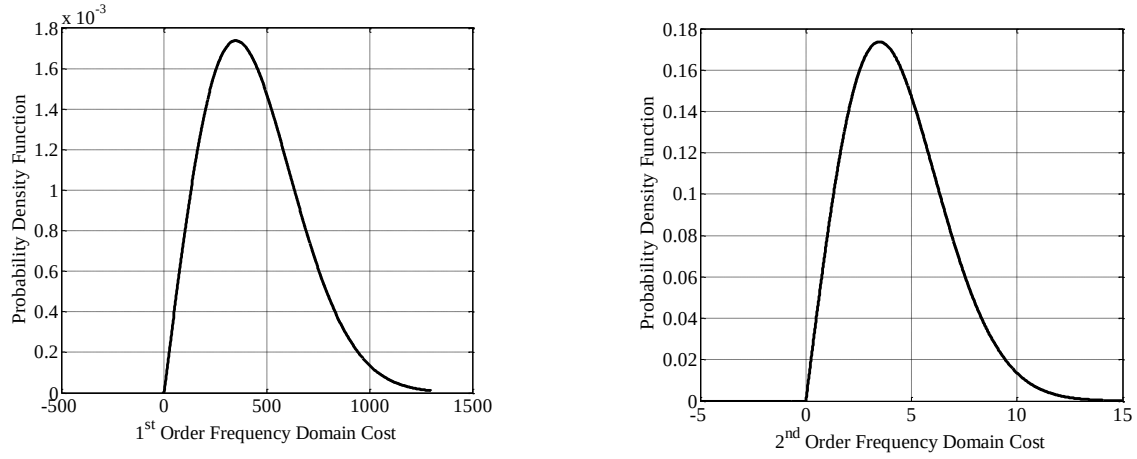

Figure 7.7. Optimal cost probability distribution for (a) first order thermal networks and (b) second order thermal networks

The limitation of first order thermal networks in reproducing the frequency response with high precision at high frequencies is apparent in Figure 7.8 and Figure 7.9 where some Bode diagrams are shown. Nevertheless for these frequencies the modulus of the frequency responses are lower compared to their gains (i.e., $G_i(j0)$). In addition, also the magnitude of the spectrum of the external inputs are negligible for these high frequencies when compared to the magnitude of the harmonic components at low frequencies (see Figure 7.6). Hence, we expect a marginal or still acceptable error when predicting building performance with simplified building models embedding first order thermal networks, i.e., G8 and Gm in Table 7.1.

From Figure 7.8 and Figure 7.9 we can also observe, in agreement with the technical literature about building model reduction, that: *i)* the loss of matching for first order system is more severe for heavy buildings with respect to light buildings and *ii)* second order thermal network improve a lot the matching of the frequency response at high frequencies. These remarks are general and can be done also for other building elements reduced via a frequency domain approach, but results are here omitted for the sake of brevity.

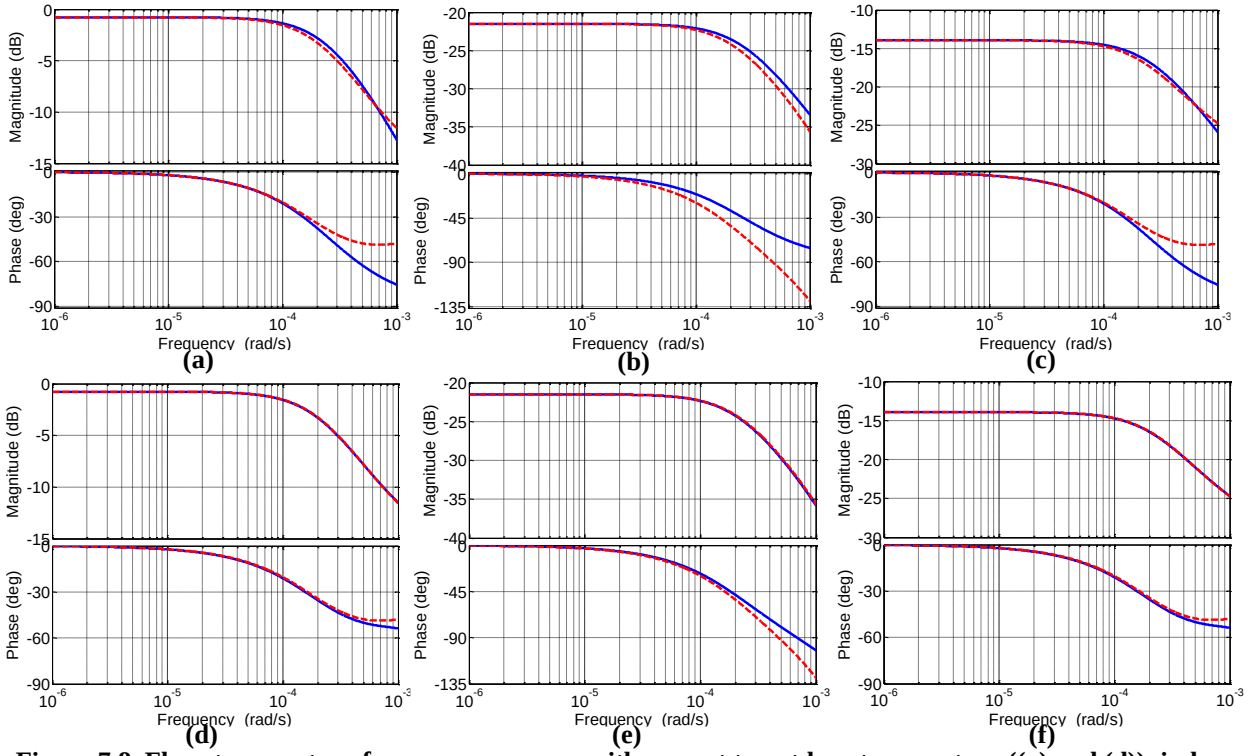

Figure 7.8. Floor temperature frequency response with respect to outdoor temperature ((a) and (d)), indoor air temperature ((b) and (e)), and solar radiation through window ((c) and (f)) for a light weight house, when first order ((a), (b), and (c)) and second order ((d), (e), and (f)) thermal networks are used. Detailed model (dashed red line) and low-order model (solid blue line).

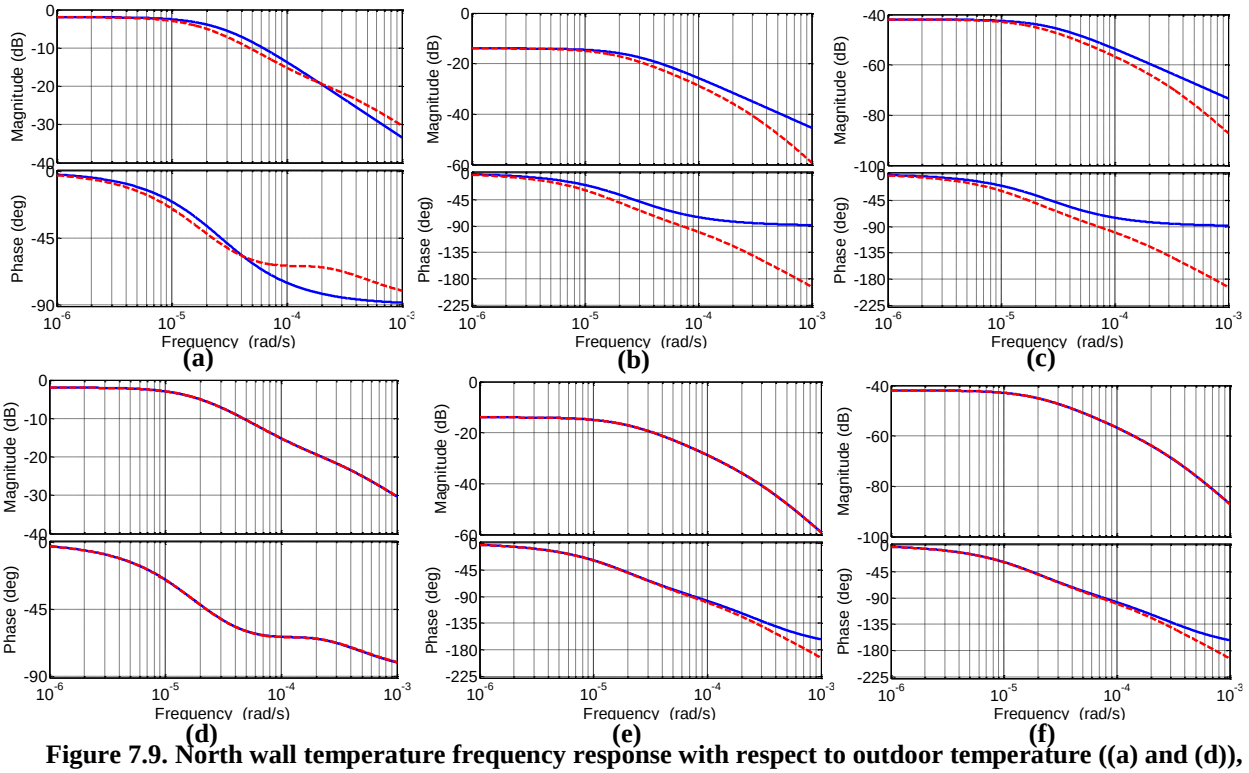

Figure 7.9. North wall temperature frequency response with respect to outdoor temperature ((a) and (d)), indoor air temperature ((b) and (e)), and solar radiation ((c) and (f)) for heavy weigh office, when first order ((a), (b), and (c)) and second order ((d), (e), and (f)) thermal networks are used. Detailed model (dashed red line) and low-order model (solid blue line).

We move now to study the position of the eigenvalues of low order building elements. As clearly indicated in Table 7.3 and Figure 7.10, there can be also a consistent variation among the eigenvalues of the low order networks and the dominant poles of the corresponding building element of the detailed model. Precisely, this variation is up to about 65% (in absolute value) in the case of first order networks. Instead, in the case of second order thermal networks, the first eigenvalue differs from the dominant pole of the corresponding building element of the detailed model up to about 11%, but the difference between the its second eigenvalue and that of the detailed model can be also of about 95%.

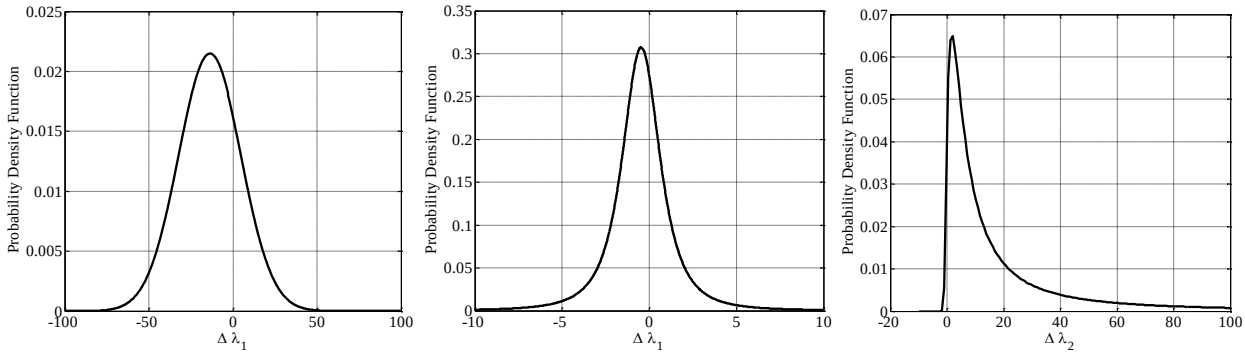

(a) **(b)** **(c)**

Figure 7.10. PDF of the percentage variation of the eigenvalues of the low order thermal networks with respect to the dominant poles of the corresponding detailed building element models (i.e., Δλ index in (7.12)); (a) $\Delta\lambda_1$ for first order networks; (b) $\Delta\lambda_1$ for second order networks and (c) $\Delta\lambda_2$ for second order networks.

Consequently, we can conclude that, if model reduction of building elements is carried out by using the dominant poles of a detailed building model, the resulting low order systems can be quite different from the optimal ones which have been identified with the procedure proposed in Section 7.1, therefore they might be not effective. In addition, when this approach is used with second order transfer functions, the resulting dynamics cannot be expressed by using the physical structure in (7.2).

Before moving to consider the result provided by the time domain identification approach, we note that in the case of the frequency domain method, often the minimization of the function (7.5) has been performed via iterative algorithms. Nevertheless, genetic algorithms have been used in those cases where the iterative methods failed. Figure 7.11 shows the evolution of the cost function with respect to the evolving of the generations required by the method in [165]. Here it is clear the effectiveness of these methods in reducing the cost function at each new generation.

To tune the parameters of the building elements for Gt models (see Table 7.1 for their definition), the minimization of (7.6) in the time domain has been carried out via iterative

methods. As initial guess for the optimization algorithm, say p_0, we have chosen the optimal parameters previously found from the identification in the frequency domain.

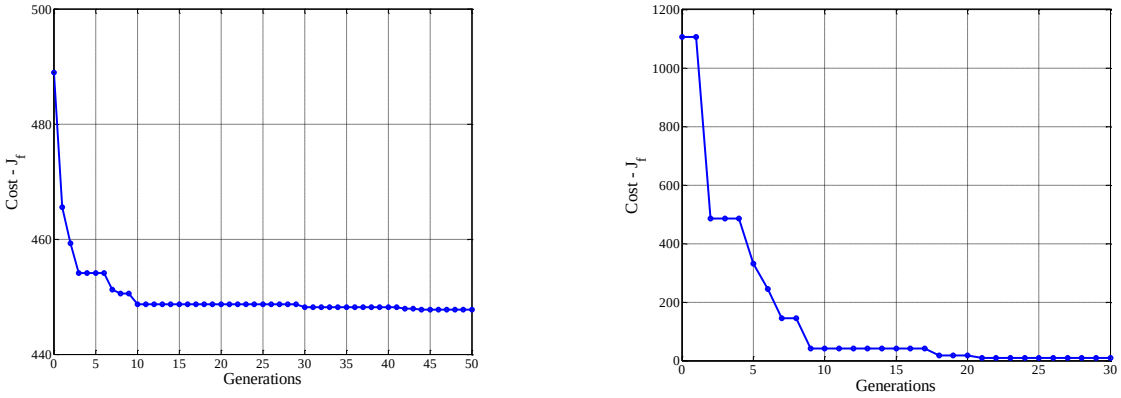

(a) **(b)**

Figure 7.11. Cost evolution when genetic algorithms are used to search for the minimum of the cost function (7.5) in the case: (a) a first order model for the south wall of a heavy house and (b) a second order model for the roof of a heavy office

In so doing, we expect to improve further the performance of the model G15 (see Table 7.1 for its definition) by taking into account also weather data of each weather zone of interest in Table 5.3. As a preliminary quantitative measure of the enhancements provided by this approach, we define the following index which measures the cost reduction from the frequency based identification to time based identification

$$\Delta J_t = 100 \frac{J_t(p_0) - J_t(p_{opt})}{J_t(p_{opt})}, \tag{7.13}$$

where p_{opt} are the optimal parameters resulting from the minimization of (7.6).

For defining an additional index to evaluate the result of time based identification, consider the following quantity

$$\Upsilon(p) = \max_{t \in \Omega} \left| \bar{y}(t) - y(t; p) \right|, \tag{7.14}$$

where $\bar{y}(t)$, $y(t; p)$ and Ω are those introduced in Section 7.1.2.

From a practical viewpoint, $\Upsilon(p)$ is the maximum error over the time range Ω between the building element temperature provided by the detailed model, i.e., $\bar{y}(t)$, and that of the low order reduced thermal network when its parameters are p, i.e., $y(t; p)$. Consequently, to evaluate the improvement in predicting the evolution of the element temperature when shifting from frequency identification to time based identification we use the following performance index

7.3 Numerical validation of the building model reduction procedure

$$\Delta T = 100\frac{\Upsilon(p_{opt}) - \Upsilon(p_0)}{\Upsilon(p_0)}. \tag{7.15}$$

Notice that the time range Ω required for computing J_t in (7.6) has been chosen as set of days in winter and summer seasons. Furthermore, the building element generating $\bar{y}(t)$ is assumed to evolve in free evolution, i.e., no additional sensible heat is provided to control the indoor air temperature.

The performance indexes computed over the 54x7=378 cases have been analyzed from a statistical viewpoint and results are concisely reported in Table 7.4 and shown in Figure 7.12.

Index	Mean	Variance	Maximum	PDF	PDF Parameters		
ΔJ_t	66.35	288.31	117.29	t-Location Scale	72.61	6.16	1.42
ΔT	61.23	310.96	114.13	t-Location Scale	66.94	7.13	1.68

Table 7.4. Statistical analysis of the identification result in the time domain.

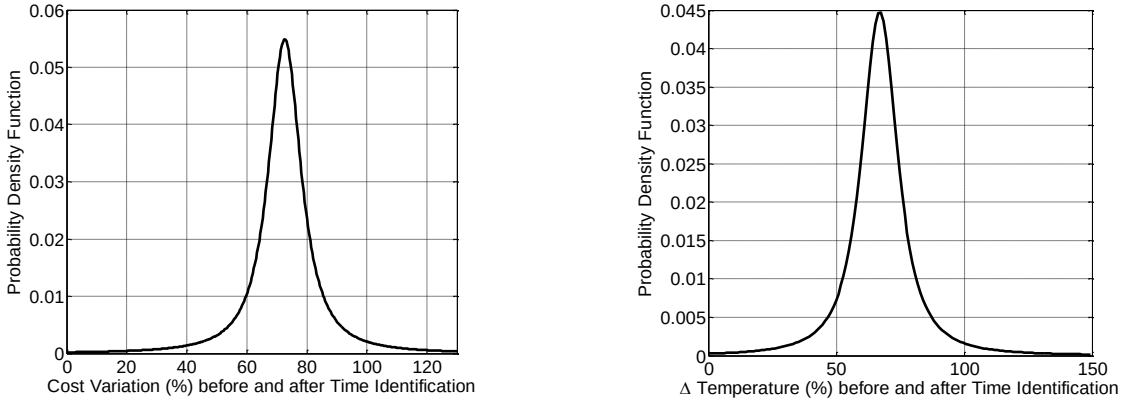

(a) **(b)**

Figure 7.12. Statistical analysis of the Identification result based in the time domain, (a) PDF of the ΔJ_t index and (b) PDF of the ΔT index

As clearly shown in Table 7.4 and Figure 7.12 time domain identification improves the temperature prediction of low order networks in Figure 7.2 with respect to the frequency based identification. Indeed, when shifting to the time domain approach there is on the average a cost reduction of about 65% and an improvement of temperature prediction of 60%.

Figure 7.13 and Figure 7.14 clearly show, for two exemplar cases, how temperature predictions improve when considering thermal networks tuned in the time domain setting with respect to the same networks whose parameters are identified by using the frequency domain approach. In these figures the area shaded in grey represents the identification data set, i.e., the temperatures, both of the detailed and low order building element models, used during the minimization of the cost function (7.6) over the time range Ω. As it is apparent, temperature

predictions improve not only over Ω but also outside (validation data set) and the residual error provided by networks tuned via the minimization of (7.6) by means of an iterative searching method with initial guess (initial point) set to the solution of the minimization of the cost function in (7.5) is always below 1°C.

Nevertheless, it is interesting to note that complete envelope models embedding building elements identified in time domain, i.e. models Gt in Table 7.1, have almost the same performance of G15 when control algorithms are used to impose some given indoor air temperature profile (see also Sections 7.3.2-7.3.4 and Appendix B for a detailed analysis).

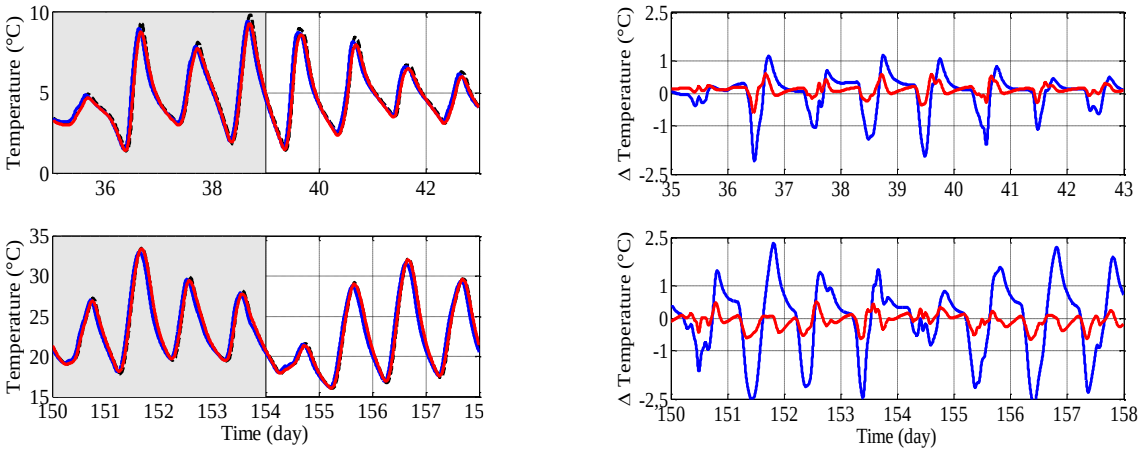

Figure 7.13. Time based identification results for the sought wall in the case of a light mall building in Denver (a) temperature profiles of the: detailed building model, i.e. $\bar{y}(t)$, (back line); second order model with parameters tuned on the basis of the frequency domain identification process, i.e., $y(t;p_0)$, (blue line); second order model with parameters tuned on the basis of the time domain identification process, $y(t;p_{opt})$, (red line); identification dataset (gray shaded area), (b) prediction errors: $\bar{y}(t)-y(t;p_0)$ (blue line) and $\bar{y}(t)-y(t;p_{opt})$ (red line).

We finally show some additional results connected to the computational effort to tune low order networks by means of both frequency and time based identification, or equivalently the computation effort required to minimize either the cost function in (7.5) or that in (7.6). Precisely, Table 7.5 and Figure 7.15 show some statistical data about the number of interactions of the iterative optimization algorithm and time required to perform the tuning of a given building element. Notice that, we indicate as N_{ij} (τ_{ij}), the number of iteration (time required) to identify the parameters of a low order thermal network in Figure 7.2 of order $i \in \{1,2\}$ and by using the method $j \in \{f,t\}$, with f and t denoting the frequency based and time based identification approach, respectively.

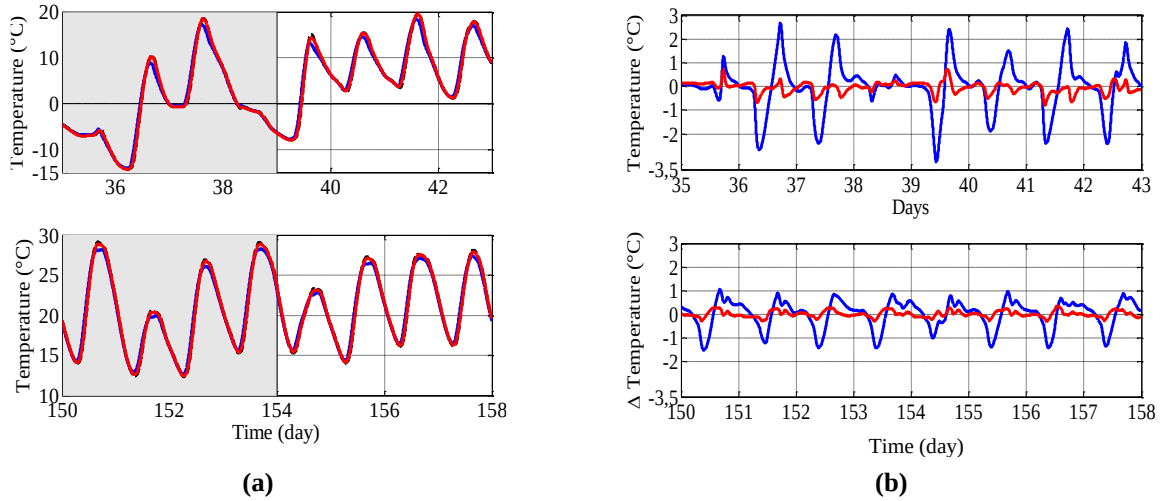

Figure 7.14. Time based identification results for the roof in the case of a heavy office building located in Milan (a) temperature profiles of the: detailed building model, i.e. $\bar{y}(t)$, (back line); second order model with parameters tuned on the basis of the frequency domain identification process, i.e., $y(t;p_0)$, (blue line); second order model with parameters tuned on the basis of the time domain identification process, $y(t;p_{opt})$, (red line); identification dataset (grey shaded area), (b) prediction errors: $\bar{y}(t)-y(t;p_0)$ (blue line) and $\bar{y}(t)-y(t;p_{opt})$ (red line).

Index	Mean	Variance	Maximum	PDF	PDF Parameters		
N_{1f} -1° order freq. based	216	$3.85\cdot10^3$	402	Inverse Gaussian	216.29	$2.9\cdot10^3$	
N_{2f}- 2° order freq. based	483	$3.50\cdot10^4$	1044	Gen. Extreme Value	0.6	110.2	270.53
N_{2t}- 2° order time based	336	$3.26\cdot10^4$	878	Gen. Extreme Value	0.12	101.49	260
τ_{1f} -1° order freq. based (s)	0.84	0.06	1.6	Inverse Gaussian	0.83	11.05	
τ_{2f}- 2° order freq. based (s)	2.32	8.46	11	Gen. Extreme Value	0.56	0.56	1.30
τ_{2t}- 2° order time based (s)	684.4	$1.72\cdot10^5$	1986	Gen. Extreme Value	0.2	228.28	498.49

Table 7.5. Statistical analysis of the identification result in terms of computational effort.

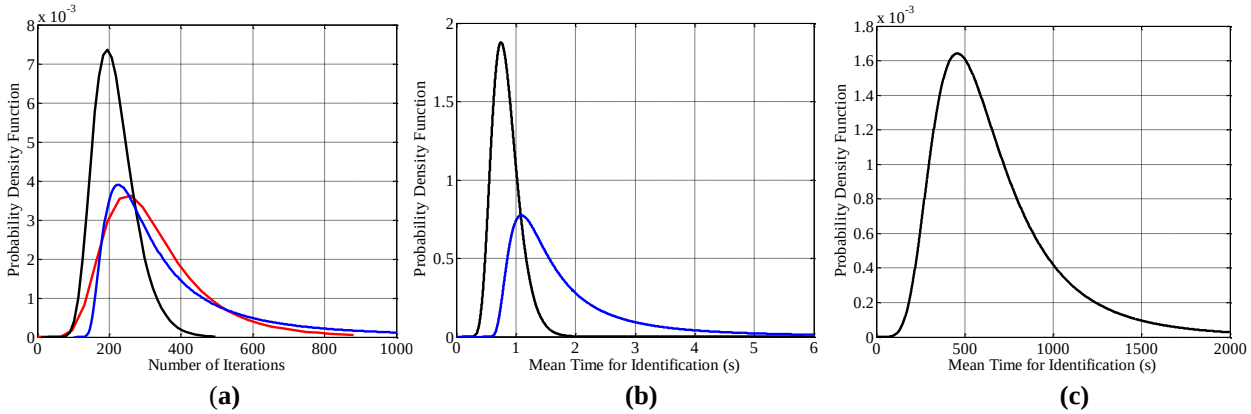

Figure 7.15. (a) PDFs of the number of iteration for identifying a building element: N_{1f} (back line), N_{2f} (blue line), N_{2t} (red line); (b) PDFs of the required time for identifying a building element: τ_{1t} (back line), τ_{2f} (blue line) (c) PDFs of the required time for identifying a building element of a second order with the time based identification approach, i.e., τ_{2t}.

Table 7.5 and Figure 7.15a clear show that the number of interactions to identify the optimal parameters of a low order model does not change too much on the basis of the order of the

thermal network or the approach used to tune them. Indeed, they have the same order of magnitude both for mean and variance (see Figure 7.15a and the first three rows of Table 7.5). On the other hand, the time required to tune the parameters for a second order thermal network via a time domain approach is much larger than that needed to tune the same network but using a frequency domain formulation. This increase of the identification time was expected. Indeed the evaluation of the cost function in the time domain, i.e., J_t in (7.6), requires to solve a set of differential equations that is much more complicated, from a numerical viewpoint, than evaluating the static function J_f in (7.5) which defines the cost index in the frequency domain identification setting. Consequently, even though the time based approach allows to obtain better predictions of the building elements temperatures (see Table 7.4 and Figure 7.12), the simulation time reduction expected when using low order building models identified with the time domain approach, e.g. the Gt model is Table 7.1, is jeopardized by the additional time required for the tuning of their low order thermal networks.

7.3.2 *Indoor air temperature and energy predictions*

In Section 7.3.1 we have analyzed the identification results both in the frequency and time domain. In this section and the next one we test the performance obtained when the low order building element models previously discussed are assembled together generating the simplified, but complete, building systems defined in Table 7.1. Furthermore we compare these performance with the white reduced models introduced in Table 7.2. Here we just recall that the low order grey models are: G8 (composed by 8 differential equations), Gm (composed by 12 differential equations), G15 and Gt (both composed by 15 differential equations); while the reduce order white box models are: W2 (composed by 2 differential equations), W15 (composed by 15 differential equations) and W22 (composed by 22 differential equations). Furthermore, the detailed model, with respect to which the performance indexes are computed, is instead composed by 71 differential equations (see Chapter 2).

In order to show the effectiveness of the proposed model reduction approach, the performance indexes defined in Section 7.2.1 have been computed for each model structure by taking into account several buildings, with different geometry and construction materials, located in different weather zones. The selected 54 case studies are those presented in detail in Section 5.3.

In this section we discuss the performance indexes defined in (7.8) and (7.9), while in the next section the indexes in (7.10) and (7.11) are analyzed for the same cases. For the indexes form (7.8) to (7.10) we have set as time range $\Theta = 1$ *week*. In so doing for each simulation we obtain

52 samples of every index and consequently 52×54 = 2808 samples for each pair *(simplified building model, performance index)* which is a satisfactory number for carrying out statistical investigations.

We first consider the performance index MaxΔT in (7.8) computed both for winter and summers weeks. Hence, we first investigate the ability to predict the indoor air temperature in free evolution by exploiting the grey box building models.

The effectiveness of the gray box modelling to predict precisely this temperature is shown both in Table 7.6 and graphically in Figure 7.16.

Maximum Variation of indoor temperature in free evolution during winter weeks						
Model	**Mean**	**Variance**	**Maximum**	**PDF**	**PDF Parameters**	
W2	5.88	7.34	14.10	Gamma	4.46	1.32
W15	0.71	0.09	1.61	Nakagami	1.56	0.58
W22	0.33	0.05	1.00	Weibull	0.36	1.44
G8	0.46	0.10	1.40	Inverse Gaussian	0.46	0.80
Gm	0.37	0.04	0.97	Inverse Gaussian	0.37	0.96
G15	0.12	0.01	0.42	Lognormal	-2.51	0.82
Gt	0.10	0.01	0.40	Inverse Gaussian	0.10	0.11
Maximum Variation of indoor temperature in free evolution during summer weeks						
Model	**Mean**	**Variance**	**Maximum**	**PDF**	**PDF Parameters**	
W2	6.73	15.91	18.69	Rayleigh	5.53	
W15	0.71	0.2	2.05	Gamma	2.84	0.25
W22	0.34	0.05	1.01	Nakagami	0.71	0.16
G8	0.39	0.04	0.99	Rayleigh	0.31	
Gm	0.25	0.02	0.67	Rician	0.19	0.15
G15	0.09	0.004	0.27	Inverse Gaussian	0.09	0.18
Gt	0.08	0.003	0.24	Inverse Gaussian	0.08	0.15

Table 7.6. Statistical analysis of the Maximum Variation in °C of the indoor temperature (MaxΔT-index) for all models in Table 7.1 and Table 7.2

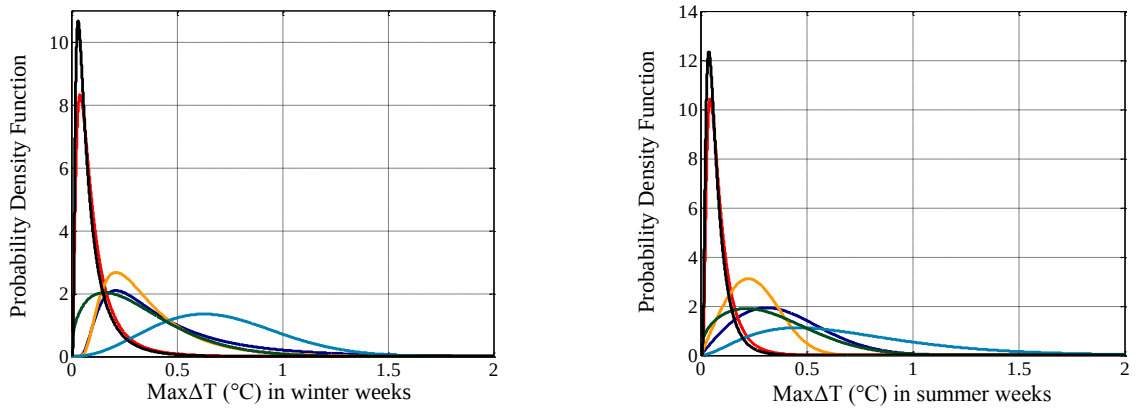

(a) **(b)**

Figure 7.16. Statistical analysis of the Maximum Variation (°C) of the indoor temperature with respect to the detailed building model (MaxΔT-index) for different simplified building models computed in (a) winter weeks and (b) summer weeks. See Table 7.1 and Table 7.2 for details on color lines.

We point out that the PDF of G15 and Gt rapidly converge to zero which implies a smaller variance and consequently a small maximum prediction error compared to the other simplified models. In addition, the prediction ability of G15 is comparable to that of Gt, which provides the best MaxΔT-index, both in terms of mean, variance and maximum prediction error and both for summer and winter weeks. Furthermore, all the grey model, except G8 during summer, provide a maximum prediction error of the indoor air temperature always below 1°C, and for G15 this error reduces to a maximum of about 0.40°C in winter and 0.27 °C in summer.

It is possible to note that the performance of grey box models are in general better than those provided by reduced order white models not only when the latter have the same order of complexity of the former, but also when considering white models with higher order, e.g., W22. In addition, both for summer and winter weeks, the prediction errors of W2 are much larger with respect to the other models and it is not reported in Figure 7.16 as its PDF was out of the scale.

Similar conclusions can be drown also when considering the performance index ΔP defined in (7.9) which measures the percentage variation of the maximum peak load (sensible load) between that provided by the detailed building model in Chapter 2 and each of the reduced models in Table 7.1 and Table 7.2, on the weekly basis. Results are collected in this case in Table 7.7 and graphically shown in Figure 7.17. Precisely, for this index performance, the model G15 and Gt provide, both for winter and summer, smaller values in terms of mean, variance, and maximum not only with respect to the white model of same complexity (W15), but also with respect to W22 which approximates the detailed building dynamics by using 22 equations (seven additional dynamical equations than G15 and Gt).

Percentage prediction error for estimating heating peak load demand during winter weeks							
Model	**Mean**	**Variance**	**Maximum**	**PDF**	**PDF Parameters**		
W2	21.44	151.02	58.30	Nakagami	0.65	610.65	
W15	2.52	5.43	9.51	Nakagami	0.89	9.58	
W22	2.72	2.18	7.14	Gen. Extreme Value	0.80	0.60	1.16
G8	6.96	8.79	15.85	Inverse Gaussian	6.96	33.04	
Gm	5.90	2.78	10.90	Gamma	11.93	0.49	
G15	1.63	3.28	7.06	Lognormal	-0.32	1.54	
Gt	1.34	2.27	5.85	LogNormal	-0.54	1.57	
Percentage prediction error for estimating cooling peak load demand during summer weeks							
Model	**Mean**	**Variance**	**Maximum**	**PDF**	**PDF Parameters**		
W2	22.76	514.17	90.78	Gen. Extreme Value	0.37	10.31	11.77
W15	8.62	29.70	24.96	t Location-Scale	7.77	2.94	2.42
W22	3.27	7.11	11.26	Gen.Extreme Value	0.91	0.41	0.37
G8	6.75	26.84	22.29	t Location-Scale	6.01	1.78	1.48
Gm	4.93	8.60	13.72	Logistic'	4.79	1.72	
G15	1.43	3.88	7.33	Gen. Extreme Value	0.91	0.33	0.30
Gt	1.18	2.70	6.10	Inverse Gaussian	3.27	5.30	

Table 7.7. Statistical analysis of the Percentage prediction error for peak load demand (ΔP -index) for all models in Table 7.1 and Table 7.2.

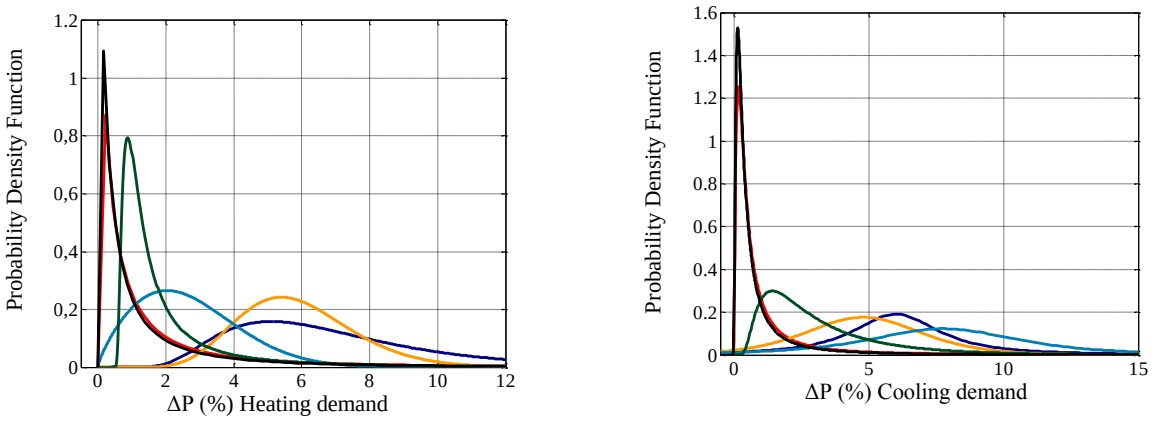

(a) **(b)**

Figure 7.17. Statistical analysis of the Percentage prediction error for peak load demand with respect to the detailed building model (ΔP-index) for different simplified building models (a) Heating (b) Cooling. See Table 7.1 and Table 7.2 for details on color lines.

Moreover, G15 and Gt have similar performance also with respect to the ΔP-index and have a narrow PDF around their mean value (see Figure 7.17).

To better appreciate the effectiveness of low order building models to reproduce indoor air temperature and demanded sensible heat predicted by a detailed but complex one, Figure 7.18 and Figure 7.19 show some time-histories for two case studies. Here we point out that for both cases, G15 and Gt provide very small prediction errors. More in detail, the prediction error of the indoor air temperature is always below 0.05°C while that on the sensible load never excesses 0.5kW. In addition, we remark that also the performance of G8 and Gm are satisfactory with a maximum prediction error on temperature of about 0.12°C in Figure 7.18 and 0.32°C in Figure 7.19, and a prediction error of the sensible load of about 2.05kW in Figure 7.18 and 0.5kW in Figure 7.19, which are consistent with data in Table 7.6 and Table 7.7

The difference between the prediction ability of grey box models with respect to low order white ones is more evident when considering the computation of the heating and cooling demands reported in Table 7.8 and Figure 7.20 which give a numerical and graphical statistical analysis of the ΔE-index in (7.9). We recall here that this index measures the percentage variation of the energy demand of a reduced order model with respect to the detailed one in Chapter 2 and it is computed for every week of the 54 case studies presented in Chapter 5 for each low order model.

Results in Table 7.8 clearly indicate that in the case of heating also the simplest grey box model designed in this chapter, i.e., G8, provides better prediction than the most complex low order white box building model, i.e., W22.

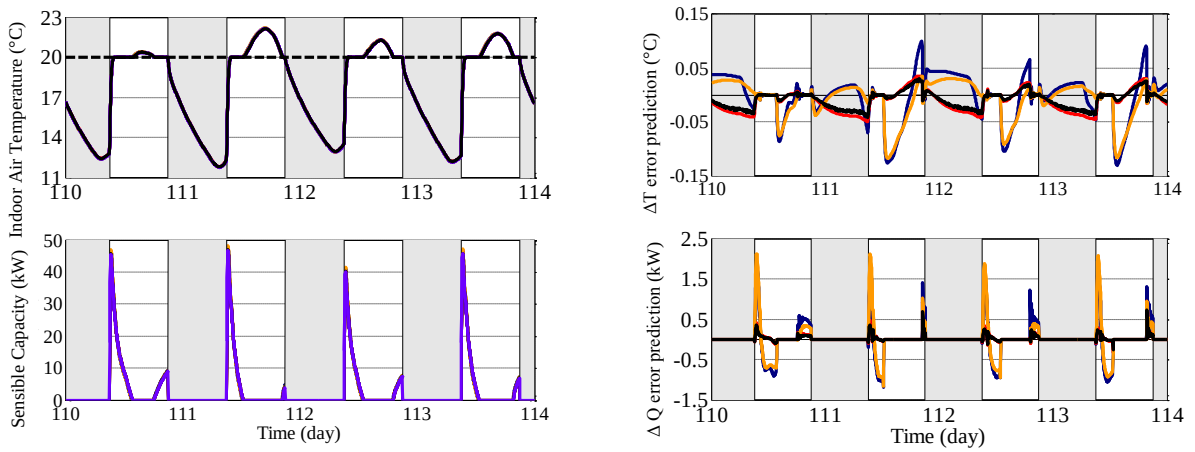

(a) **(b)**

Figure 7.18. Lightweight Mall buildings in Nice. (a) Indoor air temperature and sensible load provided by all grey simplified building models and the detailed one (purple line), and (b) corresponding prediction errors. See Table 7.1 for details on color lines for the grey box models, while the grey area denotes time intervals where the temperature control is deactivated.

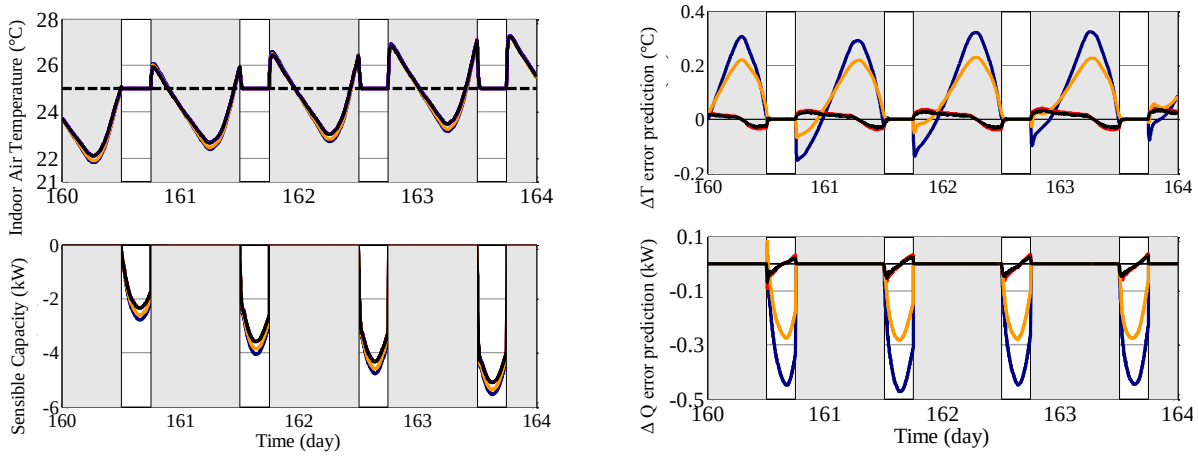

(a) **(b)**

Figure 7.19. Heavyweight Office buildings in Naples. (a) Indoor air temperature and sensible load provided by all grey simplified building models and the detailed one (purple line), and (b) corresponding prediction errors. See Table 7.1 for details on color lines for the grey box models, while the grey area denotes time intervals where the temperature control is deactivated.

Consider for example the maximum error for heating prediction, this is about 13.3% for W22 but about 4.25% for G8 and shrinks to 1.29% and 1.01% for G15 and Gt, respectively. In the case of cooling, G8 provides better predictions than W15 despite it uses 7 equations less to predict cooling demand, but its performance are worse than W22. Instead the models, Gm, G15 and Gt still outperform the white models, including W22 composed by 22 equations, having for G15 and Gt a maximum cooling prediction error of about 5.5% and 4.25%, respectively, and mean values around 1.08% and 0.83%, respectively.

Percentage prediction error for estimating heating demand during winter weeks							
Model	**Mean**	**Variance**	**Maximum**	**PDF**	**PDF Parameters**		
W2	21.86	151,13	58.74	Nakagami	0.85	628.62	
W15	5.36	8.64	14.17	Inverse Gaussian	5.36	15.14	
W22	3.82	10.00	13.30	Inverse Gaussian	3.82	3.82	
G8	0.89	1.25	4.24	Log-Normal	-0.62	1.03	
Gm	0.78	0.64	3.18	Loglogistic	-0.63	0.50	
G15	0.35	0.10	1.29	Weibull	-0.78	0.86	
Gt	0.28	0.06	1.01	Weibull	0.27	1.00	
Percentage prediction error for estimating cooling demand during summer weeks							
Model	**Mean**	**Variance**	**Maximum**	**PDF**	**PDF Parameters**		
W2	51.37	10^4	351.37	Log-Logistic	3.12	0.79	
W15	11.94	159.45	49.82	Inverse Gaussian	11.94	13.38	
W22	6.87	34.55	24.50	Gen. Extreme Value	0.41	2.31	4.15
G8	5.32	76.30	31.47	Lognormal	0.98	1.22	
Gm	3.55	20.89	16.96	Inverse Gaussian	3.55	2.52	
G15	1.08	2.17	5.49	Log-Logistic	0.36	1.00	
Gt	0.83	1.30	4.25	Log-Logistic	-1.04	0.86	

Table 7.8. Statistical analysis of the Percentage prediction error for Heating and Cooling demand (ΔE -index) for all models in Table 7.1 and Table 7.2

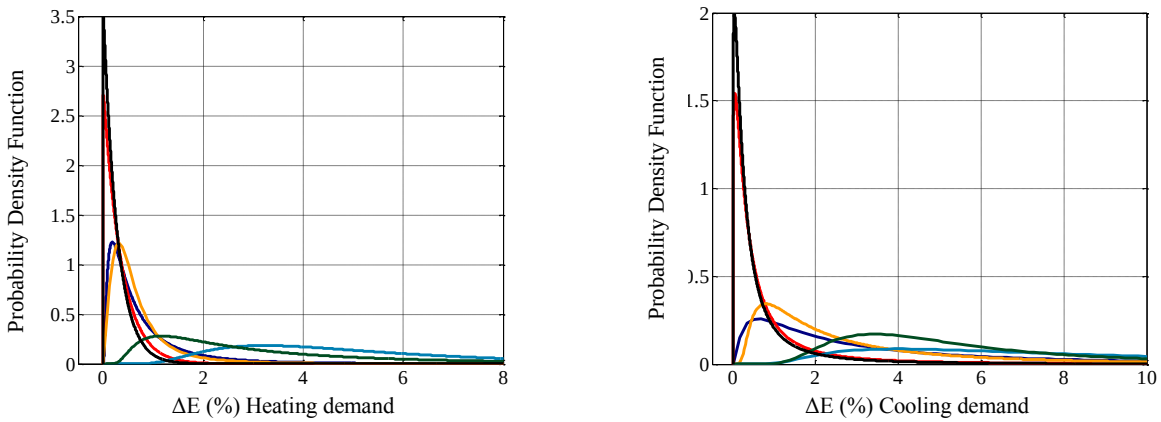

(a) **(b)**

Figure 7.20. Statistical analysis of the Percentage prediction error for Heating /Cooling demand with respect to the detailed building model (ΔE-index) for different simplified building models (a) Heating (b) Cooling. See Table 7.1 and Table 7.2 for details on color lines.

Notice that also for Figure 7.17 and Figure 7.20 the PDFs of W2 have not been reported because they were out of the scale, readers can find statistic data also for this model in Table 7.3 and Table 7.8.

7.3.3 *Comfort Predictions and simulation time*

In this section we evaluate quantitatively the ability of low order building models in Table 7.1 and Table 7.2 to predict comfort. To this aim we compute for them the performance indexes in (7.10) on the weekly basis, i.e., we set $\Theta = 1\ week$. Before showing numerical results, we point out that for each model (seven model) and for each week of the case studies (54 cases) the PMV

and PPD predictions have been computed assuming for the thermal zone an indoor air relative humidity equal to 50%.

We first consider the ability of the models to predict effectively the mean radiant temperature by means of the ΔTr–index in (7.10) which measures for each week the maximum variation of the mean radiant temperature between the reduced order model and that predicted via the detailed one in Chapter 2. Statistical results for each model are collected in Table 7.9 and shown in Figure 7.21. In particular, all models, except W2, provide a good level of prediction with a residual error that never exceed 2°C. Nevertheless, the grey models are those which better replicate the mean radiant temperature response of the detailed building system. Precisely, for G15 and Gt the maximum temperature prediction error, i.e., the ΔTr-index, is about 0.35 °C and 0.30 °C for summer weeks.

Maximum Variation of the mean radiant temperature during winter weeks							
Model	**Mean**	**Variance**	**Maximum**	**PDF**	**PDF Parameters**		
W2	5.06	3.21	10.43	Gen. Extreme Value	-0.06	1.50	4.29
W15	0.57	0.04	1.17	Nakagami	2.24	0.36	
W22	0.2	0.04	0.92	Lognormal	-1.24	0.47	
G8	0.53	0.06	1.26	Gen. Extreme Value	0.14	0.14	0.43
Gm	0.39	0.01	0.69	Gen.Extreme Value	-0.0003	0.09	0.34
G15	0.18	0.05	0.85	Gen. Extreme Value	0.46	0.04	0.11
Gt	0.15	0.03	0.66	Gen. Extreme Value	0.45	0.04	0.10
Maximum Variation of the mean radiant temperature during summer weeks							
Model	**Mean**	**Variance**	**Maximum**	**PDF**	**PDF Parameters**		
W2	2.65	1.62	6.46	Gen. Extreme Value	1.20	8.64	
W15	0.61	0.16	1.81	Nakagami	0.61	1.17	
W22	0.31	0.04	0.91	Lognormal	0.25	0.66	
G8	0.49	0.07	1.28	Gen. Extreme Value	-0.76	0.14	
Gm	0.36	0.04	0.96	Gen.Extreme Value	-1.07	0.14	
G15	0.17	0.004	0.35	Gen. Extreme Value	0.27	0.03	0.14
Gt	0.14	0.003	0.30	Gen. Extreme Value	0.25	0.02	0.12

Table 7.9. Statistical analysis of the Maximum Variation in °C of mean radiant temperature (ΔTr-index) for all models in Table 7.1 and Table 7.2

These residual errors are about three times less than that given by white models of the same complexity (W15), and about three times smaller than that provided by the white model W22 despite it contains seven additional dynamical equations. Furthermore, G15 and Gt provide a very small variance. Consequently their PDFs are narrow and concentrated around their mean values as depicted in Figure 7.21.

We consider now the error for predicting the PMV by using the performance index ΔPMV (see Section 7.2.1 for its definition). The statistical analysis for this index is reported in Table 7.10 and shown Figure 7.22. We note that the models W15 and G8 give a maximum error of about 0.7 and 0.5, respectively. Taking into account that the PMV∈ [-3, +3], these models might be inadequate for a precise estimation of the PMV despite they have often provided satisfactory

results for the previous performance indexes. In addition, it is clear from Table 7.10 that G15 and Gt are the only models which provide a maximum PMV prediction error less than double their mean values. As the maximum errors are 0.12 and 0.11 for G15 and Gt, respectively, these models seem to be promising low order systems to be used not only for the computation of energy demand but also for estimating comfort.

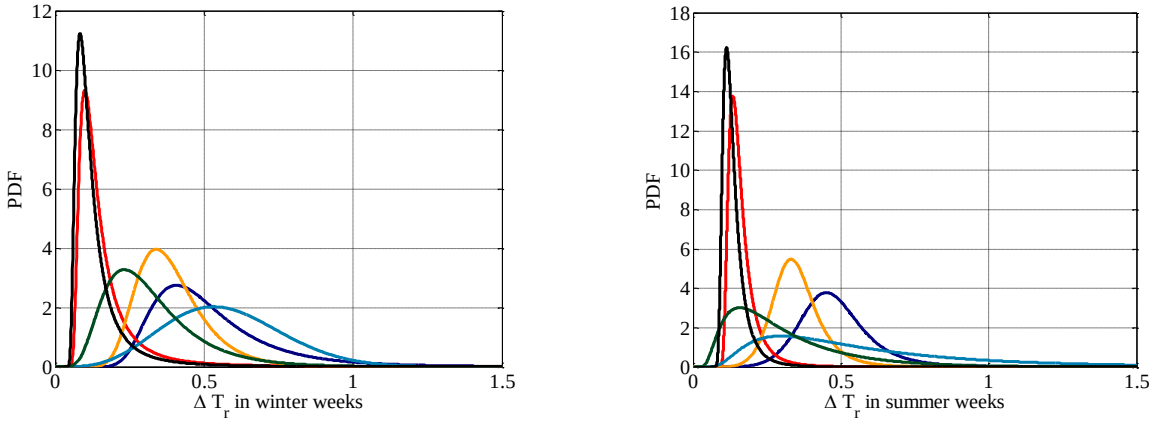

(a) **(b)**

Figure 7.21. Statistical analysis of the Maximum Variation (°C) of the mean radiant temperature with respect to the detailed building model (ΔTr-index) for different simplified building models computed in (a) winter weeks and (b) summer weeks. See Table 7.1 and Table 7.2 for details on color lines.

Maximum Variation of the PMV during winter weeks							
Model	**Mean**	**Variance**	**Maximum**	**PDF**	**PDF Parameters**		
W2	0.69	0.07	1.48	Nakagami	1.85	0.54	
W15	0.14	0.003	0.30	Gamma	6.97	0.02	
W22	0.08	0.002	0.21	Inverse Gaussian	0.08	0.33	
G8	0.11	0.003	0.27	Gen. Extreme Value	0.31	0.03	0.08
Gm	0.08	0.0008	0.17	Gen. Extreme Value	0.22	0.02	0.07
G15	0.05	0.001	0.14	Gen. Extreme Value	0.67	0.004	0.04
Gt	0.05	0.0008	0.14	Gen. Extreme Value	0.70	0.003	0.04
Maximum Variation of the PMV during summer weeks							
Model	**Mean**	**Variance**	**Maximum**	**PDF**	**PDF Parameters**		
W2	1.51	0.95	4.43	Birnbaum-Saunders	1.16	0.77	
W15	0.28	0.024	0.70	Birnbaum-Saunders	0.24	0.58	
W22	0.15	0.005	0.36	Gen. Extreme Value	0.88	0.03	0.09
G8	0.19	0.012	0.49	Gen. Extreme Value	0.09	0.04	0.17
Gm	0.14	0.007	0.39	t Location-Scale	0.14	0.03	10.71
G15	0.08	0.0002	0.12	Gen. Extreme Value	0.43	0.01	0.07
Gt	0.08	0.0001	0.11	Gen.Extreme Value	0.37	0.004	0.07

Table 7.10. Statistical analysis of the Maximum Variation of the PMV (ΔPMV-index) for all models in Table 7.1 and Table 7.2

We clearly point out that the loss of performance for the prediction of the PMV by G8 and W15 despite their acceptable performance to predict the mean radiant temperature and the indoor air temperature is mainly due to the polynomial nonlinearly which maps these temperatures onto the PMV. This static nonlinearity tends to amplify also small errors in these temperatures when computing the PMV. The loss of performance due to nonlinearities is even clearer when

considering the performance index ΔPPD for measuring the effectiveness of reduced models to predict PPD. Indeed, as the PPD is an exponential function of the PMV, also small PMV prediction errors can produce a notable error in the PPD prediction. This effect can be noted from Table 7.11 and Figure 7.23, which provide details about the statistical analysis on the ΔPPD-index. The analysis of this index reveal that also W22 is not suitable for predicting comfort as the maximum prediction error is about 20%. A quite acceptable results have been obtained by using Gm, which provides a ΔPPD of about 10%.

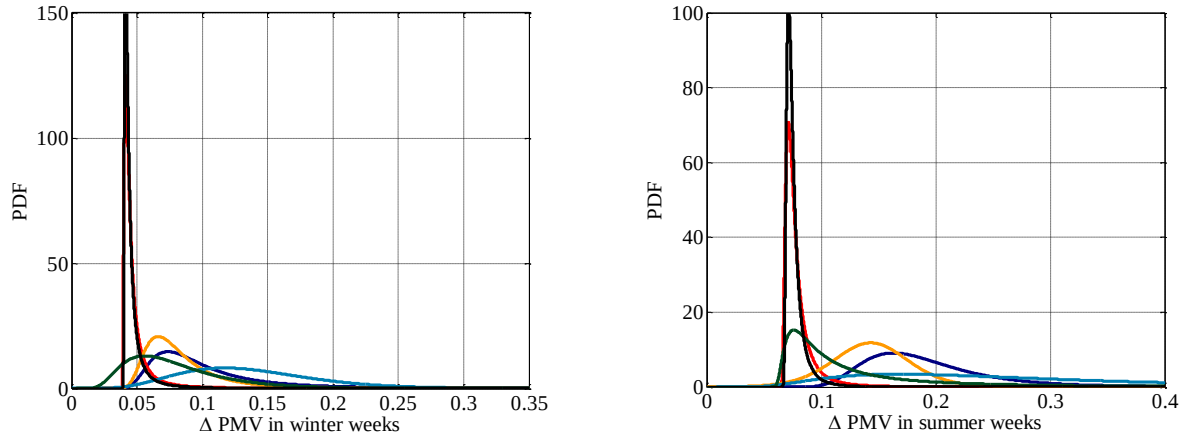

(a) **(b)**

Figure 7.22. Statistical analysis of the Maximum Variation of PMV with respect to the detailed building model (ΔPMV-index) for different simplified building models computed in (a) winter weeks and (b) summer weeks. See Table 7.1 and Table 7.2 for details on color lines.

Maximum Variation of the PPD during winter weeks							
Model	**Mean**	**Variance**	**Maximum**	**PDF**	**PDF Parameters**		
W2	30.55	180.87	70.85	Weibull	34.50	2.46	
W15	6.31	8.38	14.99	Nakagami	1.29	48.14	
W22	3.42	6.28	10.93	Birnbaum-Saunders	2.78	0.68	
G8	4.49	6.02	11.85	Gen. Extreme Value	0.21	1.30	3.41
Gm	3.65	2.04	7.93	Gen. Extreme Value	0.02	1.10	2.99
G15	2.29	2.86	7.36	Gen. Extreme Value	0.16	0.67	1.77
Gt	2.18	1.68	6.06	Log-Logistic	0.71	0.20	
Maximum Variation of the PPD during summer weeks							
Model	**Mean**	**Variance**	**Maximum**	**PDF**	**PDF Parameters**		
W2	51.42	743.92	133.24	Rician	36.22	32.22	
W15	11.56	38.37	30.14	Rayleigh	9.27		
W22	7.09	14.18	18.38	Gamma	3.35	2.11	
G8	8.22	7.57	16.47	Gen. Extreme Value	-0.06	2.38	7.02
Gm	6.30	4.37	12.57	t Location-Scale	6.25	1.85	15.15
G15	3.78	0.84	6.52	t Location-Scale	3.75	0.46	2.00
Gt	3.69	0.54	5.89	t Location-Scale	3.75	0.36	1.89

Table 7.11. Statistical analysis of the Maximum Variation of the PPD (ΔPPD-index) for all models in Table 7.1 and Table 7.2

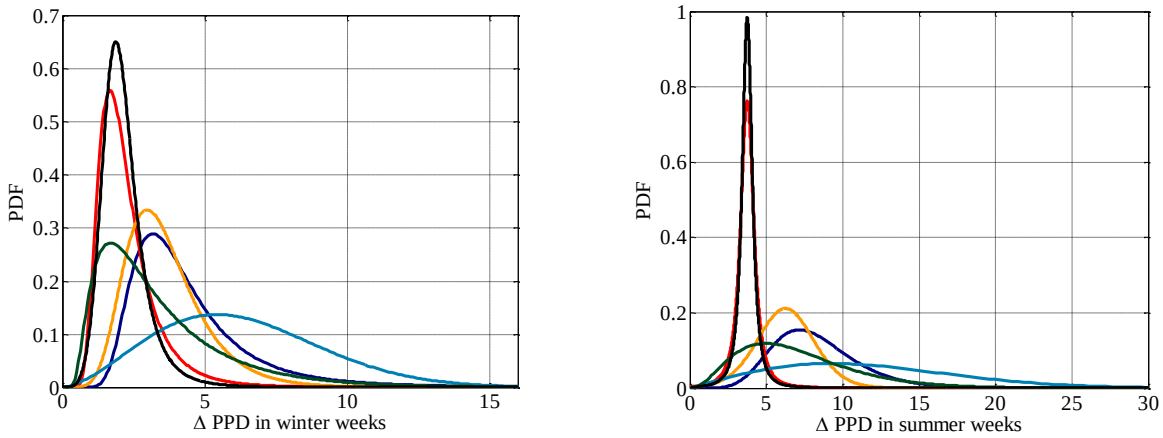

(a) **(b)**

Figure 7.23. Statistical analysis of the Maximum Variation of PPD with respect to the detailed building model (ΔPPD-index) for different simplified building models computed in (a) winter weeks and (b) summer weeks. See Table 7.1 and Table 7.2 for details on color lines.

It is interesting to point that the best results are still obtained by using G15 and Gt as they predict the PPD with and error at most of 7.36% and they are the only models to have a maximum ΔPPD-index less than 10%. The excellent performance of these models can be noted also from Figure 7.23 where it is clear that both the PDF of G15 and Gt are concentrated around their mean values, i.e., 3.78% and 3.69%, respectively.

Notice that the PDFs of W2 have not been reported in Figure 7.21, Figure 7.22 and Figure 7.23, because they were out of the scale, readers can find statistic data also for this model in Table 7.9, Table 7.10 and Table 7.11.

For the sake of completeness, Figure 7.24 and Figure 7.25 show the time-histories of the comfort predictions for the case studies considered in Figure 7.18 and Figure 7.19 when grey models are used. Here it is possible to observe that G15 and Gt provides prediction errors of the PMV always below 0.1 and an PPD prediction error always less than 5%.

We finally conclude the analysis by considering the performance index Π in (7.11), which measures the time reduction to simulate the building dynamics on a simulation horizon of one year when using low order models instead of the detailed one. For this index the statistical analysis is reported in Table 7.12 and Figure 7.26. As expected W2 and G8 provides the highest time reduction but W2 was found to be not suitable for almost all the performance index previously considered. On the other hand G15 and Gt, which have shown to be the best low order models with respect to all the performance indexes, provide also a quite consistent simulation time reduction which is on the average about 50%.

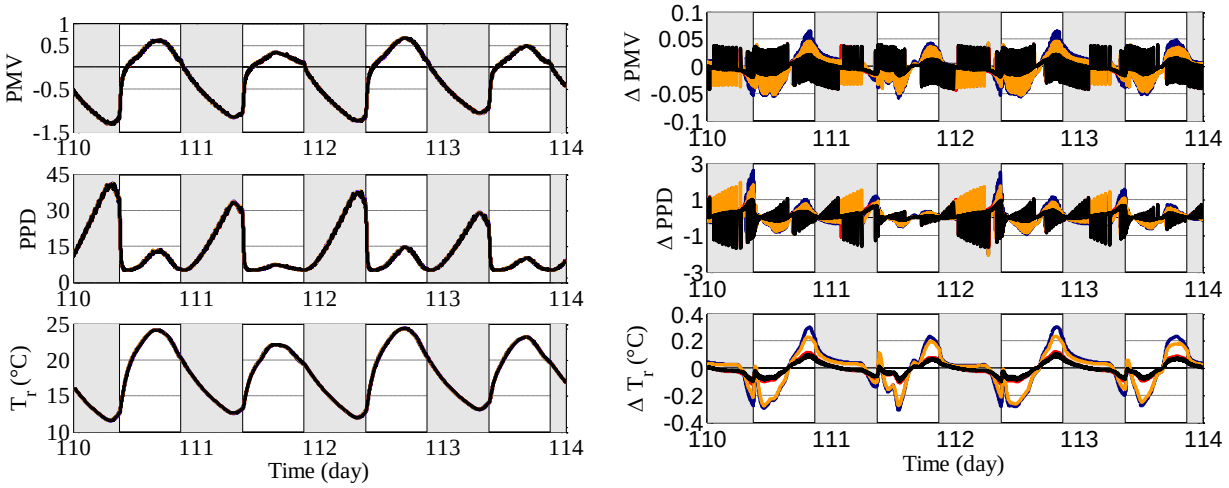

(a) **(b)**

Figure 7.24. Lightweight Mall buildings in Nice. (a) PMV, PPD and mean radiant temperature provided by all grey simplified building models and the detailed one (purple line), and (b) corresponding prediction errors. See Table 7.1 for details on color lines, while the grey area denotes time intervals where the temperature control is deactivated.

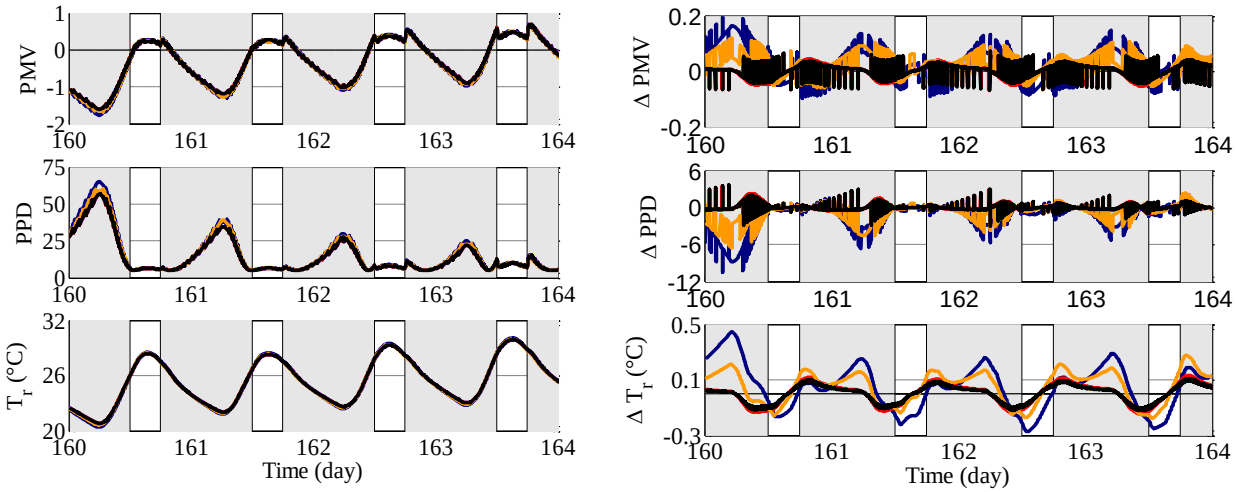

(a) **(b)**

Figure 7.25. Heavyweight Office buildings in Naples (a) PMV, PPD and mean radiant temperature provided by all grey simplified building models and the detailed one (purple line), and (b) corresponding prediction errors. See Table 7.1 for details on color, while the grey area denotes time intervals where the temperature control is deactivated.

Model	Mean	Variance	Maximum	PDF	PDF Parameters		
W2	80.64	23.92	95.31	t Location-Scale	80.82	0.72	1.13
W15	31.88	89.85	60.31	t Location-Scale	31.57	6.39	2.95
W22	31.07	108.15	62.24	t Location-Scale	31.10	4.99	2.28
G8	51.99	37.12	70.26	t Location-Scale	51.85	3.59	2.56
Gm	51.08	74.60	76.99	t Location-Scale	51.57	2.61	1.33
G15/Gt	47.66	58.79	70.66	t Location-Scale	46.95	3.13	1.88

Table 7.12. Statistical analysis of the simulation time reduction (Π-index) for all models in Table 7.1 and Table 7.2

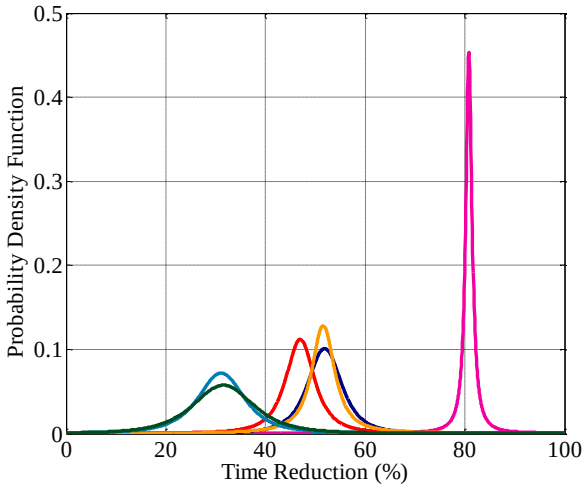

Figure 7.26. Statistical analysis of the simulation time reduction with respect to the detailed building model (Π-index) for different simplified building models in the case the simulation horizon is set to one year. See Table 7.1 and Table 7.2 for details on color lines.

7.3.4 *Overview of the identification and numerical results*

In this section we report a set of remarks which summarize the extensive quantitative analysis carried out in the previous sections for evaluating performance of low order models.

- The grey models composed by 15 equations, i.e., Gt and G15, provide always better performance than the white model with the same number of equations, i.e. W15. This is especially remarkable when predicting heating and cooling demands (see Table 7.8) and comfort. Indeed, in the case of energy demand, these low order models provide prediction errors ten times lower than W15, while for comfort G15/Gt predictions are also of about five times more precise than those given by W15 (see for example ΔPMV and ΔPPD indices in Table 7.10 and Table 7.11 computed for summer weeks). In addition, models G15/Gt outperform the model W15 in terms of indoor temperature predictions from three to five times (see Table 7.6).
- The grey box models G15 and Gt have similar or even better performance also when compared to those obtained with the white model composed by 22 dynamical equations, i.e., W22, despite this model is more complex and have seven more dynamical equations. Precisely, Gt/G15 provides predictions at least twice better with respect to W22 when considering the indoor air temperature (see Table 7.6). In the case of heating and cooling Gt/G15 models improve predictions of W22 with a maximum percentage errors that shift form 13.30% to about 1.30% for heating demand and from 24.5% to 5.5% for cooling demand (see Table 7.8). Similar performance have been obtained also when considering the prediction of peak load

demand and comfort, except for the predictions of PMV and PPD in summer weeks, where Gt/G15 works better than W22 by reducing the prediction errors of the connected performance indices of about threefold (see Table 7.10 and Table 7.11). It is important to point out that the time required to solve numerically (or equivalently, to simulate) the set of differential equations composing G15/Gt is on the average 50% less than that required by W22 (see Table 7.12). In addition the variance of the Π-index is less in the case of Gt/G15, therefore the average percentage time reduction can be obtained with higher probability when using Gt/G15 models instead of model W22.

- Except for the prediction of the maximum peak load demand, the building model composed by eight equation, i.e., G8, provides acceptable prediction errors for any building featured considered in the Section 7.3.2 and Section 7.3.3. For some of them, e.g., heating demand, PMV and PPD in summer weeks, G8 prediction errors are smaller than those provided by W22 (see Table 7.9, Table 7.10 and Table 7.11). Compared to the grey box models Gt and G15, this reduce model provides worse prediction performance and with a time reduction for building simulations that is lower than that expected. This is mainly because the time for solving the equations describing the adaptive controller in Chapter 4, which have been used for all the simulations in this chapter, does not scale with building model complexity.
- Regarding the grey box model Gm, which is composed by twelve equations, it is interesting to note that its ability to reproduce building features is better than the white box model embedding three additional equation, i.e., W15. In addition, for some building feature, e.g., heating and cooling demand, comfort, and indoor air temperature in summer weeks, this low order model have provided better performance also with respect to W22 despite it has ten less equations for capturing building dynamics. Nevertheless, its performance are worse, especially for comfort prediction, with respect those provided by G15 and Gt, and the time reduction for building simulations is comparable to these slightly more complicated grey box models.
- Despite they are used in the technical literature to design model predictive controllers [41], building models composed by two equations, one for the envelope and one for the indoor air temperature, i.e., W2, is inadequate to reproduce any feature of the detailed building model. Consequently, model based controllers can provide performance that can deviate a lot from those obtained by numerical tools embedding

such simplified building models especially when model based controllers implemented in hardware and tested experimentally.

- Models G15 and Gt provide very similar performance indexes. These performance are slightly better in the case of Gt. Nevertheless, as discussed in Section 7.3.1, even though building elements of both models require a similar number of interactions to be tuned by means of the numerical optimization process (see Table 7.5 and Figure 7.15a and Figure 7.15b), the time required to carry out a parameter identification of a building element of a Gt model is much larger than that needed to identify the same element for a G15 model. Consequently, this makes G15-models more efficient with respect to Gt-models.

From the remarks above we conclude that low order G15-models provide the better performance to reproduce building features of a detailed building model and with a consistent reduction of the simulation time. In addition these models have better performance indexes when compared to low order white box models with the same or even higher complexity. Finally, the identification time required to tune the model parameter is acceptable taking into account the just mentioned advantages.

For this reason, in the following chapter, G15 models will be used to design model predictive control algorithms. In the following section, we consider a heavyweight building as an additional case study. In accordance with the literature [28], these class of buildings are difficult to simulate and challenging to be reduced. Consequently, they provide a good benchmark to prove further the effectiveness of the proposed procedure for generating low order building models and the prediction ability of the resulting reduced order systems.

7.4 **Additional case study**

In what follows, we examine an additional case study to prove the effectiveness, of the model reduction approach illustrated in Section 7.1. Different form Section 7.3, here we consider a heavier building structure. Notice that, in accordance to the technical literature [28], these kind of buildings are known to be more difficult to be simplified. Here, we consider a typical Italian building envelope, with length, width and height equal to 20, 10 and 3.5 m, respectively. The building longitudinal axis is East–West oriented and a South facing, air filled double-glazed windows. The thickness of the building walls and floor/ceiling are 25 and 30 cm, respectively. Their stratigraphy is designed by concrete bricks (λ = 0.8 W/mK, ρ = 1800 kg/m^3, c = 840 J/kgK) and thermal insulation (λ = 0.03 W/mK, ρ = 40.0 kg/m^3, c = 1290 J/kgK). The direct solar

radiation transferred through the windows to the inside zone is assumed to be absorbed by the floor with an absorption factor of 0.3. The absorption and emission factors of interior surfaces are assumed to be equal to 0.15 and 0.9, respectively. For such zone, a ventilation rate equal to 1 Vol/h and a crowding index of 0.12 person/m^2 are taken into account.

The time horizon of interest is one year. The heating/cooling system of the thermal zone is switched on from 07:00 to 18:00, from November 1st to March 31st (heating mode) and from 12:00 to 18:00, from June 1st to September 30th (cooling mode). The indoor air temperature is controlled when it is outside the range 20-28 °C, in the case of heating mode, while in the cooling model the control system is activated when this temperature is outside the range 10-25°C. As in the previous numerical example, the relative humidity indoor air is assumed to be controlled at 50%. As weather zones we have considered all those given in Table 5.3.

The analysis in Sections 7.3.2, 7.3.3 and 7.3.4 has shown that the best compromise between the time required to identify the reduced model and the accuracy of its predictions, both in terms of energy and comport, is provided when using a second order thermal network for each building element identified by means of the frequency domain approach.

Hence, for this additional case study we have only designed G15 model, i.e., a low order model where all the elements of the building envelope are second order thermal networks (see also Table 7.1).

Figure 7.27 shows the identification result in the frequency domain for the case of south wall and floor. Compared to Figure 7.8 and Figure 7.9, for this case study there is a higher mismatch between the frequency response of the low order model and that of the detailed model, especially for the south wall. This is basically due to the presence of low frequency poles which increase, with respect to the previous case, the roll-off of the Bode diagrams of the detailed building element models. These steep slopes cannot be perfectly reproduced by means of second order thermal networks which provide at most a roll-off of -40dB/dec for the magnitude, and -90 deg/dec for the phase. On the other hand, these low frequencies poles reduce also the bandwidth of the building constructive elements. Hence, there is not the need to match precisely the frequency response of the detailed model in the entire range of the spectrum of the external inputs, i.e., up to 10^{-3} rad/s (see for example the spectrum of the radiations in Figure 7.6) as the building better filters out high frequency components. Consequently, we expect satisfactory predictions both in terms of energy and comfort as it shown in what follows. Notice that as time interval of interest for the computation of the performance indexes we have still selected the week (i.e., $\Theta = 1\ week$ in (7.8)-(7.10)).

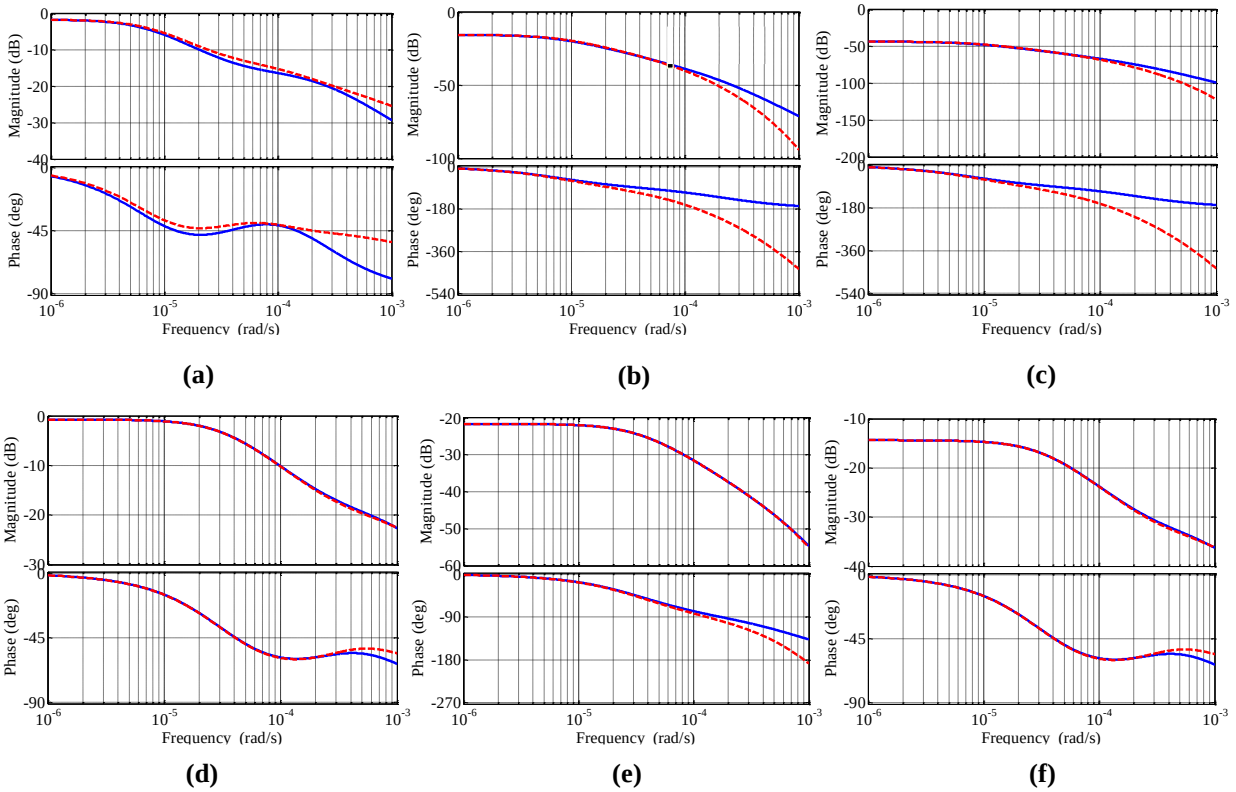

Figure 7.27. South wall temperature frequency response with respect to (a) outdoor temperature (b) indoor air temperature and (c) solar radiation. Floor temperature frequency response to (a) ground temperature (b) indoor air temperature and (c) solar radiation through window. Detailed model (dashed red line) and low-order model (solid blue line).

7.4.1 *Indoor air temperature and energy predictions*

We first investigate the effectiveness of the reduced order model to predict indoor air temperature end energy consumptions. In particular Figure 7.28 shows the PDF of the MaxΔT-index computed both for winter and summer weeks. Here it is clear that those distributions have a small mean, at most of 0.13°C, but also a small variance as the bell shapes are narrow. In addition, the maximum prediction indoor temperature error is low and never exceeds 1°C. Additional details about the PDFs in Figure 7.28 are given in Table 7.13.

Similar results are obtained also when considering the persentage difference between the maximoun heating peak load demands. In this case, better results, compared to those discussed in Section 7.3.2, have been obtained for the performance index ΔP with a maximum prediction error of about 1.11%. Hence, data provided by the low order model can be used also for the design of air conditioning systems by practitioners. As for the index MaxΔT, the probability density function takes a bell shape and its values concentrate around the mean with a small variance of about the 0.06 (see Figure 7.29a).

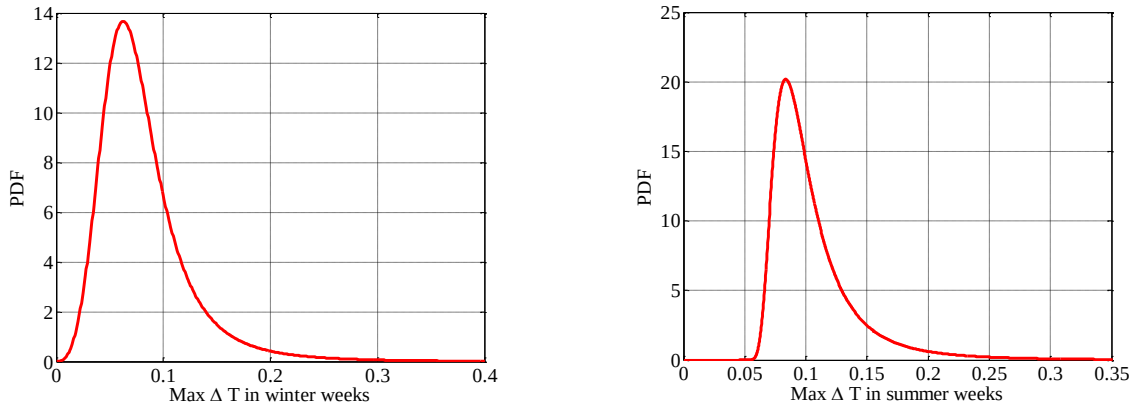

(a) **(b)**

Figure 7.28. Statistical analysis of the Maximum Variation (°C) of the indoor temperature with respect to the detailed building model (MaxΔT-index) in the case of a massive building in (a) winter and (b) summer weeks.

Regarding to the effectivness of the low order model to predict heating demand, we have detected, by computing the ΔE-indext over all the weeks of the year and for all wheater zones in Table 5.3, that on the average there is a missmatch of 0.33% between heteang demand provided by the detailed building model and that prediceted by using the low order model, while the maximoun deviation is less then 4%. Figure 7.29b depicts the shape of the PDF for the ΔE index, while all the PDF parameters are given in Table 7.13. Notice that the energy analysis for cooling is not reported here for the sake of brevity and also because for this type of building heating demand was not predominant.

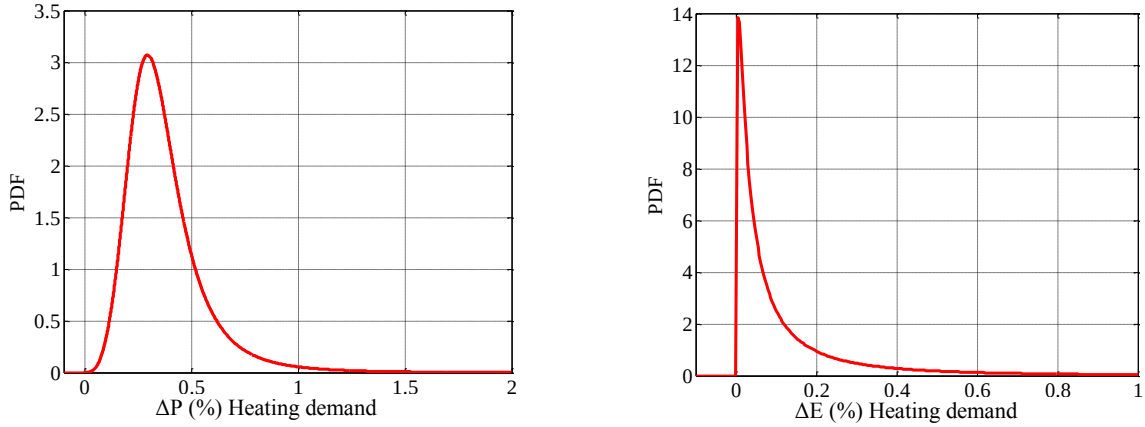

(a) **(b)**

Figure 7.29. Statistical analysis of the Percentage prediction error for (a) peak load demand (ΔP-index) and (b) Heating demand (ΔE-index) with respect to the detailed building model in the case of a massive building.

For the sake of completeness, Figure 7.30 shows the time history of the indoor air temperature and the sensible heat computed by means of the detailed building model and the reduced one (Figure 7.30a) and the corresponding prediction errors (Figure 7.30b) when the building is

located in Athens. Also in this case it is evident that for computing these quantities reduced models can be effectively used.

Index	Mean	Variance	Maximum	PDF	PDF Parameters		
MaxΔT (winter)	0.13	0.08	0.97	Log-Logistic	-2.62	0.27	
MaxΔT(summer)	0.12	0.03	0.63	Gen. Extreme Value	0.30	0.02	0.09
ΔE (heating)	0.33	1.41	3.89	Lognormal	-2.86	1.47	
ΔP (heating)	0.38	0.06	1.11	Log-logistic	-1.09	0.26	0

Table 7.13. Statistical analysis of the Maximum Variation in °C of the indoor temperature (MaxΔT-index), Percentage prediction error for peak load demand (ΔP -index), and Percentage prediction error for Heating demand (ΔE-index) with respect to the detailed building model in the case of a massive building.

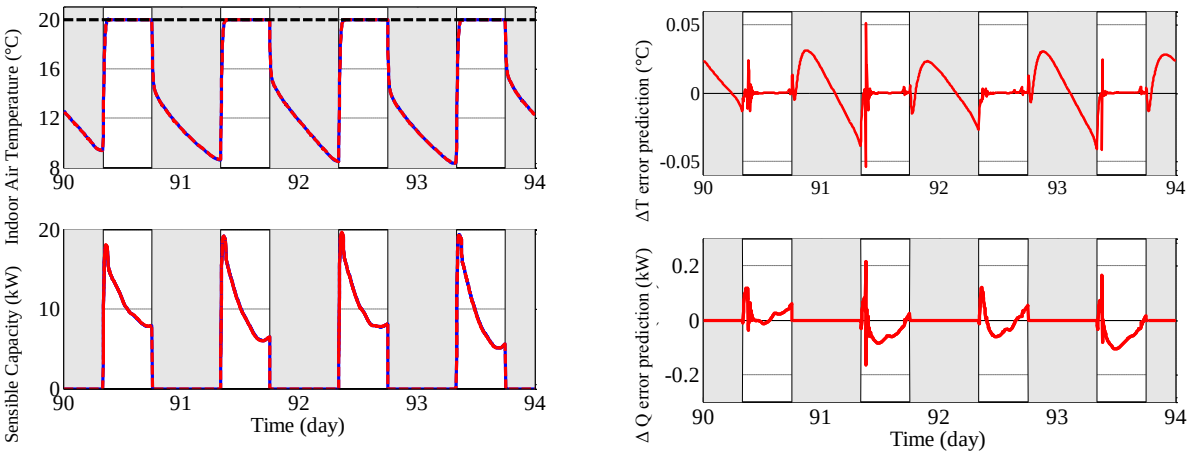

(a) **(b)**

Figure 7.30. Results in the case of Athens. (a) Indoor air temperature and sensible load, reduced model (red line) and detail model (blue line) (b) corresponding prediction errors. Grey area denotes time intervals where the temperature control is deactivated.

7.4.2 *Comfort Predictions and simulation time*

The analysis of comfort indexes has reviled that in this case the deviation of the low order model with respect to the detailed one in terms of PMV, PPD and mean radiant temperature is lower than that detected in Section 7.3.3.

Table 7.14 reports the statistical analysis of the comfort indexes ΔTr, ΔPMV and ΔPPD and shows that the mismatch between the low order and complete model is, on the average, less than 0.08 for PMV predictions, 2.30% for PPD predictions and below 0.18°C when considering the estimation of the mean radiant temperature. In addition, for all indexes the variance is low as confirmed also by the narrow bell shape of the probability density functions of such measurements depicted in Figure 7.31 and Figure 7.32 for winter and summer weeks, respectively.

For the sake of completeness the time evolution of PMV and PPD and mean radiant temperature is depicted in Figure 7.33 in the case of the Rome together with the corresponding

prediction errors. As clearly shown the model reduction approach proposed in Section 7.1 is further confirmed to give a quite precise insight of comfort in buildings.

Index	Mean	Variance	Maximum	PDF	PDF Parameters		
ΔTr (winter)	0.15	0.04	0.75	Gen. Extreme Value	0.33	0.02	0.12
ΔTr (summer)	0.18	0.001	0.27	Gen. Extreme Value	-0.02	0.02	0.16
ΔPMV (winter)	0.05	0.001	0.14	Gen. Extreme Value	0.44	0.001	0.04
ΔPMV (summer)	0.08	10^{-4}	0.11	Gen. Extreme Value	0.26	0.003	0.08
ΔPPD (winter)	2.30	1.99	6.53	t-Location-Scale	2.16	0.02	1.04
ΔPPD (summer)	1.99	2.50	6.73	Log-Logistic	-0.13	1.46	0
Π	45.96	6.16	53.40	Inverse-Gaussian	45.96	1.7E4	

Table 7.14. Statistical analysis of the Maximum Variation in °C of the mean radiant temperature (ΔTr-index), Maximum Variation of PMV (ΔPMV-index), Maximum Variation of PPD (ΔPPD-index) and simulation time reduction (Π-index) with respect to the detailed building model in the case of a massive building.

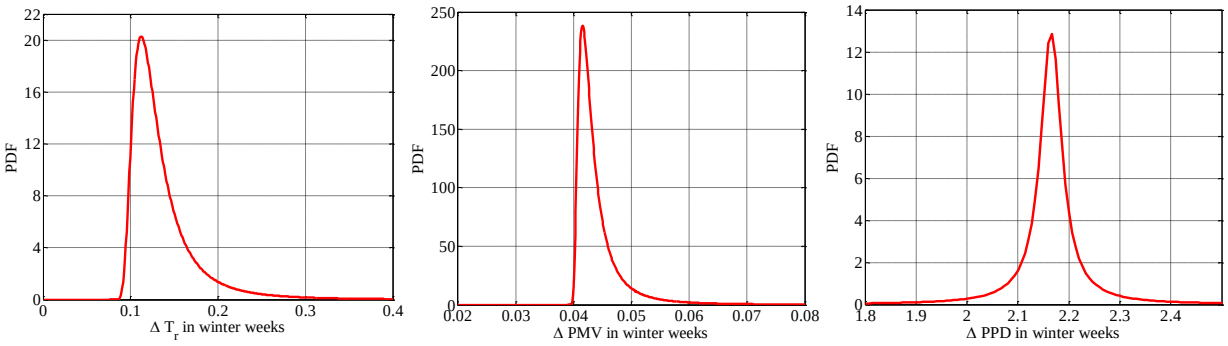

(a) **(b)** **(c)**

Figure 7.31. Statistical analysis of the Maximum Variation in °C of the mean radiant temperature (ΔTr-index), Maximum Variation of PMV (ΔPMV-index), Maximum Variation of PPD (ΔPPD-index) with respect to the detailed building model in the case of a massive building and computed for winter weeks.

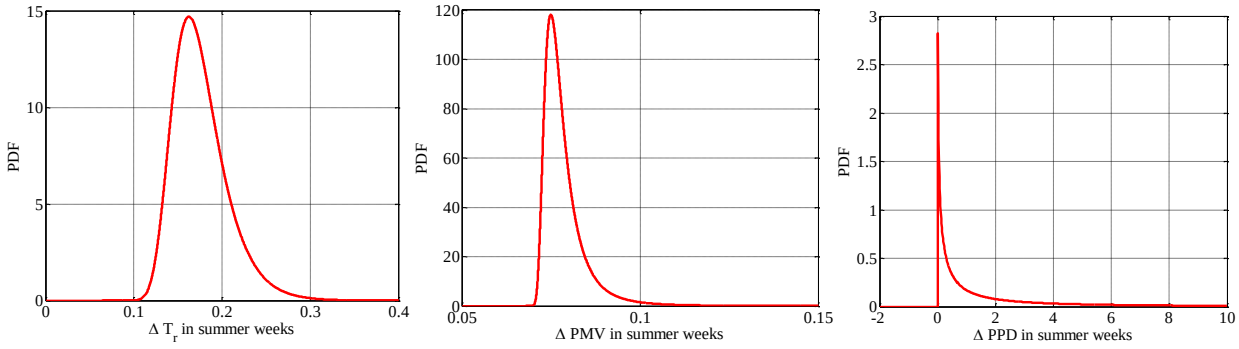

(a) **(b)** **(c)**

Figure 7.32. Statistical analysis of the Maximum Variation in °C of the mean radiant temperature (ΔTr-index), Maximum Variation of PMV (ΔPMV-index), Maximum Variation of ΔPPD (ΔPPD-index) with respect to the detailed building model in the case of a massive building and computed for summer weeks.

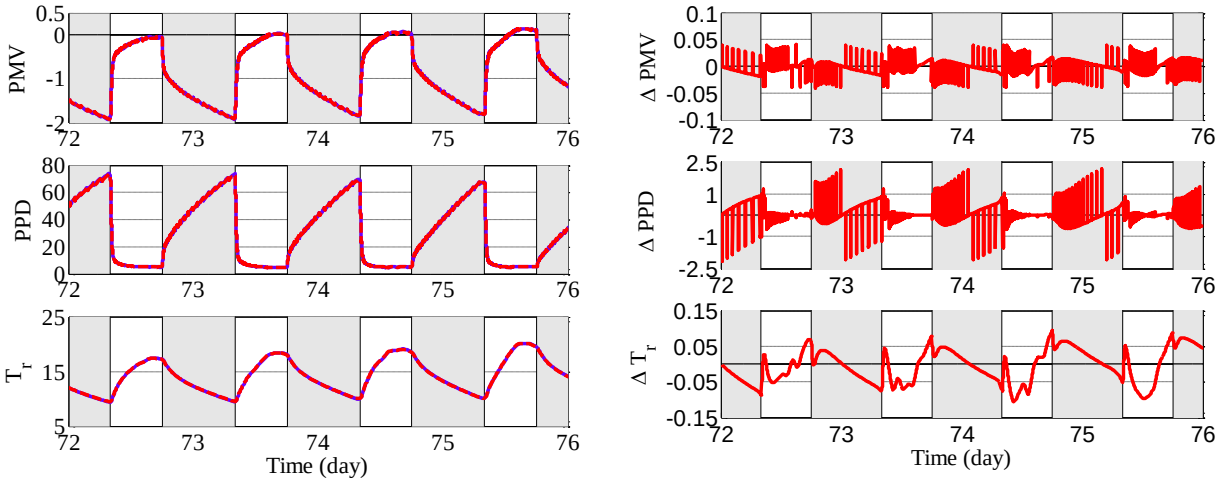

(a) **(b)**

Figure 7.33. Result in the case of Rome. (a) PMV, PPD and mean radiant temperature provided by low order building model (red line) and the detailed one (blue line), and (b) corresponding prediction errors. Grey area denotes time intervals where the temperature control is deactivated.

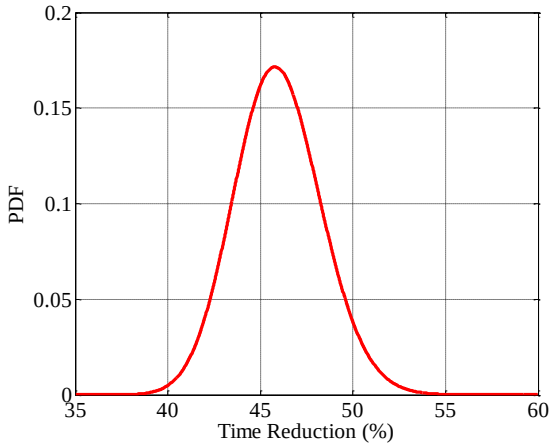

Figure 7.34. Statistical analysis of the simulation time reduction with respect to the detailed building model (Π-index) model in the case of a massive building.

Finally, we remark again that model reduction is required not only for designing model based control strategies for the control of thermo-hygrometric variables in buildings, as those in Chapter 8, but also for reducing simulation time.

Time reduction for simulating this heavyweight building is of about 46% (see Π-index in Table 7.14 and its PDF depicted in Figure 7.34). As clear shown simulation time reduction is within a range from 40% to 55%. This is a remarkable gain as in many building analysis a large amount of numerical simulations are carried out, for example, to test novel technologies for different building configurations.

7.5 **Discussion**

In this chapter we have proposed a systematic approach for deriving low order, but yet, high predictive building models from the detailed one presented in Chapter 2. Precisely, the method requires to slit the building model in its components. For each of them a simplified first or second order thermal network is used to capture its temperature dynamics. The network parameters are the result of an optimization problem based on a cost function that can be set both in the frequency domain or time domain.

To prove the effectiveness of the method, performance indexes have been introduced to measure quantitatively the deviation between the low order models and the detailed one in terms of energy and comfort predictions. Numerical results on a wide set of data have shown that reduced order models composed by second order thermal networks and identified by matching the frequency response of the detailed model provide very satisfactory performance indexes and are fast to be identified (G15 models). For these reasons they are used in the next chapter for the design of model predictive controllers with the aim of testing their performance with those given by the adaptive approach proposed in Chapter 4. Nevertheless, the model reduction method can be used in all those case where low order models are preferable with respect to detailed models, i.e., in order to *i)* reduce drastically the computation time to get an insight into building energy performance, especially when many simulations are required to evaluate them [29] *ii)* derive mathematical models when experimental data are available [30] and *iii)* simulate and evaluate energy demands of districts [31].

Chapter 8
MPC FOR THE OPTIMAL COMPUTATION OF THE SENSIBLE LOAD

In this chapter we design model predictive controllers (MPC) for the indoor air temperature control for different buildings. The aim is to compute energy demands when such model based control strategies are used on the same case studies presented in Chapter 5 for the intermittent running regime with reference set points scheduled in accordance with Table 5.4. In so doing we compare over the same case studies the performance obtained via this model based approach with those given by the adaptive solution proposed in Chapter 4. We investigate both the case when there is a perfect knowledge of the weather data and internal loads as well as the case when these data are affected by uncertainties. We show that on the case studies considered in Chapter 5, better performance are obtained by using the adaptive solution when the closed-loop systems are subjected to severe unpredicted variations of the uncontrolled system inputs. Hence, the classical MPC is considered here as a benchmark model based controller to further show the effectiveness of the adaptive solution on specific case studies. Consequently, an exhaustive comparison between predictive and adaptive control solutions which takes into account all the features of such controllers is out of the scope of the chapter.

In order to make the chapter self contained as much as possible, it opens with a brief revision of the model predictive control strategy. Then some details about its design are given for the sake of completeness. Notice that for devising MPC strategies the knowledge of the model of the process to be controlled is a key ingredient. These models must be as much predictive as possible in order to estimate precisely the indoor temperature in the future time instants. On the other hand in order to keep the computational effort of the MPC control law acceptable, these models cannot be very complicated. Consequently, we use those designed with the model reduction procedure detailed discussed in Chapter 7.

8.1 **MPC control strategy**

In this section the model predictive control strategy for generic discrete time liner system is briefly reviewed to give a reader some details about the design of this control solution. For further details the reader is referred to the wide literature about this topic as [168, 169].

Assume that then process is modelled as the following linear time invariant discrete time system

$$\begin{aligned} x(k+1) &= Ax(k) + Bu(k) + Dw(k), \\ y(k) &= Cx(k), \end{aligned} \tag{8.1}$$

where $x \in \mathbb{R}^n$ is vector state, $w \in \mathbb{R}^m$ is the vector of measurable disturbances, $u \in \mathbb{R}$ and $y \in \mathbb{R}$ are the control input and the system output, respectively. The system matrix is $A \in \mathbb{R}^{n \times n}$, the disturbance matrix is $D \in \mathbb{R}^n$, while the output and the input matrices are $B \in \mathbb{R}^n$ and $C \in \mathbb{R}^{1 \times n}$, respectively.

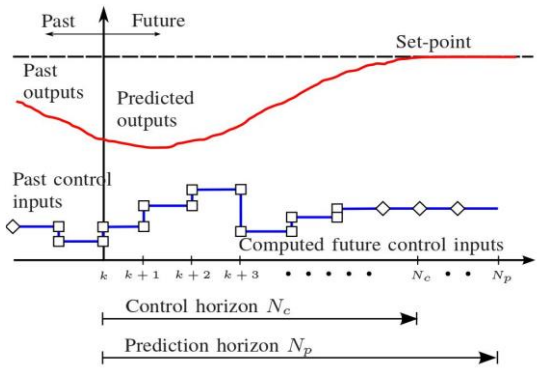

Figure 8.1. The principle of model predictive control (taken from [170]).

The control law generated by the model predictive controller is based on an iterative optimization of the system model. Precisely, at the current time instant *k* the optimal control strategy is calculated by minimizing a cost function subjected to additional constraints over a finite number of steps, say N_p, known as prediction horizon.

Usually, cost functions to be minimized are quadratic and can be expressed, for example, as

$$J = \sum_{i=k}^{k+N_p} \delta_y \left[y_r(i) - y(i) \right]^2 + \sum_{i=k}^{k+N_c} \delta_u u^2(i) \tag{8.2}$$

where $y_r(k)$ is the reference signal to be tracked and δ_u and δ_y are positive constants.

Constrains can be formulated both on system input and output, for example they can take the following form

$$
\begin{aligned}
&u_{\min} \le u(k) \le u_{\max,} \\
&\Delta u_{\min} \le \Delta u(k) \le \Delta u_{\max}, \quad \text{where} \quad \Delta u(k) = u(k) - u(k-1) \\
&y_{\min} \le y(k) \le y_{\max,}
\end{aligned}
\tag{8.3}
$$

with $u_{\min}$, $u_{\max}$, $y_{\min}$, $y_{\max}$, $\Delta u_{\min}$, and $\Delta u_{\max}$ being constants.

When the optimal control sequence is computed often only a sunset of samples (steps) of the entire control horizon N_c are applied to the system before the process described above is iterated.

Remarks.

- Only for the sake of simplicity the system in (8.1) has been supposed to be single input single output and the MCP control problem formulation for multi-input multi-output systems can be found in the literature.
- At the time instant k, the cost function in (8.2) depends on future samples of the output. For this reason a predictive model of the system to be controlled is required together with predictions of all the inputs, i.e., some predictions of the time evolution of the disturbances have to be known.
- The cost function in (8.2) depends on two terms. The first one measures the distance between the system output and the reference, while the second is a measure of the control effort. Consequently, the resulting evolution of the system output is a tradeoff between minimization of the tracking error and the magnitude of the control action.
- By means of the constrains in (8.3) it is possible to impose not only the maximum variations that the system output and control action can assume, but also the maximum rate of variation of the control action can be decided.

The problem of finding the optimal sequence for the cost (8.2) at the time k can be recast as a more standard optimization problem with constraints which allows its numerical solution.

In particular, after some algebraic manipulation the system dynamics to be considered can be rewritten as

$$
Y = Hx(k) + \Gamma_u \Delta U + \Gamma_w \Delta W \tag{8.4}
$$

where

$$
H = \begin{bmatrix} CA \\ CA^2 \\ \vdots \\ CA^{N_p} \end{bmatrix}, \qquad \Gamma_u = \begin{bmatrix} CB & 0 & \cdots & 0 \\ CAB & CB & \cdots & 0 \\ \vdots & \vdots & \cdots & \vdots \\ CA^{N_p-1}B & CA^{N_p-2}B & \cdots & CA^{N_p-N_C}B \end{bmatrix} \tag{8.5}
$$

$$\Gamma_w = \begin{bmatrix} CD & 0 & \cdots & 0 \\ CAD & CD & \cdots & 0 \\ \vdots & \vdots & \cdots & \vdots \\ CA^{N_p-1}D & CA^{N_p-2}D & \cdots & CA^{N_p-N_C}D \end{bmatrix}, \tag{8.6}$$

and

$$\begin{aligned} Y &= \begin{bmatrix} y(k) & y(k+1) & \ldots & y(k+N_p) \end{bmatrix}, \\ \Delta U &= \begin{bmatrix} \Delta u(k) & \Delta u(k+1) & \ldots & \Delta u(k+N_c-1) \end{bmatrix}, \\ \Delta W &= \begin{bmatrix} w(k) & w(k+1) & \ldots & w(k+N_p) \end{bmatrix}. \end{aligned} \tag{8.7}$$

Taking into account (8.4)-(8.7), after additional algebraic manipulations the optimal control sequence can be found by solving the following quadratic programming problem

$$\min_{\Delta U} \left[\Delta U^T \Psi \Delta U + 2\Phi \Delta U \right] \tag{8.8}$$

subject (8.3), where

$$\begin{aligned} \Psi &= \Gamma_u^T \delta_y \Gamma_u + \delta_u I \\ \Phi^T &= -\Gamma_u^T \delta_y \left(Y_r - Hx(k) - \Gamma_u \Delta W \right) + \Delta U \delta_u U \end{aligned} \tag{8.9}$$

and

$$\begin{aligned} Y_r &= \begin{bmatrix} y_r(k) & y_r(k+1) & \ldots & y_r(k+N_p) \end{bmatrix}, \\ U &= \begin{bmatrix} u(k-1) & u(k) & \ldots & y_r(k+N_c-2) \end{bmatrix}. \end{aligned} \tag{8.10}$$

Notice that the problem (8.8) depends on the state *x(k)*.

Addition details about the numerical MPC formulation and its numerical solution can be found in [168-170].

8.2 **Design of MPC for computation of the sensible heat**

Section 8.1 has pointed out that the key ingredients to design an MPC algorithm are: *i)* a predictive model of the system to be controlled so that when applying the optimal control sequence to the real system the resulting evolution is as close as possible to the expected one, *ii)* the weights δ_u and δ_y which characterize the cost function (8.2) as well as the predictive and control horizons and *iii)* the constraints in (8.3). In particular we remark that the model of the system should not only be predictive but also as simple as possible to reduce the complexity of the optimization problem.

In the case of the temperature control there is an additional design choice to be made which is connected to discretization of the building dynamics. Indeed, indoor air temperature evolves in the continuous time domain. On the other hand the system model in (8.1) for the design of MPC algorithms is set in the discrete time domain. Consequently, there is the need to use some discretization method to map the former onto the latter.

For the case studies in Chapter 5 for the intermittent running regime with reference set points scheduled in accordance with Table 5.4, we have made the following choices.

- As building model to be used during the optimization of the cost function (8.2) we exploited those designed in Chapter 7. Indeed, these models have shown to be simple, fast to be integrated numerically and they provide accurate predictions of the indoor air temperature, energy demand and comfort. More in details, we use G15 models which have provided the best values of the performance indices introduced in Chapter 7 and their identification is not time consuming. Here, we just recall that a G15 model is composed by a set of second order thermal networks (one for each building element) and the parameters of each network are so that its frequency response matches that of the corresponding element of the detailed building model in Chapter 2.
- As discretization method we have considered the zero order hold (ZOH). In so doing the resulting discrete time system is still strictly proper (i.e., the system output does not depend directly on the input [96]) and consequently the MatLab optimization procedures can be exploited to for the numerical solution of the problem. Here, we recall that given a liner time invariant continuous time system of the form

$$\begin{aligned} \dot{x} &= A_c x + B_c u + D_c w, \\ y &= C_c x, \end{aligned} \tag{8.11}$$

it is possible to map it onto a discrete time system of the form (8.1) via the following transformations

$$A = e^{A_c T_s}, \quad B = \int_0^{T_s} e^{A_c \sigma} B_c d\sigma, \quad D = \int_0^{T_s} e^{A_c \sigma} D_c d\sigma \tag{8.12}$$

where T_s is the sampling time.

In the case of temperature control, this parameter has been chosen so that aliasing phenomena are avoided [171].

- The prediction horizon has been chosen so that it is possible to capture well the temperature dynamics while the control horizon is a quarter of the prediction one.

- The weighs of the cost function (8.2) has been selected as a tradeoff between reduction of energy consumption and thermal comfort for the occupants. Indeed in the case of temperature control the first term in (8.2) measures the distance between the actual temperature and that required set point, while the latter takes into account the heating/cooling required during the control horizon.
- Constraints in (8.3) has been set so that it is always possible to achieve the reference temperatures.

8.3 **Numerical Results**

In this section we evaluate the numerical results of the MPC strategy for the indoor air temperature control for all the case studies in Chapter 5 when intermit running regime is used and the indoor air humidity is assumed to be controlled a 50%. In what follows some results, exemplar with respect to the energy building dynamic behaviour, are presented.

We start considering the time evolution for a sample day for some lightweight office buildings in cold winter zones. As clearly shown in Figure 8.2a the indoor temperature is controlled over the hours of interested for this kind of buildings as specified in Table 5.4. Notice that such table also reports the control activation ranges, comprised by the indoor air temperature set points, which change, according to the selected schedules, from winter (heating dominated) to summer (cooling dominated) season and vice versa.

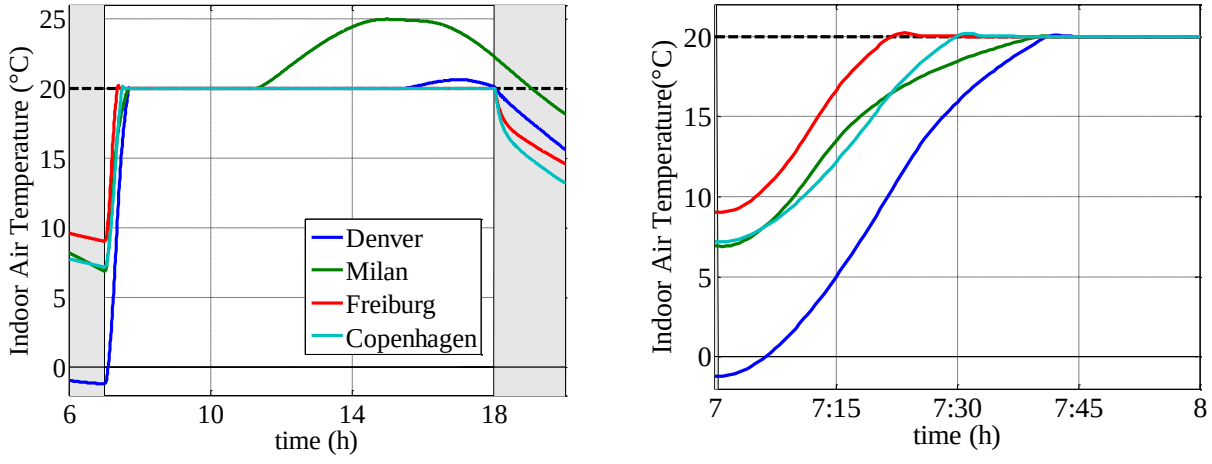

(a) **(b)**

Figure 8.2. Winter season (53th day of the year). (a) Indoor air temperature evolution of some lightweight office buildings in cold winter zones over a set of hours; (b) transient dynamics. Grey shaded areas denote the time range where the MPC controller is deactivated according to Table 5.4.

To better investigate the transient dynamics when the MPC temperature controller is switched on, Figure 8.2b shows the indoor air temperature evolution over the first hour after the activation

of the controller. It is interesting to note that the resulting indoor temperature evolution towards the required set point is not assigned a priori but depends on the weather data and which constraints become active. Consequently, different relaxation times are obtained (see Figure 8.2b).

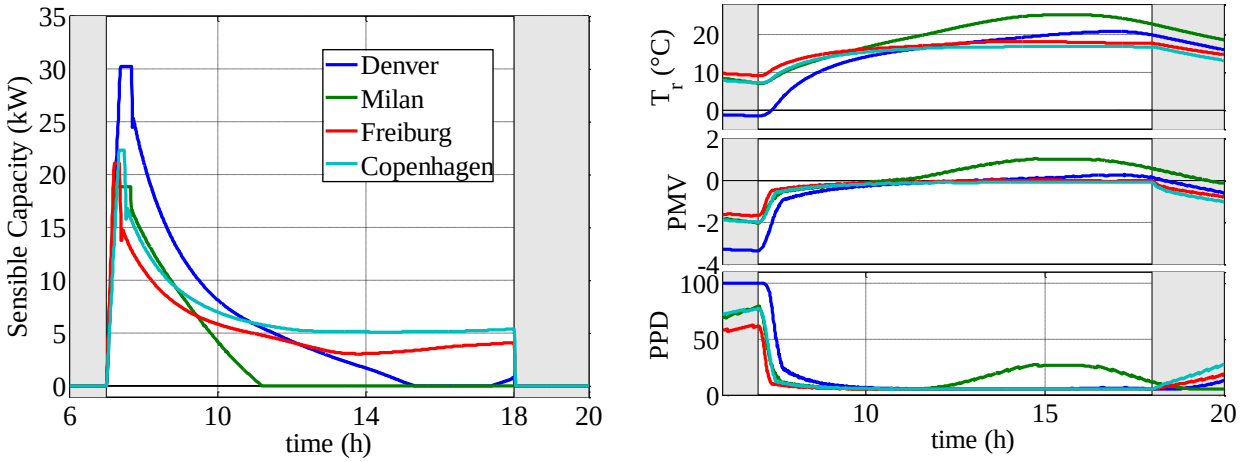

Figure 8.3. Winter season (53th day of the year). (a) Sensible heat and (b) Comfort indices for some lightweight office buildings in cold winter zones over a set of hours (b) transient dynamics. Grey shaded areas denote the time range where the MPC controller is deactivated according to Table 5.4.

The required sensible heat is instead reported in Figure 8.3a. In particular in the case of some weather zones (Denver and Milan) the algorithm automatically decides to set the heating demand to zero therefore allowing the free floating of the temperature within the acceptable range (see also Table 5.4), and in the case of Denver, the controller is restored for a short time around 18:00 before it is deactivated. The realise of the temperature for Denver and Milan is mainly due to the higher solar radiations which are depicted in Figure 8.4 for the sake of completeness. The MPC algorithm can predict, via the building model, that these radiations can lead the indoor air temperature inside the acceptable range (see Table 5.4.) without any addition heating load. Hence, for some hours the heating demand is reduced to zero (see Figure 8.3a) and then the indoor air temperature increases. In the case of Denver there is a smaller free floating region not only because solar radiations for this weather zone are smaller when compared to those in Milan, but also because the outdoor air temperature is lower in the case of Denver, but time histories of the outdoor temperatures are not reported here for the sake of brevity.

Figure 8.3b shows that when the controller is activate, the comfort indexes are acceptable. Only for the case of Milan there is small increase of PMV and PPD during the free floating regime. Similar results are obtained during summer season, as shown in Figure 8.5 and Figure

8.6 for some warm weather zones. We remark that in this case it is even more evident how constraints effect the resulting relaxation time and comfort.

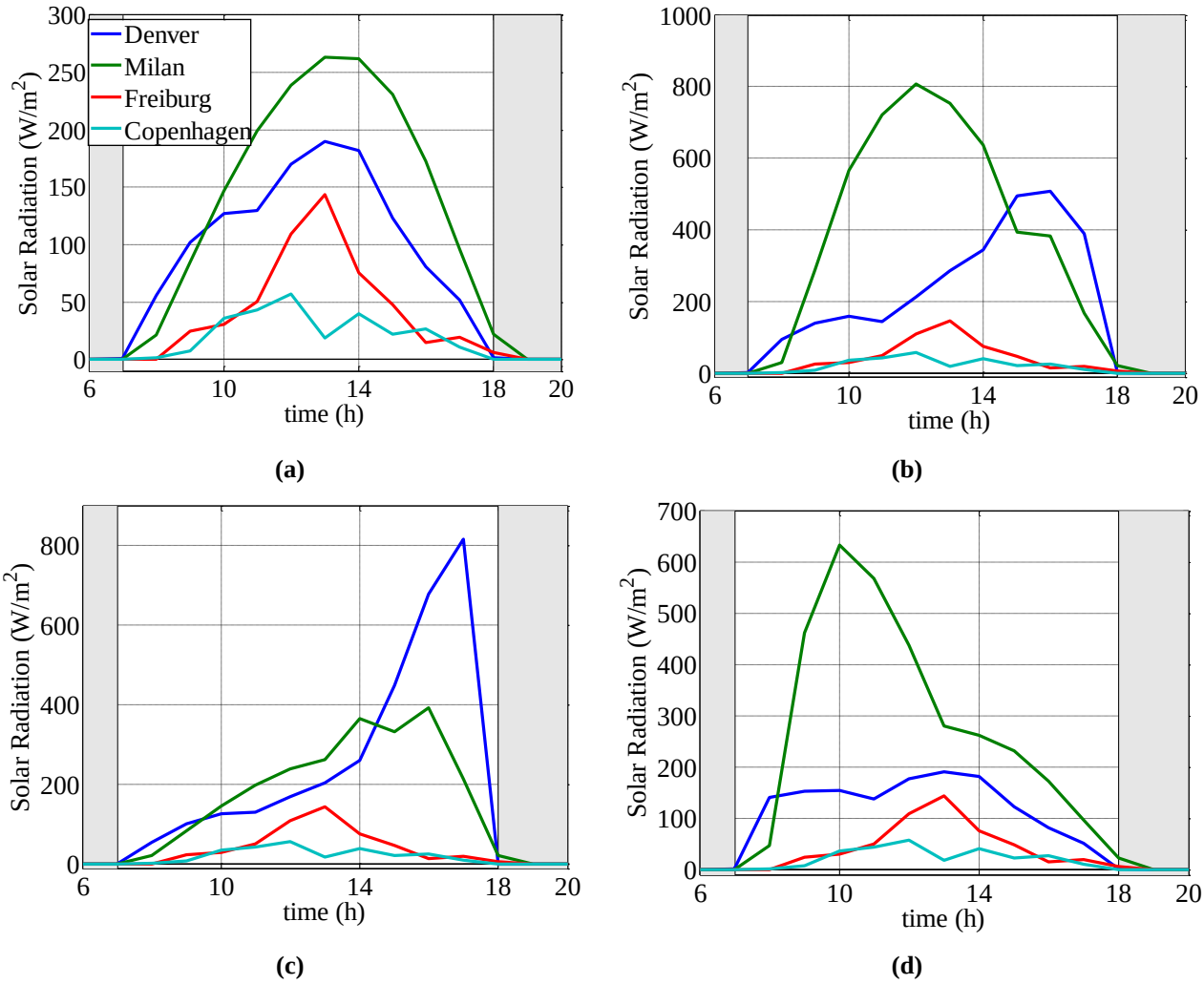

Figure 8.4. Winter season (53th day of the year).Solar radiation (a) north (b) south (c) east and (d) west walls. Grey shaded areas denote the time range where the MPC controller is deactivated according to Table 5.4.

Indeed, Figure 8.5 shows that the time to reach the required set point is about 30 min in the case of Nice and Rome, but it is about one hour for Athens and it increases to one hour and half for Naples. As a consequence for the latter two weather zones the comfort indexes enter definitely in a satisfactory range, e.g. PPD less than 20%, after a longer transient (see also Figure 8.6b).

In order to analyze the system performance with respect to comfort, the time histories of PMV, PPD and mean radiant temperature, T_{mr} , (see Section 2.3), are assessed all over the year. For the investigated case studies, such analysis showed that good PMVs and PPDs are achieved.

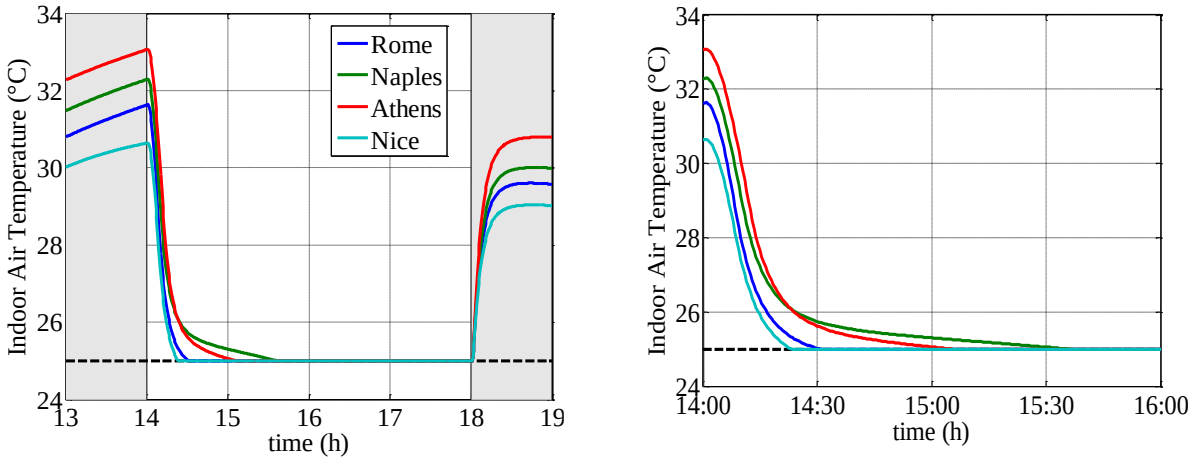

(a) **(b)**

Figure 8.5. Summer season (220th day of the year). (a) Indoor air temperature evolution of some lightweight office buildings in cold winter zones over a set of hours; (b) transient dynamics. Grey shaded areas denote the time range where the MPC controller is deactivated according to Table 5.4.

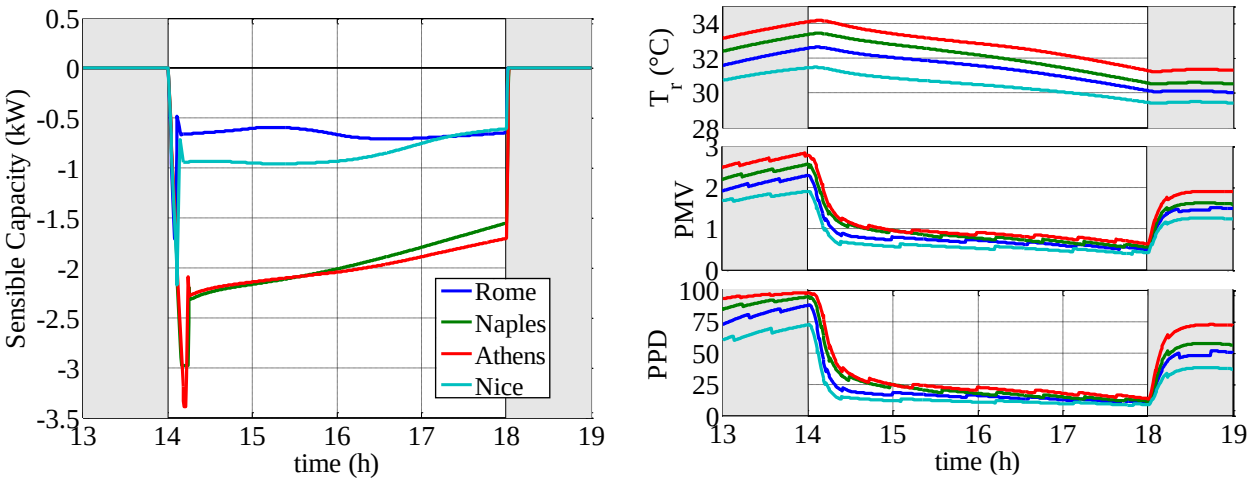

(a) **(b)**

Figure 8.6. Summer season (220th day of the year). (a) Sensible heat and (b) Comfort indices for some lightweight office buildings in cold winter zones over a set of hours (b) transient dynamics. Grey shaded areas denote the time range where the MPC controller is deactivated according Table 5.4.

It particular via a precise prediction of the system dynamics it is possible to restore satisfactory comfort levels which were lost during control deactivation because of the change of the external conditions and the variable internal thermal loads. In what follows thermal comfort performance are discussed taking into some sample days, simulated buildings and weather locations. In particular, Figure 8.7 and Figure 8.8 show the thermal comfort (described by means of PMV, PPD and T_{mr}) related to the simulated Mall and Office buildings located in some weather zones with cold winters and hot summers, respectively. Precisely, Figure 8.7 refers to several winter days, ranging from January 22nd to 28th related to lightweight buildings located in

Freiburg, Copenhagen, Milan and Denver. Here, it is clearly shown that during the steady state regime (subsequent to the switching on transient time), very good PMVs (always included between -0.5 and 0) and PPDs (always less than the 10%) are achieved, despite low values of the mean radiant temperature T_{mr} .

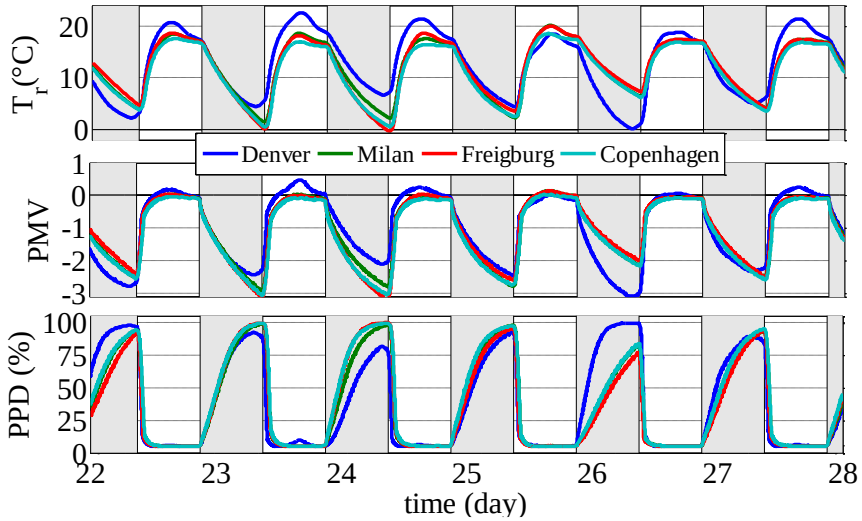

Figure 8.7. Lightweight Mall buildings in cold winter zones. Time history of PMV, PPD and T_{mr}. Grey shaded areas denote the time range where the MPC controller is deactivated according to Table 5.4.

Similar results are obtained during the summer season, as shown in Figure 8.8. Such figure refers to the days ranging from June 29nd to July 5th (i.e. 180th - 186th days of the year) and to the heavyweight Office buildings located in Athens, Naples, Jerusalem and Rome. Here, as a result of the optimal performance of the control actions, good PMVs (always included between 0 and 0.5) and PPDs (always less than the 15%) are obtained during the steady state regime.

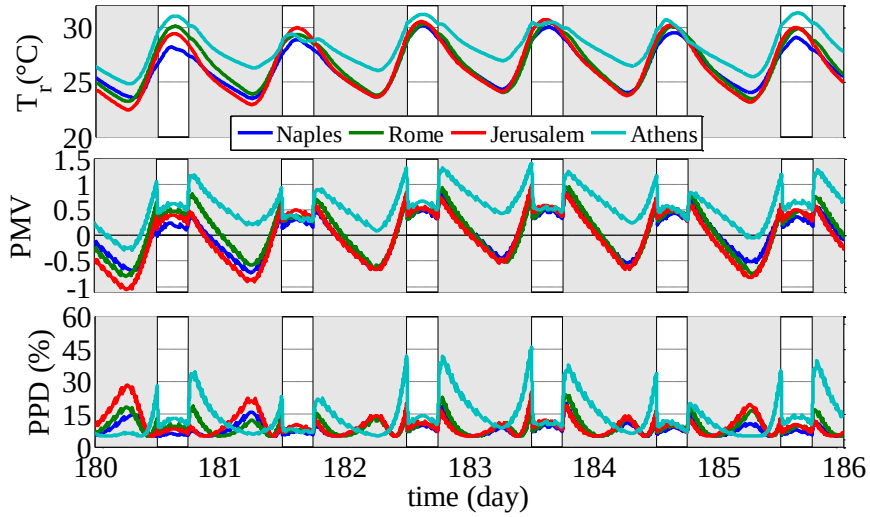

Figure 8.8. Heavyweight office in hot summer zones. Time history of PMV, PPD and T_{mr}. Grey shaded areas denote the time range where the MPC controller is deactivated according to Table 5.4.

To complete the analysis, we show the dynamic trends of the indoor air temperature and the control action (sensible heating/cooling to add or subtract to the space) required for the optimal temperature control. Such analysis takes into account the same weather zones, buildings, and weather conditions investigated in Figure 8.7 and Figure 8.8.

In particular, Figure 8.9a refers to the case of lightweight Mall buildings in Freiburg, Copenhagen, Milan and Denver, while Figure 8.9b is referred to some hot summer days in Athens, Nice, Jerusalem and Rome for heavyweights office buildings. As in Chapter 5, in these figures it is possible to observe a proportional dependence of the control actions occurring in the investigated weather conditions. In case of cold winter days as the indoor temperature goes much lower the required set point during control deactivation (*g*ray shaded areas), therefore when the controller is switched on, high sensible heat must be provided to the zone to recover comfort fast.

A similar result can be observed in case of hot summer days, as depicted in Figure 8.9b. Here, it is clearly shown that the farther the indoor from the set point, the higher the cooling requirements.

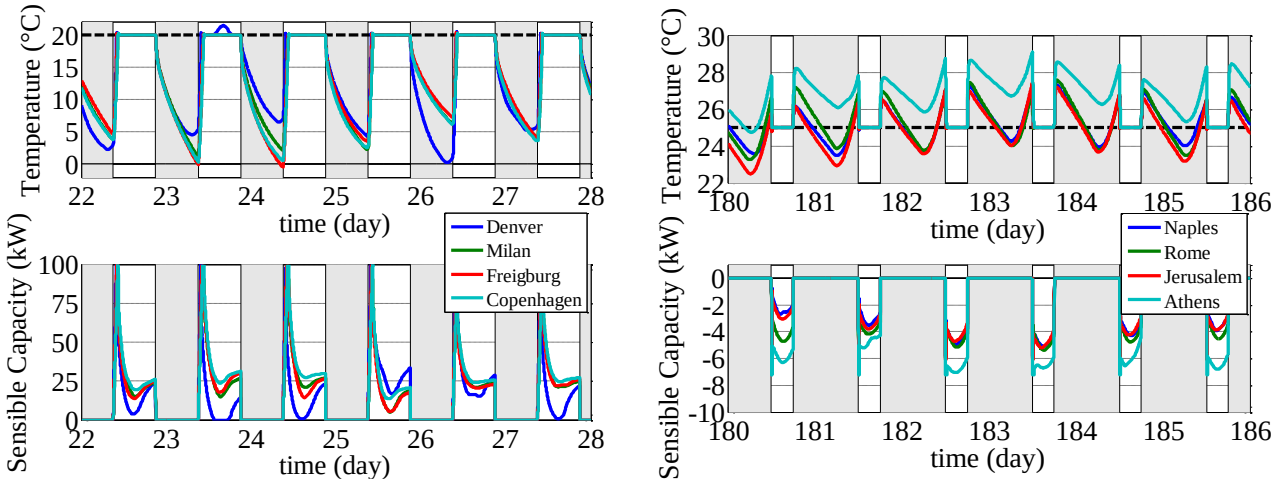

Figure 8.9. Control actions in the case (a) Lightweight Mall buildings in cold winter zones and (b) Heavyweight office in hot summer zones. Grey shaded areas denote the time range where the MPC controller is deactivated according to Table 5.4.

8.4 **Comparison with the MRAC approach**

In this section we compare the cooling/heating required to control the indoor air temperature when either the MPC strategy (designed in Section 8.2) or the model reference adaptive algorithm (designed in Chapter 5) are used. Specifically, the analysis is carried out under two

different operative conditions: *(i)* the weather data and internal loads are perfectly known, and *(ii)* predictions of the weather data and the internal loads are affected by random uncertainties. Precisely we assume that these measurements are affected by an error of about ±20%. Again, as case of studies we consider all those presented in Chapter 5 for the intermittent running regime with reference set points scheduled in accordance with Table 5.4.

Table 8.1 collects the yearly percentage energy variations when the model predictive controller replaces the model reference adaptive algorithm for the computation of the heating (H) and cooling (C) demands in the case of perfect knowledge of weather data and the internal loads. Hence, entries of Table 8.1 are computed as

$$100\frac{|E_{MRAC}|-|E_{MPC}|}{|E_{MRAC}|} \tag{8.13}$$

with E_{MRAC} (E_{MCP}) being the energy required for heating or cooling the thermal zone of interest when the model reference adaptive algorithm (the model predictive controller) is used. Consequently, negative values of (8.13) indicates that better energy performance have been obtained when the adaptive approach has been exploited to tame the building dynamics. Analogously, positive values of (8.13) means that the predictive strategy has performed better for that specific case. From Table 8.1 the following remarks can be drown.

Weather zone	**Mode**	**House**		**Office**		**Mall**	
		Light (kWh/m^{2}y)	**Heavy** (kWh/m^{2}y)	**Light** (kWh/m^{2}y)	**Heavy** (kWh/m^{2}y)	**Light** (kWh/m^{2}y)	**Heavy** (kWh/m^{2}y)
Copenhagen	*H*	-0.89	-0.80	0.07	-0.03	3.10	1.97
	C	-1.42	-1.19	0.64	1.11	1.36	1.48
Denver	*H*	-1.46	-2.16	0.04	-1.01	2.36	0.83
	C	-0.98	-0.18	-0.10	1.78	3.48	2.12
Freiburg	*H*	-1.01	-1.18	-0.38	-0.64	2.43	1.15
	C	-1.47	-2.26	-0.13	-0.24	1.05	3.46
Milan	*H*	-0.82	-0.76	-0.08	-0.19	3.14	0.74
	C	-0.56	0.43	-0.28	1.95	1.15	1.29
Rome	*H*	-2.10	-1.99	-0.82	-1.18	1.78	-0.43
	C	0.07	-0.90	-0.70	0.23	0.85	0.86
Nice	*H*	-1.51	-2.32	-0.37	-0.98	3.29	0.07
	C	0.18	0.42	-0.13	1.12	0.71	1.51
Naples	*H*	-2.24	-2.30	-0.81	-1.31	2.59	-0.32
	C	0.72	0.52	-0.58	1.87	0.913	0.84
Jerusalem	*H*	-2.25	-3.64	-0.44	-1.30	2.52	-0.23
	C	0.82	-0.34	-0.51	0.35	0.93	1.14
Athens	*H*	-1.89	-2.76	-0.89	-1.27	0.11	-0.86
	C	1.03	1.57	-0.35	1.98	0.94	1.27

Table 8.1. Percentage energy variation, heating (H) and cooling (C), when the model reference adaptive controller is replaced with MPC strategy in the case of perfect knowledge of the weather data and internal loads computed by using (8.13).

Remarks

- The model reference adaptive strategy has performed better with respect to the predictive controller for 58 times out of 108 energy analysis. Specifically, the required yearly heating is smaller when the adaptive approach is used for 38 times out of 54 case studies. On the other hand the MPC has shown to be more effective for the optimal computation of the cooling demand as the required cooling energy is smaller than that obtained when the adaptive controller is inserted in the control loop 36 times out of 54.
- The MRAC strategy performs better than the predictive one especially for buildings of small and medium sizes (houses and offices). Precisely, for the case of houses the MRAC approach requires smaller energy demands 27 times out of 36 energy analyses (heating and cooling for nine weather zones, lightweight and heavyweight buildings). Instead, for office buildings the adaptive strategy is more convenient under the energy consumption viewpoint 25 times out of 36. On the other hand for buildings of large size (defined malls in Chapter 5), the MPC performs better than the MRAC algorithm as the energy consumption for controlling the indoor air temperature is smaller 32 times out of 36.
- The MRAC strategy is less energy consuming for lightweight buildings 28 times out of 54 case studies, and 27 times out of 54 case studies for heavyweight buildings.
- From Table 8.1 is possible to note that, in the case of perfect knowledge of the weather data, there is a slight difference between the energy performance provided by the adaptive control solution and the predictive strategy. Indeed the maximum heating positive percentage variation is 3.29% and it has been obtained in the case heavyweight mall in Nice. Instead, the maximum heating negative percentage variation is -3.64% and it has been detected in the case of heavyweight house in Jerusalem. Also the cooling demands required by the adaptive and predictive strategies are comparable. In this case, the maximum cooling positive percentage variation is 3.48% (lightweight mall in Denver), while the maximum cooling negative percentage variation is -1.47% (lightweight house in Freiburg).

We point out that in this working condition both the adaptive and the model based control solutions have similar energy performance as both can effectively impose the required scheduling in Table 5.4. Consequently, in steady state regime both controllers compensate disturbances to keep the desired set-point indoor air temperature.

Consider now the case where the weather data and the internal loads are known with a random uncertainty of about ±20% .Table 8.2 reports the yearly percentage energy variations when the model predictive controller replaces the model reference adaptive algorithm for the computation of the heating (H) and cooling (C) demands in this case.

Weather zone	**Mode**	**House**		**Office**		**Mall**	
		Light (kWh/m^2y)	**Heavy** (kWh/m^2y)	**Light** (kWh/m^2y)	**Heavy** (kWh/m^2y)	**Light** (kWh/m^2y)	**Heavy** (kWh/m^2y)
Copenhagen	*H*	-1,66	-1,01	-0,58	-0,23	2,83	1,55
	C	-1,58	-5,1	-4,73	-49,78	-59,42	-65.28
Denver	*H*	-2,84	-2,47	-1,6	-1,32	1,6	0,62
	C	-1,03	-1,09	-2,03	-5,56	-4,94	-38,98
Freiburg	*H*	-2,26	-1,44	-1,42	-0,88	1,95	0,91
	C	-1,62	-3,56	-3,5	-12,71	-17,34	-53,29
Milan	*H*	-2,11	-1,2	-1,37	-0,6	2,5	0,44
	C	-0,61	-0,55	-2,41	-5,87	-13,42	-85,49
Rome	*H*	-6,44	-3,42	-4,32	-2,24	0,01	-1,12
	C	0,07	-1,44	-1,39	-3,69	-8,69	-24,01
Nice	*H*	-7,07	-4,59	-4,57	-2,53	1,38	-0,87
	C	0,16	-0,37	-2	-4,86	-14,62	-63,4
Naples	*H*	-7,01	-3,7	-4,68	-2,55	0,66	-1,2
	C	0,68	0,04	-1,17	-1,82	-8,2	-23,44
Jerusalem	*H*	-8,76	-5,77	-5,69	-3,06	0,04	-1,32
	C	0,82	-0,76	-0,83	-3,2	-7,33	-25,82
Athens	*H*	-10,21	-5,36	-6,94	-3,09	-2,93	-2,17
	C	1,03	1,23	-0,79	-0,02	-3,81	-7,84

Table 8.2. Percentage energy variation, heating (H) and cooling (C) computed by using (8.13), when the model reference adaptive controller is replaced with MPC strategy in the case of the weather data and internal loads affected by uncertainties.

When weather data available to the model based controller are affected by uncertainties, closed-loop performance, both in terms of tracking of the required temperature set point and demanded heating/cooling, get worsen. In particular the following remarks can be drown.

Remarks

- The model reference adaptive strategy has performed better with respect to the predictive controller for 89 times out of 108 energy analysis. Specifically, the required energy demand is smaller when the adaptive approach is used 42 times out of 54 case studies when computing heating, and 47 times out of 54 case studies when considering cooling demands.
- In the case of heating, the model based strategy performs better than the adaptive one only in the case of lightweight mall buildings and some heavyweight mall buildings located in cold weather zones (i.e., Copenhagen, Denver, Freiburg, and Milan).

Nevertheless the energy reduction is limited and never exceeds 2.83% (lightweight mall buildings in Copenhagen).

- In the case of cooling, the predictive control approach outperform the adaptive algorithm mainly for some lightweight house buildings located in warm weather zones (Rome, Nice, Naples, Jerusalem and Athens). In this specific case, the advantage in replacing the model reference adaptive controller is even slighter as the maximum energy reduction is 1.03% (lightweight house building in Athens).
- There are several cases where the model reference adaptive algorithm outperform the model based control strategy in terms of heating/cooling demands. In particular in the case of heating, the adaptive control method for computing the sensible heat provides an energy reduction which on the average is 3.2%. The maximum heating energy reduction by using the MRAC algorithm instead of the predictive one is about 10.21% (lightweight house building in Athens).
- When the weather data are affected by uncertainties the model reference adaptive control algorithm in Chapter 4 results to be more energy saving that the model based approach when computing cooling demands. In particular cooling demands are on the average 16.2% smaller when the adaptive controller is inserted in the control loop. For some cases we have also detected a cooling energy greater than 50% (e.g., heavyweight mall buildings in Nice and Milan).

It is important to point out that the model reference adaptive controller was found to be remarkably more convenient, under the energy consumption viewpoint, for those cases where the model based controller has shown poor tracking performance of the reference temperature set points defined in Table 5.4 due to the presence of unexpected variations of the weather data. In this regard, Figure 8.10 shows the temperature dynamics and the required sensible heat provided by both control strategies in the case of a heavyweight office building in Milan over a summer day (243^{th} day of the year, August 31^{st}). For this day, overestimated weather data and internal loads were available to the MPC controller. Consequently, the peak of the sensible heat to be removed (cooling) is higher at the control activation, and even though the indoor air temperature enters in the admissible range at the very beginning (see Table 5.4), the required sensible heat does not converge to zero. This is mainly because the controller is assuming wrongly higher outdoor air temperature and solar radiations in future time instants, therefore it requires to subtract additional heat with the aim of keeping the indoor air temperature within the admissible range of variations.

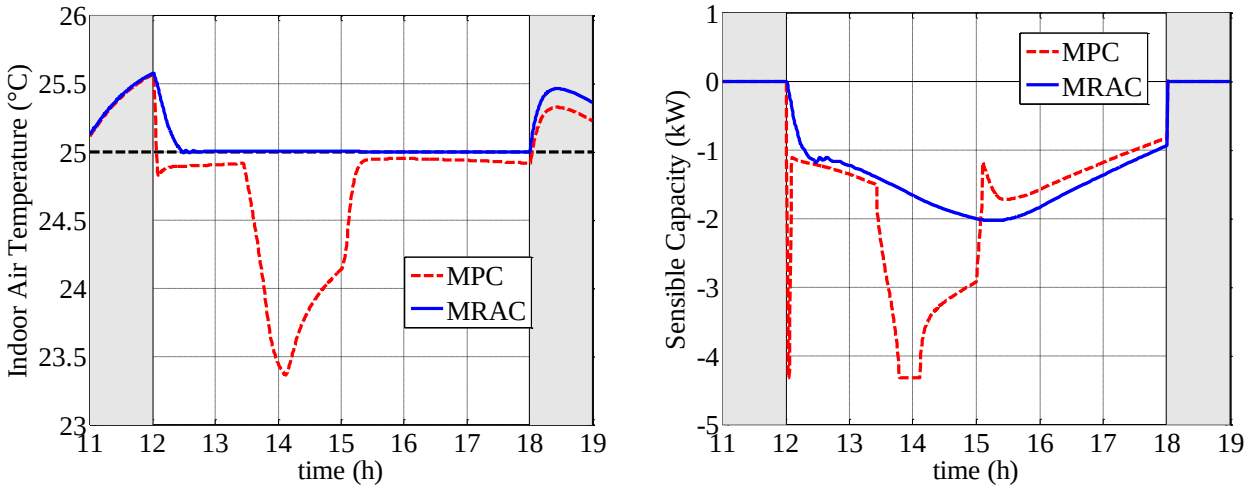

(a) **(b)**

Figure 8.10. Heavyweight Office in Milan, 245th day of the year: (a) indoor air temperature, (b) sensible capacity (control action).Grey shaded areas denote the time range where controllers are deactivated according to Table 5.4.

The effect of uncertainty on the weather data becomes even more evident from 13:30 to 15:30 when the outdoor temperature and the solar radiations increase. In particular the indoor temperature is reduced to 23.5°C which implies additional cooling despite an indoor air temperature of 25°C is acceptable according to the scheduling in Table 5.4. We remark that in this case the MRAC approach in Chapter 4 keeps constantly the indoor air temperature at the acceptable upper bound and consequently a smaller control action (sensible load) is required. Hence, a less yearly cooling demand is achieved. Precisely, the MRAC strategy requires about 5.87% less cooling energy with respect to the model based solution (see Table 8.2).

Another unwanted dynamic induced when weather data are not precisely known and predictive solutions are used is the misdetection of activation and deactivation of the controller. To better analyse this effect, Figure 8.11 shows the case of a lightweight mall in Athens during the 80th day of the year (February 26th). For this building configuration there is not the need to control the indoor air temperature between 14:00 and 16:45. Hence, the adaptive controller is deactivated allowing the free floating of the indoor air temperature in the preassigned range (see Table 5.4). On the other hand during the 80th day of the year, underestimated weather data and internal loads are available to the MPC strategy. Hence, the control algorithm decides to provide to the thermal zone an additional positive sensible heat which in turns increase the indoor air temperature without improving comfort. It is also interesting to note that for this case study, uncertainties on weather data and internal loads induce an overshoot at control activation and a steady state error of about 0.5 °C (see zoom in Figure 8.11a).

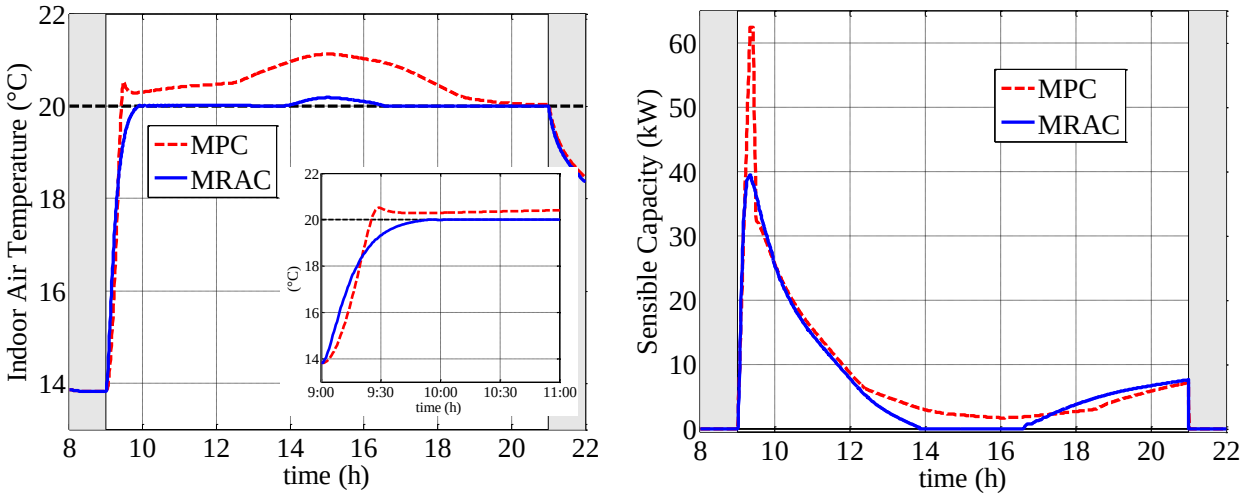

(a) **(b)**

Figure 8.11. Lightweight Mall in Athens, 80th day of the year: (a) indoor air temperature, (b) sensible capacity (control action).Grey shaded areas denote the time range where controllers are deactivated according to Table 5.4.

A similar unwanted behaviour has been also detected in case of a lightweight house in Athens during the 50th day of the year (February 19th). As clearly shown in Figure 8.12, for this case, underestimated weather data and internal loads induce saturation of the control variable at the control activation (Figure 8.12b) and an overshoot of 2.5 °C with respect to the low admissible indoor air temperature bound (see also Table 5.4). Furthermore, also for these operative conditions, there is a misdetection of the control deactivation which occurs at 12:30 instead of 11:30.

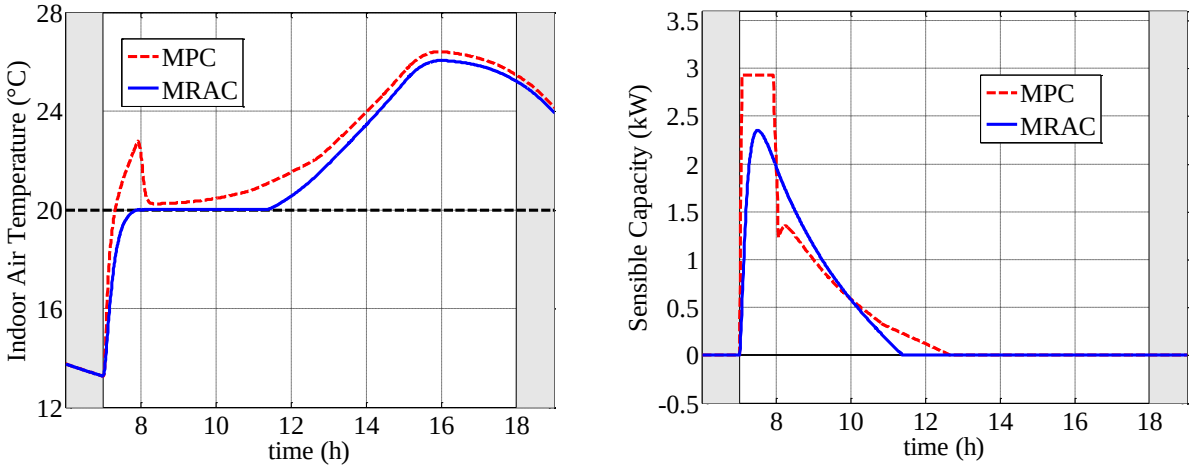

(a) **(b)**

Figure 8.12. Lightweight House in Athens, 50th day of the year: (a) indoor air temperature, (b) sensible capacity (control action).Grey shaded areas denote the time range where controllers are deactivated according to Table 5.4.

Similar additional and unnecessary heating has been also observed for several winter days. Consequently, the model based strategy is less convenient of about 10.21% with respect to the adaptive solution when uncertainties jeopardize model based control performance as reported in Table 8.2. Also additional unnecessary cooling have been also detected when the predictive algorithm is inserted in the control loop in the case of uncertain working conditions. For instance, in Figure 8.13 it is depicted the case of a Heavyweight Mall in Rome during the 185th day of the year (July 4th). In particular we note that during the time range of interest, i.e., from 11:00 to 21:00 (see also Table 5.4 for the scheduling policy), there is the need for cooling only from about 15:00 to 19:45 in order to keep the indoor air temperature in the required range (see Table 5.4). On the other hand, as overestimated weather data and internal loads are available to the predictive strategy, an unnecessary cooling is provided over the entire day. Such additional cooling has been observed also for other days of this specific case study when input data are affected by uncertainties. Consequently, the overall yearly cooling is about 24% smaller when the adaptive algorithm replaces the model based control approach (see Table 8.2).

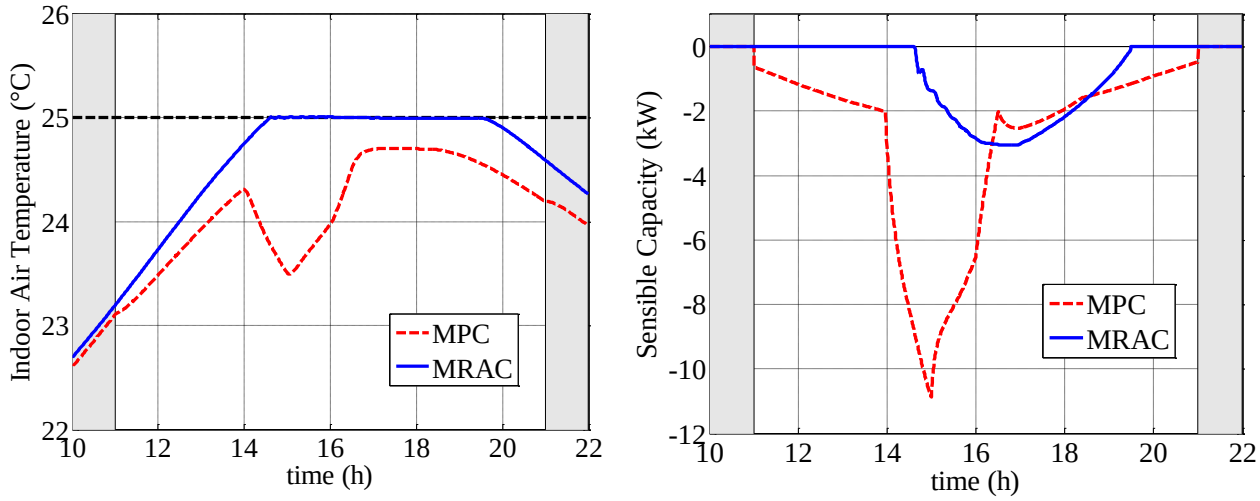

(a) **(b)**

Figure 8.13. Heavyweight Mall in Rome, 185th day of the year: (a) indoor air temperature, (b) sensible capacity (control action).Grey shaded areas denote the time range where controllers are deactivated according to Table 5.4.

It is interesting to note that for all case studies analysed form Figure 8.10 to Figure 8.13, the model reference adaptive controller in Chapter 4 has shown to provide satisfactory tracking performance also in the case of input uncertainties. This is mainly due to the ability of the control algorithm to adjust its gains also to unexpected variations of the weather data and internal loads. For the sake of completeness, Figure 8.14 shows the adaptive gains for the cases discussed above whose dynamics depend on the actual indoor air temperature evolution.

From the implementation viewpoint in the in-house code DETECt, we remark that the time required for simulating the building dynamics when the predictive algorithm is used in the control loop is larger than that obtained when the adaptive algorithm is exploited for their regulation. The increase of simulation time is up to ten times. This is mainly due to the need to solve online the optimization problem (8.8).

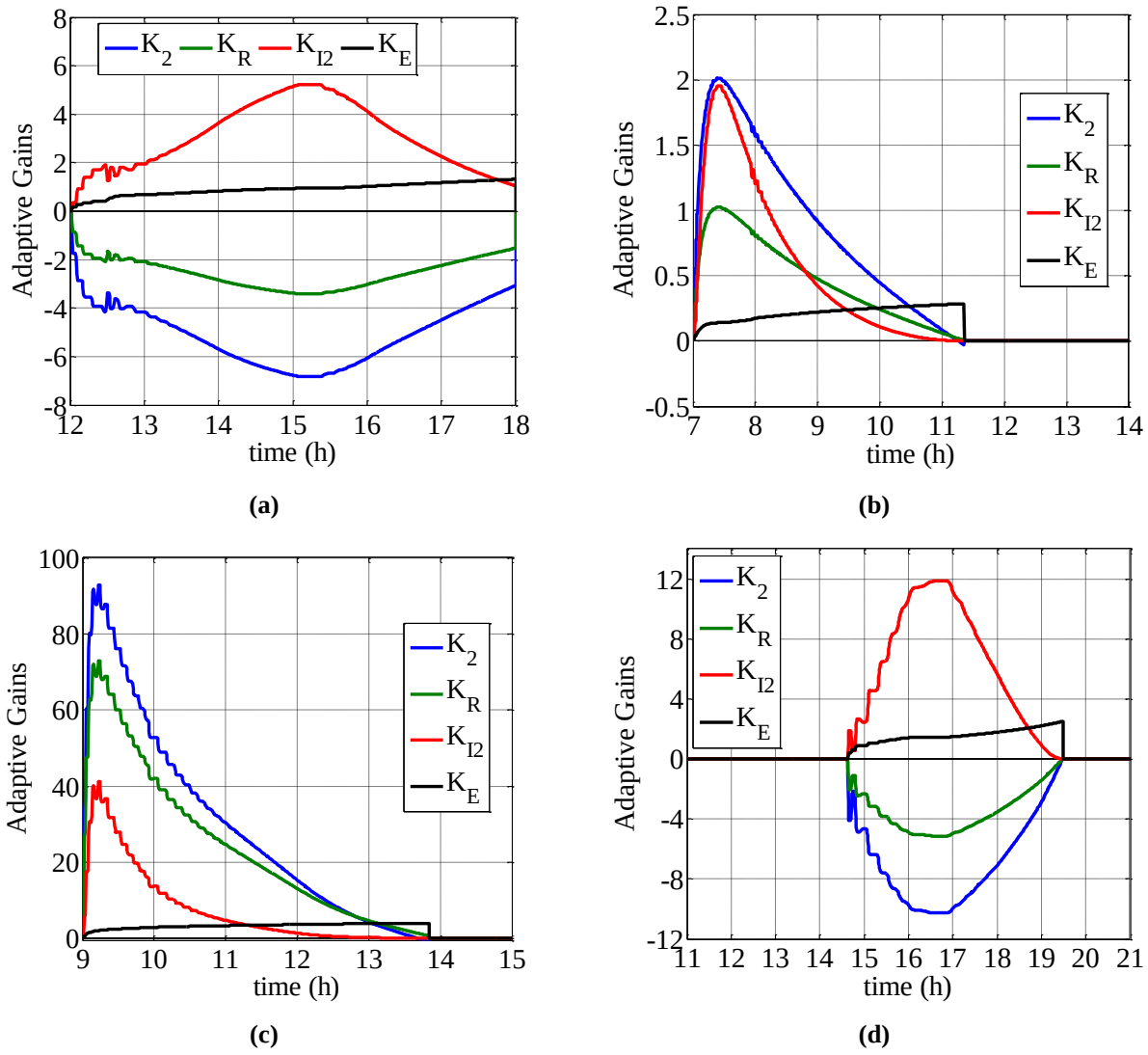

Figure 8.14. Evolution of the adaptive gains for some case studies (a) Heavyweight Office in Milan, 245th day of the year (b) Lightweight Mall in Athens, 80th day of the year (c) Lightweight House in Athens, 50th day of the year (d) Heavyweight Mall in Rome, 185th day of the year.

8.5 **Discussion**

The aim of this chapter was twofold. In the first part we have designed for the buildings in Chapter 5, in the case of intermittent running regime with scheduling policy in Table 5.4, model predictive control strategies. As this control method requires building models that are at the same

time predictive and simple to simplify the online solution of dynamic optimization problems, the low order building systems in Chapter 7 have been exploited during the control design. Several case studies have shown the effectiveness of the approach in the case of perfect knowledge of weather data and internal loads. In the second part of the chapter a comparison, in terms of heating/cooling demands, between the model based strategy and the model reference adaptive control solution in Chapter 4 has been carried out both in the case of perfect knowledge of the weather data and internal loads as well as when these measurements are affected by uncertainties. Numerical results have shown that in the former case the controllers have similar performance. This is mainly because both are effective solutions to impose the indoor air temperature in accordance with the scheduling in Table 5.4. Instead, in the latter working condition, the adaptive control approach has resulted to be more convenient than the model based solution under the energy saving viewpoint. The increase of energy consumption in the case of severe uncertain weather conditions and internal loads is mainly caused by the lack of robustness of classical model based control algorithms to face unexpected changes of the input data. On the other hand the adaptive control method provides always satisfactory tracking of the reference signals via adaptation of the control gains on the basis of the actual difference between the building dynamics and those of the reference model. We point out that an in-depth comparison between the predictive and adaptive solutions is out of the scope of the thesis as additional features should be taken into account for such a comparison which have been left out in this work. For example predictive solutions might be re-designed by using the formalisms of stochastic dynamical systems to manage better uncertain data. Consequently, the comparison here proposed has the only aim to further show the robustness of the model reference adaptive strategy in Chapter 4 when applied to buildings to impose precisely the required preassigned set points to the thermohygrometric variables of interest.

Chapter 9
CONCLUSION

In this thesis, a novel Enhanced Model Reference Adaptive Control (EMRAC) scheme is presented. The reference model is obtained by a Linear-Quadratic (LQ) optimization and it is developed for controlling nonlinear building dynamics by imposing to them optimal profiles of the thermohygrometric variables. The proposed LQ-EMRAC strategy enhances the classical MRAC adaptive algorithm with additional adaptive actions, necessary to increase its ability to deal with high variable external disturbances, parameter uncertainties and unmodelled dynamics. The goal of this control scheme is to strictly control the thermohygrometric behaviour of buildings in uncertain conditions (also for guaranteeing indoor comfort). This is obtained through the control ability to appropriately and automatically vary its control gains, without requiring a precise a priori knowledge of the building dynamics and/or its external disturbances. In fact, with respect to alternative adaptive approaches, the proposed control law relies on a minimal knowledge of the system dynamics and it can be easily implemented.

The LQ-EMRAC control scheme has been embedded in a new release of DETEC, a dynamic building energy performance simulation. In this new code release, an additional tool for the dynamic assessment of several comfort indexes (PMV, PPD, mean radiant temperature) has been also included. Through this tool, the LQ-EMRAC performance (in terms of control robustness against disturbances) was extensively analysed through the development of different case studies. In particular, they refer to: i) three different building uses (small house, office building and large commercial mall); ii) two diverse building envelopes (lightweight and heavyweight); iii) nine different weather zones (ranging from cold winter climates to temperate Mediterranean ones). Energy and comfort analyses were also carried out for continuous and intermittent control system operating strategies, as well as for different choices of the optimal reference profiles. Additional tests have been performed by taking into account the nonlinear thermal behaviour of roof and walls integrated with Phase Change Materials (PCM).

Simulation results show that the proposed control strategy is able to impose the required reference behaviours to both indoor air temperature and humidity, in any simulated conditions and for both the continuous and intermittent regimes. As a result, indoor air temperature and

humidity tracking mean squared errors, for each investigated case study, resulted to be always negligible. Due to such accurate thermohygrometric control, high occupants' comfort levels are also achieved, obtaining good PMVs (ranging from -0.5 to 0.75) and PPDs (less than 10% in winter and 20% in summer) for all the investigated case studies.

In addition, due to the LQ-EMRAC ability, simulation results also show: i) smooth transitions of both the indoor air temperature and humidity during transient operations; ii) bounded dynamic behaviours of the adaptive gains; iii) bounded sensible and latent heating and cooling control actions. These features have been also detected in the case of the control of multi-zone systems where a set to thermal zones are completely included in others and each of them has different thermohygrometric requirements. As during the design state the thermal coupling between zones were not considered, the robustness of the adaptive solution to unmodeled dynamics remain proven. Furthermore, due to the typical features of the LQ-EMRAC, its implementation in the real environment only requires measured data, being able to automatically deal with both the weather variability and the time-varying nonlinearities of the system (e.g. due to innovative energy saving solutions, PCM adoption in construction materials, etc.).

For the case studies presented in Chapter 5 when the intermittent operation policy in Table 5.4 is used, also predictive control strategies have been designed and their performance, in terms of tracking of the required set points and heating/cooling energy demand, have been compared to that given by the adaptive solution. Numerical results have shown that in the case of perfect knowledge of weather data and internal loads, these control solutions have similar performance, mainly because both strategies are able to impose the required steady-state regimes. Nevertheless in case of uncertain conditions, the adaptive controllers is still able to impose the set point temperatures and therefore also better energy performance are achieved. It is important to point out that such a comparison has been done only for the intermittent regimes in Table 5.4 where the required set points are known a priory. Consequently, an in-depth comparison between adaptive and model based solutions require additional investigations and it is still an open question.

As MPC strategies require very predictive models of the building temperature dynamics that are at the same time as simple as possible in order to facilitate the solution of the online optimization problems, in this thesis we have also proposed and implemented a systematic procedure for the generation of low order grey-box building models. Different from the approach presented in [158, 160] we have chosen as system outputs the temperatures of the surfaces of the building envelope so that also comfort can be well predicted. The effectiveness of the method

has been validated numerically by considering different case studies which are diverse with respect to the size, geometry and construction materials. The indoor air temperature, heating/cooling demands, as well as comfort indexes (i.e., man radiant temperature, PMV and PPD) predicted via the low order building models have been compared to those provided by the detailed model implemented in DETECt. The deviations between the outputs of the detailed and low order models have been quantitatively measured via a set of performance indexes which have been defined for this aim. Results confirm that for many reduced order systems such indexes take small values and therefore they can be used successfully for the design of advanced model based building controller. It is remarkable that these models can be exploited also for aims different from control design. Indeed by using reduced order models it is possible to *i)* reduce drastically the computation time to get an insight into building energy performance, especially when a large set of simulations are required to assess them [29] *ii)* derive mathematical models of building dynamics via reverse engineering methods when experimental data are available [30] and *iii)* simulate large groups of buildings organized in districts with the aim to evaluate energy performance [31]. Hence, the design of methods for the building model reduction represent an additional result.

Finally, the main contributions and conclusions of the thesis are:

- the design of a novel model reference adaptive control scheme, named LQ-EMRAC, for the control of thermohygrometric variables in buildings;
- prove analytically the effectiveness of the novel control strategy to impose in closed-loop the profiles generated via the model reference system;
- the LQ-EMRAC scheme allows to obtain very accurate regulation and fast tracking of the thermohygrometric profiles in case of stringent indoor air requirements, which are often mandatory in case of hospital units, museum display cases, laboratory chambers, etc.;
- improved reliability and usefulness of the adopted building simulation tool is obtained by embedding the LQ-EMRAC control scheme. Due to its ability to deal with a wide range of disturbances, multiple building simulations can be carried out without the need of tuning the control system for each building model. This feature is particularly useful in case of sensitivity analyses and optimization procedures, which require multiple parameters to vary during the whole optimization process;
- the design of a systematic procedure for the generation of low order building models starting from a detailed but complex one. These models can be used for a variety of

aims especially for the design of advanced model based control strategies. The performance indexes proposed in the thesis have proven their effectiveness to predict fundamental quantities, i.e., indoor air temperature, heating and cooling demands, as well as comfort indexes;

- a preliminary comparison, on very specific case studies, between the performance provided by the adaptive control solution and those given by model based controllers have been also carried out, showing that in the case of uncertain weather data adaptive controllers perform better.

Possible future research might include:

- the extension of the proposed control approach to building including renewable energy sources. Specifically, a possible investigation to solar collectors might be considered in order to propose an alternative solution to those recently presented in [172];
- an additional future research line can be the control of a group of buildings organized in thermal district. In this case the idea is to coordinate a group of buildings which share a set of energy sources so that the energy required from the resulting network is smaller than the sum of energy required by each building when they are considered as individual systems. To achieve this aim more advanced design methods, e.g., complex networks [173], can be exploited.

Appendix A
ADAPTIVE CONTROL: A BRIEF OVERVIEW

According to many dictionaries, to adapt means to change (oneself) so that one's behavior will conform to new or changed circumstances. Hence, intuitively an adaptive controller can modify its behavior in response to changes in the dynamics of the process and in presence of the disturbances. Consequently, it is not a case that in the last fifty years adaptive control theory has been proved to be one of the most promising techniques to control complex plants whose dynamics are affected by disturbances and unknown parameters [137]. In this thesis, according to [137] we refer to an adaptive controller as a controller with adjustable parameters and a mechanism for adjusting them. In so doing an adaptive scheme is characterized via two loops. One loop is a normal feedback with the process and the controller, and the other one is the parameter adjustment loop.

The aim of this appendix is to provide to the reader some basic concepts and definitions about adaptive control as the control solution proposed for buildings in Chapter 4 belongs to a subclass of this set of controllers.

A.1 Basic concepts about adaptive control

According to the definition in [137], reported above, a generic adaptive controller can be represented as shown in Figure A. 1. The way of changing the controller gains in response to changes in the plant behavior and disturbances distinguishes one scheme from another. The method used to modify the control parameters is often referred to as *adaptive law*, *update law* or *adjustment mechanism*.

A first way to classify adaptive strategies is to look how the adaptive law is combined with the control law. On the basis of the coupling between the inner loop and the outer loop in Figure A. 1, we distinguish *indirect adaptive control* (see Figure A. 2a) and *direct adaptive control* (see Figure A. 2b).

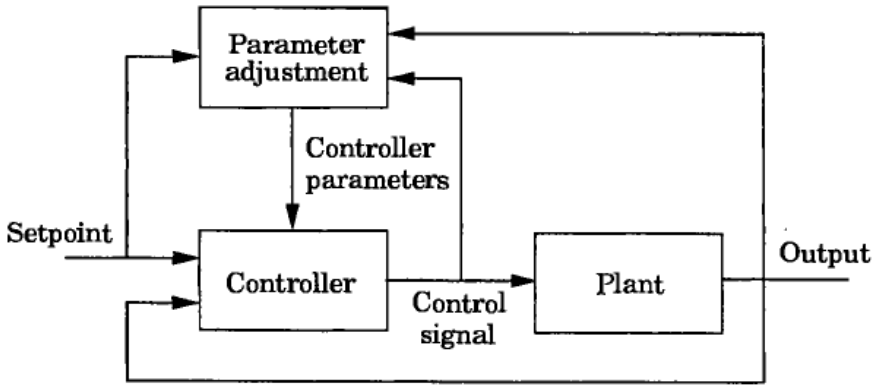

Figure A. 1. Generic adaptive control scheme (taken from [137])

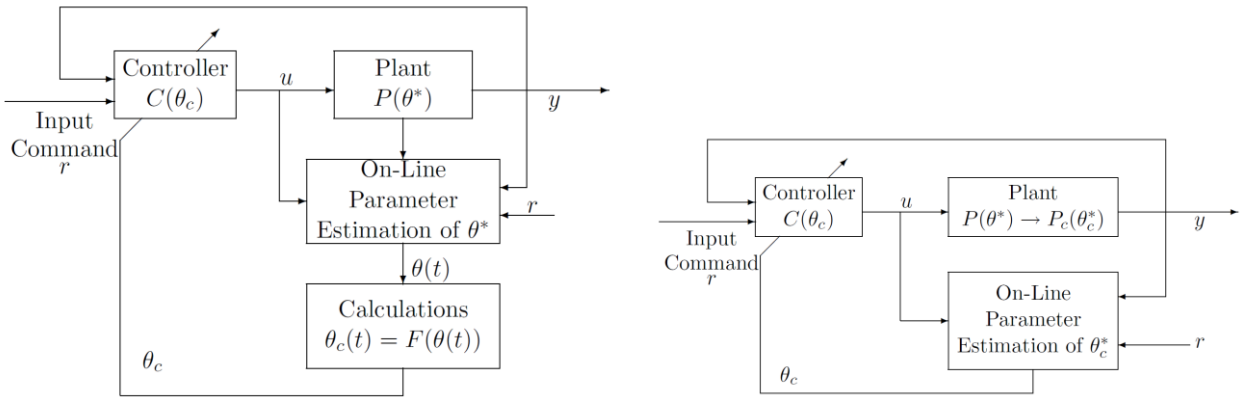

(a) **(b)**

Figure A. 2. (a) Indirect adaptive control scheme (b) Direct adaptive control scheme (taken from [140])

For the former class, plant parameters θ^*, supposed to be unknown, are estimated on line and the time varying control parameters, say $\theta_c(t)$, are computed by solving an algebraic equation of the form $\theta_c(t)=F(\theta(t))$ with $\theta(t)$ being the estimate of θ^* at the time t. Since the update law is based explicitly on the plant parameters, this kind of the adaptive approach is also known as *explicit adaptive control*.

In the case of direct adaptive strategies, the control parameters are directly updated without any online estimations of the plant paramters. Often the adaptive law is given as a set of integral-differential equations that are based on some measurable variables of the plant. When it is possible to re-parameterize the model of the plant in terms of the control parameters, i.e., when it is possible to construct what is known as *implicit model of the plant*, then it is possible to convert an indirect control scheme in a direct one. For this reason direct adaptive controllers are also known as *implicit adaptive controllers*.

In all the previous control schemes the adaptive mechanism makes the closed loop dynamics nonlinear and time varying. The theory adopted to design the control action and to show the

effectiveness of the closed loop to track the input signal can be exploited for a further classification of the adaptive strategies. Mainly sensitivity approach, passivity theory and Lyapunov techniques have been widely used over the years. The pros and cons of each approach are briefly discussed below.

Sensitivity. This method, introduced in the 1960s, was among the first approaches to design controllers able to adapt their parameters. At each time the derivative of the control parameter vector, i.e., $d\theta_c/dt$, is in the direction that minimizes a given performance function. This derivative is called *sensitivity function*, and its on line computation is the main drawback of this methodology. In fact, despite of the simplicity of the method, the sensitivity function almost always depends on the plant parameters, that are supposed to be unknown. When approximations of the sensitivity function are adopted, like the well-known M.I.T. rule, it is difficult to prove rigorously closed-loop stability or bounded tracking error [137].

Lyapunov Techniques. The problem of designing the adaptive law is formulated as a stability problem of a nonlinear dynamical system. In closed loop the dimension of the state space is augmented by the control parameters. The adaptive law is chosen so that the derivative of a candidate Lyapunov function is negative definite along the closed loop trajectories. In so doing, classical Lyapunov direct methods ensure stability and bounded adaptive gains [139]. The main challenge here is to find a Lyapunov function as their construction is systematically possible only for some classes of dynamical systems.

Passivity. In this case, the inner and the outer loop of the control system in Figure A. 1 are often reshaped as a suitable feedback system such that only the feedback dynamics depend on the adaptive gains. Using this decomposition the feedforward system and the feedback system are independently designed and made passive [139]. Passivity theory ensures that the dynamics produced by the interaction between the feedforward and the feedback paths are still passive, hence boundedness of all the signals inside the loop remains proven. The fundamental advantage of this approach is that it is possible to prove stability in closed loop without taking into account the mutual interaction between parts of the control system.

A.2 Classification of adaptive control schemes

As we mentioned before, an adaptive controller may be considered as the result of a coupling between a control law with an adjustment mechanism. The way these ingredients are mixed generates different adaptive controllers with different properties. Nevertheless, many adaptive schemes in the literature belongs to one of the following generic set: *gain scheduling*, *model-*

reference adaptive control, *self tuning regulators*, and *dual control* [137] which are shown in Figure A. 3. In want follows we will give a brief description of each of them not only for the sake of completeness, but also to better frame the control strategy proposed in Chapter 4 for the control of buildings.

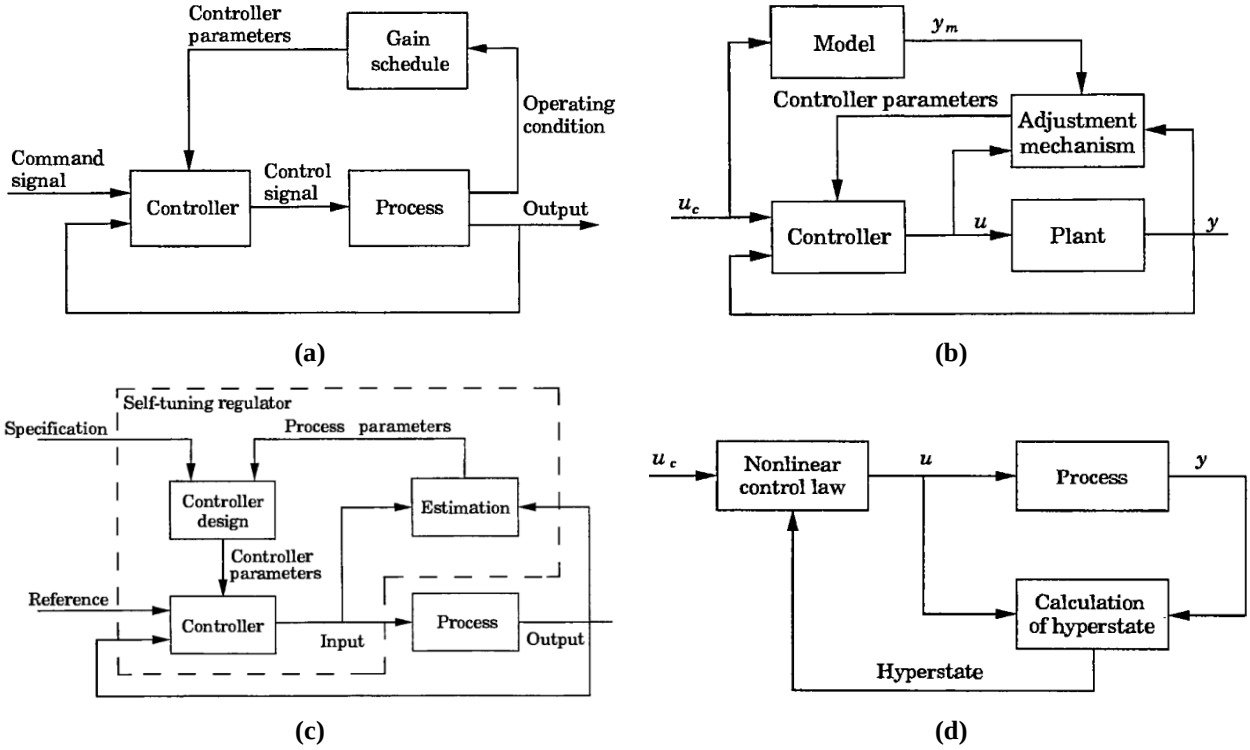

Figure A. 3. Possible of adaptive control schemes: (a) gain scheduling (b) model-reference adaptive control (c) self-tuning regulator (d) dual control (taken from [137]).

A.2.1 Gain Scheduling

One of the earliest and most intuitive approach to adaptive control is gain scheduling (see Figure A. 3a). It was introduced in the 1950 and 1960 to control aircraft with high performance. It can be used for those cases where there exists a set of measurable variables, named also *auxiliary measurements*, whose determine the set of the operating conditions of the plant. For each operating regime the mathematical model of the plant is assumed to be well-known. Hence, it is possible to tune off-line the control parameter vector according to a preassigned control objective. The key idea behind gain scheduling algorithms is to select on-line the control parameters in agreement with the actual operating condition. Often the set of control parameter vectors are stored in a look-up table and they are selected, or scheduled, as function of the current operating regime.

Remarks

1. Gain scheduling is particularly convenient when the plant dynamics depend in a well-known fashion on a small set of variables which can be easily measured and define the operating regime and the mathematical plant description.
2. One of the main advantage of this approach is that the control parameters can change as quickly as the auxiliary measurements, providing therefore a fast adaptation of the overall control system to a different working condition. On the other hand these switches make the overall control scheme a switching one, hence asymptotic stability could depend on the switching frequency [105].
3. Even if this control approach does not need complex online computations, for each operating condition is required to design a control parameter vector, then the design effort could be time consuming especially when the amount of operating regimes is not small.
4. Since the controller is scheduled only on the basis of the actual auxiliary measurements. If there is a discrepancy between the actual plant dynamics and the model used to design the controller, then in some working condition the control objective could not to be achieved. The incapability to accommodate the controller to uncertain plants is due to the off-line design of the control parameters. The absence of a real learning capability is the main drawback of the gain scheduling approach, and historically, it has been a matter of a controversy whether this control scheme should be considered an adaptive system or not.

A.2.2 Model-reference adaptive control

This adaptive control strategy can be adopted when the control specifications are given in terms of a reference model. Hence, the reference model dynamics represent how the process output should respond to the command signal. Intuitively, the aim in the case of Model Reference Adaptive Control (MRAC) is to find an adaptive feedback control law that changes the dynamics of the plant so that its input-output dynamics are exactly those of the reference model.

In the MRAC literature mainly two schemes have been proposed, i.e., *series high-gain* and *paralle*l schemes. Nevertheless the most common are parallel schemes as that shown in Figure A. 3b. Also in this case, the inner loop is an ordinary feedback loop composed by the process and the controller. The outer loop adjusts the controller parameters so that the difference between process output y and the reference model output y_m converge to zero. Even if the formulation of the model reference adaptive control is easy and appealing, finding adaptation laws to solve the

MRAC problem is not trivial. A quite standard procedure to design an MRAC scheme can be found in [24] and it is based on hyperstability theory developed by Popov [144] which can be set in the more general context of passivity theory [174]. Indeed, the methodology proposed by Landau in [24] to prove stability can be thought as a procedure that makes the closed loop dynamics passive. Briefly, the proposed design approach is based on recasting the closed-loop system, which includes also the adaptive gains, as a feedback system. Then passivity of both blocks are studied and imposed separately. Passivity theorem is finally used to assure dissipativity of the overall system and consequently the convergence of the plant dynamics to those of the reference model.

The main advantage of this approach is the possibility to study performance of adaptive systems by studying the main blocks composing the control scheme (after its recast) without considering interaction between these blocks as far as they can be made passive.

A.2.3 Self-Tuning Regulators

The design of a Self Tuning Regulator (STR) scheme needs a fixed structure of the inner controller and relations whose map the plant parameters onto the parameters of the controller. Since the plant parameters are unknown recursive estimators, as those proposed in [163], can be exploited to identify plant parameters. When computing the control gains, the estimates of the plant parameters are assume to be the real parameters values, this approach is known in the literature as *certainty equivalence principle*.

A typical STR scheme is shown in see Figure A. 3c. Again, the adaptive controller can be thought composed by two loops. The inner loop consists of the process and an ordinary feedback controller. The parameters of the controller are adjusted in accordance with the output of the recursive estimator. The block labeled *Controller design* maps the plant parameter estimates onto the control parameters so that tracking of the reference signal is assured.

According to the previous description STR strategies are indirect adaptive strategies. Nevertheless for some schemes belonging to this family it is possible to re-parameterize the process so that the model can be expressed in terms of the controller parameters. This simplifies the control scheme because the block *Control Design* in Figure A. 3c disappears and the parameters of the inner controller are updated directly. In that cases the STR algorithm reduces to an explicit adaptive strategy.

Remarks.

1. The main advantages of STR control strategies are: *(i)* just the structure of the mathematical model of the plant has to be known, but not its parameters; *(ii)* the flexibility with respect to the control design methodology (linear quadratic, PID, minimum variance just to name few) and to the identification algorithm (recursive least square, maximum likelihood, extended Kalman filtering and so on).
2. To perform its task, often parameter estimators need the use of probing control signals or perturbations. In fact, in order to ensure the convergence to plant parameters the input to the parameter estimator has to satisfy a set of conditions. This set of conditions are referred to as *persistent excitation (PE)*. Obviously, the persistent excitation property strongly depends on the estimator strategy, i.e., each estimator algorithm is characterized by a set of conditions to be satisfied in order to guarantee convergence to zero of the estimation error. Since the input to the parameters estimator is generated by the inner loop, often it is not possible to guarantee a priori persistent excitation. Hence, extra (probing) signals have to be added.
3. The main drawback of the STR strategy is that the stability analysis of the overall control scheme turns to be complicated because in general it is not possible to separate the inner loop dynamics form the outer loop dynamics.

A.2.4 Dual Control

Dual control schemes were the results of an attempt to formulate adaptive control as a solution of an optimization problem. According to this approach, the system and its environment are described by stochastic models. In particular, the plant parameters are modeled as a set of differential equations with zero right-hand side and an initial distribution that reflects the parameters uncertainty. The control objective is to minimize the expected value of a loss function, which is a scalar function of the augmented state (state variables and plant parameters) and the control action [116].

The solution of the problem can be obtained in principle by using stochastic dynamic programming. The resulting feedback controller, reported in Figure A. 3d, is one whose parameters are changed online (adaptive controller) by means of a nonlinear function that maps the hyperstate into the space control variables. Notice that the *hyperstate* is defined as the conditional probability distribution of the augmented state with respect to the measurements (output and input of the plant).

The main drawback of the dual control, that makes it unfeasible for practical problems, is that the hyperstate has to be computed online. In principle, the hyperstate belongs to an infinite dimensional vector space and it is the solution a complex nonlinear filtering problem which is difficult and time consuming to solve.

A.3 Discussion

In this Appendix basic concepts and definitions about adaptive control has been reviewed for the sake of completeness. Even though adaptive schemes can deal with plant parameters uncertainties each of them has pros and cons. Precisely, even though the gain scheduling schemes are easy to be implemented and allow a fast reconfiguration of the controller, they need the existence of a set of scheduling variables that can characterize the system response precisely. Self tuning schemes based on parameter estimators require instead some persistent excitation conditions to ensure closed loop stability, while dual control strategies are difficult to actuate, except for some specific systems. Consequently, in this thesis MRAC algorithms have been designed to solve the control problem in buildings. Indeed these strategies allow a systematic design of the control action to guarantee convergence to zero of the difference of the system dynamics and that of the reference model.

Appendix B
MODEL REDUCTION: ADDITIONAL RESULTS

In this appendix we give additional details about the results of the model reduction approach proposed in Chapter 7. In particular in the first part we report for the sake of completeness the mathematical expressions of the probability density functions used throughout that chapter. In particular for each of them we point out its parameter vector, say ζ, which is reported in some tables of Chapter 7. Instead, in the second part of the appendix additional details about the performance indexes introduced in Section 7.2.1 and computed separately for each model, for each building shape, size and type, i.e., for all cases introduced in Chapter 5, are presented in summarizing tables.

B.1 Probability density functions

Normal Distribution

$$f(x) = \frac{1}{\sigma\sqrt{2\pi}} e^{\frac{1}{2}\left(\frac{x-\mu}{\sigma}\right)^2} \qquad \zeta = [\mu \quad \sigma]$$

where μ is the mean value of the distribution and σ is the variance.

Rayleigh Distribution

$$f(x) = \frac{x}{b^2} e^{\frac{-x^2}{2b^2}} \qquad \zeta = [b]$$

where b is the scale parameter of the distribution.

t-Location Scale Distribution

$$f(x) = \frac{\Gamma\left(\frac{\nu+1}{2}\right)}{\sigma\sqrt{\nu\pi}\Gamma\left(\frac{\nu}{2}\right)} \left[\frac{\nu + \left(\frac{x-\mu}{\sigma}\right)^2}{\nu} \right]^{-\left(\frac{\nu+1}{2}\right)} \qquad \zeta = [\mu \quad \sigma \quad \nu]$$

where μ is the Location, σ is the Scale parameter and ν is the degrees of freedom parameter

Generalized Extreme Value Distribution

$$f(x) = \frac{1}{\sigma} e^{-\left(1+k\frac{(x-\mu)}{\sigma}\right)^{-\frac{1}{k}}} \left(\left(1 + k\frac{(x-\mu)}{\sigma}\right)^{-1-\frac{1}{k}} \right) \qquad \zeta = \begin{bmatrix} k & \sigma & \mu \end{bmatrix}$$

where k is the shape parameter, σ is the Scale parameter and μ is the location parameter.

Inverse Gaussian

$$f(x) = \sqrt{\frac{\lambda}{2\pi x^3}} e^{-\frac{\lambda}{2x\mu^2}(x-\mu)^2} \qquad \zeta = \begin{bmatrix} \mu & \lambda \end{bmatrix}$$

where μ is the scale parameter and λ is the shape parameter.

Generalized Pareto

$$f(x) = \left(\frac{1}{\sigma}\right)\left(1 + k\frac{(x-\theta)}{\sigma}\right)^{-1-\frac{1}{k}} \qquad \zeta = \begin{bmatrix} k & \sigma & \theta \end{bmatrix}$$

shape parameter $k \neq 0$, scale parameter σ, and threshold parameter θ.

Weibull

$$f(x) = \left(\frac{b}{a}\right)\left(\frac{x}{a}\right)^{b-1} e^{-(x/a)^b} \qquad \zeta = \begin{bmatrix} a & b \end{bmatrix}$$

shape parameter b and scale parameter a.

Rician

$$f(x) = I_0\left(\frac{xs}{\sigma^2}\right)\frac{x}{\sigma^2} e^{-\left(\frac{x^2+s^2}{2\sigma^2}\right)} \qquad \zeta = \begin{bmatrix} s & \sigma \end{bmatrix}$$

with non centrality parameter $s \geq 0$ and scale parameter $\sigma > 0$, for $x > 0$. I_0 is the zero-order modified Bessel function of the first kind.

Extreme Value

$$f(x) = \sigma^{-1} \exp\left(\frac{x-\mu}{\sigma}\right) \exp\left(-\exp\left(\frac{x-\mu}{\sigma}\right)\right) \qquad \zeta = \begin{bmatrix} \mu & \sigma \end{bmatrix}$$

location parameter μ and scale parameter σ.

Birnbaum Saunders

$$f(x) = \frac{1}{\sqrt{2\pi}} \exp\left\{ -\frac{\left(\sqrt{x/\beta} - \sqrt{\beta/x}\right)^2}{2\gamma^2} \right\} \left(\frac{\left(\sqrt{x/\beta} + \sqrt{\beta/x}\right)}{2\gamma x} \right) \qquad \zeta = [\beta \quad \gamma]$$

with scale parameter β > 0 and shape parameter γ > 0, for x > 0.

Beta

$$f(x) = \frac{1}{B(a,b)} x^{a-1}(1-x)^{b-1} I_{(0,1)}(x) \qquad \zeta = [a \quad b]$$

where B(·) is the Beta function. The indicator function I(0,1)(x) ensures that only values of x in the range (0 1) have nonzero probability.

Gamma

$$f(x) = \frac{1}{b^a \Gamma(a)} x^{a-1}(1-x)^{b-1} e^{-\frac{x}{b}} \qquad \zeta = [a \quad b]$$

where Γ(·) is the Gamma function.

Logistic

$$f(x) = \frac{\exp\left\{ \frac{x-\mu}{\sigma} \right\}}{\sigma\left(1 + \exp\left\{ \frac{x-\mu}{\sigma} \right\} \right)^2} \qquad \zeta = [\mu \quad \sigma]$$

where μ is the mean and σ is the scale parameter.

Log-Logistic

$$f(x) = \frac{1}{\sigma} \frac{1}{x} \frac{e^z}{\left(1 + e^z\right)^2} \quad \text{where} \quad z = \frac{\log(x) - \mu}{\sigma} \qquad \zeta = [\mu \quad \sigma]$$

where μ is the Log-mean and σ is the Log-scale parameter.

Lognormal

$$f(x) = \left[x\sigma\sqrt{2\pi} \exp\left(\frac{-(\ln x - \mu)^2}{2\sigma^2} \right) \right]^{-1} \qquad \zeta = [\mu \quad \sigma]$$

where μ is the Log mean and σ is the Log standard deviation.

B.2 Additional results

B.2.1 Maximum weekly Variation of Indoor temperature in free evolution

Distribution of the Maximum Variation of indoor temperature in free evolution during winter weeks for W2 model						
	Mean	**Variance**	**PDF**	**Parameters**		
Light Bestest	8.01	1.05	Extreme Value	8.47	0.80	
HeavyBestest	9.59	4.33	Generalized Extreme Value	-0.63	2.27	9.23
Light Office	4.32	0.74	Log-Logistic	1.44	0.11	
Heavy Office	5.83	1.69	Log-Logistic	1.74	0.12	
Light Mall	3.18	1.89	InverseGaussian	3.18	16.99	
Heavy Mall	4.35	3.95	BirnbaumSaunders	3.95	0.45	
Distribution of the Maximum Variation of indoor temperature in free evolution during summer weeks for W22 model						
	Mean	**Variance**	**PDF**	**Parameters**		
Light Bestest	11.74	1.58	Normal	11.74	1.08	
HeavyBestest	11.58	2.05	Weibull	12.19	9.71	
Light Office	6.50	0.33	Logistic	6.50	0.32	
Heavy Office	6.22	0.73	Rician	6.16	0.86	
Light Mall	2.30	0.15	Generalized Extreme Value	0.12	0.25	2.12
Heavy Mall	2.02	0.25	Log-logistic	0.67	0.13	

Table B.1. Distribution of Temperature variation in free evolution for W2 Model

Distribution of the Maximum Variation of indoor temperature in free evolution during winter weeks for W15 model						
	Mean	**Variance**	**PDF**	**Parameters**		
Light Bestest	1.01	0.02	Generalized Extreme Value	-0.80	0.14	1.00
HeavyBestest	0.97	0.10	Generalized Extreme Value	-0.35	0.34	0.92
Light Office	0.73	0.01	Extreme Value	0.77	0.06	
Heavy Office	0.67	0.02	Rician	0.66	0.13	
Light Mall	0.40	0.01	Generalized Extreme Value	0.04	0.08	0.34
Heavy Mall	0.45	0.03	Log-Logistic	-0.85	0.19	
Distribution of the Maximum Variation of indoor temperature in free evolution during summer weeks for W15 model						
	Mean	**Variance**	**PDF**	**Parameters**		
Light Bestest	1.41	0.005	Gamma	440.66	0.003	
HeavyBestest	0.89	0.01	Log-Logistic	-0.12	0.06	
Light Office	0.83	0.01	Generalized Extreme Value	0.05	0.06	0.79
Heavy Office	0.49	0.03	Generalized Pareto	-0.45	0.37	0.23
Light Mall	0.38	0.01	Weibull	0.42	5.09	
Heavy Mall	0.26	0.01	Gamma	9.83	0.03	

Table B.2. Distribution of Temperature variation in free evolution for W15 Model

Distribution of the Maximum Variation of indoor temperature in free evolution during summer weeks for W22 model						
	Mean	**Variance**	**PDF**	**Parameters**		
Light Bestest	0.63	0.0002	t Location-scale	0.64	0.02	0.96
HeavyBestest	0.49	0.03	Generalized Pareto	-0.91	0.52	0.22
Light Office	0.43	0.01	t Location-scale	0.47	0.02	0.97
Heavy Office	0.23	0.01	Generalized Pareto	-0.82	0.30	0.07
Light Mall	0.10	0.12	Logistic	0.09	0.003	
Heavy Mall	0.10	0.0005	InverseGaussian	0.10	1.68	
Distribution of the Maximum Variation of indoor temperature in free evolution during summer weeks for W22 model						
	Mean	**Variance**	**PDF**	**Parameters**		
Light Bestest	0.61	0.001	Generalized Extreme Value	0.38	0.01	0.60
HeavyBestest	0.58	0.005	Generalized Extreme Value	0.28	0.03	0.55
Light Office	0.35	0.01	Generalized Pareto	-1.17	0.39	0.17
Heavy Office	0.31	0.05	Generalized Pareto	-0.78	0.21	0.20
Light Mall	0.09	0.0001	Generalized Pareto	-2.14	0.22	0.02
Heavy Mall	0.12	0.0001	Extreme Value	0.13	0.02	

Table B.3. Distribution of Temperature variation in free evolution for W22 Model

Distribution of the Maximum Variation of indoor temperature in free evolution during winter weeks for G8 model						
	Mean	**Variance**	**PDF**	**Parameters**		
Light Bestest	0.23	0.004	BirnbaumSaunders	0.22	0.27	
HeavyBestest	0.92	0.05	Gamma	17.48	0.05	
Light Office	0.20	0.002	Log-Logistic	-1.60	0.11	
Heavy Office	0.72	0.02	Generalized Extreme Value	0.02	0.12	0.65
Light Mall	0.18	0.003	Generalized Extreme Value	0.11	0.03	0.15
Heavy Mall	0.52	0.03	Generalized Extreme Value	0.12	0.12	0.44
Distribution of the Maximum Variation of indoor temperature in free evolution during summer weeks for G8 model						
	Mean	**Variance**	**PDF**	**Parameters**		
Light Bestest	0.39	0.01	Weibull	0.43	5.80	
HeavyBestest	0.66	0.01	Log-Logistic	-0.43	0.09	
Light Office	0.25	0.003	Weibull	0.28	4.99	
Heavy Office	0.54	0.02	Generalized Extreme Value	0.18	0.09	0.47
Light Mall	0.14	0.45	t Location-Scale	0.14	0.01	1.82
Heavy Mall	0.37	0.02	Generalized Extreme Value	0.15	0.08	0.31

Table B.4. Distribution of Temperature variation in free evolution for G8 Model

Distribution of the Maximum Variation of indoor temperature in free evolution during winter weeks for Gm model						
	Mean	**Variance**	**PDF**	**Parameters**		
Light Bestest	0.25	0.01	Gamma	10.70	0.02	
HeavyBestest	0.66	0.02	Nakagami	5.00	0.46	
Light Office	0.20	0.03	Nakagami	3.64	0.04	
Heavy Office	0.52	0.01	Log-Logistic	-0.66	0.10	
Light Mall	0.17	0.03	Generalized Extreme Value	0.11	0.04	0.15
Heavy Mall	0.39	0.02	BirnbaumSaunders	0.36	0.37	
Distribution of the Maximum Variation of indoor temperature in free evolution during summer weeks for Gm model						
	Mean	**Variance**	**PDF**	**Parameters**		
Light Bestest	0.33	0.01	Weibull	0.36	5.24	
HeavyBestest	0.39	0.01	Generalized Extreme Value	0.15	0.05	0.35
Light Office	0.20	0.003	Weibull	0.22	4.23	
Heavy Office	0.33	0.01	Generalized Extreme Value	0.14	0.06	0.28
Light Mall	0.10	0.0001	Logistic	0.10	0.01	
Heavy Mall	0.20	0.01	InverseGaussian	0.20	1.44	

Table B.5. Distribution of Temperature variation in free evolution for GM Model

Distribution of the Maximum Variation of indoor temperature in free evolution during winter weeks for G15 model						
	Mean	**Variance**	**PDF**	**Parameters**		
Light Bestest	0.15	0.001	Normal	0.15	0.03	
HeavyBestest	0.05	0.0001	Logistic	0.05	0.01	
Light Office	0.30	0.06	t Location-Scale	0.30	0.05	2.09
Heavy Office	0.03	0.0001	InverseGaussian	0.03	0.26	
Light Mall	0.08	0.001	InverseGaussian	0.08	0.68	
Heavy Mall	0.07	0.0004	InverseGaussian	0.07	0.71	
Distribution of the Maximum Variation of indoor temperature in free evolution during summer weeks for G15 model						
	Mean	**Variance**	**PDF**	**Parameters**		
Light Bestest	0.17	0.0005	Normal	0.17	0.02	
HeavyBestest	0.05	0.00003	Generalized Extreme Value	-0.04	0.005	0.05
Light Office	0.20	0.01	Generalized Extreme Value	0.02	0.03	0.18
Heavy Office	0.04	0.00002	Log-Logistic	-3.20	0.06	
Light Mall	0.06	0.0001	Generalized Extreme Value	0.003	0.01	0.05
Heavy Mall	0.05	0.0001	Generalized Pareto	-0.38	0.02	0.03

Table B.6. Distribution of Temperature variation in free evolution for G15 Model

Distribution of the Maximum Variation of indoor temperature in free evolution during winter weeks for GT15 model						
	Mean	**Variance**	**PDF**	**Parameters**		
Light Bestest	0.12	0.0005	Normal	0.12	0.02	
HeavyBestest	0.04	0.0001	Weibull	0.04	3.74	
Light Office	0.25	0.04	t Location-Scale	0.25	0.04	2.10
Heavy Office	0.03	0.00001	InverseGaussian	0.03	0.22	
Light Mall	0.07	0.001	InverseGaussian	0.07	0.58	
Heavy Mall	0.06	0.0003	InverseGaussian	0.06	0.60	
Distribution of the Maximum Variation of indoor temperature in free evolution during summer weeks for GT15 model						
	Mean	**Variance**	**PDF**	**Parameters**		
Light Bestest	0.14	0.0004	Normal	0.14	0.02	
HeavyBestest	0.04	0.00002	Generalized Extreme Value	-0.04	0.004	0.04
Light Office	0.17	0.001	Generalized Extreme Value	0.02	0.02	0.15
Heavy Office	0.03	0.00002	Log-Logistic	-3.37	0.06	
Light Mall	0.05	0.0001	Generalized Extreme Value	0.003	0.01	0.04
Heavy Mall	0.04	0.0001	Generalized Pareto	-0.38	0.02	0.03

Table B.7. Distribution of Temperature variation in free evolution for GT15 Model

B.2.2 Heating/Cooling mismatches

Distribution of Weekly Energy and Peak variation during winter and summer weeks for the W2 Model						
	Mean	**Variance**	**PDF**	**Parameters**		
Light Bestest						
ΔE_c	5.13	23.68	Nakagami	0,33	50,06	
ΔP_c	11.10	34.93	Generalized Pareto	-1,23	24,57	0,10
ΔE_h	25.93	197.51	Generalized Pareto	-0,63	34,32	4,84
ΔP_h	39.52	2.31	Log-Logistic	3,68	0,02	
HeavyBestest						
ΔE_c	5.99	14.54	Nakagami	0,69	50,37	
ΔP_c	7.36	54.20	Exponential	7.36		
ΔE_h	33.05	137.65	Generalized Pareto	-0,55	26,28	16,07
ΔP_h	24.75	24.92	Log-Logistic	3,20	0,05	
Light Office						
ΔE_c	22.79	142.26	Generalized Pareto	0,11	9,52	12,11
ΔP_c	15.04	88.44	Generalized Pareto	-0,77	26,64	0,03
ΔE_h	16.83	106.67	Generalized Pareto	-0,51	22,11	2,17
ΔP_h	29.80	1.26	t Location-Scale	29,80	0,62	2,89
Heavy Office						
ΔE_c	32.85	$5\ 10^3$	Log-Logistic	3,11	0,46	
ΔP_c	38.89	165.64	Log Logistic	3,61	0,17	
ΔE_h	28.36	89.23	Generalized Pareto	-0,64	23,39	14,10
ΔP_h	11.77	3.08	Log-Logistic	2,45	0,08	
Light Mall						
ΔE_c	43.86	10^3	Gen Ex Value	0,34	12,25	30,36
ΔP_c	11.79	38.58	t Location-Scale	11,79	2,24	1,44
ΔE_h	8.89	37.24	Generalized Pareto	-0,38	11,19	0,79
ΔP_h	20.77	3.27	Generalized Extreme Value	-0,02	1,45	19,97
Heavy Mall						
ΔE_c	76.20	10^4	Generalized Pareto	0,28	49,43	7,39
ΔP_c	15.96	457.53	Log-Logistic	2,25	0,53	
ΔE_h	17.67	20.02	Generalized Pareto	-0,43	8,68	11,59
ΔP_h	3.41	4.97	Generalized Pareto	-0,67	5,69	0,004

Table B.8. Distribution of Energy Variation for W2 Model

Distribution of Weekly Energy and Peak variation during winter and summer weeks for the W15 Model						
	Mean	**Variance**	**PDF**	**Parameters**		
Light Bestest						
ΔE_c	3.51	1.84	Generalized Pareto	-0.51	2.92	1.59
ΔP_c	6.85	1.44	Generalized Pareto	-0.51	2.57	5.14
ΔE_h	8.76	4.19	Birnbaum Saunders	8.53	0.23	
ΔP_h	3.36	1.31	Nakagami	2.27	12.62	
Heavy Bestest						
ΔE_c	8.32	3.96	Inverse Gaussian	8.32	145.73	
ΔP_c	8.10	1.91	Nakagami	8.70	67.70	
ΔE_h	9.03	8.11	Generalized Pareto	-0.44	5.62	5.13
ΔP_h	1.47	0.98	Generalized Pareto	-0.59	2.32	0.01
Light Office						
ΔE_c	6.22	11.02	Generalized Pareto	-0.07	3.81	2.67
ΔP_c	8.81	4.66	Weibull	9.64	4.65	
ΔE_h	5.41	0.72	Inverse Gaussian	5.41	220.33	
ΔP_h	1.28	0.12	Log-Logistic	0.21	0.15	
Heavy Office						
ΔE_c	9.30	12.87	Inverse Gaussian	9.30	62.64	
ΔP_c	7.61	7.68	Log-Logistic	1.97	0.19	
ΔE_h	4.90	1.99	Generalized Pareto	-0.53	3.10	2.87
ΔP_h	4.13	0.37	Generalized Pareto	-0.72	1.63	3.19
Light Mall						
ΔE_c	5.46	17.00	Log Logistic	1.52	0.32	
ΔP_c	2.58	4.71	Generalized Extreme Value	0.59	0.64	1.29
ΔE_h	2.92	0.39	Generalized Pareto	-0.55	1.42	2.00
ΔP_h	1.33	0.07	Rician	1.31	0.26	
Heavy Mall						
ΔE_c	10.68	67.95	Generalized Pareto	-0.06	9.34	1.92
ΔP_c	5.80	14.21	Birnbaum Saunders	4.83	0.64	
ΔE_h	2.16	0.24	Generalized Pareto	-0.57	1.12	1.45
ΔP_h	4.25	0.06	Generalized Extreme Value	-0.12	0.21	4.15

Table B.9. Distribution of Energy Variation for W15 Model

Distribution of ΔE and ΔP during winter and summer weeks for the W22 Model						
	Mean	**Variance**	**PDF**	**Parameters**		
Light Bestest						
ΔE_c	3.40	0.65	Generalized Pareto	-0.70	2.13	2.16
ΔP_c	1.39	0.21	Generalized Pareto	-0.46	0.92	0.76
ΔE_h	6.71	5.00	Birnbaum Saunders	6.37	0.33	
ΔP_h	5.64	1.93	Gamma	16.54	0.34	
HeavyBestest						
ΔE_c	5.52	2.19	Inverse Gaussian	5.52	76.83	
ΔP_c	3.32	0.85	Generalized Pareto	-0.79	2.88	1.72
ΔE_h	8.74	10.87	Generalized Pareto	-0.39	6.15	4.32
ΔP_h	6.31	1.58	Inverse Gaussian	6.31	158.87	
Light Office						
ΔE_c	4.10	6.04	Generalized Extreme Value	0.36	0.80	3.21
ΔP_c	1.86	0.61	Gamma	5.68	0.33	
ΔE_h	2.78	0.65	Logistic	2.78	0.44	
ΔP_h	1.17	0.01	Generalized Extreme Value	-0.02	0.09	1.12
Heavy Office						
ΔE_c	6.67	17.10	Generalized Extreme Value	0.28	1.83	4.93
ΔP_c	4.07	3.31	Log Logistic	1.32	0.22	
ΔE_h	4.02	2.07	Generalized Pareto	-0.43	2.81	2.06
ΔP_h	1.53	0.04	Log Logistic	0.42	0.07	
Light Mall						
ΔE_c	2.56	1.52	Log-Logistic	0.85	0.23	
ΔP_c	1.01	0.13	Log-Logistic	-0.04	0.18	
ΔE_h	0.94	0.08	Generalized Pareto	-0.61	0.70	0.50
ΔP_h	0.87	0.01	Weibull	0.91	11.61	
Heavy Mall						
ΔE_c	6.18	15.67	Birnbaum Saunders	5.16	0.63	
ΔP_c	2.90	3.07	Log-Logistic	0.94	0.28	
ΔE_h	1.18	0.10	Generalized Pareto	-0.58	0.72	0.73
ΔP_h	0.95	0.02	Logistic	0.95	0.07	

Table B.10. Distribution of Energy Variation for W22 Model

Distribution of ΔE and ΔP during winter and summer weeks for the G8 Model						
	Mean	**Variance**	**PDF**	**Parameters**		
Light Bestest						
ΔE_c	1.95	0.03	Generalized Extreme Value	-0.008	0.14	1.88
ΔP_c	5.83	0.02	Inverse Gaussian	5.83	1.2 10^4	
ΔE_h	1.09	0.54	Gamma	2.23	0.49	
ΔP_h	5.37	0.02	Log-logistic	1.68	0,015	
HeavyBestest						
ΔE_c	5.54	1,45	Log-logistic	1,69	0.12	
ΔP_c	7.80	1.36	Log-logistic	2.04	0.08	
ΔE_h	1.93	3.81	Nakagami	0.29	7.54	
ΔP_h	11.04	3.93	Inverse Gaussian	11.04	342,53	
Light Office						
ΔE_c	1.76	0.33	Generalized extreme value	0.30	0.23	1.52
ΔP_c	5.31	1.96	Generalized Pareto	-2.40	11.52	1.93
ΔE_h	0.61	0.63	Log-logistic	-0.78	0.41	
ΔP_h	5.03	0.02	Log Logistic	1.61	0.014	
Heavy Office						
ΔE_c	5.94	19.85	Generalized extreme value	0.34	1.53	4.27
ΔP_c	7.1	7.24	Log-logistic	1.90	0.19	
ΔE_h	0.95	0.90	Exponential	0.95		
ΔP_h	10.41	1.93	Birnbaum Saunders	10.33	0.13	
Light Mall						
ΔE_c	0.43	0.19	Log-logistic	-1.32	0.51	
ΔP_c	1.59	3.24	Extreme Value	0.39	0.50	0.99
ΔE_h	0.29	0.0044	Generalized extreme value	0.13	0.04	0.26
ΔP_h	3.22	0.09	Weibull	3.35	12.85	
Heavy Mall						
ΔE_c	10.67	149.74	Inverse Gaussian	10.67	8.12	
ΔP_c	8.30	43.99	Log-logistic	1.93	0.33	
ΔE_h	0.66	0.20	Nakagami	0.63	0.64	
ΔP_h	8.14	0.39	Rician	8.12	0.63	

Table B.11. Distribution of Energy Variation for G8 Model

Distribution of ΔE and ΔP during winter and summer weeks for the Gm Model						
	Mean	**Variance**	**PDF**	**Parameters**		
Light Bestest						
ΔE_c	1.78	0.02	Generalized Pareto	-0.28	0.24	1.60
ΔP_c	5.50	0.01	Log-logistic	1.70	0.01	
ΔE_h	1.30	0.89	Generalized Pareto	-0.22	1.39	0.17
ΔP_h	5.32	0.05	Generalized Extreme Value	0.30	0.88	5.23
HeavyBestest						
ΔE_c	3.80	0.45	Log-logistic	1.32	0.09	
ΔP_c	5.77	0.40	Logistic	5.77	0.35	
ΔE_h	1.08	1.16	Exponential	1.08		
ΔP_h	7.62	0.95	Generalized Extreme Value	-0.02	0.78	7.18
Light Office						
ΔE_c	1.53	0.15	Generalized Pareto	0.03	0.36	1.16
ΔP_c	4.74	1.72	Generalized Pareto	-2.26	10.08	1.65
ΔE_h	0.70	0.35	Birnbaum Saunders	0.53	0.82	
ΔP_h	4.99	0.01	Generalized Extreme Value	-0.04	0.08	4.94
Heavy Office						
ΔE_c	4.01	7.78	Generalized Extreme Value	0.33	1.01	2.94
ΔP_c	4.21	5.41	t Location-Scale	4.21	0.64	1.44
ΔE_h	0.67	0.33	Generalized Extreme Value	0.19	0.32	0.41
ΔP_h	8.03	0.56	Inverse Gaussian	8.03	921.68	
Light Mall						
ΔE_c	0.62	0.50	Generalized Extreme Value	0.39	0.20	0.38
ΔP_c	1.26	1.67	Log-Logistic	-0.01	0.37	
ΔE_h	0.27	0.01	Generalized Extreme Value	0.32	0.03	0.24
ΔP_h	3.42	0.06	Generalized Extreme Value	-0.44	3.25	3.36
Heavy Mall						
ΔE_c	4.60	39.90	Inverse Gaussian	4.60	2.45	
ΔP_c	3.73	24.16	Log-Logistic	1.02	0.41	
ΔE_h	0.57	0.04	Rician	0.52	0.22	
ΔP_h	6.65	0.10	Rician	6.64	0.32	

Table B.12. Distribution of Energy Variation for GM Model

Distribution of ΔE and ΔP during winter and summer weeks for the G15 Model						
	Mean	**Variance**	**PDF**	**Parameters**		
Light Bestest						
ΔE_c	0.33	0.02	Generalized Pareto	-1.41	0.71	0.03
ΔP_c	0.75	0.03	Generalized Pareto	-1.26	0.79	0.40
ΔE_h	0.72	0.02	Generalized Pareto	-0.51	0.33	0.51
ΔP_h	1.30	0.01	Extreme Value	1.37	0.10	
HeavyBestest						
ΔE_c	0.06	0.001	Rayleigh	0.05		
ΔP_c	0.27	0.02	Logistic	0.27	0.03	
ΔE_h	0.10	0.01	Beta	0.59	4.95	
ΔP_h	0.11	0.005	Nakagami	0.71	0.02	
Light Office						
ΔE_c	1.88	0.85	Generalized Pareto	-0.03	0.98	0.93
ΔP_c	1.92	5.25	t Location-Scale	5.87	0.32	0.99
ΔE_h	0.47	0.14	Weibull	0.51	1.28	
ΔP_h	5.25	0.05	Generalized Extreme Value	0.13	0.14	5.24
Heavy Office						
ΔE_c	0.29	0.01	Log-logistic	-1.28	0.18	
ΔP_c	0.29	0.02	Rayleigh	0.23		
ΔE_h	0.07	0.004	Exponential	0.066		
ΔP_h	0.11	0.003	Rayleigh	0.08		
Light Mall						
ΔE_c	0.53	0.39	Log-Logistic	-1.19	0.55	
ΔP_c	0.31	0.09	Generalized Extreme Value	0.29	0..13	0.18
ΔE_h	0.49	0.004	Generalized Pareto	-0.39	0.12	0.4
ΔP_h	0.83	0.008	Logistic	0.83	0.05	
Heavy Mall						
ΔE_c	1.06	1.62	Generalized Pareto	0.25	0.67	0.17
ΔP_c	0.78	0.44	Log-Logistic	-0.44	0.34	
ΔE_h	0.14	0.003	Birnbaum Saunders	0.13	0.40	
ΔP_h	1.54	0.02	Weibull	1.60	14.45	

Table B.13. Distribution of Energy Variation for G15 Model

Distribution of Weekly Energy and Peak variation during winter and summer weeks for the GT15 Model						
	Mean	**Variance**	**PDF**	**Parameters**		
Light Bestest						
ΔE_c	0.26	0.01	Generalized Pareto	-1.46	0.57	0.03
ΔP_c	0.61	0.02	Generalized Pareto	-1.14	0.60	0.34
ΔE_h	0.56	0.01	Generalized Pareto	-0.50	0.25	0.39
ΔP_h	1.07	0.01	Extreme Value	1.13	0.09	
HeavyBestest						
ΔE_c	0.05	0.002	Rayleigh	0.04		
ΔP_c	0.22	0.002	Extreme Value	0.24	0.03	
ΔE_h	0.08	0.01	Beta	0.60	6.63	
ΔP_h	0.09	0.003	Nakagami	0.66	0.01	
Light Office						
ΔE_c	1.46	0.51	Generalized Pareto	-0.03	0.76	0.72
ΔP_c	4.85	1.34	t Location-Scale	4.85	0.28	1.01
ΔE_h	0.36	0.08	Weibull	0.39	1.28	
ΔP_h	4.44	0.04	Generalized Extreme Value	0.01	0.15	4.35
Heavy Office						
ΔE_c	0.23	0.007	Log Logistic	-1.53	0.18	
ΔP_c	0.24	0.02	Rayleigh	0.19		
ΔE_h	0.25	0.003	Exponential	0.05		
ΔP_h	0.09	0.002	Rayleigh	0.07		
Light Mall						
ΔE_c	0.41	0.23	Log Logistic	-1.44	0.55	
ΔP_c	0.25	0.05	Generalized Extreme Value	0.26	0.11	0.15
ΔE_h	0.38	0.002	Generalized Pareto	-0.40	0.09	0.31
ΔP_h	0.65	0.01	Beta	21.98	11.92	
Heavy Mall						
ΔE_c	0.82	0.97	Generalized Pareto	0.25	0.52	0.13
ΔP_c	0.66	0..31	Log-Logistic	-0.61	0.34	
ΔE_h	0.11	0.002	Birnbaum Saunders	0.10	0.40	
ΔP_h	1.24	0.01	Logistic	1.24	0.06	

Table B.14. Distribution of Energy Variation for GT15 Model

B.2.3 Comfort Analysis

Distribution of Comfort Indexes Variation for W2 Model						
Comfort Analysis in Light Bestest for Winter Weeks						
Index	**Mean**	**Variance**	**PDF**	**Parameters**		
ΔPMV	0,83	0,02	Log-Logistic	-0,20	0,08	0
ΔPPD	40,30	32,71	Logistic	40,17	3,11	0
ΔTr	5,50	3,49	Inverse Gaussian	5,50	48,00	0
Comfort Analysis in Light Bestest for Summer Weeks						
ΔPMV	3,01	0,12	Normal	3,01	0,34	0
ΔPPD	83,91	41,16	Generalized Extreme Value	-0,58	6,99	82,61
ΔTr	4,29	1,59	Weibull	4,75	3,90	0
Comfort Analysis in HeavyBestest for Winter Weeks						
ΔPMV	0,94	0,03	Logistic	0,94	0,09	0
ΔPPD	39,86	75,87	t Location-Scale	39,64	4,84	2,17
ΔTr	5,51	3,52	Generalized Extreme Value	0,15	1,25	4,58
Comfort Analysis in HeavyBestest for Summer Weeks						
ΔPMV	2,42	0,16	Normal	2,42	0,40	0
ΔPPD	76,23	79,20	Extreme Value	80,35	7,20	0
ΔTr	2,82	0,40	Generalized Extreme Value	0,069	0,45	2,53
Comfort Analysis in Light Office for Winter Weeks						
ΔPMV	0,56	0,03	Generalized Extreme Value	0,19	0,11	0,47
ΔPPD	24,99	114,14	Generalized Extreme Value	0,34	5,76	19,23
ΔTr	5,10	3,17	Gamma	8,06	0,63	0
Comfort Analysis in Light Office for Summer Weeks						
ΔPMV	1,50	0,02	Logistic	1,50	0,09	0
ΔPPD	63,63	44,49	Extreme Value	66,65	5,14	0
ΔTr	2,18	0,79	Generalized Pareto	-0,43	1,92	0,80
Comfort Analysis in Heavy Office for Winter Weeks						
ΔPMV	0,69	0,07	Generalized Extreme Value	0,25	0,16	0,55
ΔPPD	29,76	215,19	Inverse Gaussian'	29,76	113,79	0
ΔTr	5,49	3,18	Inverse Gaussian'	5,49	54,00	0
Comfort Analysis in Heavy Office for Summer Weeks						
ΔPMV	1,12	0,06	Nakagami	5,39	1,32	0
ΔPPD	46,49	215,91	Generalized Pareto	-1,22	65,49	15,38
ΔTr	2,87	0,52	Inverse Gaussian	2,87	48,74	0
Comfort Analysis in Light Mall for Winter Weeks						
ΔPMV	0,49	0,04	Inverse Gaussian	0,49	2,65	0
ΔPPD	22,16	127,21	Generalized Pareto	-0,46	24,12	5,38
ΔTr	4,06	2,35	Nakagami	1,88	18,85	0
Comfort Analysis in Light Mall for Summer Weeks						
ΔPMV	0,57	0,06	Log-Logistic	-0,61	0,12	0
ΔPPD	23,94	54,99	Birnbaum-Saunders	22,84	0,31	0
ΔTr	1,14	0,63	Generalized Extreme Value	0,27	0,35	0,81
Comfort Analysis in Heavy Mall for Winter Weeks						
ΔPMV	0,60	0,07	Gamma	5,04	0,12	0
ΔPPD	26,25	220,32	Generalized Pareto	-0,80	43,51	2,60
ΔTr	4,71	1,94	Gamma	11,69	0,40	0
Comfort Analysis in Heavy Mall for Summer Weeks						
ΔPMV	0,44	0,02	Generalized Extreme Value	0,14	0,08	0,38
ΔPPD	14,38	49,90	Gamma	3,98	3,61	0
ΔTr	2,59	0,50	Lognormal	0,92	0,26	0

Table B.15. Distribution of Comfort Indexes variation for W2 Model

Distribution of Comfort Indexes Variation for W15 Model						
Comfort Analysis in Light Bestest for Winter Weeks						
Index	**Mean**	**Variance**	**PDF**	**Parameters**		
ΔPMV	0,20	0,001	t Location-Scale	0,21	0,005	0,91
ΔPPD	9,70	3,80	Generalized Extreme Value	-1,02	1,69	9,75
ΔTr	0,79	0,02	Generalized Extreme Value	-0,87	0,13	0,79
Comfort Analysis in Light Bestest for Summer Weeks						
ΔPMV	0,57	0,002	Nakagami	42,24	0,32	0
ΔPPD	21,50	7,02	Generalized Extreme Value	-0,006	2,14	20,25
ΔTr	1,38	0,013	Weibull	1,43	14,22	0
Comfort Analysis in HeavyBestest for Winter Weeks						
ΔPMV	0,17	0,003	Generalized Pareto	-1,44	0,28	0,06
ΔPPD	6,81	14,85	Generalized Pareto	-0,97	11,86	1,16
ΔTr	0,60	0,03	Beta	5.00	3,38	0
Comfort Analysis in HeavyBestest for Summer Weeks						
ΔPMV	0,32	0,001	Beta	53,32	113,53	0
ΔPPD	13,46	5,06	Log-Logistic	2,59	0,09	0
ΔTr	0,65	0,007	Beta	21,88	11,64	0
Comfort Analysis in Light Office for Winter Weeks						
ΔPMV	0,15	0,0004	Generalized Extreme Value	-0,67	0,02	0,14
ΔPPD	7,59	2,07	Generalized Extreme Value	-0,82	1,50268	7,46
ΔTr	0,64	0,008	t Location-Scale	0,62	0,03	1,27
Comfort Analysis in Light Office for Summer Weeks						
ΔPMV	0,32	0,0007	Normal	0,32	0,03	0
ΔPPD	15,00	5,51	Generalized Extreme Value	-0,54	2,56	14,48
ΔTr	0,75	0,007	Birnbaum-Saunders	0,75	0,11	0
Comfort Analysis in Heavy Office for Winter Weeks						
ΔPMV	0,13	0,0003	Weibull	0,13	8,15	0,13
ΔPPD	5,15	2,41	Weibull	5,71	3,80	5,15
ΔTr	0,49	0,02	Log-Logistic	-0,75	0,13	0,49
Comfort Analysis in Heavy Office for Summer Weeks						
ΔPMV	0,18	0,003	Generalized Pareto	-0,44	0,11	0,10
ΔPPD	7,64	7,24	Inverse Gaussian	7,64	62,61	0
ΔTr	0,35	0,01	Generalized Pareto	-0,51	0,22	0,20
Comfort Analysis in Light Mall for Winter Weeks						
ΔPMV	0,09	0,00046	Inverse Gaussian	0,09	1,96	0
ΔPPD	4,39	0,73	Weibull'	4,74	5,85	0
ΔTr	0,49	0,03	Inverse Gaussian	0,49	4,00	0
Comfort Analysis in Light Mall for Summer Weeks						
ΔPMV	0,19	0,001	Extreme Value	0,20	0,03	0
ΔPPD	7,02	5,50	Generalized Pareto	-0,74	5,98	3,67
ΔTr	0,34	0,002	Lognormal'	-1,09	0,14	0
Comfort Analysis in Heavy Mall for Winter Weeks						
ΔPMV	0,09	0,001	Log-Logistic	-2,41	0,17	0
ΔPPD	4,20	3,72	Weibull	4,75	2,34	0
ΔTr	0,42	0,04	Birnbaum-Saunders	0,38	0,45	0
Comfort Analysis in Heavy Mall for Summer Weeks						
ΔPMV	0,11	0,001	Generalized Pareto	-0,22	0,04	0,08
ΔPPD	4,80	2,47	Log-Logistic	1,53	0,18	0
ΔTr	0,20	0,002	Inverse Gaussian	0,20	3,76	0

Table B.16. Distribution of Comfort Indexes variation for W15 Model

istribution of Comfort Indexes Variation for W22 Model						
Comfort Analysis in Light Bestest for Winter Weeks						
Index	**Mean**	**Variance**	**PDF**	**Parameters**		
ΔPMV	0,13	10^{-6}	Inverse Gaussian'	0,13	629,77	0
ΔPPD	6,49	0,15	Extreme Value'	6,66	0,28	0
ΔTr	0,50	0,0002	t Location-Scale'	0,50	0,007	1,73
Comfort Analysis in Light Bestest for Summer Weeks						
ΔPMV	0,23	0,0001	Generalized Extreme Value'	-0,046	0,009	0,23
ΔPPD	11,84	0,14	t Location-Scale'	11,79	0,20	2,11
ΔTr	0,64	0,005	Beta'	29,14	16,49	0
Comfort Analysis in HeavyBestest for Winter Weeks						
ΔPMV	0,10	0,001	Generalized Pareto	-0,95	0,09	0,06
ΔPPD	4,04	4,68	Generalized Pareto	-0,93	6,25	1,16
ΔTr	0,33	0,01	Generalized Pareto	-0,89	0,36	0,14
Comfort Analysis in HeavyBestest for Summer Weeks						
ΔPMV	0,23	10^{-4}	t Location-Scale	0,23	0,004	1,95
ΔPPD	11,92	0,51	Extreme Value	12,18	0,42	0
ΔTr	0,45	0,004	Generalized Pareto	-0,72	0,18	0,34
Comfort Analysis in Light Office for Winter Weeks						
ΔPMV	0,10	0,0004	Generalized Extreme Value	-1,04	0,02	0,11
ΔPPD	4,32	1,21	Generalized Pareto	-0,99	4,16	2,11
ΔTr	0,38	0,005	t Location-Scale	0,37	0,02	1,19
Comfort Analysis in Light Office for Summer Weeks						
ΔPMV	0,14	0,002	Generalized Pareto	-1,10	0,15	0,08
ΔPPD	6,33	4,29	Generalized Extreme Value	0,20	1,32	5,27
ΔTr	0,29	0,005	Generalized Pareto	-0,92	0,23	0,17
Comfort Analysis in Heavy Office for Winter Weeks						
ΔPMV	0,06	10^{-4}	Inverse Gaussian	0,06	1,01	0
ΔPPD	1,87	1,14	Generalized Extreme Value	0,54	0,38	1,31
ΔTr	0,22	0,004	Inverse Gaussian	0,22	2,85	0
Comfort Analysis in Heavy Office for Summer Weeks						
ΔPMV	0,12	0,002	Generalized Pareto	-1,03	0,12	0,07
ΔPPD	5,34	4,74	Generalized Pareto	-0,66	5,30	2,24
ΔTr	0,23	0,002	Generalized Extreme Value	-0,53	0,05	0,22
Comfort Analysis in Light Mall for Winter Weeks						
ΔPMV	0,06	0,006	Logistic	0,05	0,002	0
ΔPPD	2,58	12,03	t Location-Scale	2,17	0,07	0,70
ΔTr	0,34	0,14	Log-Logistic	-1,19	0,20	0
Comfort Analysis in Light Mall for Summer Weeks						
ΔPMV	0,07	10^{-6}	Weibull	0,078	46,17	0
ΔPPD	3,79	0,06	Extreme Value	3,90	0,18	0
ΔTr	0,12	0,001	Generalized Extreme Value	0,18	0,02	0,10
Comfort Analysis in Heavy Mall for Winter Weeks						
ΔPMV	0,04	4,06	Inverse Gaussian	0,04	1,55	0
ΔPPD	1,25	0,08	Log-Logistic	0,21	0,12	0
ΔTr	0,17	0,005	Birnbaum-Saunders	0,16	0,39	0
Comfort Analysis in Heavy Mall for Summer Weeks						
ΔPMV	0,07	10^{-5}	Extreme Value	0,08	0,0036	0
ΔPPD	3,37	0,40	Extreme Value	3,64	0,44	0
ΔTr	0,13	0,0002	Logistic	0,13	0,008	0

Table B.17. Distribution of Comfort Indexes variation for W22 Model

Distribution of Comfort Indexes Variation for G8 Model						
Light Bestest during Winter Weeks						
Index	**Mean**	**Variance**	**PDF**	**Parameters**		
ΔPMV	0,072	10^{-4}	Inverse Gaussian	0,07	3,16	0
ΔPPD	3,36	0,35	Lognormal	1,20	0,17	0
ΔTr	0,38	0,011	Generalized Extreme Value	0,05	0,08	0,33
Light Bestest during Summer Weeks						
ΔPMV	0,20	0,0008	Log-Logistic	-1,64	0,08	0
ΔPPD	9,16	5,37	Weibull	10,06	4,53	0
ΔTr	0,54	0,008	Weibull	0,58	7,26	0
HeavyBestest during Winter Weeks						
ΔPMV	0,17	0,002	Generalized Pareto	-0,50	0,10	0,10
ΔPPD	7,04	6	Gamma	8,09	0,87	0
ΔTr	0,73	0,03	Genalized Extreme Value	0,04	0,13	0,65
HeavyBestest during Summer Weeks						
ΔPMV	0,26	0,002	Generalized Extreme Value	0,08	0,03	0,24
ΔPPD	10,68	6,38	Inverse Gaussian	10,68	203,40	0
ΔTr	0,62	0,01	Log-Logistic	-0,49	0,09	0
Light Office during Winter Weeks						
ΔPMV	0,08	0,0001	Generalized Extreme Value	-0,34	0,01	0,07
ΔPPD	3,45	0,41	Gamma	29,34	0,12	0
ΔTr	0,44	0,01	Generalized Extreme Value	0,08	0,087	0,39
Light Office during Summer Weeks						
ΔPMV	0,16	0,0004	t Location-Scale	0,17	0,004	1,11
ΔPPD	6,15	2,16	Gamma	17,62	0,35	0
ΔTr	0,45	0,006	Extreme Value	0,48	0,06	0
Heavy Office during Winter Weeks						
ΔPMV	0,14	0,0006	Generalized Extreme Value	0,04	0,02	0,12
ΔPPD	5,51	3,15	Birnbaum-Saunders	5,23	0,32	0
ΔTr	0,64	0,03	Generalized Extreme Value	0,12	0,11	0,56
Heavy Office during Summer Weeks						
ΔPMV	0,22	0,001	t Location-Scale	0,21	0,02	2,04
ΔPPD	9,13	6,03	Nakagami	3,54	89,29	0
ΔTr	0,49	0,01	Generalized Extreme Value	0,18	0,07	0,43
Light Mall during Winter Weeks						
ΔPMV	0,07	0,006	t Location-Scale	0,07	0,009	3,09
ΔPPD	2,98	10,83	Generalized Extreme Value	0,20	0,49	2,44
ΔTr	0,45	0,13	Generalized Extreme Value	0,27	0,07	0,37
Light Mall during Summer Weeks						
ΔPMV	0,17	0,06	t Location-Scale	0,15	0,007	1,61
ΔPPD	7,09	4,79	t Location-Scale	7,10	0,82	3,51
ΔTr	0,47	0,34	t Location-Scale	0,41	0,03	2,22
Heavy Mall during Winter Weeks						
ΔPMV	0,11	0,001	t Location-Scale	0,11	0,01	2,24
ΔPPD	4,59	3,31	'Nakagami'	1,68	24,35	0
ΔTr	0,52	0,04	Generalized Extreme Value	0,20	0,12	0,42
Heavy Mall during Summer Weeks						
ΔPMV	0,17	0,001	Inverse Gaussian	0,17	3,45	0
ΔPPD	7,24	5,47	Nakagami	2,51	57,80	0
ΔTr	0,40	0,01	Generalized Extreme Value	0,18	0,07	0,34

Table B.18. Distribution of Comfort Indexes variation for G8 Model

Distribution of Comfort Indexes Variation for Gm Model						
Comfort Analysis in Light Bestest for Winter Weeks						
Index	**Mean**	**Variance**	**PDF**	**Parameters**		
ΔPMV	0,07	9,77	Log-Logistic	-2,75	0,07	0
ΔPPD	3,10	0,30	Log-Logistic	1,12	0,09	0
ΔTr	0,34	0,01	Inverse Gaussian	0,34	3,05	0
Comfort Analysis in Light Bestest for Summer Weeks						
ΔPMV	0,17	0,0004	t Location-Scale	0,18	0,007	1,40
ΔPPD	7,98	2,69	Generalized Extreme Value	-0,62	1,81	7,68
ΔTr	0,47	0,009	Weibull	0,51	5,87	0
Comfort Analysis in HeavyBestest for Winter Weeks						
ΔPMV	0,13	0,0005	Weibull	0,135	6,56	0
ΔPPD	5,10	2,36	Weibull	5,66	3,72	0
ΔTr	0,41	0,007	Log-Logistic	-0,906	0,109	0
Comfort Analysis in HeavyBestest for Summer Weeks						
ΔPMV	0,17	0,0005	Inverse Gaussian	0,175	10,71	0
ΔPPD	7,76	1,946	Rician	7,639	1,40	0
ΔTr	0,33	0,002	Lognormal	-1,107	0,148	0
Comfort Analysis in Light Office for Winter Weeks						
ΔPMV	0,067	10^{-4}	Log-Logistic	-2,70	0,074	0
ΔPPD	3,133	0,269	Gamma	36,53	0,085	0
ΔTr	0,417	0,016	Inverse Gaussian	0,417	4,821	0
Comfort Analysis in Light Office for Summer Weeks						
ΔPMV	0,15	0,0006	Generalized Extreme Value	-0,750	0,025	0,14
ΔPPD	5,54	2,73	Generalized Pareto	-0,610	3,94	3,12
ΔTr	0,37	0,004	Weibull	0,400	6,45	0
Comfort Analysis in Heavy Office for Winter Weeks						
ΔPMV	0,10	0,0002	Log-Logistic	-2,27	0,084	0
ΔPPD	4,33	1,871	Generalized Pareto	-0,92	4,82	1,72
ΔTr	0,41	0,013	Generalized Extreme Value	0,127	0,076	0,357
Comfort Analysis in Heavy Office for Summer Weeks						
ΔPMV	0,14	0,0006	Generalized Extreme Value	0,039	0,019	0,13
ΔPPD	6,38	2,46	Gamma	16,65	0,38	0
ΔTr	0,29	0,003	Inverse Gaussian	0,298	8,10	0
Comfort Analysis in Light Mall for Winter Weeks						
ΔPMV	0,06	e-04	Logistic'	0,064	0,0050	0
ΔPPD	2,60	0,319	Generalized Extreme Value'	0,115	0,402	2,321
ΔTr	0,41	0,012	Generalized Extreme Value'	0,194	0,069	0,355
Comfort Analysis in Light Mall for Summer Weeks						
ΔPMV	0,12	0,038	Logistic'	0,11	0,0018	0
ΔPPD	5,46	5,118	Log-Logistic'	1,66	0,113	0
ΔTr	0,37	0,226	t Location-Scale'	0,338	0,038	2,927
Comfort Analysis in Heavy Mall for Winter Weeks						
ΔPMV	0,08	0,0004	Inverse Gaussian'	0,08	1,12	0
ΔPPD	3,63	2,919	Generalized Pareto'	-1,09	6,41	0,61
ΔTr	0,36	0,0166	Generalized Extreme Value'	0,263	0,0771	0,294
Comfort Analysis in Heavy Mall for Summer Weeks						
ΔPMV	0,11	0,0005	Generalized Extreme Value'	0,257	0,013	0,098
ΔPPD	4,76	1,94	Logistic'	4,70	0,744	0
ΔTr	0,31	0,003	Lognormal'	-1,172	0,179	0

Table B.19. Distribution of Comfort Indexes variation for GM Model

Distribution of Comfort Indexes Variation for G15 Model						
Comfort Analysis in Light Bestest for Winter Weeks						
Index	**Mean**	**Variance**	**PDF**	**Parameters**		
ΔPMV	0,05	10^{-5}	Log-Logistic	-2,97	0,05	0
ΔPPD	2,46	0,12	Generalized Extreme Value	-0,50	0,38	2,37
ΔTr	0,11	10^{-3}	Generalized Extreme Value	0,10	0,02	0,10
Comfort Analysis in Light Bestest for Summer Weeks						
ΔPMV	0,09	10^{-5}	Generalized Extreme Value	0,02	0,004	0,09
ΔPPD	4,29	0,10	Generalized Extreme Value	-0,51	0,34	4,21
ΔTr	0,14	0,0003	Rician'	0,13	0,02	0
Comfort Analysis in HeavyBestest for Winter Weeks						
ΔPMV	0,04	10^{-6}	Log-Logistic	-3,18	0,01	0
ΔPPD	1,77	0,14	Generalized Extreme Value	-0,68	0,43	1,72
ΔTr	0,11	0,0006	Weibull	0,12	5,43	0
Comfort Analysis in HeavyBestest for Summer Weeks						
ΔPMV	0,07	10^{-6}	Weibull	0,072	111,21	0
ΔPPD	3,34	0,11	Generalized Extreme Value	-0,54	0,37	3,26
ΔTr	0,14	0,0002	Lognorma	-1,99	0,10	0
Comfort Analysis in Light Office for Winter Weeks						
ΔPMV	0,08	0,0007	Log-Logistic	-2,5297	0,12	0
ΔPPD	4,17	0,59	Gamma'	29,097	0,14	0
ΔTr	0,47	0,024	Birnbaum-Saunders	0,453	0,32	0
Comfort Analysis in Light Office for Summer Weeks						
ΔPMV	0,11	0,0003	Generalized Pareto	-0,50	0,04	0,08
ΔPPD	4,89	1,34	Generalized Pareto	-0,44	2,28	3,31
ΔTr	0,28	0,007	Birnbaum-Saunders	0,27	0,31	0
Comfort Analysis in Heavy Office for Winter Weeks						
ΔPMV	0,04	10^{-7}	t Location-Scale	0,041	0,0003	2,589
ΔPPD	1,71	0,140	Generalized Pareto	-1,348	1,892	0,857
ΔTr	0,11	0,0006	Weibull	0,12	5,134	0
Comfort Analysis in Heavy Office for Summer Weeks						
ΔPMV	0,07	10^{-6}	Weibull	0,0712	60,67	0
ΔPPD	3,04	0,378	Generalized Pareto	-1,385	3,291	1,56
ΔTr	0,14	0,0002	Log-Logistic	-1,970	0,0607	0
Comfort Analysis in Light Mall for Winter Weeks						
ΔPMV	0,05	0,006	Logistic	0,042	0,00075	0
ΔPPD	2,18	11,09	Logistic	1,79	0,029	0
ΔTr	0,16	0,149	Logistic	0,138	0,0037	0
Comfort Analysis in Light Mall for Summer Weeks						
ΔPMV	0,07	e-06	t Location-Scale	0,073	0,0004	1,64
ΔPPD	3,79	0,059	Extreme Value	3,87	0,143	0
ΔTr	0,16	0,0004	Rician	0,16	0,019	0
Comfort Analysis in Heavy Mall for Winter Weeks						
ΔPMV	0,04	10^{-6}	Rician	0,043	0,002	0
ΔPPD	1,45	0,18	Gamma	11,58	0,13	0
ΔTr	0,13	0,0005	Lognormal	-2,03	0,16	0
Comfort Analysis in Heavy Mall for Summer Weeks						
ΔPMV	0,07	10^{-5}	Rician	0,07	0,003	0
ΔPPD	3,40	0,41	Generalized Extreme Value	-0,72	0,67	3,32
ΔTr	0,15	0,0004	Beta'	52,27	293,07	0

Table B.20. Distribution of Comfort Indexes variation for G15 Model

Distribution of Comfort Indexes Variation for GT15 Model						
Comfort Analysis in Light Bestest for Winter Weeks						
ΔPMV	0,05	10^{-5}	Generalized Extreme Value	-0,003	0,004	0,02
ΔPPD	2,41	0,09	Generalized Extreme Value	-0,50	0,32	2,34
ΔTr	0,09	0,0005	Generalized Extreme Value	0,11	0,01	0,08
Comfort Analysis in Light Bestest for Summer Weeks						
ΔPMV	0,08	1e-5	Log-Logistic	-2,48	0,02	0
ΔPPD	4,17	0,06	Generalized Extreme Value	-0,45	0,26	4,10
ΔTr	0,11	0,0002	'Normal'	0,11	0,02	0
Comfort Analysis in HeavyBestest for Winter Weeks						
ΔPMV	0,04	10^{-6}	Generalized Extreme Value	-0,15	0,001	0,04
ΔPPD	1,79	0,15	Generalized Extreme Value	-0,77	0,43	1,75
ΔTr	0,09	0,0004	Weibull	0,10	5,43	0
Comfort Analysis in HeavyBestest for Summer Weeks						
ΔPMV	0,07	10^{-7}	Logistic	0,07	0,0003	0
ΔPPD	3,43	0,08	Generalized Extreme Value	-0,51	0,30	3,36
ΔTr	0,12	0,0001	'Lognormal'	-2,17	0,10	0
Comfort Analysis in Light Office for Winter Weeks						
ΔPMV	0,07	0,0004	t Location-Scale	0,07	0,006	1,70
ΔPPD	3,52	0,36	Log-Logistic	1,25	0,09	0
ΔTr	0,39	0,02	Birnbaum-Saunders	0,37	0,33	0
Comfort Analysis in Light Office for Summer Weeks						
ΔPMV	0,09	0,0002	Generalized Pareto	-0,36	0,02	0,07
ΔPPD	4,33	0,78	Generalized Extreme Value	0,01	0,68	3,93
ΔTr	0,23	0,005	'Birnbaum-Saunders'	0,22	0,31	0
Comfort Analysis in Heavy Office for Winter Weeks						
ΔPMV	0,04	1,55	t Location-Scale	0,04	0,0002	2,07
ΔPPD	1,72	0,14	Generalized Pareto	-1,30	1,78	0,88
ΔTr	0,09	0,0004	Weibull	0,10	5,17	0
Comfort Analysis in Heavy Office for Summer Weeks						
ΔPMV	0,07	10^{-6}	Weibull	0,071	74,99	0
ΔPPD	3,07	0,41	Generalized Pareto	-1,48	3,46	1,53
ΔTr	0,12	0,0002	Log-Logistic	-2,14	0,06	0
Comfort Analysis in Light Mall for Winter Weeks						
ΔPMV	0,05	0,004	Logistic	0,04	0,0006	0
ΔPPD	2,15	6,54	Logistic	1,89	0,023	0
ΔTr	0,13	0,10	Logistic	0,12	0,003	0
Comfort Analysis in Light Mall for Summer Weeks						
ΔPMV	0,07	10^{-7}	Log-Logistic	-2,62	0,005	0
ΔPPD	3,77	0,05	Generalized Extreme Value	-0,80	0,20	3,75
ΔTr	0,14	0,0003	'Rician'	0,14	0,02	0
Comfort Analysis in Heavy Mall for Winter Weeks						
ΔPMV	0,04	10^{-6}	Lognormal	-3,15	0,03	0
ΔPPD	1,49	0,16	Nakagami	3,61	2,39	0
ΔTr	0,11	0,0003	'Gamma'	39,49	0,003	0
Comfort Analysis in Heavy Mall for Summer Weeks						
ΔPMV	0,07	10^{-6}	Logistic	0,07	0,001	0
ΔPPD	3,43	0,41	Generalized Extreme Value	-0,70	0,65	3,33
ΔTr	0,12	0,0002	Nakagami	16,01	0,017	0

Table B.21. Distribution of Comfort Indexes variation for GT15 Model

B.2.4 Simulation time reduction

Distribution of Time Reduction for 2eq Model						
	Mean	**Variance**	**PDF**	**Parameters**		
Light Bestest	82.58	4.88	Generalized Extreme Value	-1,14	2,06	82,71
Heavy Bestest	80.91	0.93	Generalized Extreme Value	0,27	0,43	80,51
Light Office	81.50	0.94	Generalized Extreme Value	2,52	0,09	80,90
Heavy Office	82.02	7.57	Generalized Extreme Value	0,63	0,63	80,59
Light Mall	82.17	5.01	Generalized Extreme Value	1,27	0,59	80,67
Heavy Mall	80.51	0.60	Generalized Extreme Value	0,56	0,32	79,94

Table B.22. Time Reduction for 2eq Model

Distribution of Time Reduction for 8eq Model						
	Mean	**Variance**	**PDF**	**Parameters**		
Light Bestest	52.68	66.43	Generalized Extreme Value	-1,20	7.34	53.32
Heavy Bestest	52.07	8.74	Inverse Gaussian	52.07	10^4	
Light Office	55.16	20,02	Generalized Extreme Value	0.52	1,92	52,06
Heavy Office	53.06	47.13	Generalized Extreme Value	2.01	0.99	48.66
Light Mall	51.71	30.78	Log Logistic	3.94	0.06	
Heavy Mall	46.94	25.21	Weibull	49.10	11.32	

Table B.23. Time Reduction for 8eq Model

Distribution of Time Reduction for 12eq Model						
	Mean	**Variance**	**PDF**	**Parameters**		
Light Bestest	56.47	9.71	Inverse Gaussian	56.47	10^4	
Heavy Bestest	49.55	27.60	t Location-Scale	50.61	0.91	0.87
Light Office	53.16	3.65	Inverse Gaussian	53.16	10^4	
Heavy Office	54.02	50.11	Generalized Extreme Value	5.11	1.00	50.50
Light Mall	51.90	51.33	Logistic	51.90	3.95	
Heavy Mall	46.52	35.28	Generalized Extreme Value	-1.01	5.91	46.55

Table B.24. Time Reduction for 12eq Model

Distribution of Time Reduction for 15eq Model						
	Mean	**Variance**	**PDF**	**Parameters**		
Light Bestest	52.20	24.23	Generalized Extreme Value	0.34	1.74	50.33
Heavy Bestest	46.60	9.10	Inverse Gaussian	46.60	10^4	
Light Office	50.71	35.00	Generalized Extreme Value	0.53	2.28	46.91
Heavy Office	45.98	70.16	t Location-Scale	45.98	1.97	1.07
Light Mall	48.95	43.73	Generalized Extreme Value	0.98	1.86	44.91
Heavy Mall	44.62	3.85	Inverse Gaussian	44.62	10^4	

Table B.25. Time Reduction for 15eq Model

Distribution of Time Reduction for 22eq Model						
	Mean	**Variance**	**PDF**	**Parameters**		
Light Bestest	36.11	51.46	Generalized Pareto	-1.10	26.93	23.29
Heavy Bestest	30.37	14.85	Generalized Pareto	-1.06	13.99	23.57
Light Office	37.59	86.42	Generalized Pareto	-1.12	35.52	20.85
Heavy Office	32.44	86.07	BirnbaumSaunders	31.60	0.28	
Light Mall	31.04	36.09	Inverse Gaussian	31.04	828.90	
Heavy Mall	22.32	60.56	Generalized Pareto	-2.10	54.94	4.58

Table B.26. Time Reduction for 22eq Model

BIBLIOGRAPHY

[1] Agency IIE. Transition to Sustainable Buildings. Strategies and Opportunities to 2050. 2013.
[2] Diakaki C, Grigoroudis E, Kolokotsa D. Towards a multi-objective optimization approach for improving energy efficiency in buildings. Energy and Buildings. 2008;40:1747-54.
[3] Commission EE. Energy efficiency in buildings.
[4] 15232 CE. Energy performance of buildings-impact of building automation, controls and building management.
[5] Dounis A, Caraiscos C. Advanced control systems engineering for energy and comfort management in a building environment. A review Renewable and Sustainable Energy Reviews. 2009;13:1246-61.
[6] Li X, Wen J. Review of building energy modeling for control and operation. Renewable and Sustainable Energy Reviews. 2014;37:517-37.
[7] Foucquier A, Robert S, Suard F, Stéphan L, Jay A. State of the art in building modelling and energy performances prediction: A review. Renewable and Sustainable Energy Reviews. 2013;23:272-88.
[8] Riederer P. Matlab/Simulink for building and HVAC simulation: State of the art. Ninth International IBPSA Conference2005.
[9] Buonomano A, Palombo A. Building energy performance analysis by an in-house developed dynamic simulation code: An investigation for different case studies. Applied Energy. 2014;113:788-807.
[10] Antonopoulos KA, Koronaki EP. On the dynamic thermal behaviour of indoor spaces. Applied Thermal Engineering. 2001;21 929-40.
[11] Bigot D, Miranville F, Fakra AH, Buildings HBHEa. A nodal thermal model for photovoltaic systems: Impact on building temperature fields and elements of validation for tropical and humid climatic conditions. Energy and Buildings. 2009;41:1117-26.
[12] Borderon J, Virgone J, Cantin R. Modeling and simulation of a phase change material system for improving summer comfort in domestic residence. Applied Energy. 2015:288-96.
[13] Kwak Y, Huh J-H, Jang C. Development of a model predictive control framework through real-time building energy management system data. Applied Energy. 2015:1-13.
[14] Široký J, Oldewurtel F, Cigler J, Prívara S. Experimental analysis of model predictive control for an energy efficient building heating system. Applied Energy. 2011;88:3079-87.
[15] Chou J-S, Bui D-K. Modeling heating and cooling loads by artificial intelligence for energy-efficient building design. Energy and Buildings. 2014;82:437-46.
[16] Candanedo JA, Dehkordi VR, Saberi-Derakhtenjani A, Athienitis A-K. Near-optimal transition between temperature setpoints for peak load reduction in small buildings. Energy and Buildings. 2015;87:123-33.
[17] Shaikh PH, Mohd NB, Nallagownden P, Elamvazuthi I, Ibrahim T. A review on optimized control systems for building energy and comfort management of smart sustainable buildings. Renewable and Sustainable Energy Reviews. 2014;34:409-29.
[18] Paris B, Eynard J, Grieu S, Talbert T, Polit M. Heating control schemes for energy management in buildings. Energy and Buildings. 2010;42 1908–17.

[19] Panão MJNO, Rebelo MP, Camelo SML. How low should be the energy required by a nearly Zero-Energy Building? The load/generation energy balance of Mediterranean housing. Energy and Buildings. 2013;61:161-71.
[20] Desideri U, Arcioni L, Leonardi D, Cesaretti L, Perugini P, al EAe. Design of a multipurpose "zero energy consumption" building according to European Directive 2010/31/EU: Life cycle assessment. Energy and Buildings.
[21] Karatasou S, Santamouris M, Geros V. Modeling and predicting building's energy use with artificial neural networks: Methods and results. Energy and Buildings. 2006;38:949-58.
[22] Wetter M. Modelica-based modeling and simulation to support research and development in building energy and controls systems. Journal of Building Performance Simulation. 2009;2:143-61.
[23] Anderson BDO, Moore. JB. Linear Optimal Control: nglewood Cliff NJ, Prentice Hall; 1971.
[24] Landau I. Adaptive Control, the model reference approach1979.
[25] Wang S. Dynamic simulation of a building central chilling system and evaluation of EMCS on-line control strategies. Building and Environment. 1998;33:1-20.
[26] Buonomano A, Palombo A. Nzebs design and simulation: a new tool for dynamic energy performance analyses. Proceedings of the 27th International Conference on Efficiency, Cost, Optimization, Simulation and Environmental Impact of Energy Systems, ECOS 20142014.
[27] Buonomano A, Luca GD, Montanaro U, Palombo A. Innovative technologies for NZEBs: an energy and economic analysis tool and a case study of a non-residential building in Mediterranean climate. Energy and Buildings. 2015;http://dx.doi.org/10.1016/j.enbuild.2015.08.037.
[28] Harish VSKV, Kumar A. A review on modeling and simulation of building energy systems. Renewable and Sustainable Energy Reviews. 2016;56:1272-92.
[29] Kramer R, J. van Schijndel, Schellen H. Simplified thermal and hygric building models: A literature review Frontiers of Architectural Research. 2012;1:318-25.
[30] Viot H, Sempey A, L. Mora, Batsale J-C. Fast on-Site Measurement Campaigns and Simple Building Models Identification for Heating Control. Energy Procedia. 2015;78: 812-7.
[31] Lauster M, Teichmann J, Fuchs M, Streblow R, Mueller D. Low order thermal network models for dynamic simulations of buildings on city district scale. Building and Environment. 2014;73:223-31.
[32] Buonomano A, Montanaro U, Palombo A, Vicidomini M. NZEBs in Mediterranean climates: energy design and optimization for a non-residential building. Energy Procedia. 2015;82:458-64.
[33] Buonomano A, Montanaro U, Palombo A, Santini S. Dynamic building energy performance analysis: A new adaptive control strategy for stringent thermohygrometric indoor air requirements. Applied Energy. 2016;163:361–86.
[34] IEA SHC. Annex 43/SHC Task 34 - Testing and Validation of Building Energy Simulation Tools. Comparative Test Case Specification. 2003-2007.
[35] ISO International Organization for Standardization. ISO/DIS 13790:2008: Thermal Performance of Buildings – Calculation of Energy Use for Space Heating and Cooling. Geneva, 2008.
[36] CEN European Committee for Standardizations. EN 15265:2007 - Thermal Performance of buildings – Calculation of Energy Use for Space Heating and Cooling – General Criteria and Validation Procedures. Brussels, 2007.
[37] Judkoff R, Neymark J. International Energy Agency Building Energy Simulation Test (BESTEST) and Diagnostic Method. NREL/TP-472-6231. 2005.

[38] ANSI ASHRAE American Society of Heating Refrigerating and Air-Conditioning Engineers. Standard 140. Standard Method of Test for the Evaluation of Building Energy Analysis Computer Programs. 2004.
[39] CEN European Committee for Standardizations. EN ISO 13791 - 13792. Thermal performance of buildings – Calculation of internal temperatures of a room in summer without mechanical cooling. General criteria and validation procedures - Simplified Methods. Brussels, 2004.
[40] Ramallo-González AP, Eames ME, Coley DA. Lumped parameter models for building thermal modelling: An analytic approach to simplifying complex multi-layered constructions. Energy and Buildings. 2013;60 174-84.
[41] Ghiaus C, Hazyuk I. Calculation of optimal thermal load of intermittently heated buildings. Energy and Buildings. 2010;42:1248-58.
[42] Joudi A, Svedung H, Rönnelid M. Energy efficient surfaces on building sandwich panels - A dynamic simulation model. Energy and Buildings. 2011;43 2462-7.
[43] US Department of Energy. EnergyPlus.
[44] University of Wisconsin Madison. TRNSYS. 2012.
[45] Crawley DB, Hand JW, Kummert M, Griffith BT. Contrasting the capabilities of building energy performance simulation programs. Building and Environment. 2008;43 661-73.
[46] Al-Homoud MS. Computer-aided building energy analysis techniques. Building and Environment. 2001:421-33.
[47] Xu X, Wang S. A simplified dynamic model for existing buildings using CTF and thermal networks modes. International Journal of Thermal Sciences. 2008;47 1249-62.
[48] Mathews EH, Richards PG, Lombard C. A first order thermal model for building design. Energy and Buildings. 1994;21 133-45.
[49] De Witt MH, Driessen HH. ELAN - A computer model for building energy design. Building and Environment. 1988;23 285-9.
[50] Lombard C, Mathews EH. A two port envelope model for building heat transfer. Building and Environment. 1999;34:19-30.
[51] Maile T, Fischer M, Haymaker J, V. B. Formalizing Approximations, Assumptions, and Simplifications to Document Limitations in Building Energy Performance Simulation. CIFE Working - Stanford University. 2010.
[52] VanderVeken J, Saelens D, Verbeeck G, Hens H. Comparison of steady-state and dynamic building energy simulation programs. Proceedings of the international Buildings IX ASHRAE conference on the performance of exterior envelopes of whole buildings. 2004.
[53] Pisello AL, Goretti M, Cotana F. A method for assessing buildings' energy efficiency by dynamic simulation and experimental activity. Applied Energy. 2012;97 419-29.
[54] Neymark J, Judkoff R, Knabe G, Le H-T, Durig M, Glass A, et al. Applying the building energy simulation test (BESTEST) diagnostic method to verification of space conditioning equipment models used in whole-building energy simulation programs. Energy and Buildings. 2002;34 917-31.
[55] Virote J, Neves-Silva R. Stochastic models for building energy prediction based on occupant behavior assessment. Energy and Buildings. 2012;53 183.
[56] Ryan MR, Sanquist TF. Validation of building energy modeling tools under idealized and realist conditions. Energy and Buildings. 2012;47:375-82.
[57] Chuah JW, Raghunathan A, Jha NK. ROBESim: A retrofit-oriented building energy simulator based on EnergyPlus. Energy and Buildings. 2013;66:88-103.
[58] Tsilingiris PT. Parametric space distribution effects of wall heat capacity and thermal resistance on the dynamic thermal behavior of walls and structures. Energy and Buildings. 2006;38 1200-11.

[59] Kontoleon KJ. Dynamic thermal circuit modelling with distribution of internal solar radiation on varying façade orientations. Energy and Buildings. 2012;47 139-50.
[60] Goya S, Barooah P. A method for model-reduction of non-linear thermal dynamics of multi-zone buildings. Energy and Buildings. 2012;47 332-40.
[61] Tsilingiris PT. On the transient thermal behaviour of structural walls - the combined effect of time varying solar radiation and ambient temperature. Technical note. Renewable Energy. 2002;27 319-36.
[62] Buonomano A, Calise F, Palombo A. Buildings dynamic simulation: Water loop heat pump systems analysis for European climates. Applied Energy. 2012;91:222-34.
[63] Buonomano A, Calise F, Palombo A. Solar heating and cooling systems by CPVT and ET solar collectors: A novel transient simulation model. Applied Energy. 2013;103:588-606.
[64] Sahlin P, Eriksson L, Grozman P, Johnsson H, Shapovalov A, Vuolle M. Whole-building simulation with symbolic DAE equations and general purpose solvers. Building and Environment. 2004;39 949-58.
[65] Pedersen L. Use of different methodologies for thermal load and energy estimations in buildings including meteorological and sociological input parameters. Renewable and Sustainable Energy Reviews. 2007;11:998-1007.
[66] Tuhus-Dubrow D, Krarti M. Genetic-algorithm based approach to optimize building envelope design for residential building. Building and Environment. 2010;23 1574-81.
[67] Wong SL, Wan KKW, Lam TNT. Artificial neural networks for energy analysis of office buildings with daylighting. Applied Energy. 2010 87 551–7.
[68] CEN European Committee for Standardizations. EN ISO 13786:1999. Thermal Performance of Building Components. Dynamic Thermal Characteristics. Calculation Methods. 1999.
[69] Martin K, Erkoreka A, Flores I, Odriozola M, Sala JM. Problems in the calculation of thermal bridges in dynamic conditions. Energy and Buildings. 2011;43 529-35.
[70] Kusuda T. Thermal response factors for multi-layered structures of various heat conduction systems. ASHRAE Transactions. 1969;75 246-67.
[71] Bueno B, Norford L, Pigeon G, Britter R. A resistance-capacitance network model for the analysis of the interactions between the energy performance of buildings and the urban climate. Building and Environment. 2012;54 116-25.
[72] Crabb JA, Murdoch N, Penman JM. A simplified thermal response model. Building Services Engineering Research and Technology. 1987;8:13-9.
[73] Tindale A. Third order lumped parameter simulation method. Building Services Engineering Research and Technology. 1993;14 87-97.
[74] Bacher P, Madsen H. Identifying suitable models for the heat dynamics of buildings. Energy and Buildings. 2011;43 1511-22.
[75] Waters JR, Wright AJ. Criteria for the distribution of nodes in multilayer walls in finite-difference thermal modelling. Building and Environment. 1985;30:151-62.
[76] Holopainen R, Tuomaala P, Piippo J. Uneven gridding of thermal nodal networks in floor heating simulations. Energy and Buildings. 2007;39:1107-14.
[77] Bring A, Sahlin P, Vuolle M. IEA SHC Task 22-Subtask B-Models for Building Indoor Climate and Energy Simulation. Dept of Building Sciences Stockholm, KTH. December 1999.
[78] Skrjanc I, Zupancic B, Furlan B, Krainer A. Theoretical and experimental FUZZY modelling of building thermal dynamic response. Building and Environment. 2001;36:1023-38.
[79] Freire RZ, Mazuroski W, Abadie MO, N. M. Capacitive effect on the heat transfer through building glazing systems. Applied Energy. 2011;88 4310–9.
[80] Berdahl P, Martin M. Emissivity of clear skies. Solar Energy. 1984;32 663-5.
[81] Roux JJ, Teodosiu C, Covalet D, Chareille R. Validation of a glazed space simulation model using full-scale experimental data. Energy and Buildings. 2004;36 557–65.

[82] Bergman TL, Lavine AS, Incropera FP, D.P. D. Fundamentals of Heat and Mass Transfer. 7th ed. John Wiley & Sons. 2011.
[83] Gebhart B. A new method for calculating radiant exchanges. ASHRAE Transactions. 1959;92 95-104.
[84] Kreider JF, Rabl A. Heating and cooling of buildings. New York (NY): McGraw-Hill. 2009.
[85] Duffie JA, Beckman WA. Solar energy thermal processes. New York, Wiley. 1974.
[86] Jamil Ahmad M, Tiwari GH. Evaluation and comparison of hourly solar radiation models. Short communication. International Journal of Energy Research. 2009;33 538-52.
[87] Ghiaus C. Linear algebra solution to psychometric analysis of air-conditioning systems. Energy. 2014;74:555-66.
[88] Soares N, Costa J, Gaspar AR, Santos P. Review of passive PCM latent heat thermal energy storage systems towards buildings' energy efficiency. . Energy and Buildings. 2013;59:82-103.
[89] Cabeza LF, Castell A, Barreneche C, Gracia Ad, Fernández AI. Materials used as PCM in thermal energy storage in buildings: A review. Renewable and Sustainable Energy Reviews. 2011;15:554-62.
[90] Toppi T, Mazzarella L. Gypsum based composite materials with micro-encapsulated PCM: Experimental correlations for thermal properties estimation on the basis of the composition. Energy and Buildings. 2013;57:227-36.
[91] 7730:2006 EI. Eronomics of thermal environment – Anaslytical determination and interpretation of thermal comfort using calculation of the PMV and PPD indices and local thermal comfort criteria.
[92] d'Ambrosio Alfano F. R., Ianniello E., Palella B. I. PMV–PPD and acceptability in naturally ventilated schools. Building and Environment. 2013;67:129–37.
[93] ASHRAE American Society of Heating Refrigerating and Air-Conditioning Engineers. ASHRAE handbook, Fundamentals - Chapter 7. Atlanta, 2009
[94] Tsilingiris PT. The influence of heat capacity and its spatial distribution on the transient wall thermal behavior under the effect of harmonically time-varying driving forces. Building and Environment. 2006:590-601.
[95] Mathworks. MATLAB.
[96] Franklin GF, Powell JD, Emami-Naeini A. Feedback Control of Dynamic Systems: Addison Wesley; 1993.
[97] Zhou JQ, Claridge DE. PI tuning and robustness analysis for air handler discharge air temperature control. Energy and Buildings. 2012;44 1-6.
[98] Buonomano A, Montanaro U, Palombo A, Santini S. Indoor Air Temperature Control in Buildings via an Optimal Tuned PI Strategy. International Journal of Engineering and Innovative Technologies. 2014;4:77-85.
[99] Vrecko D, Vodopivec N, Strmcnik S. An algorithm for calculating the optimal reference temperature in buildings. Energy and Buildings. 2009;41:182–9.
[100] Ghiaus C. Linear algebra solution to psychometric analysis of air-conditioning systems. Energy. 2014;74:555–66.
[101] Denga S., Wang R.Z., Dai Y.I. How to evaluate performance of net zero energy building – A literature research. Energy. 2014;71.
[102] Ghiaus C., Hazyuk I. Calculation of optimal thermal load of intermittently heated buildings. Energy and Buildings. 200;42:1248 – 58.
[103] Hazyuk I, Ghiaus C, Penhouet D. Optimal temperature control of intermittently heated buildings using Model Predictive Control: Part I - Building modeling. Building and Environment. 2012;51:379 - 87.
[104] 55-2004 AA. Thermal environmental conditions for human occupancy. American Society of Heating Refrigerating and Air-conditioning Engineers Inc, Atlanta, USA. 2004.
[105] Liberzon D. Switchings in Systems and Control: Birkhauser; 2003.

[106] Bernardo Md, Budd C, Champneys A, Kowalczyk. P. Bifurcations and Chaos in Piecewise-Smooth Dynamical Systems: theory and applications: Springer; 2006.
[107] Mosterman PJ. An overview of hybrid simulation phenomena and their support by simulation packages. Hybrid Systems: Computation and Control: Springer-Verlag; 1999. p. 165-77.
[108] Boiko I. Discontinuous Control Systems: Frequency-Domain Analysis and Design: Birkhauser; 2008.
[109] Branicky MS. Studies in Hybrid Systems: Modeling, Analysis, and Control. Cambridge: Massachusetts Institute of Technology; 1995.
[110] ISO International Organization for Standardization, ISO 8601:2004 , Numeric representation of Dates and Time. 2004.
[111] Sakarovitch J. Elements of automata theory: Cambridge University Press; 2009.
[112] Ruivo CR, Ferreirac PM, Vazc DC. Prediction of thermal load temperature difference values for the external envelope of rooms with setback and setup thermostats. Applied Thermal Engineering. 2013;51:980 – 7.
[113] Dounis A, Caraiscos C. Advanced control systems engineering for energy and comfort management in a building environment—A review. Renewable and Sustainable Energy Reviews. 2009;13:1246-61.
[114] Paris B, Eynard J, Grieu S, Talbert T, Polit M. Heating control schemes for energy management in buildings. Energy and Buildings. 2010;42:1908-17.
[115] Zhou JQ, Claridge DE. PI tuning and robustness analysis for air handler discharge air temperature control. Energy and Buildings. 2012;44:1-6.
[116] Astroman KJ, Hagglund T. Theory, Design, and Tuning. 2nd-Edition ed: ISA; 1995.
[117] Leithead WE, Leith DJ. Survey of gain-scheduling analysis and design. International Journal of Control. 2000;73:1001–25.
[118] Astrom KJ, Hagglund T. Advanced PID Control: ISA; 2006.
[119] Chapra SC, Canale RP. Numerical Methods for Engineers - Sixth Edition: McGraw-Hill; 2010.
[120] Mohammadpour J, Scherer C. Control of linear parameter varying systems with applications: Springer; 2012.
[121] Buonomano A, Montanaro U, Palombo A, Santini S. Building temperature control using an enhanced MRAC approach. European Control Conference 2015. p. 3629-2634.
[122] Soroka E, Shaked. U. On the robustness of LQ regulators. IEEE Transactions on Automatic Control. 1984;29:664–5.
[123] Zang C, Fu. M. A revisit to the gain and phase margins of linear quadratic regulators. IEEE Transactions on Automatic Control. 1996;41:1527–30.
[124] Stoten DP. The adaptive minimal control synthesis algorithm with integral action. International Conference on Industrial Electronics, Control, and Instrumentation1995. p. 1646 – 51.
[125] Bernardo Md, Stoten. DP. A new extended minimal control synthesis algorithm with an application to the control of chaotic systems. Conference on Decision and Control1997. p. 1902 - 7.
[126] Stoten DP, H.Benchoubane. Robustness of a minimal controller synthesis algorithm. International Journal of Control. 1990;51:850–61.
[127] Feldbaum AA. Optimal control systems: Accademic Press, New York; 1965.
[128] N.M.Filatov, Unbehauen. H. Survey of adaptive dual control methods. IEEE International Journal of Control Theory Application. 2000:118–28.
[129] Miklovicova E, Hejda I, Cervenka V, Bouslimani. M. Optimal adaptive control using the delta operator: a case study. International Conference on Systems, Man and Cybernetics1993. p. 223–8.

[130] El-Farra NH, Christofides PD. Robust optimal control of nonlinear systems. American Control Conference1999. p. 124–8.
[131] Huang T. A note on adaptive optimal control of ion accelerator facilities. IEEE Transactions on Nuclear science. 1990:1461–6.
[132] Iftar A. Robust optimal control for uncertain systems. IEEE International Conference on Systems Engineering. 1989:119–22.
[133] Rusnak I, Guez. A. Optimal adaptive control of uncertain stochastic linear systems. American Control Conference1995.
[134] Soos A, Malik. OP. An H2 optimal adaptive power system stabilizer. IEEE Transactions on Energy Conversion. 2002:143–9.
[135] Svantesson T, Olsson. G. Optimal adaptive control of an ash stabilization batch mixing process using change detection. International Conference on Control Applications2000. p. 109–14.
[136] Impe JFv, Bastin G. Optimal adaptive control of fed-batch fermentation processes with multiple substrates. Conference on Control Applications1993.
[137] Astrom K., Wittenmark B. Adaptive Control, 2nd edition: Addison-Wesley Publishing Company, Inc.; 1995.
[138] Anderson B.D.O., Moore J.B. Linear Optimal Control.
[139] Khalil H. K. Nonlinear Systems, 3rd edition2001.
[140] Ioannou P., Fidan B. Adaptive Control Tutorial: Advances in Design and Control2006.
[141] Utkin VI. Sliding Modes in Control and Optimization: Springer-Verlag; 1992.
[142] di Bernardo M., Montanaro U., Santini S. Novel hybrid MRAC-LQ control schemes: Synthesis, analysis and applications. International Journal of Control. 2008;81 940-61.
[143] Slotine J., Li W. Applied Nonlinear Control1991.
[144] Popov VM. Hyperstability of Control Systems: Springer-Varlag; 1973.
[145] di bernardo M., di Gaeta A., Montanaro U., Santini S. Synthesis and experimental validation of the novel LQ-NEMCSI adaptive strategy on an electronic throttle valve. IEEE Transactions on Control Systems Technology. 2010;18:1325-37.
[146] Bergman T. L., Lavine A. S., Incropera F. P., DeWitt D. P. Fundamentals of Heat and Mass Transfer - 7th edition2011.
[147] Judkoff R, Neymark J. International Energy Agency Building Energy Simulation Test (BESTEST) and Diagnostic Method. NREL/TP-472-6231. 2005.
[148] Evola G, Marletta L, Sicurella F. A methodology for investigating the effectiveness of PCM wallboards for summer thermal comfort in buildings. Building and Environment. 2013;59:517-27.
[149] Narendra K. S., Annaswamy A.M. Stable Adaptive Systems: Prentice Hall; 1989.
[150] LeBlanc MH. The physics of thermal exchange between infants and their environment. Medical Instrumentation. 1987;21:11-5.
[151] Lyon A. Applied physiology: temperature control in the newborn infant. Current Paediatrics. 2004;14:137-44.
[152] Zermani MA, Feki E, Mami A. Building simulation model of infant-incubator system with decoupling predictive controller. IRBM. 2014;35:189-201.
[153] Buonomano A, Montanaro U, Palombo A, Santini S. Multi-zone buildings thermo-hygrometric analysis: a novel dynamic simulation code based on adaptive control. Building Simulation Applications 2015 - 2nd IBPSA-Italy Conference. Bolzano2015. p. 109-18.
[154] Buonomano A, Montanaro U, Palombo A, Santini S. Adaptive control for building thermo-hygrometric analysis: a novel dynamic simulation code for indoor spaces with multi-enclosed thermal zones. 6th International Building Physics Conference (IBPC 2015). Turin 2015.

[155] Buonomano A, Montanaro U, Palombo A, Santini S. Adaptive control for building thermo-hygrometric analysis: a novel dynamic simulation code for indoor spaces with multi-enclosed thermal zones. Energy Procedia. 2015;78:2190-5.
[156] Pedro A, Sala A. Multivariable Control Systems: An Engineering Approach: Springer; 2004.
[157] G.Verghese. Getting to the Gray Box: Some Challenges for Model Reduction. American Control Conference2009. p. 5-6.
[158] Wang S, Chen Y. A novel and simple building load calculation model for building and system dynamic simulation. Applied Thermal Engineering. 2001;21:683-702.
[159] S.W. Wang, Xu XH. Simplified building model for transient thermal performance estimation using GA-based parameter identification. International Journal of Thermal Sciences. 2006;45:419-32.
[160] Zhu N, Wang S, Xu X, Ma Z. A simplified dynamic model of building structures integrated with shaped-stabilized phase change materials. International Journal of Thermal Sciences. 2010;49:1722-31.
[161] Phillips Cl, J.M.Parr, Riskin EA. Signals, systems and Transforms: Prentice Hall; 2007.
[162] Hespanha JP. Linear System Theory: Princeton university press; 2009.
[163] Ljung L. System Identification: Theory for the User: Prentice Hall.
[164] Nocedal J, Wright S. Numerical Optimization. second edition ed: Springer; 2006.
[165] Cantone I, Marucci L, Iorio F, Ricci MA, Belcastro V, Bansal M, et al. A Yeast Synthetic Network for In Vivo Assessment of Reverse-Engineering and Modeling Approaches. Cell. 2009;137:172–81.
[166] Coley DA. An Introduction to Genetic Algorithms for Scientists and Engineers: World Scientific Pub Co Inc; 1999.
[167] Sheppard M. allfitdist matlab function, available at www.mathworks.com. 2012.
[168] Camacho EF, Bordons C. Model Predictive Control: Springer-Verlag; 2004.
[169] Kwon WH, (Autore) SH. Receding Horizon Control: Model Predictive Control for State Models: Springer-Verlag; 2005.
[170] Ferhatbegovic T, Palensky P, Fontanella G, Basciotti D. Modelling and design of a linear predictive controller for a solar powered HVAC system. 2012. p. 869-74.
[171] Franklin G, Powell JD, Workman ML. Digital Control of Dynamic Systems: Addison-Wesley; 1997.
[172] Lemos JM, Neves-Silva NR, Igreja JM. Adaptive control of Solar Energy Collector Systems2014.
[173] Wu CW. synchronization in complex networks of nonlinear dynamical systems: World Scientific Publishing Company; 2007.
[174] Brogliato B, Lonzano R, Masheke B, Egeland O. Dissipative Systems Analysis and control: Theory and Applications: Springer; 2007.

LIST OF PUBLICATIONS

Journal papers

1. A. Buonomano, U. Montanaro, A. Palombo and S. Santini, *Dynamic building energy performance analysis: a new adaptive control strategy for stringent thermohygrometric indoor air requirements*, Applied Energy, vol. 163, pages 361-386, February 2016.

2. A. Buonomano, G. De Luca, U. Montanaro and Adolfo Palombo, *Innovative technologies for NZEBs: an energy and economic analysis tool and a case study of a non-residential building in Mediterranean climate*, in press in Energy and Building. Available online (http://dx.doi.org/10.1016/j.enbuild.2015.08.037).

3. A. Buonomano, U. Montanaro, A. Palombo and S. Santini, *Indoor Air Temperature Control in Buildings via an Optimal Tuned PI Strategy*, *International Journal of Engineering and Innovative Technologies*, volume 4, issue 4, pages 77-85, October 2014.

4. A. Buonomano, U. Montanaro, A. Palombo and M. Vicidomini, *NZEBs in Mediterranean climates: energy design and optimization for a non-residential building*, Energy Procedia, vol. 82, pages 458-464, December 2015.

5. A. Buonomano, U. Montanaro, A. Palombo and S. Santini, *Adaptive control for building thermo-hygrometric analysis: a novel dynamic simulation code for indoor spaces with multi-enclosed thermal zones*, Energy Procedia, vol. 78, pages 2190-2195, November 2015.

Conference papers

1. A. Buonomano, U. Montanaro, A. Palombo and M. Vicidomini, *NZEBs in Mediterranean climates: energy design and optimization for a non-residential building*, 70th Conference of the ATI Engineering Association, Rome (Italy), 9-11 September 2015 (this article has been published also in Energy Procedia, see the previous list).

2. A. Buonomano, U. Montanaro, A. Palombo and M. Vicidomini, *Energy saving technologies for non-residential NZEB in Mediterranean climate*, Latin American and European Conference on Sustainable Buildings and Communities, pages 649-658, Guimaraes (Portugal), 21-23 July 2015.

3. A. Buonomano, U. Montanaro, A. Palombo and S. Santini, *Building temperature control using an enhanced MRAC approach*, 14th European Control Conference, pages 3634-3639, Linz (Austria), 15-17 July 2015.

4. A. Buonomano, U. Montanaro, A. Palombo and S. Santini, *Adaptive control for building thermo-hygrometric analysis: a novel dynamic simulation code for indoor spaces with multi-enclosed thermal zones*, 6th International Building Physics Conference (IBPC 2015), Turin (Italy), 14-17 June 2015 (this article has been published also in Energy Procedia, see the previous list).

5. A. Buonomano, U. Montanaro, A. Palombo and S. Santini, *Multi-zone buildings thermo-hygrometric analysis: a novel dynamic simulation code based on adaptive control*, Building Simulation Applications 2015 - 2nd IBPSA-Italy Conference, pages 109-118, Bolzano (Italy), 4-6 February 2015

Submitted papers

1. A. Buonomano, U. Montanaro, A. Palombo and S. Santini, *Model reduction of buildings for control applications: a quantitative analysis of energy demand and thermohygrometric comfort*, submitted abstract to 11th Conference on Sustainable Development of Energy, Water and Environment Systems, September 2016.

2. A. Buonomano, F. Calise, U. Montanaro and A. Palombo, *Solar heating and cooling systems for residential applications: a comparison among different system layouts and technologies*, submitted abstract to 11th Conference on Sustainable Development of Energy, Water and Environment Systems, September 2016.

3. A. Buonomano, U. Montanaro, A. Palombo and S. Santini, *Energy and comfort analysis of PCM materials embedded in the building envelope*, submitted abstract to 11th Conference on Sustainable Development of Energy, Water and Environment Systems, September 2016.